National Library of Canada
Bibliothèque nationale du Canada

Canadian Theses Service
Services des thèses canadiennes

Ottawa, Canada
K1A 0N4

CANADIAN THESES
THÈSES CANADIENNES

NOTICE

The quality of this microfiche is heavily dependent upon the quality of the original thesis submitted for microfilming. Every effort has been made to ensure the highest quality of reproduction possible.

If pages are missing, contact the university which granted the degree.

Some pages may have indistinct print especially if the original pages were typed with a poor typewriter ribbon or if the university sent us an inferior photocopy.

Previously copyrighted materials (journal articles, published tests, etc.) are not filmed.

Reproduction in full or in part of this film is governed by the Canadian Copyright Act, R.S.C. 1970, c. C-30.

AVIS

La qualité de cette microfiche dépend grandement de la qualité de la thèse soumise au microfilmage. Nous avons tout fait pour assurer une qualité supérieure de reproduction.

S'il manque des pages, veuillez communiquer avec l'université qui a conféré le grade.

La qualité d'impression de certaines pages peut laisser à désirer, surtout si les pages originales ont été dactylographiées à l'aide d'un ruban usé ou si l'université nous a fait parvenir une photocopie de qualité inférieure.

Les documents qui font déjà l'objet d'un droit d'auteur (articles de revue, examens publiés, etc.) ne sont pas microfilmés.

La reproduction, même partielle, de ce microfilm est soumise à la Loi canadienne sur le droit d'auteur, SRC 1970, c. C-30.

THIS DISSERTATION
HAS BEEN MICROFILMED
EXACTLY AS RECEIVED

LA THÈSE A ÉTÉ
MICROFILMÉE TELLE QUE
NOUS L'AVONS REÇUE

Canada

NL-339 (r. 86/06)

THE UNIVERSITY OF ALBERTA

KINETICS AND EQUILIBRIA OF ELECTRON TRANSFER REACTIONS: $A^{\cdot} + B = A + B^{\cdot}$. DETERMINATION OF ELECTRON AFFINITIES. STRUCTURE AND STABILITIES OF IONS $A^{\cdot}$, $B^{\cdot}$ AND ADDUCT IONS $A^{\cdot}.B$, AND $B^{\cdot}.A$

by

SWAPAN KUMAR CHOWDHURY

A THESIS

SUBMITTED TO THE FACULTY OF GRADUATE STUDIES AND RESEARCH

IN PARTIAL FULFILMENT OF THE REQUIREMENTS FOR THE DEGREE

OF DOCTOR OF PHILOSOPHY

DEPARTMENT OF CHEMISTRY

EDMONTON, ALBERTA

SPRING, 1987

Permission has been granted to the National Library of Canada to microfilm this thesis and to lend or sell copies of the film.

The author (copyright owner) has reserved other publication rights, and neither the thesis nor extensive extracts from it may be printed or otherwise reproduced without his/her written permission.

L'autorisation a été accordée à la Bibliothèque nationale du Canada de microfilmer cette thèse et de prêter ou de vendre des exemplaires du film.

L'auteur (titulaire du droit d'auteur) se réserve les autres droits de publication; ni la thèse ni de longs extraits de celle-ci ne doivent être imprimés ou autrement reproduits sans son autorisation écrite.

ISBN 0-315-37613-9

THE UNIVERSITY OF ALBERTA

RELEASE FORM

NAME OF AUTHOR SWAPAN KUMAR CHOWDHURY

TITLE OF THESIS KINETICS AND EQUILIBRIA OF ELECTRON TRANSFER REACTIONS: $A^{\cdot} + B = A + B^{\cdot}$. DETERMINATION OF ELECTRON AFFINITIES. STRUCTURE AND STABILITIES OF IONS $A^{\cdot}$, $B^{\cdot}$ AND ADDUCT IONS $A^{\cdot}.B$, AND $B^{\cdot}.A$

DEGREE FOR WHICH THESIS WAS PRESENTED DOCTOR OF PHILOSOPHY

YEAR THIS DEGREE GRANTED SPRING, 1987

Permission is hereby granted to THE UNIVERSITY OF ALBERTA LIBRARY to reproduce single copies of this thesis and to lend or sell such copies for private, scholarly or scientific research purposes only.

The author reserves other publication rights, and neither the thesis nor extensive extracts from it may be printed or otherwise reproduced without the author's written permission.

(SIGNED) Swapan k. Chowdhury

PERMANENT ADDRESS:
Vill. Dakinagar, P.O. Gohira
P.S. Raozan, Chittagong
Bangladesh

DATED Feb. 9 1987

THE UNIVERSITY OF ALBERTA

FACULTY OF GRADUATE STUDIES AND RESEARCH

The undersigned certify that they have read, and recommend to the Faculty of Graduate Studies and Research, for acceptance, a thesis entitled KINETICS AND EQUILIBRIA OF ELECTRON TRANSFER REACTIONS: $A^{\cdot} + B = A + B^{\cdot}$. DETERMINATION OF ELECTRON AFFINITIES. STRUCTURE AND STABILITIES OF IONS $A^{\cdot}$, $B^{\cdot}$ AND ADDUCT IONS $A^{\cdot}.B$, AND $B^{\cdot}.A$ submitted by SWAPAN KUMAR CHOWDHURY in partial fulfilment of the requirements for the degree of DOCTOR OF PHILOSOPHY.

P. Kebarle

Supervisor

D. S. Hogan

Dennis Tanner

T. B. Grieve

T. B. McMahon

External Examiner

Date Feb 9 /1987

Dedication

To

My parents

ABSTRACT

The gas phase electron transfer reactions: $A^- + B = A + B^-$, where A and B are substituted benzenes, substituted naphthalenes, azulene, perfluoro aromatic systems, sulfurhexafluoride, perfluoromethylcyclohexane, benzo- and naphthoquinones, maleic and phthalicanhydride, di- and tetracyanoethylene and small molecules like SO_2, NO_2, CS_2, CH_3NO_2 etc. were studied with a pulsed electron high pressure mass spectrometer.

The rate constants for 77 reactions were determined. The majority, when exothermic, proceeded with rate constants k_1 which were near the Langevin-ADO collision limit. However, when SF_6 and perfluoromethylcyclohexane were used, k_1 was observed to be very small, and was found toincrease with the increase of exothermicity of the reaction. The slowness was attributed to a large energy barrier in the reaction coordinate which decreases as the exothermicity increases. The barrier is due to a large geometry change between SF_6^- and SF_6, and stability differences between $SF_6^-.B$ and $SF_6.B^-$.

Determination of equilibrium constants K_1 leads to an evaluation of the ΔG_1^0. While the temperature dependence of K_1 provides, via van't Hoff plots, ΔH_1^0 and ΔS_1^0 changes. These measurements permit the construction of interconnecting ΔH_1^0, ΔS_1^0 and ΔG_1^0 scales containing 100 molecules. The electron affinities EA(A) of all compounds in the ΔH_1^0 scale were determined by anchoring the scale to the precisely known electron affinity of SO_2. The resulting electron affinity scale extends from 0.5 to 3.2 eV. $\Delta H_a^0(A)$ (= - EA(A)), $\Delta S_a^0(A)$ and $\Delta G_a^0(A)$ data for electron attachment process ($A + e \rightarrow A^-$) was also obtained.

The equilibria: $A^- + Sl = A^-.Sl$ and $A^- + B$ (or A) $= A^-.B$ (or $A^-.A$), where A and B are 27 different substituted nitrobenzenes and quinones and Sl are the solvent molecules: MeOH, MeCN, DMSO, DMF and THF were studied also. A decrease of binding energy in $A^-.Sl$ with increasing electron affinity of A was observed. The decrease is attributed to increasing charge delocalization in A^- with the increase of EA(A). The observed changes in bond energies for the adducts $A^-.B$ were examined and possible structures of the $A^-.B$ and $A.B^-$ adducts are proposed.

Acknowledgement

I wish to express my sincere appreciation and gratitude to Professor Paul Kebarle for his continued interest, invaluable advice and encouragement throughout the course of this work.

The measurements described in chapters 4 and 5 were done in collaboration with Dr. E. P. Grimsrud, whose assistance and suggestions are gratefully acknowledged. I wish to thank Dr. G. Caldwell for doing some initial electron transfer equilibria measurements and Dr. T. Heinis for performing some cross-check measurements described in chapter 4.

The author would like to thank other members of the mass spectrometry group for their assistance, especially Dr. J. Sunner for his occasional help with the instrumental problems and helpful discussions.

I wish to thank my friend Dr. Dipak Ghosh, who kindly proof-read the manuscript with care and patience and also helped me with the use of textform in typing the thesis. I take this opportunity to thank all other friends and well wishers, for their co-operation.

The financial support provided by the University of Alberta as teaching and research assistantships is gratefully acknowledged.

Table of Contents

Chapter — Page

Dedication iv

ABSTRACT v

Acknowledgement vi

List of Tables xii

List of Figures xiv

Abbreviation xviii

1. INTRODUCTION 1

1.1 The Scope and Objective of the Present Study 1

1.2 Methods Used in the Past for the Determination of Electron Affinities 3

1.2.1 Methods Based on Electron Affinity Measurements in Gas Phase 3

1.2.2 Methods Based on Electron Affinity Measurements in Solution 9

1.3 Formation of Negative ions in Gas Phase: Electron Capture in the Absence of Third Body Collision. 11

1.4 Electron Transfer Reactions in Gas Phase: Measurements of Kinetics and Equilibria. 14

1.5 Conditions and Apparatus for the Measurements of ET Kinetics and Equilibria. 17

1.5.1 The Pulsed High Pressure Mass Spectrometry (HPMS) 17

1.5.2 Pulsed Ion Cyclotron Resonance Spectrometry (ICR) 19

1.5.3 The Flowing Afterglow Method (FAG) 20

2. EXPERIMENTAL 21

2.1 General 21

2.2 The Apparatus: High Pressure Mass Spectrometer 21

2.3 Chemicals 27

3. KINETICS OF ELECTRON TRANSFER REACTIONS 28

3.1 Introduction 28

3.2 Well Behaved and Fast Reactions 28

3.2.1 Measurements and Results 28

3.2.2 Discussion of the Results of Kinetics of Electron Transfer Reactions 32

3.3 Slow Electron Transfer Kinetics Involving SF_6, $CF_3C_6F_{11}$, Etc. 42

3.3.1 Background 42

3.3.2 Results of Slow Electron Transfer Reactions Involving SF_6, $CF_3C_6F_{11}$ and Their Negative Ions 44

3.3.3 Discussions 47

4. ELECTRON AFFINITIES FROM ELECTRON TRANSFER EQUILIBRIA MEASUREMENTS 57

4.1 Measurements and Results 57

4.1.1 Electron Transfer Equilibria 57

4.1.2 Scales of ΔG^0_1, ΔS^0_1, and ΔH^0_1 66

4.1.3 Electron Affinities and Other Thermochemical Quantities: ΔH^0_a, ΔS^0_a, and ΔG^0_a for Electron Attachment Reaction 89

4.2 Discussion of Results Obtained from Electron Transfer Equilibria Measurements .. 95

4.2.1 Comparison of Relative EAs Obtained in the Present Investigation with Those Reported by Fukuda and McIver 102

4.2.2 Electron Affinities. Structure and Stabilities of Radical Anions. Effects of Substituents on Electron Affinities 105

4.2.3 Comparison of EAs from Gas Phase ET-Equilibria Obtained in the Present Study with those Deduced from the Measurements in Solution 138

4.2.4 Autodetachment Lifetimes of Negative Ions and the Electron Affinities of Neutral Molecules 141

4.3 Entropy Changes on Electron Attachment 142

5. THERMAL ELECTRON DETACHMENT RATE CONSTANTS. THE ELECTRON DETACHMENT FROM AZULENE NEGATIVE ION 146

5.1 Introduction 146

5.2 Measurements and Results: Reaction Mechanisms and Determination of Thermal Detachment Rate Constant 147

5.3 Discussion of Thermal Detachment Rate Constants and Electron Attachment-Detachment Equilibria 160

6. BINDING ENERGIES OF ION-NEUTRAL COMPLEXES INVOLVING CHARGE DELOCALIZED NEGATIVE IONS 165

6.1 Introduction 165

6.2 Bonding of Charge Delocalized Anions to Protic and Dipolar Aprotic Solvent Molecules 167

6.2.1 Measurements and Results 167

6.2.2 Discussion of Bond Energies in $A^-.Sl$ and Their Significance to the Solvation of A^- in Polar and Dipolar Aprotic Solvent 175

6.3 Binding Energies in $A^-.B$ and $A^-.A$, where A and B are NO_2, Nitrobenzenes, Quinones and Perfluoromolecules 184

6.3.1 Measurements and Results 184

6.3.2 Discussion of Results 191

7. APPLICATION OF ELECTRON AFFINITIES AND THE STABILITIES OF A^- AND ADDUCTS OF A^- IN NEGATIVE ION ANALYTICAL MASS SPECTROMETRY 213

8. SUGGESTIONS FOR FURTHER WORK 224

8.1 Determination of Electron Affinities 224

8.1.1 Polycyclic Aromatic Hydrocarbons, PAHs 224

8.1.2 Extension of the Electron Affinity Scale to Higher Electron Affinity Values 225

8.2 Determination of Binding Energies of Charge Delocalized Anions with Multiple Solvent Molecules 227

8.3 Meisenheimer Type Complexes 228

BIBLIOGRAPHY: 230

List of Tables

3.1 Rate constants k_1 for exothermic electron transfer reactions (1.1): $A^- + B \rightarrow A + B^-$ involving NO_2 at 423K..... 33

3.2 Rate constants k_1 for electron transfer reactions (1.1) involving substituted benzenes at 423K..... 34

3.3 Rate constants k_1 for exothermic electron transfer reactions (1.1) involving perfluorobenzenes..... 35

3.4 Rate constants for electron transfer reactions (1.1) involving benzo- and naphthoquinones and di- and tetracyanoethylene..... 35

3.5 Exothermic electron transfer rate constants for reactions involving azulene and naphthalenes..... 36

3.6 Exothermic electron transfer rate constants for reactions involving SF_6 and C_7F_{14}..... 46

3.7 Binding energies in adducts $A^-.B$ involving SF_6 and C_7F_{14}..... 54

4.1 $\Delta G^0_1(423K)$, ΔH^0_1, and ΔS^0_1 values for electron transfer reactions (1.1) from van't Hoff plots..... 87-88

4.2 $\Delta G^0_a(423K)$, ΔH^0_a, and ΔS^0_a for electron attachment to SO_2..... 91

4.3 Electron affinities and other thermochemical data for electron attachment reaction: $A + e = A^-$..... 96-101

4.4 Relative electron affinities of substituted nitrobenzenes..... 117

4.5 Separation of field effect and resonance effect of substituents on the electon affinity of substituted nitrobenzenes..... 119

4.6 Comparison of resonance effect of substituents on the electron affinity of nitrobenzene with those on the gas phase phenol acidity..... 120

4.7 Comparison of the field effect of substituents on the electron affinity of nitrobenzene with those on the gas phase phenol acidity..... 121

4.8 Substituent constants based on electron affinities of substituted nitrobenzenes..... 124

4.9 Effect of substituents on the electron affinity of substituted nitrobenzenes and substituted perfluorobenzenes..... 132

5.1 Kinetic data for electron detachment and attachment reactions and diffusion of ions and electron..... 153

5.2 Thermal electron detachment rate constants for detachment from azulene negative ion..... 163

6.1 Thermochemical data for reactions: $A^- + Sl = A^-.Sl$, where Sl are solvent molecules..... 170

6.2 Thermochmical results from van't Hoff plots for reactions: $A^- + Sl = A^-.Sl$..... 171

6.3 Thermochmical data for the reaction $NO_2^- + A = NO_2^-.A$ obtained directly from van't Hoff plots..... 189

6.4 Thermochemical data for the stability of adducts of NO_2^- and rate constants for oxynegative ion formation by reaction of NO_2^- with substituted nitrobenzenes. 190

6.5 Thermochemical results for the stability of adducts of 1,2-dinitrobenzene negative ion. 192

6.6 Binding energies in Cl^--A. 194

6.7 Thermochemical data for the reaction: $A^- + A = A^-.A$.....195

List of Figures

2.1 Simplified diagram of the ion source 22

2.2 Main components of the electron beam mass spectrometer. 24

2.3 Pulsing sequence 26

3.1a-b Log of ion intensities as a function of time showing the achievement of equilibrium. .. 29

3.2 Concentration changes of ions due to electron transfer: (a) 4-FNB$^-$ to BQ, (b) 3-CF_3NB$^-$ to 4-NO_2NB for different concentrations of 4-NO_2NB. 31

3.3 Plot of pseudo-first-order rate constant for electron transfer to 4-NO_2NB against concentration of 4-NO_2NB. 37

3.4 Time dependence of ion intensities in percent of total ion current. 38

3.5 Intensities of ions observed after a short electron pulse with various perfluoro compounds and nitrobenzenes in the ion source. 41

3.6 Temperature dependence of rate constants for electron transfer from SF_6^- 45

3.7 Reaction coordinate with internal energy barrier used to explain temperature dependence of gas phase S_N2 type reactions 48

3.8 Reaction coordinate for the reaction $SF_6^- + B \rightarrow SF_6 + B^-$, where B = 3-$CF_3$NB 51

3.9a-b Observed ion intensities as a function of time of SF_6^-, nitrobenzene negative ions and their adducts. 52

4.1 Tests of invariance of equilibrium constants K_1 with changing pressure of ion source. 59

4.2A-C Measurements of electron transfer equilibria involving SF_6^- and substituted nitrobenzenes. 61

4.3a-b Tests of invariance of equilibrium constants of electron transfer reactions involving SF_6^- with total ion source pressure and partial pressure of 4-CNNB 63

4.4 Intensity changes observed in the equilibria measurement of the reaction involving $C_7F_{14}^-$ 64

4.5a-b Time dependence of ion intensities observed after ionising pulse to the ion source containing C_6F_6 and substituted nitrobenzenes. 65

4.6 Invariance of electron transfer equilibrium constants, (a) with total pressure, (b) with the ratio of partial pressures of A and B for reactions involving perfluorobenzenes 67

4.7 Free energy change ΔG_1^0 ladder for electron transfer reaction (1.1) involving some reference molecules and SO_2. 68

4.8 A continuous ΔG_1^0 scale for electron transfer reactions (1.1). 69-71

4.9 An additional ΔG_1^0 scale for electron transfer reactions (1.1) involving TCNE and perfluoro compounds. 72

4.10 Ion intensity versus time plot for the reaction involving fluoranil negative ion and

TCNE..... 74

4.11 van't Hoff plots of equilibrium constants for electron transfer reactions..... 75

4.12 van't Hoff plots of equilibrium constants for electron transfer reactions..... 76

4.13 van't Hoff plots of equilibrium constants for electron transfer reactions..... 77

4.14 van't Hoff plots of equilibrium constants for electron transfer reactions..... 78

4.15 van't Hoff plots of equilibrium constants for electron transfer reactions..... 79

4.16 van't Hoff plots of equilibrium constants for electron transfer reactions..... 80

4.17 van't Hoff plots of equilibrium constants for electron transfer reactions..... 81

4.18 van't Hoff plots of equilibrium constants for electron transfer reactions..... 82

4.19 Ladder for ΔH_1^0 changes for electron transfer reactions (1.1) from van't Hoff plots..... 83

4.20 An additional ladder for ΔH_1^0 changes from van't Hoff plots..... 84

4.21 Ladder for ΔS_1^0 changes for electron transfer reactions from van't Hoff plots..... 85

4.22 An additional ladder for ΔS_1^0 from van't Hoff plots..... 86

4.23 Comparison of ΔG_a^0 values for electron attachment reaction involving substituted nitrobenzenes from the present investigation with those reported by Fukuda and McIver, measured with the help of a pulsed ICR spectrometer.....103

4.24 Comparison of ΔG_a^0 values for electron attachment reaction involving substituted benzo- and naphthoquinones from the present investigation with those reported by Fukuda and McIver, measured with the help of a pulsed ICR spectrometer.....104

4.25 Plot of electron affinities of substituted benzenes, naphthalenes, anthracenes, cyanobenzenes and nitrobenzenes versus Hammet substituent constants based on gas phase phenol acidities.....108

4.26 Comparison of relative electron affinities of substituted nitrobenzenes with those of substituted cyanobenzenes.....111

4.27 Plot of net charge distribution in position 1 and 2 of naphthalene plotted against the electron affinities of substituted naphthalenes.....113

4.28 Comparison of relative electron affinities of substituted nitrobenzenes with gas phase acidities of substituted phenols.....115

4.29 Plot of electron affinities of substituted nitobenzenes versus substituent constants based on gas phase phenol acidities.....122

4.30 Plot of electron affinities of CH_3 and Cl substituted benzoquinones versus number of substituents.....129

4.31 Time dependence of intensities of ions observed after electron pulse in the ion source containing methane and hexafluorobenzene.....134

4.32 Comparison of electron affinities obtained in the present investigation with those from half wave reduction potential and charge transfer spectroscopic measurements in solution. 139

5.1 Observed ion intensities of azulene negative ion and $C_7F_{14}^-$ after an ionising electron pulse 149

5.2 Plot of $\nu(Az^-)$ versus temperature. 151

5.3 Plot of $\nu(Az^-)$ versus the pressure of C_7F_{14}. 152

5.4 Plot of experimental points for $\nu_N(Az^-) = \nu(Az^-) - \nu_{tr}(Az^-)$ versus pressure of C_7F_{14} 155

5.5 Arrhenius plot of electron detachment rate constants for electron detachment from Az^- ..157

5.6 Time dependence of ions after ionising electron pulse; (A) with methane and perfluoro methycyclohexane, (B) with methane and azulene, and (C) with methane, azulene and perfluoro methylcyclohexane. 158

5.7 Dependence of electron detachment rate constant on total pressure. 161

6.1 Ion intensities observed after ionising electron pulse in the ion source containing 1,2-dinitrobenzene, MeOH and MeCN. 168

6.2 Plot showing invariance of equilibrium constants with total ion source pressure for the reaction: $A^- + Sl = A^-.Sl$, where Sl are solvent molecules. 172

6.3 van't Hoff plots of equilibrium constants of equilibria: $A^- + Sl = A^-.Sl$. 173

6.4 Plot of ΔG^0 and ΔH^0 for the reaction: $A^- + Sl = A^-.Sl$ versus the electron affinity of A. 174

6.5 Plot of $E_{1/2}$, the half wave reduction potential values for some benzo- and naphthoquinones versus electron affinities of quinones. 178

6.6a-b Observed ion intensity changes after ionising pulse in the source containing methane, NO_2, and dinitrobenzenes. 186

6.7 Plot of equilibrium constants for the reaction: $NO_2^- + A = NO_2^-.A$ versus total ion source pressure. 187

6.8 van't Hoff plots of equilibrium constants for the reactions: $NO_2^- + A = NO_2^-.A$. 188

6.9 van't Hoff plots of equilibrium constants for reactions: $A^- + B = A^-.B$. 193

6.10 Plot of ΔH^0 for reactions: $NO_2^- + A = NO_2^-.A$ versus the electorn affinities of A. 198

6.11 Plot of $D(2\text{-}NO_2NB^-\text{-}A)$ against $D(NO_2^-\text{-}A)$. 201

6.12 Plot of binding energies $D(A^-\text{-}A)$ versus electron affinities of A 203

6.13 Plot of binding energies of Cl^- to A versus substituent constants based on gas phase phenol acidities 204

6.14 Plot of binding energies of Cl^- to A versus dipole moments of A. 207

6.15 Possible bonding structures of $SF_6^-.B$ and $SF_6.B^-$, where B= 3-CF_3NB. 209

6.16 Structures of $F^-.C_6F_6$ and $F^-.C_6H_6$ from theoretical calculations due to Hiraoka et al. (ref. 170). 211

7.1 Shown are electron affinities of four different classes of compounds. 215

7.2a-b Formation of phenoxy anion by reaction of NO_2^- with 3,5-dinitrobenzonitrile at 125 and 250°C. 221

7.3 Pulsed electron negative ion mass spectrum of fluoranil: (a) methane + fluoranil, (b) methane + fluoranil + NO_2. 222

Abbreviation

Az = Azulene

BN = Benzonitrile

BQ = p-benzoquinone

CI = Collisional Ionisation technique

CTS = Charge transfer spectroscopic method

DMF = Dimethyl formamide

DMSO = Dimethyl sulfoxide

EA = Electron affinity

ECD = Electron capture detector

ECT = Endothermic charge transfer method

ETE = Electron transfer equilibrium method

FAB = Fast atom bombardment

ICR = Ion cyclotron resonance method

HPMS = High pressure mass spectrometer

HWP = Half wave reduction potential

KB = Kinetic bracketing technique

LPD = Laser photodetachment method

MaAn = Maleic anhydride

Me = CH_3

NB = Nitrobenzene

NICI = Negative ion chemical ionisation

NpQ = 1,4-naphthoquinone

NpT = Naphthalene

Sl = Solvent molecule

Sv = Scavenger

TCNE = Tetracyano ethylene

1. INTRODUCTION

1.1 The Scope and Objective of the Present Study

The present study which involves negative ions in gas phase consists of three parts. The first part involves the measurements of the rate constants, k_1 of the exothermic electron transfer reactions (1.1), where A and B are various organic

$$A^- + B \underset{k_{-1}}{\overset{k_1}{\rightleftharpoons}} A + B^- \qquad (1.1)$$

and inorganic molecules. The second part describes the determination of electron affinities of molecules A and B through measurements of the equilibria (1.1). The third part deals with the determination of the binding energies of ion neutral adducts, such as $A^-.Sl$, A_2^-, $A^-.B$ etc., where Sl are different protic and aprotic solvent molecules.

Negative ions play an important role in Ion-molecule chemistry, Photochemistry and Photophysics[1]. The chemistry of negative ions has its origin as early as 1939, since Widlt[2] showed that H^- photoabstraction could be a major source of opacity in the solar infrared spectrum. In the past decades there has been a considerable development of the negative ion chemistry in the gas phase. This involves negative ion spectroscopic studies[3,4], gas phase ion-molecule equilibria measurements[5] and collisional studies with charged and uncharged particle beams[1].

One of the fundamental properties of the molecular negative ion is the electron affinity, EA of the neutral molecule. The electron affinity of a molecule is defined as the difference in energy between the neutral molecule plus an electron at rest at infinity and the molecular negative ion, when both the negative ion and the neutral molecule are in their ground electronic, vibrational and rotational states. Thus $-\Delta E^\circ_a = EA(A)$. ΔE°_a is the electron attachment energy to A, equation (1.2).

$$A + e^- = A^- \qquad (1.2)$$

Only those molecules which have positive electron affinity form stable negative ions in the gas phase.

The electron affinities of molecules are of interest not only in areas where gas phase negative ions are present, such as, ionosphere[6], electron capture detector for gas chromatography[7-9], radiation chemistry[10], negative ion analytical mass spectrometry[5,13-16]; but also in a much wider field of condensed phase chemistry[17-18]. The vast application of charge transfer complexes in organic, catalytic and biological processes indicates that studies involving charge-transfer complexes represent an active research area where the knowledge of electron affinities are important[19-20]. Many organic reactions in solution are interpreted to be occurring through single electron transfer (SET)[21-23]. The role of electron affinities of large organic molecules and the electron transfer reactions involving them in biological systems have been discussed by Lovelock[7], Rich[24], and Christophrou[25]. For example, quinones are compounds with high electron affinities. They are an integral part of membrane bound mitocondrial, photosynthetic and bacterial electron transport chains[24]. One such chain involves the bc complex, a multiprotein electron transfer device which is found in many respiratory and photosynthetic electron-transfer chains and which is capable of transducing electrical energy into osmotic energy. The recent book by Trumpower[26] provides very informative overview on the importance of quinones in biological energy conserving systems.

Another area in biochemistry where electron transfer is thought to occur is the reaction between carcinogenic hydrocarbons and proteins[7]. It has always been of question which one of them is the electron acceptor. In general, toxic action is known to be due to the ability of some compounds to cause a disturbance in the electron transport by trapping electrons. The trapping of electrons is harmful when it is irreversible. When a dissociative capture occurs, a highly reactive potentially harmful free radical may be formed[7].

The measurement of electron affinities, electron transfer rates etc. will provide information that may help answer many vital questions related to the biological processes involving electron transfer.

In spite of the tremendous significance of electron affinities, reliable electron affinity values are still scarce, especially so for large organic molecules, because such molecules are unaccessible to many methods used in the past for the determination of electron affinities. Very recently Christophorou et al.[27] published an extensive review on the measurements of electron affinities of atoms, radicals and neutral molecules. More than 30 different experimental methods are described and available electron affinities from various theoretical, semiempirical and experimental sources also are given[27]. Unfortunately a critical discussion on the electron affinity values is not provided even though one observes numerous disagreements between the reported values[27] from different methods. In many cases the electron affinity of the same molecule is spread over more than 1.0 eV. The uneven reliability of the methods and the fact that EAs for many important molecules have not been determined necessitates the development of methods for rapid and reliable determination of electron affinities especially for large, complex polyatomic organic molecules.

1.2 Methods Used in the Past for the Determination of Electron Affinities

There are numerous methods, that have been used in the past for the determination of electron affinities of atoms, radicals and molecules. Here only some of them which are relevant to the present investigation will be discussed. The experimental methods can be grouped into two major classes based on whether the determinations were made in gas phase or in the condensed phase.

1.2.1 Methods Based on Electron Affinity Measurements in Gas Phase

The most important gas phase methods are: i) Optical and ii) Chemical methods.

i) Optical Methods

In optical methods the most loosely bound electron from a molecular negative ion is detached by photons, equation (1.3). In photoelectron spectroscopy, PES, one uses a fixed

$$A^- + h\nu \rightarrow A + e^- \qquad (1.3)$$

frequency light source and measures the energy of the ejected electrons. In photodetachment technique, PDS, one varies the frequency of the light source and observes the wavelength dependence of the photodetachment. Since the binding energies of electrons in most negative ions lie in the range of 0.5 - 3.0 eV, the photodetachment techniques of either kind are well suited to the determination of electron affinities, since the intense light sources are available in this energy range. For diatomic[3] and small polyatomic molecules[4] where the photodetachment spectrum can often be completely resolved, one obtains at high resolution, rotational and vibrational spacings from which not only a highly accurate adiabatic electron affinity can be deduced, but also the rotational and vibrational constants, and thus bond distances and bond energies in the negative ion are obtained[3]. The analysis of the photodetachment spectrum of OH^- and OD^- provides an example of such accurate determinations[3]. The transitions between the negative ion and the neutral are governed by the Franck-Condon principle. Thus if there is a substantial geometry change in going from the negative ion to the neutral, the 0-0 transition, corresponding to the adiabatic electron affinity may be too weak to observe. If the observed vibrational structure in the photodetachment spectra cannot be resolved an accurate determination of electron affinity is not possible in such cases. The EA determination is further aggravated, when the negative ion contains internal excitation induced by the method used for its production. In such cases the observed threshold curve often cannot be interpreted and thus an accurate electron affinity determination cannot be made. This problem is reduced to a large extent in ICR photodetachment technique. The ions have the opportunity to lose most of the vibrational excitation energy while trapped in the ICR cell. The review articles by Lineberger et

al.[3] and Brauman et al.[4] provide in-depth information regarding the determination of electron affinities by these powerful optical methods.

ii) Chemical Methods

Three important methods can be included in this subgroup; pulsed electron Capture Detector, PECD Technique ; Atom or Ion Impact Studies and Exothermic Electron Transfer, EET Method.

Pulsed Electron Capture Detector Technique

PECD technique was originally developed by Lovelock[7-8] for use in gas chromatography. Later Wentworth and coworkers[28-34] developed and employed the method towards the determination of electron affinities of polyatomic molecules and radicals. In this technique free electrons are generated from the ionisation of a mixture of gases by high energy β-particles. The secondary electrons formed from the interaction of β-particles with the bath gas (Ar or methane) are readily thermalized as a result of collision with the bath gas. The concentration of electrons is then measured and compared with the electron concentration observed under identical condition after introduction of the reactant. A steady state kinetic model was developed by Wentworth and coworkers[34] which led, in its simplest form, to the equation (1.4).

$$K \propto T^{-3/2} e^{EA/kT} \qquad (1.4)$$

K is defined as the electron capture coefficient, and relates to the electron concentration before and after the sample introduction. The other parameters have their usual significance. Electron affinities are obtained from the plot of $\log KT^{3/2}$ against $1/T$. Electron affinities of some substituted aromatic aldehydes and ketones, naphthalenes and anthracenes[31], small molecules[30] e.g., NO, O_2, CS_2, COS, N_2O; radicals[29] such as NO_2, CH_3COO etc. were determined and a

lower limit for the electron affinity of nitrobenzene, SF_6, and naphthoquinone[30] was provided. However, this method is limited to electron affinity values which are less than 0.8 eV. This limitation makes this method unsuitable for the electron affinity determinations of most biologically and chemically important molecules.

Atom or Ion Impact Studies

In atom impact studies, alkali atoms such as Cs, K, Na and Li and in negative ion impact studies H^-, halides, O^-, S^- etc. are used as projectiles. The former technique is known as collisional ionisation (CI) and the latter is known as endothermic charge transfer (ECT).

In the collisional ionisation method one determines the dependence of the relative cross section for reaction (1.5) on the translational energy of the reactants.

$$A + B \rightarrow A^+ + B^- \qquad (1.5)$$

The electron affinity of B is given by the equation (1.6),

$$EA(B) = IP(A) - E_{th}(B^-) \qquad (1.6)$$

where IP(A) is the ionisation potential of A and $E_{th}(B^-)$ is the threshold energy for the formation of B^-. Helbing and Rothe[35] were the first to employ the alkali atom collisional ionisation technique to determine molecular electron affinities. They used a velocity selected Cs beam to study the translational energy dependence of the reaction: $Cs + Br_2 \rightarrow Cs^+ + Br_2^-$. To produce a Cs beam of known translational energy Cs^+ ions are formed by surface ionisation on a heated filament and are accelerated through a nickel grid. The ions are converted to neutral atoms by charge exchange. The remaining Cs^+ ions are electrostatically deflected. The Cs atom beam is then passed through the velocity selector. The Br_2 beam emerges from an array of

sintered glass capillaries and intersects the Cs beam perpendicularly. The Cs^+ formed by collisions in the crossed beam are accelerated and detected by an electron multiplier. In addition to Rothe[35-39], Lacman et al.[40-41] and Compton and coworkers[42-46] also successfully determined electron affinities of many large molecules by the collisional ionisation technique. Electron affinities of some 30 molecules were determined by this technique.

In the endothermic charge transfer method, a negative ion projectile A^- impacts on a target molecule B and one measures the translational energy threshold to produce B^- via (1.7), in a tendem mass spectrometer which is capable of producing a mass and energy resolved ion beam.

$$A^- + B \rightarrow A + B^- \qquad (1.7)$$

The translational energy of the beam can be controlled over a range from 0.3 to 170.0 eV with a resolution of ± 0.3 eV. The ion beam reacts with neutrals in a field free collision chamber kept at pressures of 5 - 30 mtorr. Product ions emerging from the collision chamber are reaccelerated, mass analyzed and detected with an electron multiplier in the pulsed counting mode.

The electron affinity of B is then given by equation (1.8).

$$EA(B) = EA(A) - E_{th}(B^-) \qquad (1.8)$$

Tiernan and coworkers[47-50] and Rafaey and Franklin[51-55] used this method for the determination of electron affinities.

Both the heavy particle projectile methods outlined above have major shortcomings: (i) only lower limits to EAs are deduced, (ii) the thresholds are sensitive to the target-gas temperature, (iii) in some cases the actual threshold is difficult to determine because of the

nature of cross section, and (iv) in cases where the target molecules form a gas at room temperature, the Doppler broadening caused by the motion of the target molecules can have serious effects on the observed threshold.

Exothermic Electron Transfer Method (EET).

EET method also known as 'kinetic bracketing technique' is one in which the electron affinity is obtained by observing the rates of ion-molecule reaction (1.1) involving electron transfer:

$$A^- + B \rightarrow A + B^- \qquad (1.1)$$

If A^- transfers an electron to B, then the reaction (1.1) is exothermic. Now if B^- transfers an electron to some other molecule C one may conclude that EA(A)<EA(B)<EA(C). Using a series of A and C one can in principle bracket the electron affinity of an unknown molecule or radical B quite closely, provided electron affinities of A and C are known from other techniques.

Fehsenfeld et al.[56-57] measured the exothermic electron transfer rate constants of a few reactions of atmospheric interest, with the help of a flowing afterglow apparatus and the electron affinity of NO_2 is bracketed to be 2.38±0.06 eV. Streit[58-59] recently obtained the electron affinity of SF_4 and SF_6 via kinetic bracketing technique. By examining a series of electron transfer reactions involving SF_4 and SF_4^-, the EA of SF_4 is determined to be 2.35±0.1 eV[58]. Similarly, the electron affinity of SF_6 is determined to be 1.0±0.2 eV[59].

This method while useful, sometimes leads to serious error in electron affinity measurements for some obscure reasons. For example, the electron affinity of SO_2(EA=2.2±0.1 eV) and nitrobenzene (EA=2.1±0.1 eV) obtained via this procedure by Fukuda and McIver[60] is about 1.0 eV higher than the values obtained by many absolute and relative methods[49,51,61-65].

In addition to the three chemical methods discussed above determination of absolute EAs for some typical π-acceptors were carried out also by Page et al.[66-67] using "Magnetron Technique". The determinations in the magnetron technique is complicated, because the reactions take place in the vicinity of a filament and thus at high temperatures and sometimes other ions apart from A^- may be the dominant species in the plasma. Klots et al.[68] evaluated electron affinities of some molecules from the IP and charge transfer energies in solution, EAs of which were determined earlier by the magnetron method, because of the "past notorious unreliability" of the magnetron method. They subsequently established[68] that in cases where A^- is the only ion in the plasma, electron affinities determined by Magnetron method are generally in good agreement with those obtained from other methods.

1.2.2 Methods Based on Electron Affinity Measurements in Solution

Electron affinity determinations were made earlier also in solution phase. Two different techniques have been employed mainly. They are: measurements of (i) absoption energy of π-charge transfer complexes, and (ii) polarographic half wave reduction potential.

(i) Spectroscopic Measurements of Charge Transfer Energies.

A charge transfer complex is a partial or complete transfer of an electron in solution from one component (donor D) with high ionisation potential to the other (acceptor A) with high electron affinity. When a charge transfer complex is formed, a new characteristic absorption band in the visible or ultraviolet region is observed. The relation[19,20] between the energy corresponding to charge transfer absorption band, the vertical ionisation potential I_D of the donor D and the vertical electron affinity, EA_A of the acceptor A is given by equation (1.9).

$$E_{CT} = I_D - (EA_A + G_1 \cdot G_0) + (\beta_0^2 + \beta_1^2)/[I_D - (EA_A + G_1 \cdot G_0)] \quad (1.9)$$

Where G_0 and G_1 are respectively, sums of several terms of interaction energies between donors and acceptors in the ground DA state and in the excited D^+A^- state. The terms β_0 and β_1 are matrix elements for the resonance interaction between D,A and D^+,A^-. For a series of donor-acceptor complexes of the same bond type, G_0-G_1 is essentially constant and may be represented as C and $(\beta_0^2 + \beta_1^2)$ is also a constant but very small, thus equation (1.9) reduces to equation (1.10).

$$h\nu_{CT} = I_D - EA_A + C \qquad (1.10)$$

Thus, using a donor of known ionisation potential I_D the electron affinity of an unknown molecule A, can be determined from the experimental determination of charge transfer absorption energy $h\nu_{CT}$ through equation (1.10), provided the value of C is known. In order to obtain the value of C, one measures the frequency ν_{CT} for the charge transfer maximum absorption band of a fixed donor with a series of molecules of known electron affinities as acceptors. Then from the plot of $h\nu_{CT}$ versus EA_A a constant value for I_D+C could be obtained from the intercept. For details about the determination of EA from E_{CT} see the article by Foster[19].

(ii) Polarographic Half Wave Reduction Potential Measurements

Electron affinity can be obtained by reducing a substance A on a dropping mercury electrode[17] in a medium of low proton activity to avoid rapid protonation of the primary product A^-. The potential determining step in the polarographic reduction of a compound has been assumed to be the reversible addition of an electron to the neutral molecule A. The diffusion coefficients of the parent molecule and the radical anion are assumed to be identical.

The following sequence of reactions could be considered:

$$A(gas) + e^- = A^-(gas) \qquad -\Delta E_0 = EA$$

$A^-(gas) + A(solution) = A(gas) + A^-(solution)$ $\quad \Delta G_{solv}$

$e^-(in\ Hg) = e^-(gas)$ $\quad \phi_{Hg} = -4.54$ eV

$Hg(liq) + Cl^-(1N,aq) = 1/2Hg_2Cl_2 + e^-(Hg)$ $\quad E^o$(satu. calomel electrode)

$Cl^-(satu.\ Hg_2Cl_2) = Cl^-(1N,aq)$

The absolute potential of a saturated calomel electrode is calculated to be -0.50 V[17]. Thus one deduces equation (1.11) from the above sequence of reactions.

$$E_{1/2} = EA - \Delta G_{solv} - 5.07\ eV \qquad (1.11)$$

Chen and Wentworth[29] deduced electron affinities of a large number of molecules from the half wave reduction potential values obtained from the literature.

The main problem associated with the methods for the determination of electron affinities in solution is that the changes in solvation energy $\Delta G_s^0 = \Delta G_s^0(A^-) - \Delta G_s^0(A)$ are not well known. Thus a constant value for ΔG_s^0 is assumed[29] to deduce electron affinities from $E_{1/2}$ and E_{CT} values. In fact as will be shown in chapters 4 and 6 later, the solvation free energy change is not a constant but is a quantity which depends on the extent to which the negative charge in the radical anion is delocalized. Thus the EA values deduced from the results obtained from solution based techniques are not the true "electron affinities" and are affected by the solvation energy.

1.3 Formation of Negative ions in Gas Phase: Electron Capture in the Absence of Third Body Collision.

An electron is said to be attached if it is "temporarily" held up for a time at least greater than its normal "transit time" across the molecule and the electron molecule system is known as a "resonance". Mandl[70] classified such resonances as: (i) shape resonances, (ii) electronically excited Feshbach resonances, and (iii) Nuclear excited Feshbach resonances. In the

case of a shape resonance, the electron molecule interaction potential possesses a centrifugal barrier built in by the orbital angular momentum of the colliding particles. The electron is then temporarily held up at the potential well exists due to the barrier. Shape resonances usually lie at low (0 to ~4 eV) energies and have life times, τ ranging from $\sim 10^{-15}$ to $\geq 10^{-10}$ s. A shape resonance lies above the neutral-molecule potential energy curve i.e., the electron affinity is negative and it decays back into the target plus a free electron.

In electron excited Feshbach resonances, the incident electron is captured with the simultaneous excitation of one of the electrons of the target molecule i.e., these resonances arise when the interaction potential between the excited target molecule and the incident electron is strong enough to support a bound state, which lies below the parent state and decays via autodetachment or if energetically permitted via dissociative attachment (1.12). When

$$XY + e^- \rightarrow X^- + Y \qquad (1.12)$$

decaying into the parent state is not energetically possible such resonances have long life time, τ because decaying into nonparent states when possible involves changes in configuration and therefore is not fast.

Nuclear excited Feshbach resonances are similar to electron excited Feshbach resonances in that the negative ion-state lies below the parent ground state exhibiting a positive electron affinity. In nuclear excited Feshbach resonances the loss of energy by the captured electron goes solely to the vibrational modes of the molecule.

In large polyatomic structures, other modes of electron trapping are possible, such as, geometrical changes accompanying the collision and capture processes connected with the specific portion of the molecule. There is little known about them at the present time.

Thus, an electron of energy E_e when attached to a molecule forms a molecular ion with total energy E^* according to equation (1.13).

$$e(E_e) + A(E) \underset{\tau(E^*)}{\overset{\sigma(E_e)}{\rightleftharpoons}} A^-(E^*) \qquad (1.13)$$

The width of the attachment resonance, Γ is related to the life time through the uncertainty principle $\tau.\Gamma \simeq h$.

The cross section σ is related to the life time through the principle of detailed balance, equation (1.14).

$$\sigma(E_e)\tau(E^*) = \rho^-(E^*)/v\rho^0(E) \qquad (1.14)$$

Where v is the velocity of the electron and ρ^- and ρ^0 designate the density of states of the negative ion and the neutral molecule respectively. The life time of the ion against autodetachment, τ is a function of the total internal energy E^* which is the sum of the incident electron energy, E_e and the electron affinity EA of the molecule A.

When a complex molecule attaches a slow electron, the the total energy E^* is shared among the various degrees of freedom of the ion. Inspection of equation (1.14) shows that if $\rho^-(E^*)$ is large the life time and the cross section can be large. For negative ions with life times greater than 1.0 μs, it is possible to study these resonances directly (for review see refs. 1 and 25) and their their life times as a function of E^*.

Depending on the magnitude of τ, three classes of negative ions have been distinguished[25].

i) Extremely short lived ($10^{-15} < \tau \leq 10^{-12}$ s): these are observed as resonances in electron scattering and/or in dissociative attachment studies.

ii) Moderately short lived ($10^{-12} < \tau \leq 10^{-6}$ s) : these can be stablized in high (1 to 1000 torr) and very high (>1000 torr) pressure swarm experiments.

iii) Long lived ($\tau > 10^{-6}$ s): these can be observed and studied in conventional mass spectrometers, after subsequent stabilization by third body collision.

1.4 Electron Transfer Reactions in Gas Phase: Measurements of Kinetics and Equilibria.

The concept of electron transfer (ET) is very familiar to any one interested in the chemistry of life processes. The major life-sustaining process on this planet is critically dependent on ET reactions[71]: Photosynthesis, in which the primary photon capture gives rise to chlorophyll excited state, is followed by a series of extremely fast ET steps and the released electron becomes available for chemical work. Dioxygen metabolism is another important biological process in which the superoxide ion (O_2^-), a one electron reduced species, is a ubiquitious component of all aerobic systems[71].

Single electron transfer reaction in solution from alkali metals to unsaturated organic compounds has been of synthetic importance for many years (e. g., Bouveault-Blanc and Zinc reductions, Birch reductions, Acyloin condensation etc.)[72-73]. The recognition that ET can also occur readily from organic nucleophiles Nu^- is of more recent [74].

Occurrence of electron transfer reaction in solution involving simple systems like, Fe(II) and Fe(III), Ce(III) and Ce(IV) etc. was demonstrated in the early fifties. In fact, electron transfer reactions involving biological systems have been one of the most active persuits to the present. The recent review article by Eberson[71] provides a large number of recent reviews involving electron transfer reactions in solution in different areas of chemistry and biochemistry. Marcus theory[21,75] has been successful in explaining features of electron transfer reactions in solution in terms of two mechanisms: the inner-sphere transfer mechanism involving a bridging ligand or molecule and the outer-sphere transfer mechanism, involving reorganisation of solvent molecules after electron transfer.

The subject of gas phase electron transfer reactions is also an old one. As early as 1959, Henglein et al.[76] recognized that electron transfer froma negative ion to the neutral in the gas phase is fast when exothermic. However, the subsequent development was quite slow. Only few literature references involving electron transfer reactions from negative ions in gas phase were available until recently. Ferguson and coworkers reported[56-57] the measurement of kinetics of electron transfer reactions involving O^-, O_2^-, O_3^-, CO_3^-, Cl_2^-, SH^-, NO_2^- etc. Grabowski et al.[64] determined the rate constants of ET reactions involving SO_2 and SO_2^- with the help of flowing

afterglow apparatus (FAG) and selected ion flow tube (SIFT). As mentioned earlier Streit[58-59] recently reported the kinetics of ET reactions of SF_4 and SF_6 and their negative ions.

If the rates of electron transfer reactions (1.1) in the forward and reverse direction can be made fast compared to the observed time scale by selecting appropriate conditions, the ET equilibria can be obtained and the equilibrium constant K_1 can be determined. The measurement of electron transfer equilibria involving negative ions is a new field. Fukuda and McIver[77-80] were the first to demonstrate that the ET equilibria (1.1) can be measured for compounds whose negative ions A^- and B^- can be generated in a mass spectrometer source by thermal electron capture. They[77-80] used pulsed ICR technique to measure ET equilibria (1.1). Later Caldwell and Kebarle[63] also showed that the ET equilibria (1.1) can also be measured with the help of a pulsed electron high ion source pressure mass spectrometer (HPMS). Once the equilibrium constant is determined the evaluation of thermochemical data follows established procedure.[5,13-16]

Measurement of the relative concentrations of A^- and B^- at equilibrium together with the concentration of the neutral species A and B leads to the evaluation of the equilibrium constant K_1 and the free energy change ΔG_1^0 via reactions (1.15) and (1.16).

$$K_1 = \{[B^-][A]\}/\{[B][A^-]\} \tag{1.15}$$

$$- RT\ln K_1 = \Delta G_1^0 \tag{1.16}$$

Determination of K_1 at different temperatures leads to ΔS_1^0 and ΔH_1^0 via van't Hoff plots. Therefore, relative electron affinities of A and B are obtained through equations (1.17) and (1.18).

$$\Delta G_1^0 = \Delta H_1^0 - T\Delta S_1^0 \tag{1.17}$$

$$\Delta H_1^0 = EA(A) - EA(B) \tag{1.18}$$

From the measurements of equilibria (1.1) at different temperatures involving many different compounds of varying electron affinities one can construct ladders of ΔH_1^0 and ΔS_1^0. The absolute electron affinities of all compounds which are part of the continuous enthalpy change ladder can be obtained by anchoring the above results to the precisely determined thermochemical quantities for electron attachment to a standard molecule, whose electron affinity is well stablished in the literature. We chose in the present study the electron attachment energy ΔH_a^0, equation (1.2), of SO_2 as such a standard obtained from the electron photodetachment threshold measurement due to Hall[61].

$$A + e^- \rightarrow A^- \qquad (1.2)$$

The selection of SO_2 as a standard is justified by the fact that there are five other gas phase experimental determinations of the electron affinity of SO_2 by different physical methods[49,51,62,64-65] which are within ± 0.1 eV to the $EA(SO_2) = 1.1 \pm 0.1$ eV provided by Hall[61].

The entropy changes $\Delta S_a^0(A)$ were also obtained in the present study from the ΔS_1^0 ladder by calibrating the ladder with the entropy change for electron attachment to SO_2. The entropy change for electron attachment to sulfur dioxide molecule is evaluated from the known geometries and vibrational frequencies of SO_2 and SO_2^-. A stationary electron convention was used, in which the translational thermal energy of the electron is neglected. The calculation of enthalpy, entropy and free energy changes on electron attachment to SO_2 and thus the determinations for other molecules A and B from the various thermochemical ladders will be discussed in chapter 4, which deals with the results and discussions of EA measurements.

As mentioned earlier Fukuda and McIver[77-80] reported measurements of relative electron affinities via electron transfer equilibria measurements obtained with the help of a pulsed ICR spectrometer. No temperature dependence of the electron transfer equilibria (1.1) is obtained[77-80] and thus relative electron affinity values provided are only in terms of free

energy change ΔG_1^0. They did not anchor their ΔG_1^0 scale with the literature electron affinity of a standard and therefore, no absolute electron affinity value was obtained. Their attempt, to obtain absolute electron affinity for SO_2 and nitrobenzene[60]; benzophenone, hexafluorobenzene, naphthoquinone, benzoquinone, etc.[77] by kinetically bracketing with the known electron affinities of $(CH_3)_3CO$ and CH_3O radicals led to erroneous results. In the result section, chapter 4, a comparison with the Fukuda's relative electron affinity results[77-80] from equilibria measurements with those from the present investigation are provided.

1.5 Conditions and Apparatus for the Measurements of ET Kinetics and Equilibria.

Rate constants of exothermic electron transfer reactions were measured by flowing afterglow apparatus by Ferguson et al.[56-57], Streit[58-59], and Grabowski et al.[64], while rate constants and equilibria measurements in the present investigation are made with the help of a pulsed high pressure mass spectrometer. McIver et al.[60,77-80] did not report any determination of ET rate constants, but their equilibria measurements were performed with the help of a pulsed ICR spectrometer.

The following criteria must be met for thermal ion-molecule equilibria measurements: i) The reactants and products must be in thermal equilibrium with the surroundings. Excess energies present in the reactants and products must be removed prior to the achievement of the equilibrium. ii) Sufficient residence time must be allowed for the system to reach equilibrium and finally, iii) the rates of forward and reverse reactions of equilibria (1.1) must be faster than other competitive reactions, if any, involving the reactants and products participating in equilibria (1.1).

1.5.1 The Pulsed High Pressure Mass Spectrometry (HPMS)

This is the technique used in the present study. A brief description of the method follows. A detailed description of the apparatus and the experimental procedures will be given in the following chapter. The pulsed high pressure mass spectrometer, used in the present study

consists of a temperature controlled (-190° to 650°C) reaction chamber in which a suitable reaction mixture at 2.0 to 10.0 torr total pressure is irradiated by short electron pulses, generally 5-20 μs. The ions created by a given electron pulse react and reach equilibrium as they diffuse towards the walls of the ion source. Ions diffusing to the vicinity of a very narrow slit (3 x 0.01 mm) are carried by gas flow into an evacuated region pumped by a high capacity pumping system. Scheme 1.1 describes the sequence of reactions which occur in a typical electron transfer reaction after a short electron pulse.

Scheme 1.1

$$CH_4 + e\ (2\ kv) \rightarrow CH^+_4,\ CH^+_3,\ \text{.....etc.} + 2e$$

$$A + e = [A^-]^* \xrightarrow{[M]} A^- + M^*$$

$$B + e = [B^-]^* \xrightarrow{[M]} B^- + M^*$$

$$A^- + B = A + B^-$$

$$A^-,\ B^- \rightarrow \text{Diffuse to the walls.}$$

Each ion undergoes several thousand collisions, while diffusing in the field free ion source. After they enter the high vacuum region through the narrow slit, they are accelerated by a weak electric field, mass analyzed and detected by an electron multiplier. The electron multiplier is coupled to a time resolved multiscalar where the observed ion intensities are stored. The multiscalar is synchronized with the start of the electron pulse.

The criteria established for the measurements, at a given temperature, were the followings: i) the equilibrium constant K_1 should be independent of the ratio of the concentrations of the neutral reactants, A and B over a reasonable range (1 to 10) at a constant

carrier gas pressure; ii) in a mixture of fixed concentration ratio of A and B, K_1 should be independent of the bath gas pressure over at least a factor of 3; and iii) in a given measurement the reactant and product concentration ratio from which K_1 was derived (see equation (1.15)), should be constant for a sufficient period of time (a few tens of minutes) to ensure that flow of a constant neutral concentration ratio exists throughout. These criteria were satisfied for all measurements including those at different temperatures for van't Hoff plots in the present investigation.

1.5.2 Pulsed Ion Cyclotron Resonance Spectrometry (ICR)

The pulsed, trapped ion ICR spectrometer used for the study of ET equilibria[78] was developed by McIver[81] for the determination of rate constants and long reaction sequences. The introduction of electron pulsing and ion trapping makes the mode of operation of pulsed, trapped ion ICR spectrometer different from the conventional ICR spectrometers[82].

The ions are produced in a rectangular cell (1x1x3.5 inch) by a short (~0.1 ms) electron pulse. The gas pressure is typically 10^{-6} torr. The ions are trapped by the magnetic field H (~13,000G) in the z direction, and in the x and y directions by small static voltages (~1 V) applied to the side plates of the cell. The ions then travel in circle in the x-y plane with a frequency $\omega_c=(qH)/(mc)$, where m and q are mass and charge. ω_c is known as cyclotron frequency. It is believed that[78] at the operating pressure ions suffer ~100 ion neutral collisions while trapped in the cell, which are considered to be sufficient for thermalization of ions to the temperature of the neutrals. The relative abundances of A and B are measured with a capacitance bridge detector.

To check if the electron-transfer is fast compared to the time scale of the experiment, ~1 s, double resonance experiments could be performed[60,77-80] by scanning the magnetic field across the resonance for an ion, first with double resonance rf turned off and then turned on. For an exothermic ET reaction, the product ion signal height was observed to decrease when the reactant ion was ejected from the cell, which confirms that the reactant ion produces the product. Similarly a check can be made for the reactant ion by ejecting the product ion.

1.5.3 The Flowing Afterglow Method (FAG)

The flowing afterglow apparatus used for the study of electron transfer reactions was developed by Ferguson and Fehsenfeld[83]. The carrier gas, most commonly He (~0.5 torr), passes with very high velocity ($v \approx 10^4$ cm/s) through the reactor tube, which is 8 cm in diameter and 1 m long. The ions are created from electron impact obtained from a heated filament mounted upstream in the tube. The neutral reactant gases are added through one or more nozzles downstream of the filament. The ions are sampled at some distance d downstream of the neutral reactant inlet, by bleeding a small part of the gas through a small orifice into a evacuated region. The ions are then mass analyzed by a quadrupole mass filter mounted in the evacuated region. The reaction time (~ms) $t=d/v$ remains constant in rate constant and equilibrium runs. The effective reaction time is obtained by integration over the flow profile, since the linear velocity at a given cross section of the tube is not constant, but is a function of the radius. This technique is well suited for rate constant measurements.

A drawback common to HPMS and FAG systems is that ion intensities are determined by bleeding gas from the ion-chamber through a sampling leak into mass analyzer located in the vacuum. Cluster break-up in the region immediately past the sampling leak could cause a serious ion-sample adulteration[84]. Collision of clusters with neutral molecules in the electric field of acceleration could cause decomposition of clusters and this breakdown of clusters outside the ion-source could lead to ion abundances different from the true equilibrium ion intensities present in the source. In contrast the ICR spectrometer has the unique advantage of detecting the ion concentrations *in situ* and does not depend on the sampling leak. Because of efficient ion trapping in an ICR spectrometer, equilibrium can be observed for second order reactions, even though the pressures of the reactants may be as low as 10^{-6} torr.

2. EXPERIMENTAL

2.1 General

The pulsed electron beam high ion-source pressure mass spectrometer, HPMS used in the present investigations, differs significantly from a conventional mass spectrometer, and is discussed in greater details elsewhere[85-87]. Only a brief description of the apparatus will be given in this chapter. Unlike in a conventional mass spectrometer, to obtain most reliable and reproducible kinetics and equilibria of ion neutral reactions such as reaction (1.1), the following conditions must be met in a HPMS: (i) the temperature of the ion-source must be known accurately and should be uniform for a prolonged period. In order to avoid getting the ion-source heated by the filament, the filament in the present instrument was mounted 30 cm away from the source and electrons are accelerated with high velocity (2 kV) to ensure the penetration of the electrons into the source which is at high pressure (3-8 torr); (ii) pressure in the ion-source should be known quite accurately; (iii) high capacity pumping system is required, because the analyzer needs high vacuum to be operated and also at that pressure the mean free path of the ions should be greater than the dimension of the apparatus.

2.2 The Apparatus: High Pressure Mass Spectrometer

Shown in Figure 2.1 is a simplified diagram of the ion chamber and in Figure 2.2 is a detailed description of the essential components: the electron gun, the ion-source, and the ion accelerating tower. The electrons emitted from the filament [1] passed through the small hole at the center of the drawout electrode [2] and were accelerated, focused and deflected by subsequent electrodes [3-8]. The electrons then passed through a shielding cylinder [9] and entered the ion-source through a narrow slit.

The ion-source is a cylindrical chamber, with inside diameter of 1/2 inch. The electron entrance slit [12] was located in one side of the ion-source towards the electron gun and the

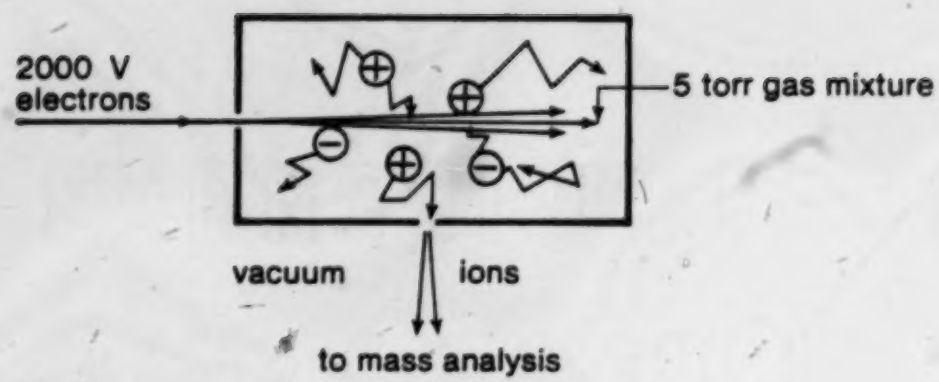

Figure 2.1. Ion trapping at high pressure. Ions generated by electron impact at high pressures (~5.0 torr) experience many thousands of collisions before reaching the wall or the exit slit. This results in collision quenching to thermal levels and achievement of reactive ion-molecule equilibria.

Figure 2.2

A. **Electron Gun**

1. Filament
2. Draw out
3. Extractor
4. First focussing and accelerating electrode
5. Second focussing and accelerating electrode
6. Third focussing and accelerating electrode
7. Horizontal deflection half plates
8. Vertical deflection half plates
9. Shielding cylinder

B. **Ion Source**

10. Copper jacket
11. Electrostatic shield
12. Electron entrance slit flange
13. Electron trap flange
14. Ion exit slit cone
15. Gas inlet
16. Kovar seal flange
17. Stainless steel support
18. Ceramic spacer

C. **Ion Acceleration Tower**

19. First cone
20. Second cone
21. Cylinder entrance
22. First cylinder
23. Second cylinder
24. Cylinder exit
25. First deflection half plate
25a. Second deflection half plate
26. Mass analysis slit
27. Mass analyzer tube

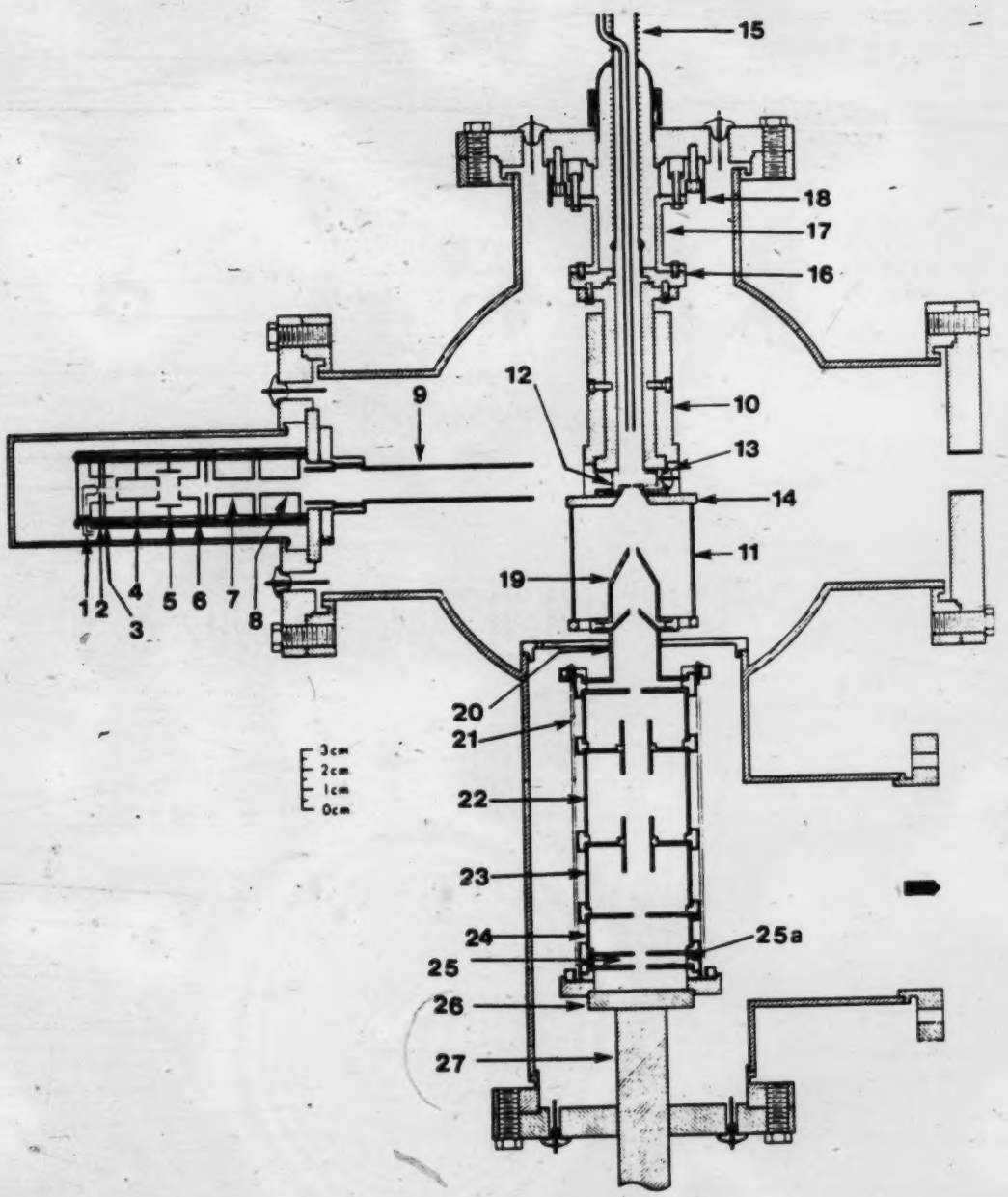

Figure 2.2. Main components of the electron beam mass spectrometer: ion source, elecron gun, and ion accelerating tower.

electron trap flange [13] on the other side. The ion exit slit [14] was located towards the ion acceleration tower. Both the electron entrance and ion exit slits were of 2 mm long and 0.015 mm wide and are made by spot welding razor blades. The ion-source is enclosed in a heating jacket [10] and the heater voltage and the temperature is controlled by manual setting of the heater voltage. The gas entered the ion source through the outer of the two concentric tubes [15] and left the ion-source through the inner tubing. The entire ion-source assembly was mounted on a cylindrical stainless steel support [17]. A thermocouple was embeded deep in the ion-source block, close to the inner wall of the source. This thermocouple was used for the measurement of ion-source temperature.

The ion accelerating tower is also shown in Figure 2.2. Ions diffusing out of the ion exit slit [14] of the ion-source were accelerated and focused on the mass analyzer entrance slit by ion accelerating tower. A stepwise acceleration of the ions was carried out by the successive electrodes [19-25a] of the ion accelerating tower.

After acceleration, the ions were magnetically mass analyzed in a 90°, 15 cm radius tube. Differential pumping was applied to the analyzer tube and thus the pressure in the tube was about 10 times lower than that of the main vacuum chamber. Mass scanning was obtained by changing the magnetic field at a constant accelerating voltage.

After mass analysis the ion current was detected by a channeltron electron multiplier (CEM 4700). The output pulses from the multiplier were then passed through a discriminator to eliminate low level noise. The output pulses from the multiplier were amplified further by an amplifier (Quard Amplifier AN201/N) before being counted. The pulses then were counted with an Ortec Model 441 rate meter and a multichannel scalar, LeCroy 3500 micro computer. The sweep of the multichannel scalar (mcs) was synchronized with the triggering pulse of the electron gun as shown in Figure 2.3. In a typical experiment, the dwell time per channel of the multichannel scalar was set at 4 μs and 512 channels were used. The number of ions arriving at the detector in the first 4 μs after the triggering pulse, was stored in the first channel. The number of ions which arrived from 5-8 μs was stored in the second channel and so on for 512 channels. In this way the change in ion intensity was followed for ~2.0 ms. The whole process

FIGURE 2.3 Pulsing Sequence with Typical Voltage and Durations.

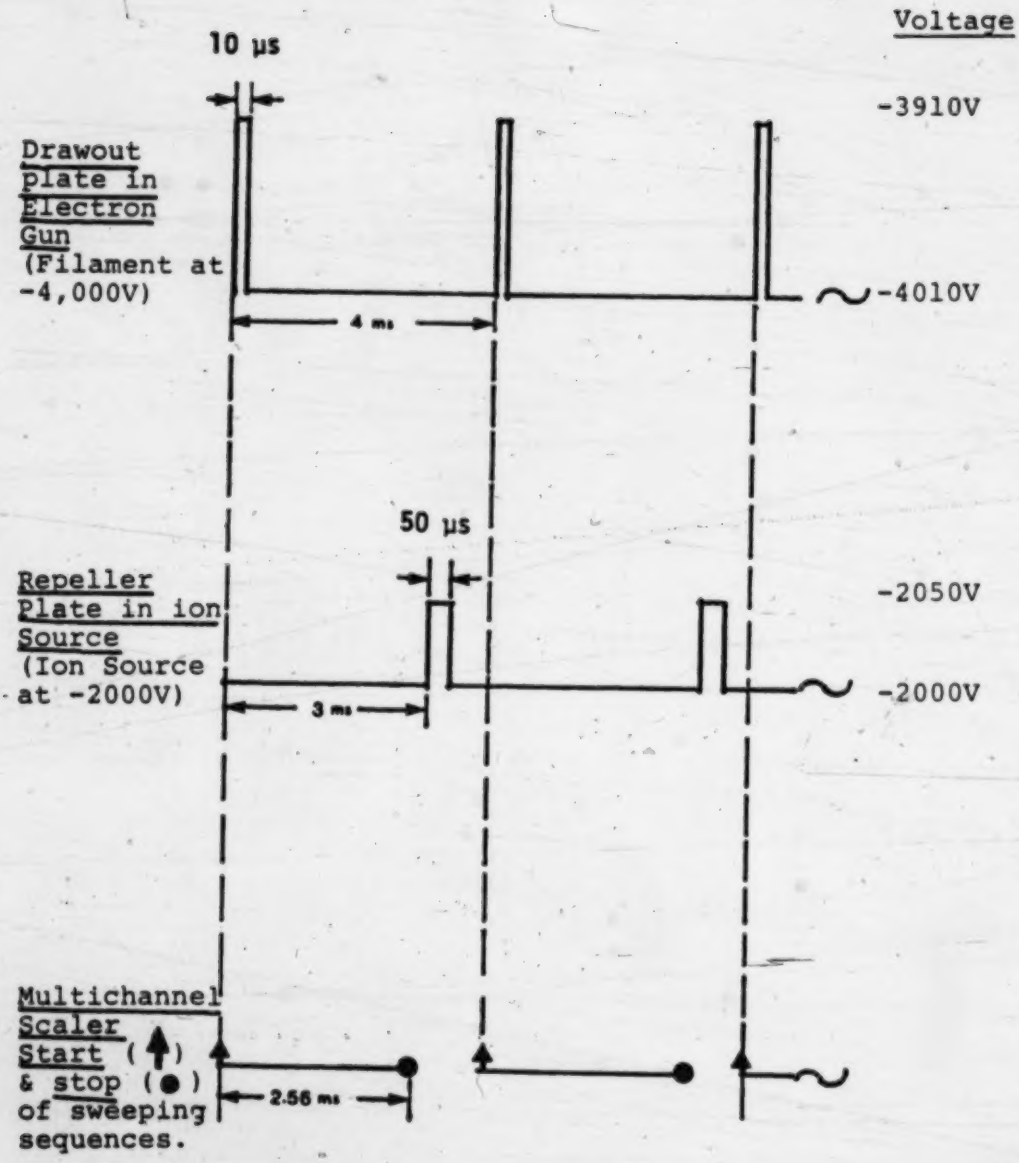

was repeated with another pulse from the electron gun. Generally data of 10,000 scans (pulses) were accumulated for each ion.

The intensities of ions accumulated in various channels could be displayed on the screen of the LeCroy computer and the intensities or the average ratios of intensities of ions displayed for any range of time were obtained directly from the computer.

2.3 Chemicals

The chemicals used in the present investigation are all of highest purity obtained from commercial suppliers. No further purification was done. Impurities which affect the measurements are detected by the observation of the negative ions that are formed due to their presence. In general, only serious difficulty with impurities occurred when measurements with a compound B were performed which contained an impurity isomer B' of higher electron affinity. This may lead to an apparent EA value higher than the true value. For this to happen the impurity has to be more than 10%. However, in no case, the impurity level was detected to be higher than 10%. The presence of lesser amounts could be detected by a very slow approach to the (false) $([B^-] + [B'^-])/[A^-]$ equilibrium in the intensity time plot, because of the low concentration of B'.

3. KINETICS OF ELECTRON TRANSFER REACTIONS

3.1 Introduction

By proper selection of the composition of the reaction mixtures, either the equilibrium constant K_1 or the rate constant k_1 of the electron transfer reaction (1.1) could be determined. In the present investigation rate constants for 77 ET-reactions involving some 35 molecules were studied. The compounds whose electron transfer reactions studied were SO_2, NO_2, substituted benzenes, azulene, substituted naphthalenes, some quinones, cyanoethylenes, perflourobenzenes, SF_6 and perfluorocycloalkanes. The electron transfer reaction involving the above group of compounds were of two different types, from the point of view of the rate of reactions. The majority of the reactions when exothermic, were observed to proceed with rate constants which were near Langevin-ADO collision limit, $k_1 \simeq 10^{-9}$ cc/(molecule.s). There were a few important exceptions, however. When SF_6 and the perfluo- alkanes and cycloalkanes, like perfluorocyclohexane C_6F_{12} and perfluomethylcyclohexane $CF_3C_6F_{11}$, were used k_1 was found to be very small, often less than 10^{-13} cc/(molecule.s). Measurements and discussions of all of these electron transfer rate constants are as follows.

3.2 Well Behaved and Fast Reactions

3.2.1 Measurements and Results

Figure 3.1(a) demonstrates a situation where B(3-CF_3nitrobenzene) has an electron affinity which is 3.1 kcal/mol higher than A(2-Clnitrobenzene). The neutral concentration ratio [A]/[B] = 14.3 was chosen to offset the advantage of the higher EA of B, which promotes higher B^-_{eq} intensity. The ions appear after about 0.1 ms delay. The ratio of $[B^-]/[A^-]$ which in

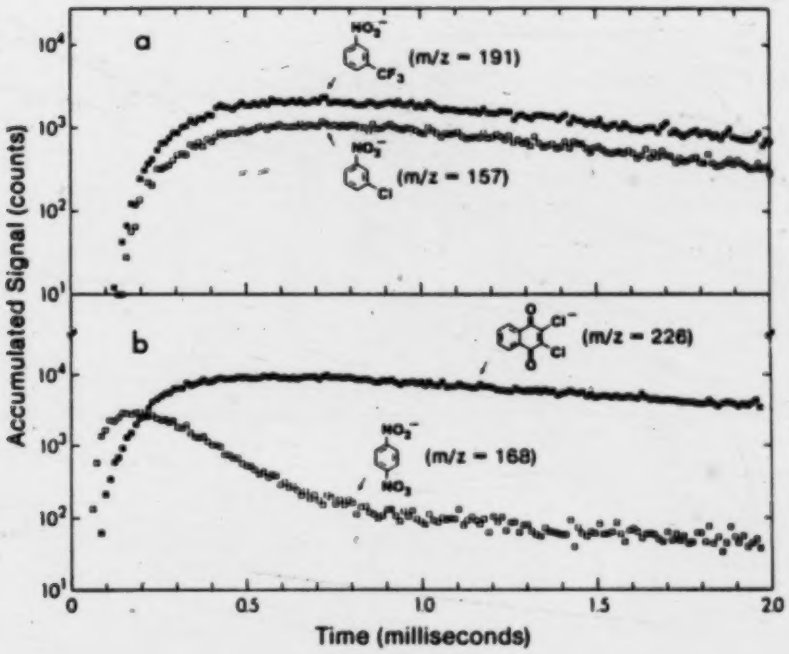

Figure 3.1. Log of ion intensities as a function of time after a 10μs electron pluse, at ion source temperature 423K. (a); ions have reached equilibrium (1.1) already at onset of ion signal. Constant $[B^-]/[A^-]$ ratio corresponds to constant vertical distance between A^- and B^-; 3.5 torr of methane, 0.53 mtorr of 3-CF_3NB and 7.6 mtorr of 3-ClNB. NB = nitrobenzene. (b); equilibrium (1.1) is reached after ~0.9 ms; 2.8 torr of methane, 0.54 mtorr of 4-NO_2NB, 0.49 mtorr of 2,3-dichloronaphthoquinone.

the log plot used, is given by the vertical distance between the two ion intensity curves is observed to be essentially constant from the very onset of the ions. This means that the equilibrium (1.1) was achieved already within the short 0.1 ms time before the ions started emerging from the ion-source. It could also be possible that the electron transfer reaction (1.1) involving those two compounds shown in Figure 3.1(a) is slow, such that no reactive change whatever is occurring within the ~2.0 ms observation time, and the constant ratio of the ion intensities could be due to the very similar diffusion coefficients of A^- and B^-, since ion diffusion to the walls of the ion source is the main ion loss mechanism.

However, a definite proof of the reactive changes in the ion intensities due to electron transfer reaction (1.1) is shown in Figure 3.1(b). The 1,4-dinitrobenzene has 4.4 kcal/mol lower electron affinity than the dichloronaphthoquinone, since the neutral concentrations were nearly equal, the 1,4-dinitrobenzene negative ion intensity is seen to decrease for some 0.7 ms and after that time log intensities of the ions became equidistant. The results in Figure 3.1(b) thus show the kinetics of the approach to the equilibrium and the constant concentration ratio of ions after the equilibrium was achieved. The slope of the initial linear portion of the dinitrobenzene intensity curve in Figure 3.1(b) could be used to obtain an approximate rate constant for the electron transfer from 1,4-dinitrobenzene negative ion to 2,3-dicholoronaphthoquinone.

More accurate rate constants were obtained for reactions when longer linear sections for the A^- decay were available. This particular condition was achieved when EA(B) is much higher than the EA(A), such that, A^- disappears essentially completely. An example of such a run is shown in Figure 3.2(a) where the log[A^-] has a long linear section. The slope of this section when converted to the natural logarithm by multiplying with 2.303, equals ν_1(obs), the observed pseudo-first-order rate constant for A^- disappearance. This is given by equation (3.1), where ν_{d,A^-} is the first order rate constant for loss of A^- by diffusion to the walls.

$$\nu_1(\text{obs}) = k_1 [B] + \nu_{d,A^-} \qquad (3.1)$$

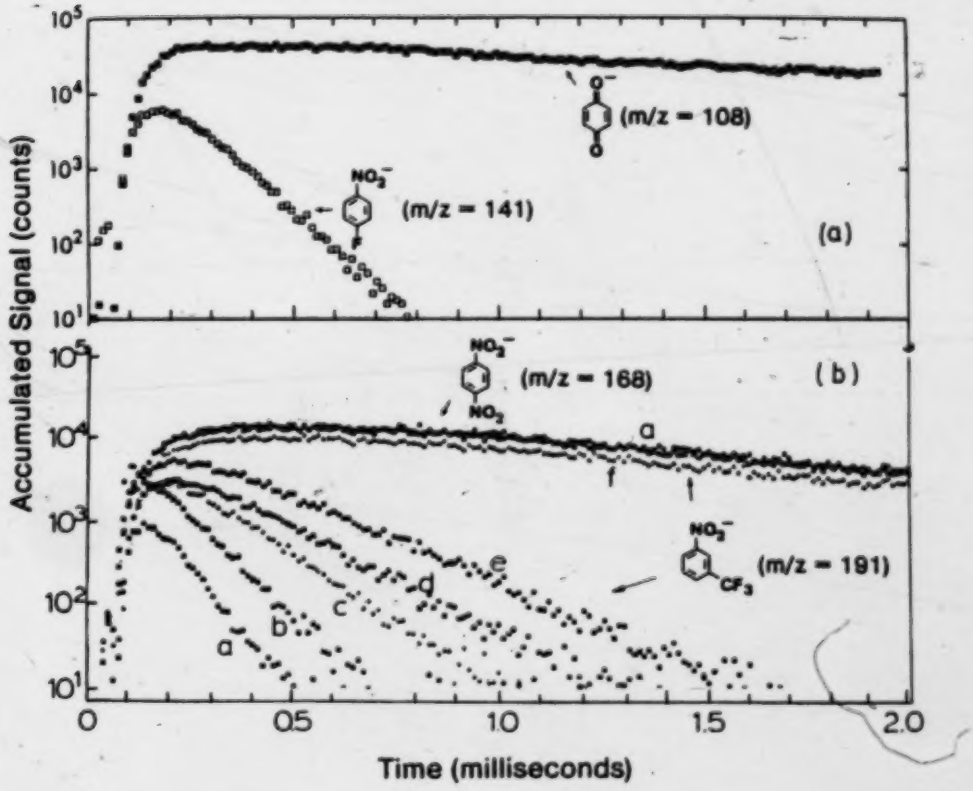

Figure 3.2. (a) Concentration changes due to electron transfer from 4-FNB anion to benzoquinone (BQ); methane, 4.0 torr; 4-FNB , 2.0 mtorr and BQ, 0.3 mtorr. (b) Electron transfer from 3-CF_3NB^- to 4-NO_2NB. The slopes of the linear portion of decaying 3-CF_3NB^- = ν_1(obs) are used for determination of rate constant k_1 (see Figure 3.3); 3-CF_3NB, 15.0 mtorr; methane, 4.0 torr; 4-NO_2NB at different pressures are: a, 0.5; b, 0.33; c, 0.25; d, 0.167; e, 0.116; f, 0.0 mtorr. T = 423K. Accumulated signal for 4-NO_2NB^- is almost identical for cases a-f, so only case a is shown.

Choosing different [B] in a series of experiments at constant T, a series of slopes ν_1(obs) were obtained as shown in Figure 3.2(a). The slopes ν_1(obs) obtained from this series were plotted against the known [B] in Figure 3.3. The straight line obtained has a slope which is equal to k_1 and intercept ν_{d,A^-}, according to equation (3.1). Equation (3.1) and Figure 3.3 show that when concentration of B is large ν_{d,A^-} is very much smaller than k_1 [B]. Under such conditions quite accurate rate constants k_1 can be obtained by determining ν_1(obs) at a given large [B]. Then assuming $\nu_{d,A^-} \simeq \nu_{d,B^-}$, k_1 can be evaluated from equation (3.1). The diffusion rate constants ν_{d,B^-} were obtained from the constant slope of ln[B^-] at long reaction times (see Figure 3.2). In fact, the very similar slopes of A^- for [B]=0, and B^- at long reaction times (shown in Figure 3.2) were obtained, which indicate that the two diffusion rate constants are similar. The majority of the experimental rate constants k_1 given in Tables 3.1 to 3.5 were obtained mostly with this second faster procedure. However, in all cases at least three different B concentrations were used to check the consistency of the evaluated k_1.

For low exothermicities, where the system rapidly approached equilibrium, the rate constants were obtained by computer fitting the observed time dependence to the theoretical (pseudo)first order reversible rate expressions. The assumption of equal diffusion loss rates for both ions was made. An example of ion intensities in such a determination is shown in Figure 3.4.

3.2.2 Discussion of the Results of Kinetics of Electron Transfer Reactions

The measured k_1(exp) were compared with the average dipole orientation, ADO-theory[88] predicted collision rate constsants k_1(ADO) also given in Tables 3.1, 3.2, 3.4 and 3.5. The ADO-theory predicted collision rate constant is given by[88] equation (3.2).

$$k_{ADO} = (2\pi q/\mu^{1/2})[\, \alpha^{1/2} + c\mu_D\, (2/\pi kT)^{1/2}\,] \qquad (3.2)$$

Table 3.1 Rate constants, k_1, for exothermic electron transfer reactions $A^- + B \rightarrow A + B^-$ involving NO_2.[a]

	A[b]	B[c]	$-\Delta H_1^0$	$k_1(exp)x10^{10}$	$k_1(ADO)x10^{10}$
1	NO_2	2,6-Cl_2NpQ	4.2	1.2	
2	3,5-$(NO_2)_2$BN	NO_2	3.1	2.2	
3	4-NO_2NB	NO_2	6.8	4.0	6.0
4	BQ	NO_2	8.9	5.0	
5	3-NO_2NB	NO_2	14.8	5.0	6.0
6	2-NO_2NB	NO_2	14.8	2.5	6.0
7	4-CNNB	NO_2	13.5	4.9	
8	2-CNNB	NO_2	15.9	5.0	
9	3-CNNB	NO_2	16.9	6.5	
10	3-CF_3NB	NO_2	20.4	4.1	
11	3-ClNB	NO_2	23.5	5.0	
12	4-ClNB	NO_2	24.0	4.3	6.0
13	2-ClNB	NO_2	26.7	4.2	
14	3-FNB	NO_2	24.6	5.8	
15	4-FNB	NO_2	27.2	4.8	
16	2-FNB	NO_2	28.2	5.4	
17	3-CH_3ONB	NO_2	28.9	5.6	
18	4-CH_3ONB	NO_2	31.9	5.0	
19	NB	NO_2	29.8	4.1	6.0
20	3-CH_3NB	NO_2	30.2	5.5	
21	4-CH_3NB	NO_2	31.0	5.0	6.0
22	2-CH_3NB	NO_2	31.7	5.4	

[a]Rate constants are in cc molecule^{-1} s^{-1}, ΔH_1^0 values in kcal/mol. All measurements are performed at 423°K.

[b]BN stands for benzonitrile, NB for nitrobenzene and BQ for 1,4-benzoquinone.

[c]NpQ stands for 1,4-naphthoquinone.

Table 3.2 Rate constants[a] k_1 for exothermic electron transfer reactions $A^- + B \rightarrow A + B^-$ involving substituted benzenes.

	A[b]	B[c]	$k_1(exp)x10^9$	$k_1(ADO)x10^9$
1	NB	4-NO_2NB	1.3	1.1
2	NB	3-NO_2NB	2.1	1.8
3	NB	3-CF_3NB	1.8	1.8
4	4-CH_3NB	3-CF_3NB	1.9	1.7
5	3-CF_3NB	4-NO_2NB	1.3	1.0
6	4-FNB	3-NO_2NB	1.9	1.8
7	4-CNBN	4-CNNB	1.2	1.1
8	2-CNBN	3-CNNB	1.4	1.8
9	3-CNBN	2-CNNB	2.1	2.4
10	2,3-$(CH_3)_2$NB	4-CNBN	1.5	1.1
11	3-CNBN	3-FNB	2.5	1.9
12	2,6-Cl_2BN	4-CH_3NB	1.7	
13	4-CF_3BN	4-CNNB	1.2	1.0
14	4-CF_3BN	3-CNNB	1.9	
15	3-CNBN	3-CNNB	1.6	1.8

[a]Rate constants are in cc/(molecule.s), all measurements are done at 423°K.

[b,c]BN stands for benzonitrile and NB for nitrobenzene.

Table 3.3 Rate constants, k_1 for exothermic electron transfer reactions (1.1), involving perfluorobenzenes C_6F_5X, where X is an electron withdrawing substitutent[a].

	A[b]	B[c]	$k_1(exp)x10^9$	Exothermicity
1	C_6F_5F	2,3-$(CH_3)_2$NB	2.0	4.6
2	C_6F_5CN	4-CNNB	1.4	11.7
3	C_6F_5CN	3-CF_3NB	2.6	4.6
4	C_6F_5CN	3-ClNB	1.3	1.8
5	C_6F_5CN	4-ClNB	1.0	1.2
6	C_6F_5CN	3-FNB	0.9	1.0
7	2-ClNB	C_6F_5CN	1.9	1.3
8	4-CNNB	1,4-$(CN)_2C_6F_4$	1.9	4.8
9	2-CH_3BQ	1,4-$(CN)_2C_6F_4$	2.2	2.4
10	1,4-$(CN)_2C_6F_4$	3,5-$(NO_2)_2$BN	1.4	5.0

[a]Rate constants are in cc/(molecule.s) and exothermicities are in kcal/mol.
[b,c]NB stands for nitrobenzene, BN for benzonitrile and BQ for 1,4-benzoquinone.

Table 3.4 Exothermic electron transfer reaction rate constants k_1, involving benzoquinones, naphthoquinones and di- and tetracyano ethylene at 423K[a].

	A[b]	B[c]	$k_1(exp)x10^9$	$k_1(ADO)x10^9$
1	3-FNB	BQ	1.4	
2	4-NO_2NB	2,6-$(Cl)_2$BQ	1.0	
3	4-NO_2NB	2,3-$(Cl)_2$NpQ	0.4	
4	2,3-$(Cl)_2$NpQ	2,6-$(Cl)_2$BQ	1.5	
5	2,6-$(Cl)_2$BQ	Cl_4BQ	0.5	
6	DCNE	4-CNNB	1.9	1.0
7	DCNE	2-NO_2NB	2.7	2.4
8	3-FNB	DCNE	0.5	0.9
9	F_4BQ	TCNE	0.8	

[a]Rate constants are in cc/(molecule.s)

[b,c]NB, BQ, NpQ, DCNE, TCNE respectively stand for nitrobenzene, 1,4-benzoquinone, 1,4-naphthoquinone, trans-1,2-dicyanoethylene, and tetracyanoethylene.

Table 3.5 Exothermic electron transfer rate constants[a] k_1, for reactions (1.1) involving azulene and naphthalenes.

	A[b]	B[c]	k_1(exp)x10^9	k_1(ADO)x10^9
1	Azulene	3-CF_3NB	1.0	1.7
2	1-NO_2NpT	4-NO_2NB	1.4	1.0
3	2-NO_2NpT	2-NO_2NB	2.6	2.1
4	1-NO_2NpT	2-NO_2NB	2.6	2.1
5	1-CNNpT	2-NO_2NpT	1.6	2.0
6	1-CNNpT	1-NO_2NpT	1.6	1.7
7	NB	1,3-$(NO_2)_2$NpT	0.6	2.0
8	3-FNB	1,3-$(NO_2)_2$NpT	0.6	1.9
9	2,3-diCH_3NB	1-NO_2NpT	2.2	1.7
10	2-CH_3NB	1-NO_2NpT	2.2	1.7

[a]Rate constants are in cc/(molecule.s). Only the reaction involving azulene is measured at 343°K, other values are obtained at 423°K.

[b,c]NB and NpT stand for nitrobenzene and naphthalene respectively.

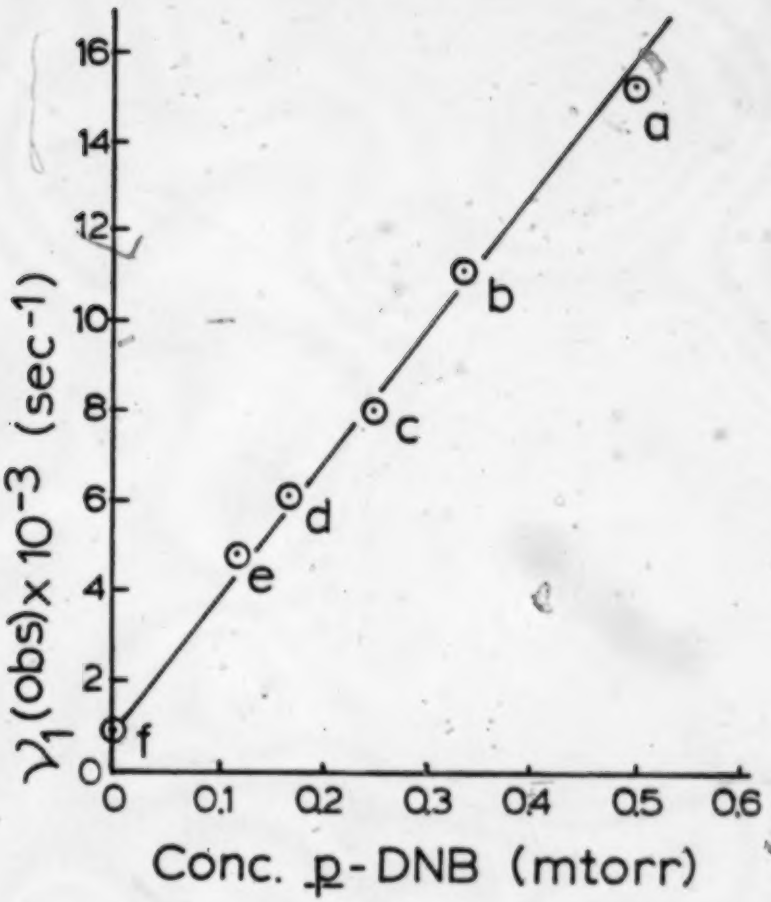

Figure 3.3. Plot of ν_1(obs), from Figure 3.2(b) against concentration of 4-NO_2NB. The slope gives the rate constant k_1 while the intercept gives the rate constant for diffusional loss to wall.

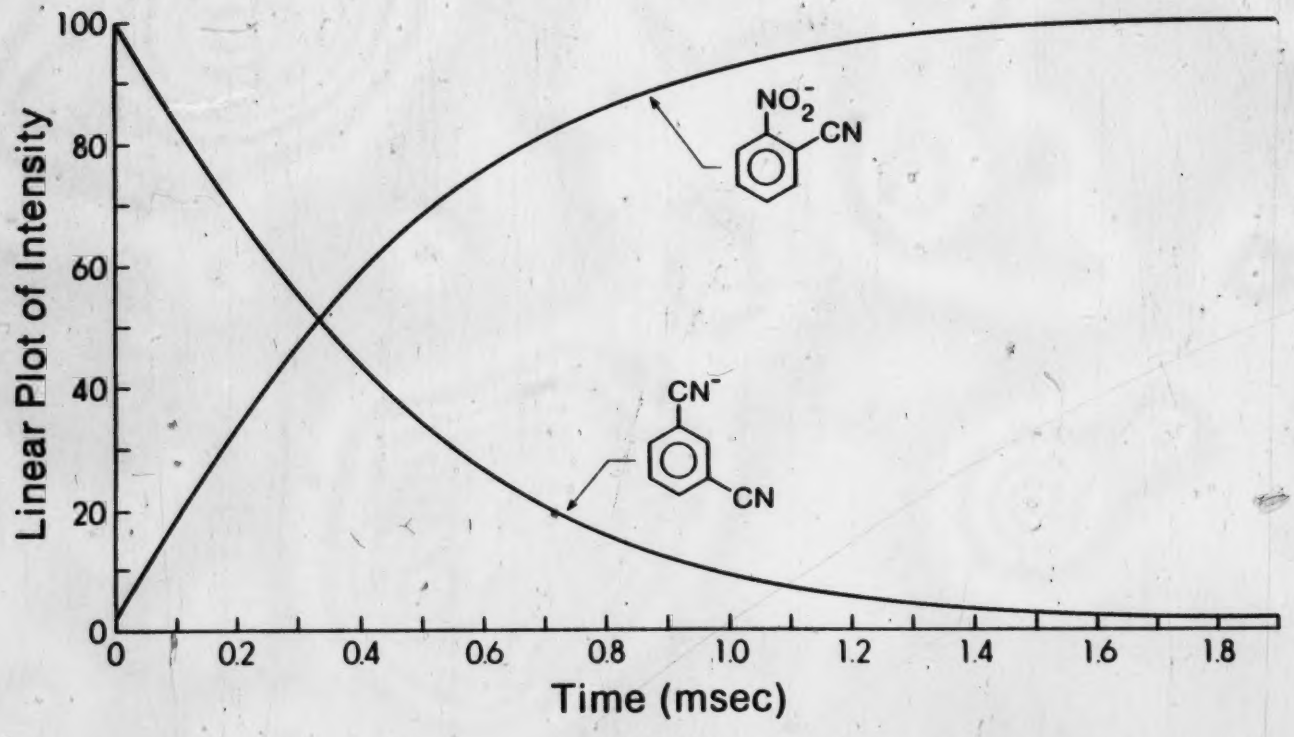

Figure 3.4. Time dependence of ion intensities in percent of total ion current. Reversible electron transfer leading slowly to equilibrium. 3.5 torr methane, 1.0 mtorr of 3-CNBN, 0.06 mtorr of 2-CNNB were present in the ion source at T = 374K in this run. BN stands for benzonitrile.

Where q is charge of the ion, μ is reduced mass of the ion-neutral system, α is polarizability of the neutral molecule, μ_D is dipole moment of the molecule and k is the Boltzman constant. c is the dipole locking constant and has a value between 0 and 1, which compensates for the effectiveness of the charge "locking in" of the dipole. It turns out that[88] at constant temperature, c is a function of $\mu_D/\alpha^{1/2}$ only. The isotropic curve of c against $\mu_D/\alpha^{1/2}$ is provided by Su[88] and the magnitude of c for a particular reaction (for any definite value of $\mu_D/\alpha^{1/2}$) could be obtained from the curve[88].

Comparison of k_1(exp) with k_1(ADO) provided in Tables 3.1 to 3.5 shows a good agreement between those two rate constants for reactions involving A and B which are substituted nitrobenzenes, cyanobenzenes and naphthalenes. Electron transfer to NO_2 also proceeded at near Langevin-ADO collision limit. Only the reactions with an exothermicity of less than 10.0 kcal/mol (see Table 3.1), k_1(exp) values were observed to be below the collision limit. This weak trend of decrease of rate constants with the decrease of the exothermicity of the reaction is probably associated with the geometry change on formation of NO_2^-. For NO_2/NO_2^- system it is the decrease in <O-N-O bond angle[89] from 134.1°(NO_2) to 115.4°(NO_2^-). The rate constants for reactions shown in Table 3.1 involving B = NO_2 and A = nitrobenzenes and quinones are lower by a factor of about 2 than those for B = nitrobenzenes (Table 3.2). This is a consequence of the relatively much lower polarizability of NO_2 and the smallness of its permanent dipole moment.

Of special interest is the effect of dipole moment of B, μ_B on the experimental rate constants k_1(exp), which is reproduced quantitatively in the Langevin-ADO theory predicted rate constants, shown in Tables 3.2 and 3.5. Reactions 1 and 2 in the Table 3.2 involving B = 1,4-dinitrobenzene and 1,3-dinitrobenzene respectively, show such dependence. Due to the presence of a dipole in the meta compound and its cancellation in the para case, ADO predicts a k_1(ADO)(meta) > k_1(ADO)(para) and this trend is quantitatively followed by the experimental rate constants, k_1(exp) shown in Table 3.2. A similar comparison could be made between electron transfer reactions 7, 8, and 9 in Table 3.2, where the trend k_1(ADO)(ortho) > k_1(ADO)(meta) > k_1(ADO)(para) is in agreement with the trend of experimental rate

constants and hence the dipole moments[90] of B.

SF_6, $CF_3C_6F_{11}$, C_6F_{12} showed unusual behavior towards electron transfer reactions. These compounds capture electrons most readily with a large electron capture rate constant[25]. However, they are totally unreactive in many electron transfer reactions (1.1) either as electron donors or as electron acceptors. Typical experimental behavior of these compounds are shown in Figure 3.5. Shown in Figure 3.5a is the time dependence of ion abundances of $CF_3C_6F_{11}^-$ and 4-FNB$^-$ in a typical run obtained after a short (~10μs) electron pulse. The intensity time dependence appears similar to that observed when there is a rapid electron transfer equilibrium shown in Figure 3.1. However, a closer examination shows that, the distance between the two logarithmic intensity plots increases with time due to a slightly faster decay of the 4-FNB$^-$. A slightly faster diffusional loss of the lighter ion 4-FNB$^-$ is expected. Shown in Figure 3.5b is the time dependence of the intensities of ions obtained after an ionising pulse from a mixture of SF_6, C_6F_{12}, $CF_3C_6F_{11}$, and 3-MeNB. Since the electron affinity of all these compounds are different (electron affinity values are provided in the next chapter, Table 4.3), one would expect a change in their relative abundances with time due to electron transfer reaction (1.1) leading to the stable ion intensities at equilibrium. What one observes instead is only a very slow decay of all ions, due to diffusion of ions to the wall. Thus observations in Figure 3.5 are more consistent with no reactive coupling between A$^-$ and B rather than a fast equilibrium.

A definite proof that there is no electron transfer (1.1) in most reactions involving perfluoro compounds was obtained by examining the intensities in runs involving these compounds and many other compounds of known electron affinities. The time dependence of intensities was like those shown in Figure 3.5. On varying the concentration of A and B, the quotient Q_1 in equation (3.3), was found to remain constant as would be the case if equilibrium (1.1) was present; however, ΔG_1^0 values evaluated

$$Q_1 = \{[B^-][A]\}/\{[A^-][B]\} \qquad (3.3)$$

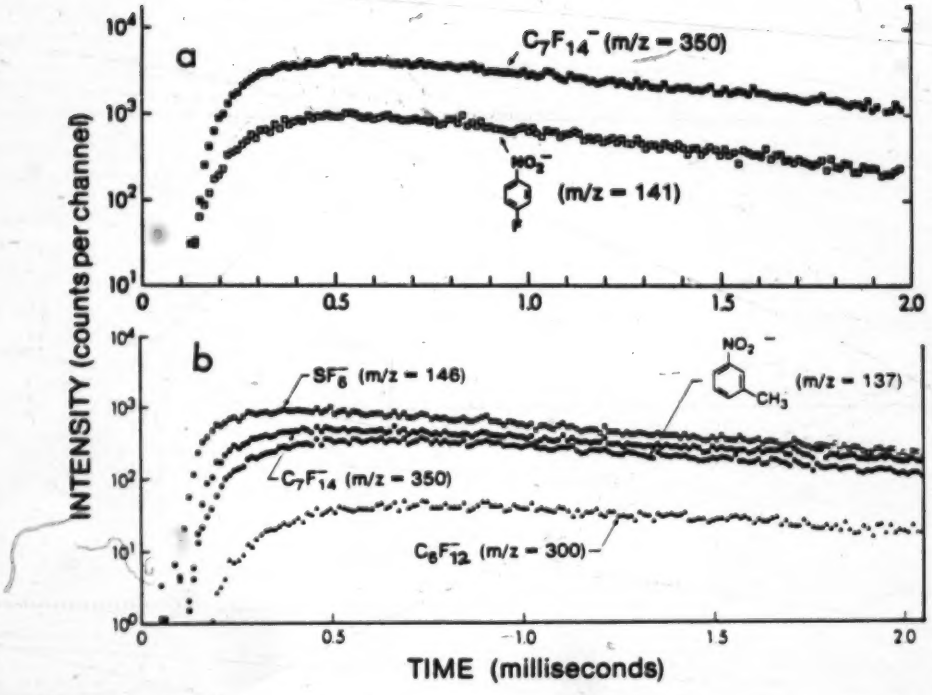

Figure 3.5. a) Intensities observed with C_7F_{14} (5.9 mtorr) and 4-FNB (5.4 mtorr) in 4.0 torr methane at 423K. Superficially, the intensities of the two anions appear equidistant and one might have assumed that ions are in rapid eqilibrium (1.1) as in Figure 3.1(a). However, behavior in the present system corresponds to total lack of electron transfer. (b) Slow electron transfer when perfluorinated compounds are involved. All negative ions observed are formed by electron capture. Intensity decreases with time only due to diffusion of ions to wall without any reactive changes. 3-CH_3NB, 7.3 mtorr; SF_6, 0.5 mtorr; C_7F_{14}, 1.0 mtorr; C_6F_{12}, 0.5 mtorr at 423K.

with the Q_1 lead to a different position to the perfluoro compounds in the EA scale for every partner used. This means that equilibrium was not present in any of these cases and that the ions A^- and B^- formed by electron capture did not react at all via (1.1). Since electron capture by A is proportional to the concentration of A, the expression (3.3) holds also in the complete absence of reactive eqilibrium. The detailed discussion about the slow electron transfer reactions involving the above group of compounds follows.

3.3 Slow Electron Transfer Kinetics Involving SF_6, $CF_3C_6F_{11}$, Etc.

3.3.1 Background

SF_6 and SF_6^- have been the subject of numerous investigations. The recent ones are: electron photodetachment studies from SF_6^-[91]; studies of negative ion chemistry of SF_6^- and electron affinity of SF_6[59,92]; determination of kinetics and thermochemistry of electron attachment to SF_6[93] and unimolecular decomposition of SF_6^-[94]. Streit[59] provided an up-to-date list of all investigations prior to his report. The interest in SF_6 is justified by the fact that, it has a very large electron capture cross section[25,95], the SF_6^{-*} formed after electron capture has a very long autodetachment life time [25,91,95-96] and SF_6^- obtained after collisional stabilization is very unreactive[59,91]. These properties made SF_6 an important and extensively used gaseous dielectric and electron scavenger[25,91,95-96]. A number of different values ranging from 0.4 to 1.5 eV has been suggested for the EA of SF_6[59].

Drzaic and Brauman reported that[91] no observable photodetachment could be detected from SF_6^- and a loose SF_6^- structure which is distorted significantly from the neutral SF_6 is suggested as the possible cause. Streit[59] with the help of a flowing afterglow apparatus investigated the following reactions involving SF_6, SF_6^-, and SF_5^- : ET reactions, dissociative ET reactions and an electron transfer equilibria in order to determine the electron affinity of SF_6. He reported that[59] NH_2^- (EA, NH_2 = 0.72 eV) transfers electron to SF_6 with the rate constant

2.0×10^{-10} cc/(molecule.s). Thus $EA(SF_6) > 0.74$ eV. In a similar fashion from other measurements involving SF_6 and SF_6^-, a value of 1.0 ± 0.2 eV is suggested[59] for the EA of SF_6. Electron affinity of SF_6 determined with the help of alkali atom collisional ionisation[44] and negative ion endothermic charge transfer method[49] are rather low; $EA(SF_6) = 0.5 - 0.6$ eV, compared to the value due to Streit and that from the present investigation, $EA(SF_6) = 1.03 \pm 0.1$ eV. The low values obtained from beam experiments for EA of SF_6 (ref. 44 and 49) were suggested[59] to be due to: (i) the threshold might have been observed at higher energy (~0.5 eV) because of low cross section for charge exchange and/or (ii) SF_6^- during atom or ion impact was in an excited state probably ~0.5 eV higher than the ground state.

Henegan et al.[93] performed RRKM calculations for the lifetime of SF_6^- toward autodetachment and an electron affinity value $EA(SF_6) = 1.4$ eV is suggested. The conclusion of Henegan et al.[93] that the structures of SF_6 and SF_6^- were similar, is in direct contrast with that of Drzaic et al.[91], who favored an structure of SF_6^- which is highly distorted from that of SF_6. The experimental life time of SF_6^- ($\tau = 25$ μs) is consistent with the $EA(SF_6) \simeq 1.0$ eV[91].

Little experimental information concerning the structure of SF_6^- is presently available. Electron spin resonance techniques have been used to probe SF_6^- formed by irradiation of SF_6 matrices with high energy electrons or γ-radiation. These studies indicate that the sulfur center is surrounded by six fluorines which are equivalent on the ESR time scale. This may be either due to an octahedral SF_6^- or to a system with six rapidly interconverting fluorine ligands.

A recent SCF calculation by P. J. Hay[98] predicts a larger S-F distance for the negative ion SF_6^-, i.e., $R_e(SF_6) = 1.567$ A vs $R_e(SF_6^-) = 1.710$ A. Hay[98] assumed an octahedral geometry for both SF_6 and SF_6^- with no Jahn-Teller distortion, but did not investigate the structures of low symmetry. Hay's results show that the electronic ground state of SF_6 is 0.9 eV higher than that for SF_6^- i.e., giving an adiabatic electron affinity of 0.9 eV.

$CF_3C_6F_{11}$ and C_6F_{12} are also known to have very high electron capture coefficients[25]. They are also very unreactive towards electron transfer reactions. Very little information is available on the electron affinity of these compounds, geometries of the neutrals and the negative ions and their reactivity towards ET reactions.

3.3.2 Results of Slow Electron Transfer Reactions Involving SF_6, $CF_3C_6F_{11}$ and Their Negative Ions

The present investigation is the first detailed and systematic study of the kinetics of electron transfer reactions involving SF_6 and perfluoro cycloalkanes. Table 3.6 summarizes the measured exothermic electron transfer rate constants, k_1, involving SF_6 and $CF_3C_6F_{11}$. Also shown in Table 3.6 are the exothermicities, ΔH_1^0 of the reactions. SF_6^- and $CF_3C_6F_{11}^-$ transfer electrons to compounds B, provided the reaction is exothermic, i.e., $EA(B) > EA(SF_6)$; and do so with low collision efficiency. The rate constants, k_1, however increase with the increase of exothermicity, $-\Delta H_1^0 = EA(B) - EA(SF_6)$ of the reaction, see Table 3.6. The reaction proceeded at collision efficiency, with an exothermicity as high as 38.7 kcal/mol or 1.7 eV. Very slow electron transfer from SF_6^- was also reported earlier by Fehsenfeld[92] among others[59,96,99].

The temperature dependence of four reactions involving exothermic electron transfer from SF_6^- to some substituted nitrobenzenes and quinones showed some interesting features. Shown in Figure 3.6 are the $\log k_f$ of the reaction (3.5) plotted against 1/T for four B molecules.

$$SF_6^- + B \rightarrow SF_6 + B^- \qquad (3.5)$$

They are tetrafluorobenzoquinone, F_4BQ (curve A); 1,4-dinitrobenzene, 4-NO_2NB (curve B); 4-CNNB (curve C) and 3-CF_3NB (curve D). Temperature dependence is almost absent when the reaction proceeds at collision efficiency (curve A), see reaction (5) in Table 3.6. Rate constants which were below collision limit, reactions (2) to (4) in Table 3.6 were found to have negative temperature dependence (curve B and C in Figure 3.6). Curve D in Figure 3.6 is for the reaction where B=3-CF_3NB, and for which reaction exothermicity is the smallest (reaction(1), Table 3.6). This reaction was found to have positive temperature dependence at lower temperatures and no temperature dependence at higher temperatures.

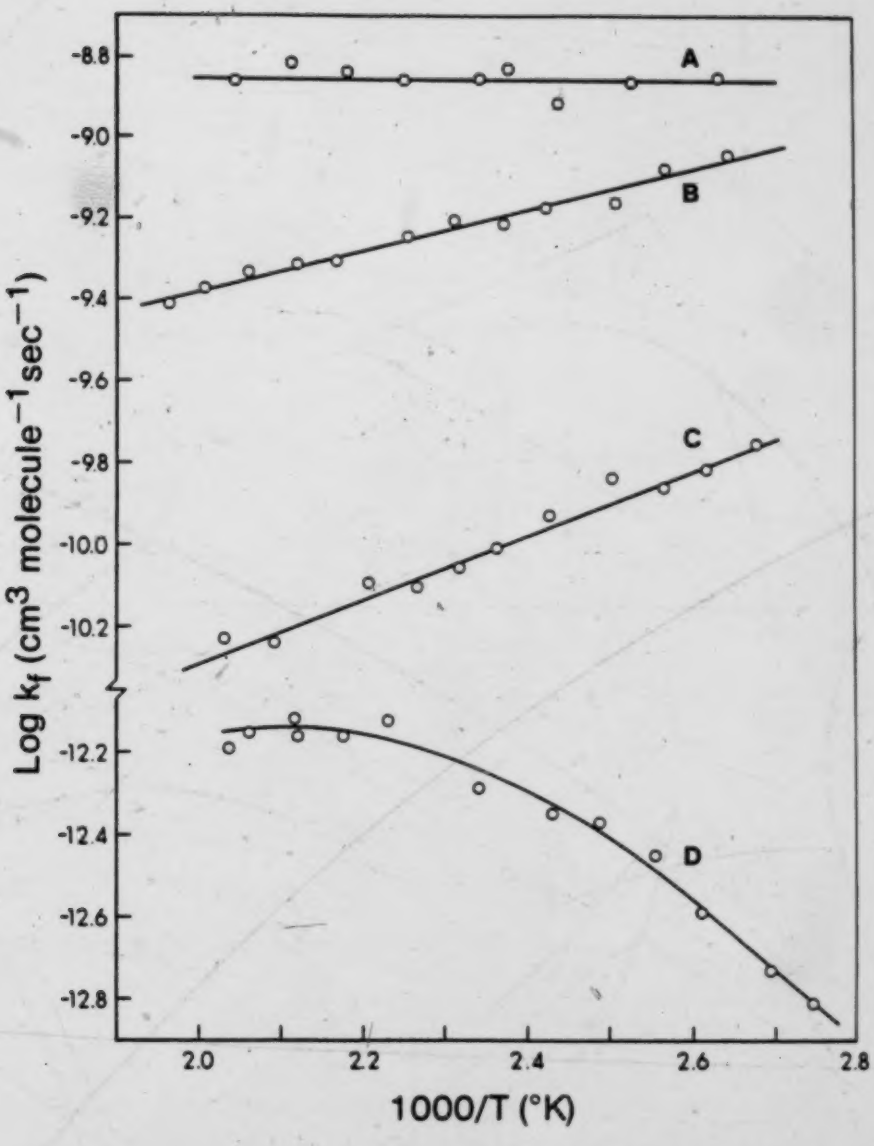

Figure 3.6. Temperature dependence of rate constants k_f for reactions $SF_6^- + B \rightarrow SF_6 + B^-$. Case A, B = tetrafluoro benzoquinone; case B, B = 1,4-dinitrobenzene; case C, B = 4-CNNB; case D, B = 3- CF_3NB The electron affinities of B and exothermicities of the reactions decrease from A to D.

Table 3.6 Exothermic electron transfer rate constants k_1 for the reaction: $A^- + B \rightarrow A + B^-$ involving SF_6 and $CF_3C_6F_{11}$ at 423 K.[a]

	A	B[b]	$-\Delta H^0_1$	k_1(exp)	$E^{\ddagger}$,[c]
1	SF_6	3-CF_3NB	8.9	5.0×10^{-13}	7.4
2	SF_6	3-NO_2NB	14.5	6.0×10^{-11}	5.4
3	SF_6	4-CNNB	15.8	1.0×10^{-10}	4.8
4	SF_6	4-NO_2NB	22.5	1.0×10^{-9}	2.9
5	SF_6	F_4BQ	38.6	1.4×10^{-9}	0.3
6	$CF_3C_6F_{11}$	3-CF_3NB	7.7	$<5.0\times10^{-13}$	
7	$CF_3C_6F_{11}$	3-NO_2NB	13.3	4.0×10^{-11}	
8	$CF_3C_6F_{11}$	4-CNNB	14.6	5.0×10^{-11}	
9	$CF_3C_6F_{11}$	4-NO_2NB	21.3	7.0×10^{-10}	
10	$CF_3C_6F_{11}$	2,6-diClBQ	32.3	8.0×10^{-10}	
11	$CF_3C_6F_{11}$	F_4BQ	37.4	1.2×10^{-9}	

[a]Rate constants all are in cc/(molecule.s) and energy terms are in kcal/mol.
[b]NB and BQ stand for nitrobenzene and 1,4-benzoquinone respectively.
[c]Energy barrier for electron transfer reaction is calculated by Richardson (ref. 104).

3.3.3 Discussions

The above observations, that electron transfer from SF_6^- proceeded with low collision efficiency, indicate the presence of a kinetic barrier in the electron transfer reaction (3.5) from SF_6^- to B molecules. This kinetic barrier is probably due to a large geometry change occurring during formation of SF_6^-. This supposition is supported by the observation of large entropy change for electron attachment to SF_6, obtained in the present investigation, $\Delta S_a^0 = 13.0$ cals/deg, SCF calculation by Hay[97] and electron photodetachment study by Brauman[91].

It is a well known fact that geometry changes between negative ion and the neutral lead to an energy barrier for electron transfer. The type of unusual behavior displayed in Fig. 3.6 for ET reactions involving SF_6^- was also observed earlier by Sen Sharma and Kebarle[100] in a different series of reactions (3.6) involving CH_3^+ transfer from $CH_3ClCH_3^+$ to B, where B were $(CH_3)_3N$, NH_3, CH_3OCH_3 etc.

$$CH_3ClCH_3^+ + B = CH_3Cl + CH_3B^+ \qquad (3.6)$$

The slowest reaction had positive temperature dependence, the faster ones with more basic B compounds had negative temperature dependence, and the most exothermic and the fastest reactions proceeded at collision rates without any T-dependence[100].

The behavior of reaction series (3.6) was explained[100] on the basis of reaction coordinates with substantial internal barriers as shown in Figure 3.7. Brauman[101] was the first to propose a kinetic model for ion molecule reactions with large internal barriers. The internal barrier in the reaction series (3.6) is due to changes in chemical bonding attendant with the formation of the chemical transition state given in formula (3.7). Other similar cases

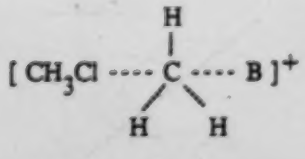

(3.7)

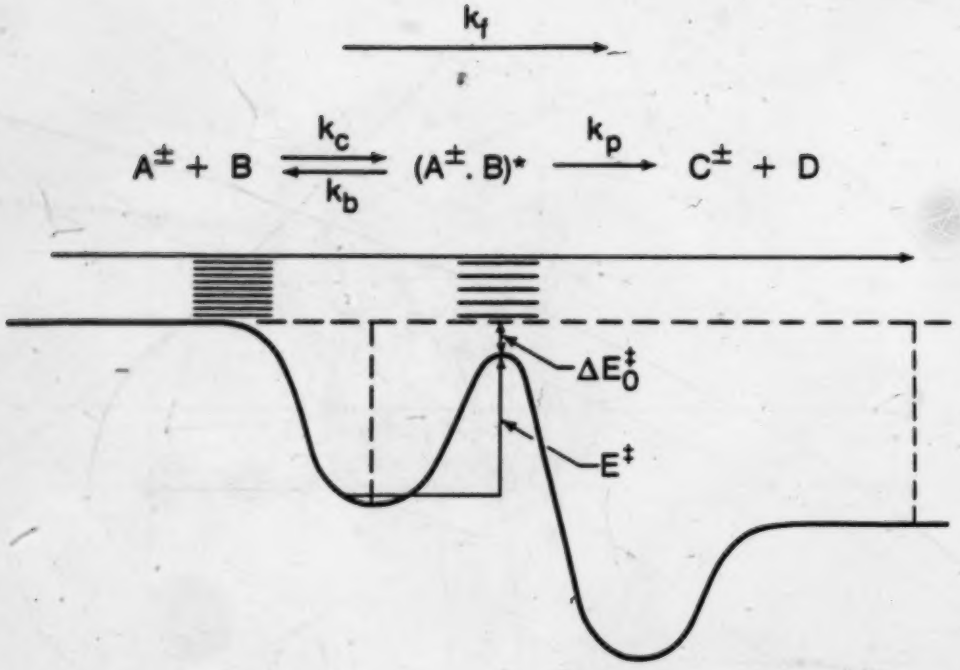

Figure 3.7. Reaction coordinate with internal energy barrier used to explain temperature dependence of rate constants for S_N2 reactions (3.6) involving CH_3^+ transfer, which have similar temperature dependence of rate constants observed in case of electron transfer from SF_6^- (Figure 3.6). $E^{\ddagger}$ is the barrier for the formation of chemical transition state.

have been discussed in the literature[100-103]. The excited complex $(A^{\pm}.B)^{*}$ (see Figure 3.7) formed by the orbiting collision with the rate constant k_c is (assumed) sufficiently long lived for energy randomization to occur within the complex[101]. $(A^{\pm}.B)^{*}$ may back decompose (k_b) or go over the barrier (k_p) and form the products (for notations see Fig. 3.7). A steady state approximation leads[101] to the equation (3.8).

$$k_f = k_p k_c/(k_p+k_b) \qquad (3.8)$$

For a small internal barrier, $-\Delta E_0^{\ddagger}$ is very large and $k_p >> k_b$ so that $k_f = k_c$ i.e., the reaction proceeds at collision rates. It is shown[101] from the RRKM statistical formalism, that when $-\Delta E_0^{\ddagger}$ is small i.e., equal to a few kcal/mol, k_p becomes smaller than k_b, so that k_f falls below the collision rate, see equation (3.8). The reason that $k_p < k_b$ even though $\Delta E_0^{\ddagger}$ is negative lies in the nature of the complexes associated with k_p and k_b. The product complex $(AB^{\pm})^{\ddagger}$ is a tight complex with low density of states because of loss of external rotation(s) of A and B, while the orbiting collision complex or the so called "precursor complex" is a loose complex with a large density of states due to retention of the external rotations of A and B.

It could be shown[100,102-103] that the experimentally observed reactions which had negative T-dependence are associated with negative $\Delta E_0^{\ddagger}$. As the temperature is increased the energy of the reactants $A^{\pm}+B$ increases. Since the density of states of the loose orbiting complex is higher than that for the tight chemical transition state, k_b increases faster than k_p, while k_c stays approximately constant. These changes lead to a decrease of k_f with temperature, see equation (3.8). The much slower reactions which had a positive temperature dependence were attributed to reaction coordinates where the internal barrier protruded above the energy level of the reactants, i.e., led to a $\Delta E_0^{\ddagger}$ that was positive[100,102-103]. In this case $\Delta E_0^{\ddagger}$ is simply the conventional Arrhenius activation energy.

The similarities between the rate constant changes for electron transfer from SF_6^- (Fig. 3.6), and those observed for reactions (3.6) and other systems[100-103] suggest that reaction

coordinates similar to those proposed for reactions (3.6), should apply also for the slow electron transfer reactions. Since only an electron is transferred, the origin of the internal barrier in reaction (3.5) must be different. The most likely origin of an internal barrier in reaction (3.5) is the occurrence of a geometry change between the ground states of SF_6 and SF_6^-. The barriers $E^{\ddagger}$ given in Table 3.6 were calculated by Richardson[104] on the basis of Marcus equation[105-106] and theoretical geometry of Hay[98] for SF_6 and SF_6^-. Richardson[104] assumed essentially minimal geometry changes from B to B^- and $D(SF_6^-\text{-}B) = D(SF_6\text{-}B^-) = 7.0\pm2.0$ kcal/mol.

The potential energy surface for electron transfer reaction (3.5) from SF_6^- is shown in Figure 3.8. The parabolic potential wells for $SF_6^-.B$ and $SF_6.B^-$ are drawn to scale potential energies for SF_6^- and SF_6 for the symmetric S-F stretch, based on SCF calculation due to Hay[98]. The reaction coordinate in this region only, is assumed to be the S-F distance, that is a minimal geometry change from B to B^- is assumed. The resulting barrier $E^{\ddagger}$ in Figure 3.8 thus represents an approximate graphical solution for the Marcus barrier, due to symmetric S-F distance changes. Figure 3.8(a) represents the potential energy surface for electron transfer from SF_6^- to B molecules, where the enthalpy changes for the formation of precursor and successor complexes are assumed to be equal and Figure 3.8(b) is drawn using experimental binding energies of the above mentioned complexes as will be discussed shortly.

In the present investigation it was possible to determine $D(SF_6^-\text{-}B)$ experimentally by studying the equilibria (3.9), at low temperatures.

$$SF_6^- + B = SF_6^-.B \qquad (3.9)$$

Since the rate of electron transfer reactions (3.5) decreases with temperature, for B=3-CF_3NB, it was possible to collisionally stabilize the SF_6^-.3-CF_3NB adduct and measure the equilibria (3.9). The ion intensity time dependence of such a lower temperature run is shown in Figure 3.9. Given are the logarithm of the measured ion-intensities of various ions as a function of

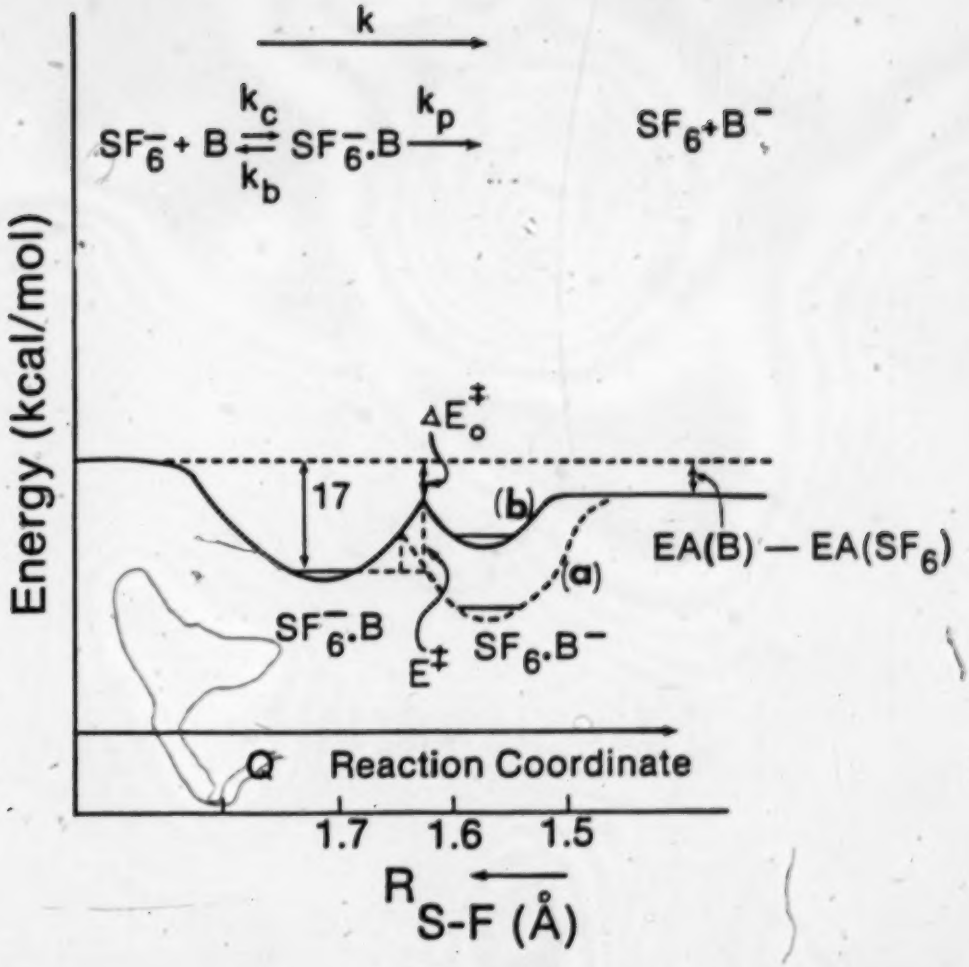

Figure 3.8. Reaction coordinate for reaction $SF_6^- + B \rightarrow SF_6 + B^-$, where B is 3-trifluoromethyl nitrobenzene. (a) Reaction coordinate with experimental $D(SF_6^-\text{-}B) = 17.0$ kcal/mol and with the assumption $D(SF_6^-\text{-}B) = D(SF_6\text{-}B^-)$. (b) Reaction coordinate with measured $D(SF_6\text{-}B^-)$. The barrier $E^\ddagger$ is assumed to be only due to geometry changes between SF_6^- and SF_6, which consists of the symmetric shortening of the S-F bonds in the region of $E^\ddagger$, therefore in the region of $E^\ddagger$ only the reaction coordinate is represented by the S-F bond length.

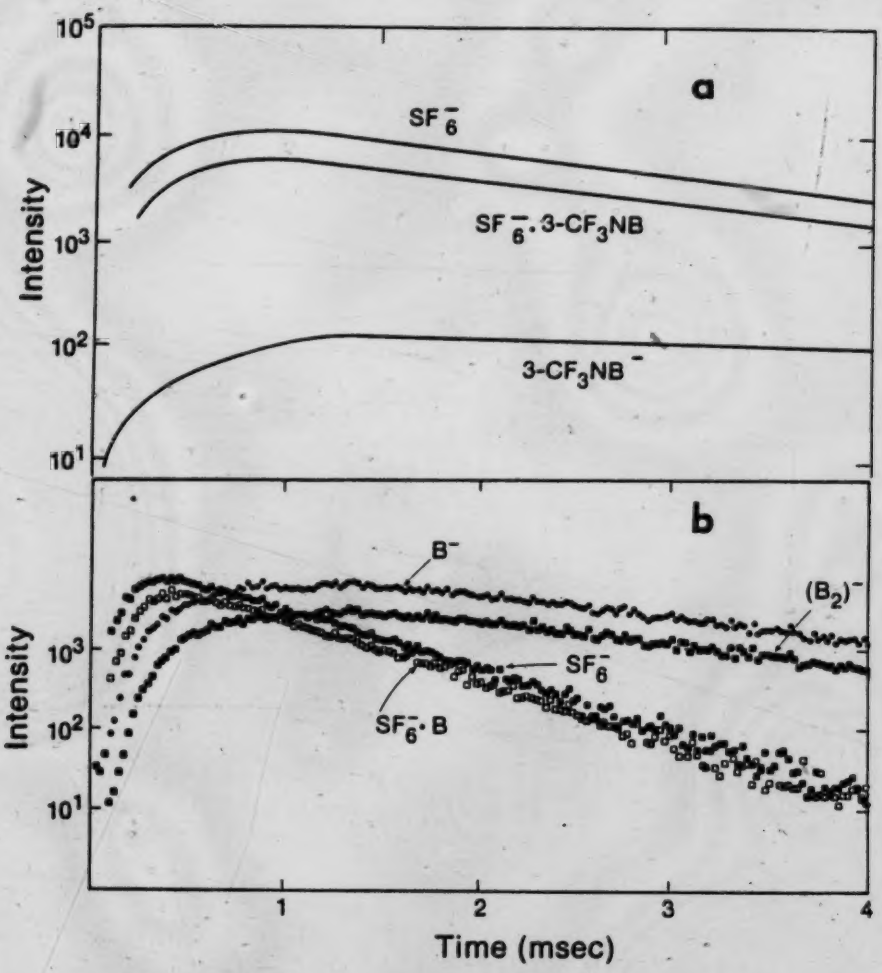

Figure 3.9. Observed ion intensities after ionising electron pulse. Ion source at 342K contains (a) 3.0 torr methane as bath gas, 113 mtorr SF_6 and 3.5 mtorr $3\text{-}CF_3NB$ = B leads to the formation of B^-. (b) Runs similar to that of (a), but with B = $3\text{-}NO_2NB$. SF_6^- and $SF_6^-.B$ are in equilibrium. B^- and $B^-.B$ are also in equilibrium. Electron transfer from SF_6 and $SF_6.B$ to B is much faster than case (a), where B is $3\text{-}CF_3NB$. T = 333K; methane, 3.0 torr; SF_6, 29.0 mtorr; and 1,3-dinitrobenzene, 0.3 mtorr. Actual experimental points are shown in case (b) but not in case (a).

time after the short electron pulse. Shown in Figure 3.9, where the ion intensities are plotted on a log scale against time, the intensities of SF_6^- and SF_6^-.3-CF_3NB (in Figure 3.9a) or SF_6^- and SF_6^-.B (in Figure 3.9b), maintain a constant vertical distance from each other.

This means that the intensity ratio of two ions SF_6^- and SF_6^-.3-CF_3NB is constant with time. The 3-CF_3NB^- is seen to have different time dependence (Fig. 3.9a). The constant ion intensity ratio obtained in Figure 3.9 shows that the equilibrium (3.9) was attained. The gradual decrease of intensities of ions in equilibrium is due to the slow diffusion of ions to the wall[5,87]. The electron transfer reaction (3.5) is still occurring, but very slowly. In the run shown in Figure 3.9a the electron transfer rate is close to the diffusion loss of 3-CF_3NB^- and this leads to the observed approximate time invariance of the 3-CF_3NB^- intensity observed after t = 1 ms.

The dimer ion $(3\text{-}CF_3NB)_2^-$ was also observed in the the run used for the Figure 3.9a. This ion which is not shown in the Figure 3.9a, had similar intensity as the monomer, 3-CF_3NB^- and ratio of these two ions was also constant with time, which means that the monomer and dimer were in equilibrium. The run shown in figure 3.9b, involves B =3-NO_2NB and the reaction (3.5) is the next slowest to B = 3-CF_3NB (see Table 3.6). The faster rate of electron transfer is evident. The ions SF_6^- and SF_6^-.3-NO_2NB decrease together i.e., they are coupled by fast electron transfer reaction. The products of ET reaction 3-NO_2NB^- and $(3\text{-}NO_2NB)_2^-$ are also in equilibrium. Even though the adduct 3-NO_2NB^-.SF_6 has the same mass (m/z = 314) as 3-$NO_2NB.SF_6^-$, significant amounts of the former complex are obviously not formed. This follows from the fact that, the mass 314 is in exact ion equilibrium with SF_6^- ion and this means practically all the (m/z=)314 ion is SF_6^-.3-NO_2NB.

Thus from the runs depicted in Figure 3.9 equilibrium constants K_{ad} and $-\Delta G^0_{ad}$ for adduct forming reaction (3.9) were obtained. Measurements at different temperatures lead to ΔH^0_{ad} and ΔS^0_{ad} via van't Hoff plots. The results are given in Table 3.7. In order to facilitate a comparison with adducts of other ions, binding energies in complexes Cl^-.B were also determined by studying equilibria like those of (3.9) involving Cl^-. A complete set of these results will be provided in chapter 6 which deals with binding energies of various ion-neutral

Table 3.7 Binding energies[a] in $A^-.B$ from the study of equilibria: $A^- + B \rightleftharpoons A^-.B$.

	A[b]	B[c]	$-\Delta G^0$	$-\Delta H^0$	$-\Delta S^0$
1	SF_6	3-CF_3NB	9.0	17.0	26.7
2	SF_6	3-FNB	7.9	15.7	26.1
3	SF_6	NB	6.7	14.9	27.5
4	$CF_3C_6F_{11}$	NB	6.7		
5	3-NO_2NB	SF_6	<1.7(333K)	<8.4[d]	
6	4-NO_2NB	SF_6	<1.9	<8.5[d]	
7	Cl	$CF_3C_6F_{11}$	<1.8		
8	Cl	SF_6	<1.8		
9	SF_6	3-NO_2NB	9.5(333K)	18.5[e]	

[a]All energies are in kcal/mol, entropies in cals/deg, standard state 1.0 atm.

[b,c]NB stands for nitrobenzene.

[d]ΔS^0 is assumed to be -20.0 cals/deg, [e]entropy change is assumed to be -27.0 cals/deg.

complexes. The significance of the binding energies in $SF_6^-.B$, comparison with $Cl^-.B$ and some interesting results of binding energies involving other perfluoro compounds, such as, C_6F_6, C_6F_5CN etc. with various negative ions will be discussed in chapter 6.

For a qualitative discussion of electron transfer reaction (3.5), involving SF_6^-, the electron transfer involving the least exothermic reaction (B = 3-CF_3NB) and $E^{\ddagger} \simeq 7.4$ kcal/mol (Table 3.6) is of special interest. For this slowest reaction k_f was lower by a factor of 10^4 relative to collision rate and the Arrhenius plot of k_f showed positive temperature dependence (Figure 3.6). For this reaction one therefore, expects $E^{\ddagger} \simeq D(SF_6^-\text{-}B)$ and $\Delta E^0 \geq 0$. However, $-\Delta H^0_{ad}$ for B = 3-CF_3NB is observed to be 17.0 kcal/mol in the present study (Table 3.7). Evidently the barrier $E^{\ddagger}$ of 7.4 kcal is now much too small (Figure 3.8a), so that reaction coordinate 3.8a leads to a large $-\Delta E^{\ddagger}_0$ and is thus inconsistent with the observed very slow kinetics. It can be shown that $\Delta E^{\ddagger}_0 = E^{\ddagger} - D(SF_6^-\text{-}B)$ from Figure 3.7. However, the reaction coordinate 3.8a was obtained by making the assumption, that the binding energies $D(SF_6^-\text{-}B) \simeq D(SF_6\text{-}B^-)$, based on which Marcus and Sutin [105] deduced the expression for the barrier in electron transfer reaction (1.1), which was used by Richardson[104] to deduce the barrier in the reaction (3.5) involving SF_6^- (as shown in Table 3.7). Obviously the equality between the stability of the precursor and the successor complexes need not be present, since the two adducts are distinct chemical entities, and may be formed by different bonding. In fact no adducts $SF_6.B^-$ were found to exist in the runs shown in Figure 3.9. The log intensities of SF_6^- and $(SF_6.B)^-$ are exactly parallel. This means that $(SF_6.B)^-$ is predominantly $SF_6^-.B$, and thus the bonding in $SF_6.B^-$ is very much weaker than that in $SF_6^-.B$.

However, an upper limit of the equilibrium constant for the formation of $SF_6.B^-$ can be deduced from the experiments shown in Figure 3.9. By estimating the possible deviation from the parallel behavior in log intensities of SF_6^- and $SF_6^-.B$ at longer reaction times, the maximum possible concentration of $SF_6.B^-$ can be estimated. Thus the maximum equilibrium constant, K_{ad}, ΔG^0_{ad} ($= -RT\ln K$) and ΔH^0_{ad} (assuming $\Delta S^0_{ad} = -25$ cal/deg) can be estimated. This value as shown in Table 3.7 is $D(SF_6\text{-}B^-) < 8$ kcal/mol.

Now incorporating $D(SF_6\text{-}B^-)$ in the reaction cordinate 3.8a, a new reaction coordinate 3.8b is obtained with a completely different picture. The electron transfer reaction based on zero point levels of the two complexes has now become endothermic rather than exothermic. The internal barrier $E^{\ddagger}$ due to SF_6 geometry change is thereby raised such that $-\Delta E_0^{\ddagger}$ is quite small again. Furthermore, since there is a change in the adduct geometries, this change must also become part of the reaction coordinate, an effect not taken into account in the evaluation of $E^{\ddagger}$ (Table 3.6 and Figure 3.8), where only S-F bond length changes are considered. Taking into account the adduct geometry changes might lead to further increase in $E^{\ddagger}$, so that $E^{\ddagger} \simeq D(SF_6^-\text{-}B)$ becomes possible and the reaction coordinate becomes compatible with the observed kinetics.

The geometry changes occurring on formation of the negative ion $CF_3C_6F_{11}^-$ from the neutral are not known, however the very low rate constant for electron transfer from $CF_3C_6F_{11}^-$ to B, Table 3.6 is probably primarily due to such a geometry change i.e., the situation in this respect is probably similar to that for SF_6 and SF_6^-. Another similarity is also present in the bonding energy changes of the adducts. Thus $CF_3C_6F_{11}^-$ bonds to NB and probably also to CF_3NB about equally well as SF_6^- (compare data for adduct reaction (3) and (4) in Table 3.7). Similarly, negative ions bond very poorly to $CF_3C_6F_{11}$ as was the case for SF_6, compare reactions (5), (7) and (8) in Table 3.7. Thus it appears that the reasons for the slow electron transfer from $CF_3C_6F_{11}^-$ are the same as those for SF_6^-. Low rate constants were observed also for perfluorocyclohexane, C_6F_{12} and it is likely that the factors involved for this and other perfluorocycloalkanes will be similar to those for SF_6 and $CF_3C_6F_{11}$.

4. ELECTRON AFFINITIES FROM ELECTRON TRANSFER EQUILIBRIA MEASUREMENTS

4.1 Measurements and Results

Part of the measurements and results presented in this chapter are collaborative works done by this author and Dr. E. P. Grimsrud, who has been in sabbatical leave in 1984/85 year in this laboratory.

4.1.1 Electron Transfer Equilibria

As outlined in chapter 1 earlier, the measurements of electron transfer equilibria (1.1) leading to the determination of electron affinities were obtained with the help of a pulsed electron high ion-source pressure mass spectrometer, described in chapter 2. A typical example of experiments leading to the determination of equilibrium constant K_1

$$A^- + B = A + B^- \qquad (1.1)$$

given by equation (1.15) are shown in Figure 3.1.

$$K_1 = \{ [A] [B^-] \} / \{ [B] [A^-] \} \qquad (1.15)$$

The pulsed electron ion-source shown in Figure 2.1 in such experiments contains typically ~5.0 torr of a bath gas most often methane and generally 0.5 to 50.0 mtorr pressures of the compounds A and B which have positive electron affinities. A short (~10-20 μs) pulse of electrons accelerated by 2000 V leads to the production of positive ions and secondary electrons in the ion source from the bath gas. The secondary electrons thus produced are brought to near

thermal energies by collision with the bath gas. Molecules A and B then capture thermal electrons to form excited $(A^-)^*$ and $(B^-)^*$. The excited negative ions are readily thermalized by collision with the bath gas. A^- and B^- then engage in electron transfer reactions with neutral molecules A and B, while diffusing towards the walls of the ion source. Electron transfer equilibria (1.1) could be achieved under suitably selected conditions.

In the ion time dependence shown in Figure 3.1(b), the compound A(1,4-dinitrobenzene) which is of lower electron affinity than B(2,3-dichloronaphthoquinone) is present in much larger concentration than B. Therefore, electron capture occurs predominantly by A and A^- concentration observed at short times (0.1 ms) after the electron pulse, is dominant. Rapid electron transfer to B leads to the decrease of A^- intensity and increase of B^- intensity. After about 0.7 ms the ratio of the intensities of these two ions (in Figure 3.1(b)) has become constant which in the logerthmic plot corresponds to a constant vertical distance between A^- and B^-. In Figure 3.1(a) the concentrations of A and B are chosen to be higher and the equilibrium is established very rapidly. In general, when equilibrium measurements were performed, the concentrations of A and B were chosen such that equilibrium establishes rapidly as shown in Figure 3.1(b). This is generally achieved with pressures of A and B in the mtorr (1 to 10 mtorr) range.

For all reactions measured checks were made of the invariance of K_1 with total pressure of the gas mixture, at a constant ratio of the partial pressures of A and B. Figure 4.1 shows, for three electron transfer reactions as an example of such invariance of K_1 with total pressure in the ion source. The equilibrium constant for every reaction was measured at 2 to 3 different P_A / P_B ratios. It was made sure that equilibrium constant K_1 is invariant of the ratio of the partial pressures A and B, and only those equilibrium constants which were independent of partial pressure ratios were used to evaluate the electron affinities and other thermochemical quantities for A and B.

Since the majority of the electron transfer reactions proceeded with rate constants which are near Langevin-ADO collision limit, equilibria (1.1) for those reactions were achieved within a very short time, generally 0.1 - 0.3 ms after the application of the electron pulse (Figure 3.1).

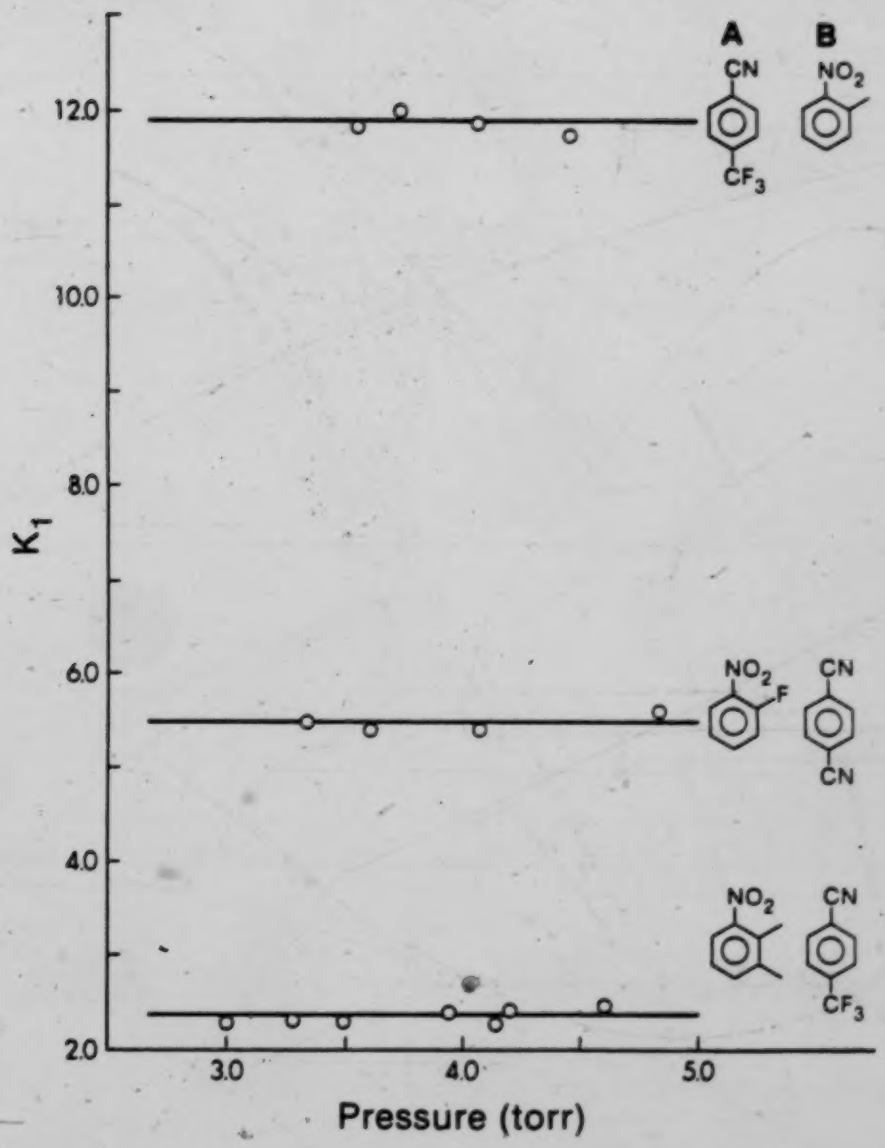

Figure 4.1. Tests of invarience of equilibrium constants K_1 with changing pressure of bath gas and pressure of A and B at constant P_A/P_B.

This was generally the case for compounds such as, SO_2, NO_2, $MeNO_2$, substituted aromatics; naphthalenes, cyanoethylenes etc. However, as discussed in the previous chapter (chapter 3), the rate constants for electron transfer reactions (3.5) involving SF_6 become immeasurably small for small exothermicities (see Table 3.6). So equilibrium for reaction (3.5) could not be achieved within the observation time, with the concentration range used for majority of the molecules at low exothermicities. To overcome this difficulty, one must use compounds B with sufficiently high electron affinities, such that, the exothermicities are large (see Table 3.6) and simultaneously boost the reverse rate by using very large concentration of SF_6. Fortunately such conditions are accessible with high pressure mass spectrometric technique. SF_6 is introduced as the major carrier gas at pressures up to 6.0 torr, while the partial pressure of B is kept in the mtorr range. The ion-intensity time dependence plots shown in Figure 4.2 illustrate this type of experiment. The intensity time dependence in plot A shows the signals in pure 5.0 torr SF_6. The SF_6^- produced by third body electron capture and SF_5^- from dissociative electron capture reaction (4.1) are observed to decrease very slowly with time.

$$SF_6 + e \rightarrow [SF_6^-]^* \rightarrow SF_5^- + F \qquad (4.1)$$
$$\underset{\longrightarrow}{[M]} \; SF_6^-$$

This decrease is due to diffusion of ions to the walls of the ion-source. The plot in Figure 4.2B shows the kinetic stage and achievement of equilibrium with B = 4-CNNB. In the first 0.2 ms the $(4\text{-CNNB})^-$ is seen to increase due to electron transfer from SF_6^-. The decrease in SF_6^- is observed due to log plot used, over a much longer period (~ 1.0 ms). Then the intensities of two ions become equidistant which means that the ion intensity ratio has become constant with time, that is, equilibrium has been reached. The SF_5^- ion showed no reactive changes. The plot

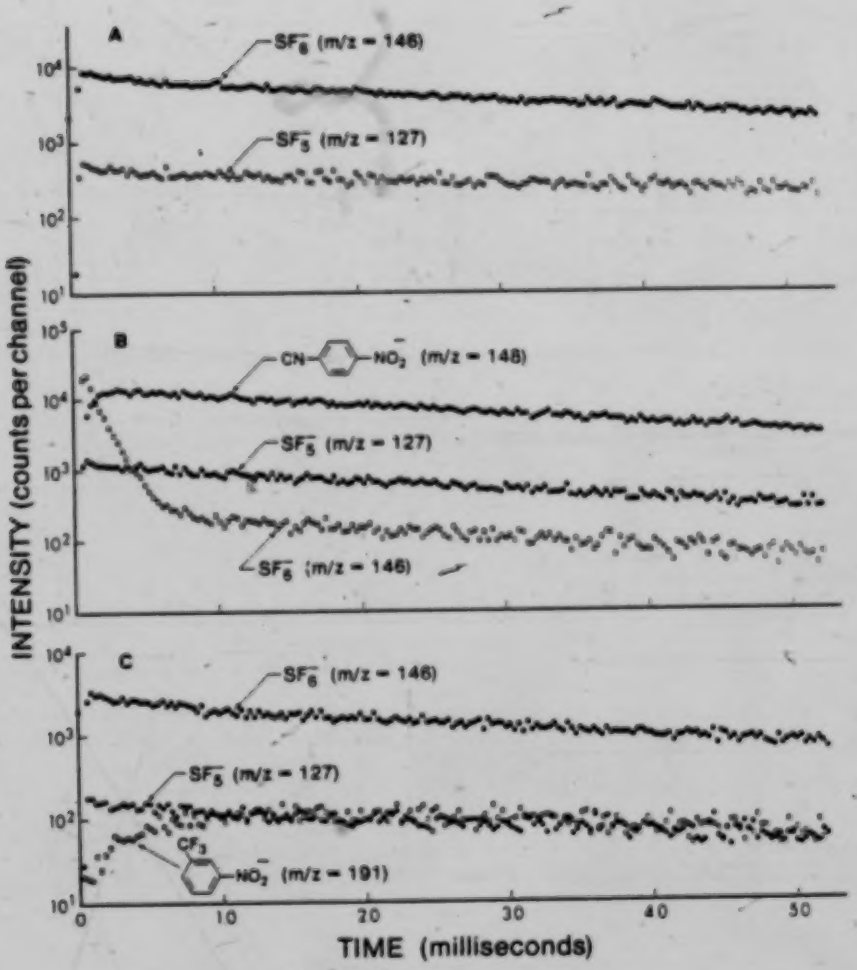

Figure 4.2. Measurement of electron transfer equilibria $SF_6^- + B = SF_6 + B^-$. (A) Neat SF_6 at 5.0 torr. SF_6^- and SF_5^- decay only due to diffussional losses at 150°C. (B) SF_6 at 5.0 torr, B = 4-CNNB at 5.0 mtorr. Equilibrium is reached after ~0.8 ms, T = 150°C. (C) SF_6 at 5.0 torr, B = 3-CF_3NB at 9.9 mtorr, at 122°C.

in Figure 4.2C shows the reactive changes and the achievement of equilibrium for B = 3-CF_3NB. The invariance of the measured equilibrium constants K_1 with the pressure of B and pressure of SF_6 is shown in Figure 4.3. Only a few compounds B had electron affinities in the appropriate range. They are 4-CNNB, 1,3-dinitrobenzene, and 3-CF_3NB and measurements with three of these were obtained. The results in terms of ΔG_1^0 will be shown in next section, in this chapter.

The electron transfer reaction with $CF_3C_6F_{11}^-$ was also slow (Table 3.6) and the equilibrium constants for electron transfer from this ion were measured in a similar way as was done for measurements involving SF_6^-. The intensity time dependence observed in one such experiment, where B = 3-CF_3NB is shown in Figure 4.4. The $CF_3C_6F_{11}^-$ and 3-CF_3NB^- ion required whole 6.0 ms to reach equilibrium i.e., a constant ion intensity ratio. Two slower side reactions leading to $C_7F_{13}^-$ (m/z =331) and $C_7F_{13}O^-$ (m/z = 347) occurred also. They were observed to have no effect on the electron transfer between $CF_3C_6F_{11}^-$ and 3-CF_3NB^-.

The electron transfer equilibria measurements involving C_6F_6 were also difficult for several reasons. As we will see shortly (section 4.2) it has low electron affinity and therefore, thermal electron detachment (loss of electron from the negative ion : $A^- \rightarrow A + e$) from $C_6F_6^-$ occurred at 150°C, a temperature at which most single temperature runs were made. The problem was more serious for the measurements of the temperature dependence of the electron transfer equilibria invoving C_6F_6. Thus the van't Hoff plots could not be extended to high temperatures, where the detachment becomes more rapid than the electron transfer equilibria. The detachment problem was partially overcome by using reference compounds whose EA is larger than C_6F_6 and thus have minimum electron detachment. The equilibria were also operated for neutral ratios where $C_6F_6^-$ was the minor ion and the reference negative ion was the major ion. Furthermore, because of the high electron affinity of the reference compounds, a large pressure ratio of hexafluorobenzene to the reference compound could be used, and this combined with the use of relatively large partial pressures of both compounds leads to efficient recapture of detached electrons by reattachment to hexafluorobenzene and the reference compounds. Results obtained under such conditions are shown in Figure 4.5.

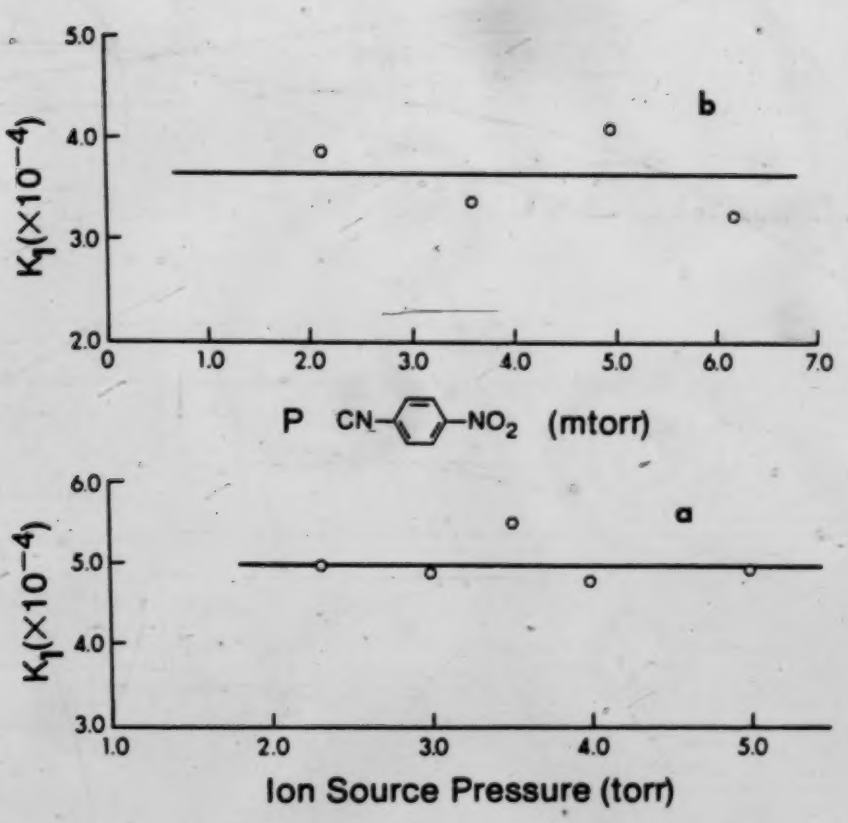

Figure 4.3. Tests of invarience of equilibrium constant of the reaction SF_6^- + 4-CNNB = SF_6 + 4-CNNB$^-$ at 160°C; (a) with ion source pressure, (b) with the pressure of 4-CNNB.

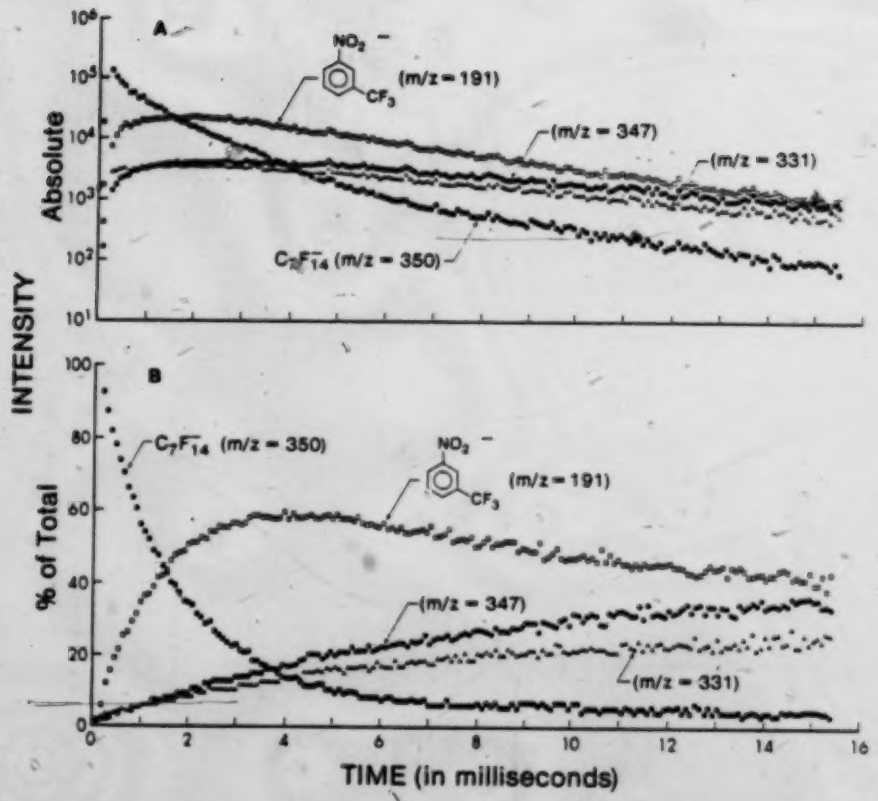

Figure 4.4. Intensity changes observed in equilibria measurement of the reaction $C_7F_{14}^-$ + 3-CF_3NB = C_7F_{14} + 3-CF_3NB$^-$. Equilibrium is reached after ~6.0 ms. Two slower side reactions leading to $C_7F_{13}^-$, m/z = 331 and $C_7F_{13}O^-$, m/z = 347 occur also. In such a run ion source contains C_7F_{14}, 3.0 torr; 3-CF_3NB, 4.3 mtorr at 175°C.

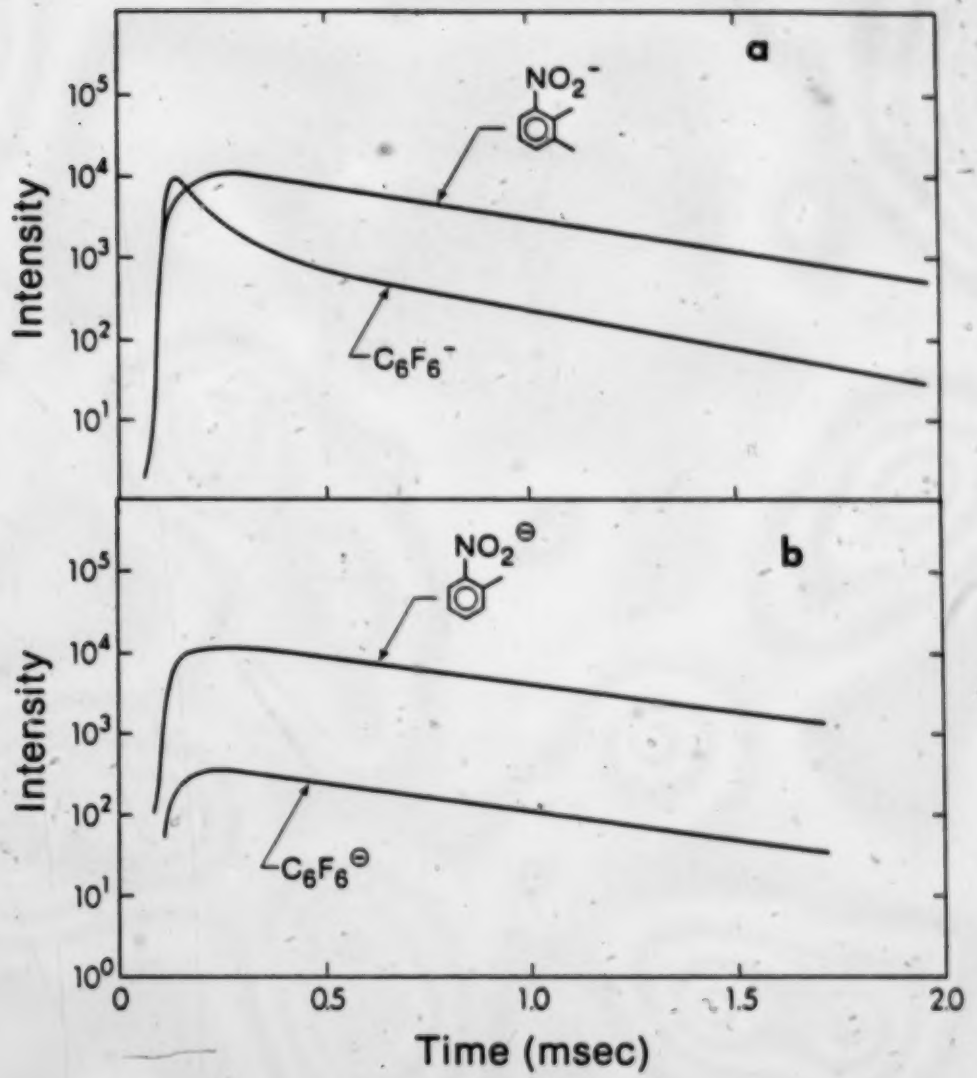

Figure 4.5. Time dependence of intensities observed after ionising pulse. (a) The ion source is at 116°C, contains 4.5 torr of methane, 0.12 mtorr 2,3-diMeNB and 14.0 mtorr of C_6F_6 gases. After a short kinetic stage both ions reach their equilibrium intensities. (b) T = 152°C, methane = 4.0 torr, C_6F_6 = 49.0 mtorr and 2-MeNB = 4.8 mtorr. Ions reach equilibrium more rapidly than in case (a) due to the higher concentrations of reactants.

Another difficulty was the observed occurrence of side reactions in the presence of traces of oxygen (~ 0.05 mtorr). Traces of oxygen lead to production or increase of intensities of the following ions of m/z: 152($C_5F_4O^-$), 171($C_5F_5O^-$), 183($C_6F_5O^-$), 205($C_6F_6.F^-$), 272($C_{10}F_8^-$), etc. A minor leak in the gas handling plant of the instrument leads to the presence of oxygen at 0.1 mtorr level. These reactions were still too slow to affect the results of electron transfer equilibria.

For electron transfer reactions involving hexafluorobenzene and other perfluorobenzene compounds, it was examined whether the equilibrium constant K_1 remains invariant with the the changing of total pressure and changing partial pressure ratio $\{P_B / P_A\}$. Examples of such measurements are shown in Figure 4.6. The results in Figure 4.6 indicate the reliability of the present investigation involving perfluorobenzenes.

4.1.2 Scales of ΔG_1^0, ΔS_1^0, and ΔH_1^0

Equilibrium constants from runs like those shown in Figures 3.1, 4.2, 4.4, 4.5 etc. lead to ΔG_1^0 values using equation (1.16).

$$- RT\ln K_1 = \Delta G_1^0 \qquad (1.16)$$

Separate measurements of such ΔG_1^0 values using different partners A and B which interconnect lead to a free energy ladder (or scale) shown in Figures 4.7, 4.8 and 4.9. The consistency in ΔG_1^0 values is better than ± 0.1 kcal/mol as can be seen in Figures 4.7 and 4.8. However, consistency in ΔG_1^0 measurements in reactions involving tetracyanoethylene (TCNE), SF_6, $CF_3C_6F_{11}$, C_6F_6 and other perfluorobenzenes was not as good as was observed in case of majority of the molecules studied and shown in Figures 4.7 and 4.8. The ΔG_1^0 values for electron transfer reactions involving TCNE and other perfluoro molecules are shown in Figure 4.9, drawn in a scale, such that the relatively poor consistency obtained in case of these

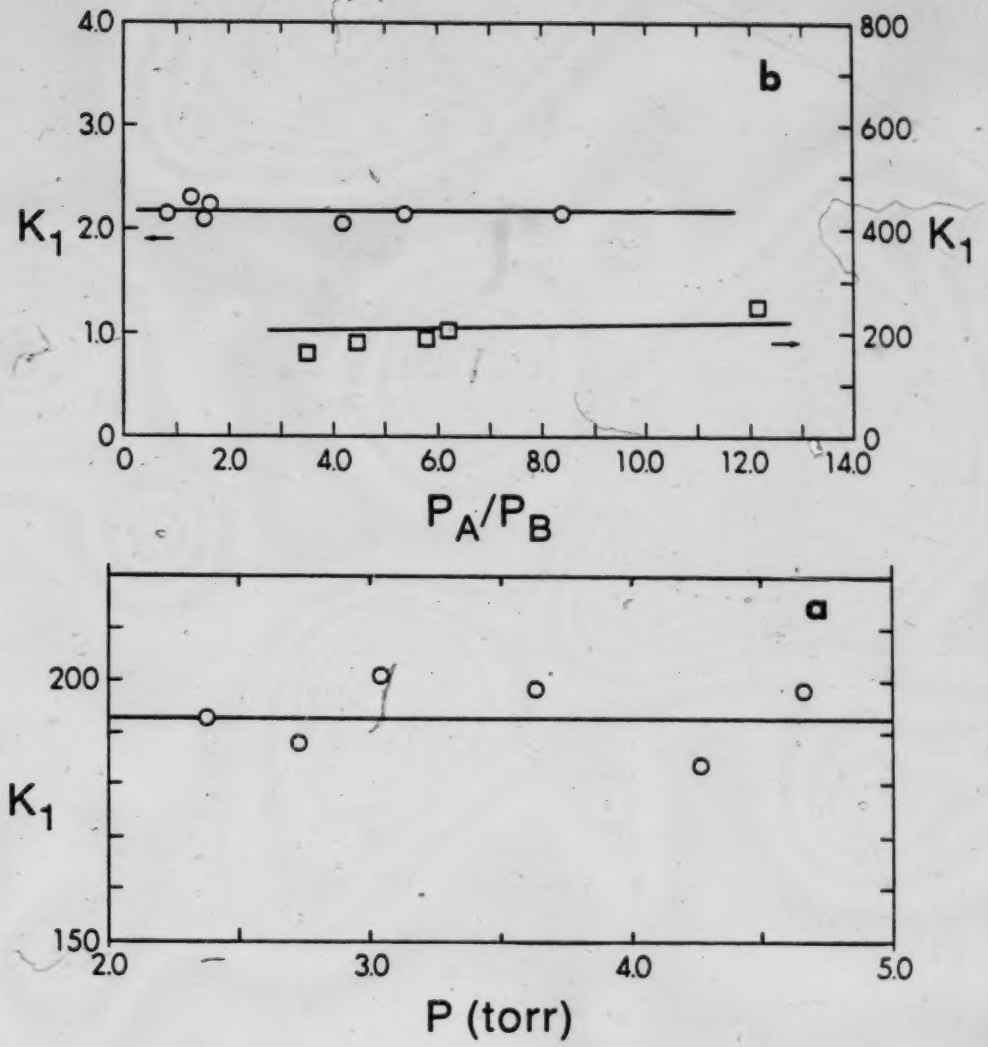

Figure 4.6. (a) Invariance of equilibrium constant K_1 with the pressure in the ion source for reactions of $C_6F_6^-$ at 150°C and at a constant pressure ratio of hexafluorobenzene and 2,3-diMeNB = 5.8. (b) Invariance of equilibrium constant K_1 with P_A/P_B ratios of (O) C_6F_5CN and 3-FNB, (□) C_6F_6 and 2,3-diMeNB.

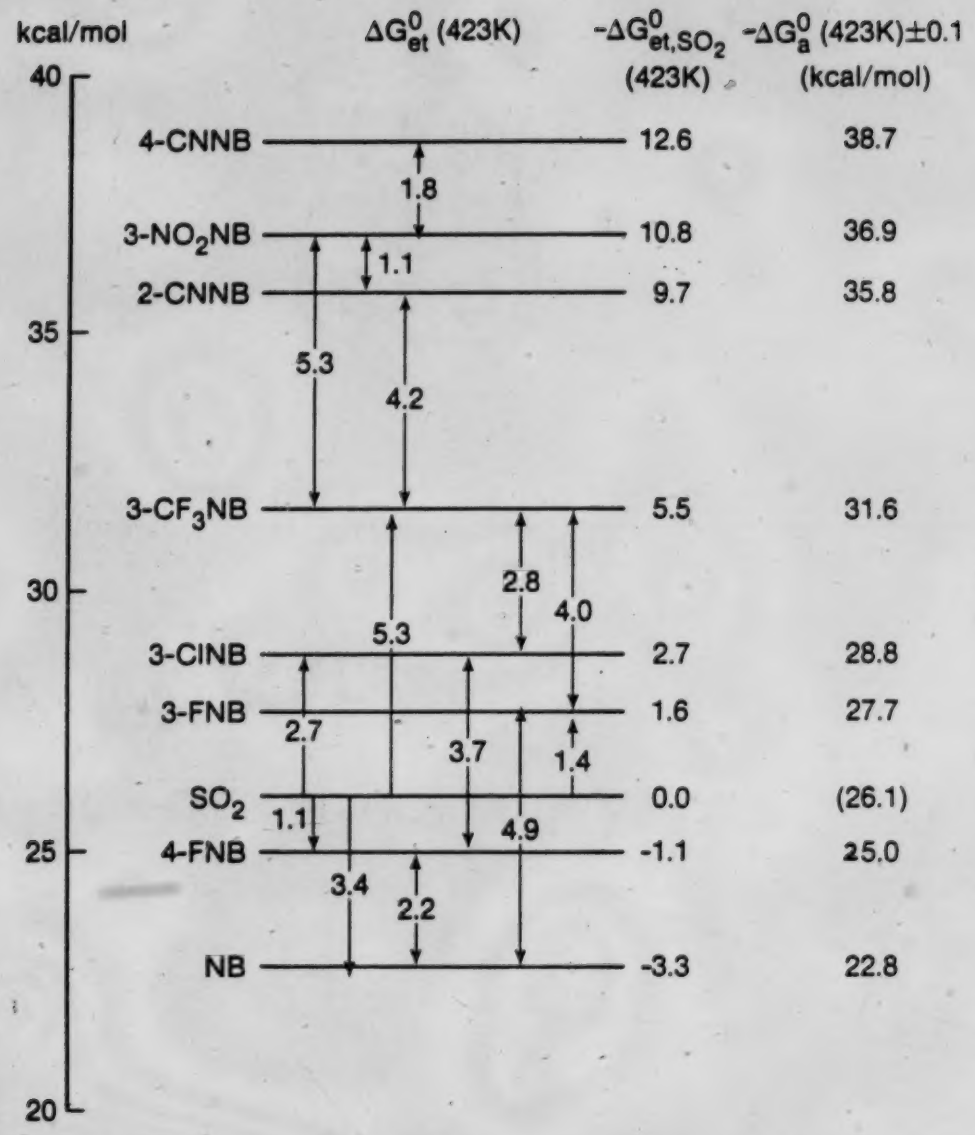

Figure 4.7. Ladder of free energy changes ΔG^0_1 at 423K obtained from equilibrium constant K_1 for reaction (1.1) $A^- + B = A + B^-$. The ΔG^0_1 values are given between double arrows connecting A and B for each equilibrium measured at 150°C. $\Delta G^0_{et,SO_2}$ is the free energy change corresponding to reactions where B = SO_2 and A = other molecules. ΔG^0_a in the right most column corresponds to free energy change for electron capture of a stationary electron: $A + e \rightarrow A^-$. $-\Delta G^0_a(SO_2)$ = 26.1 kcal/mol can be evaluated from the literature value (ref. 61) $EA(SO_2)$ = 25.3 kcal/mol. Therefore, free energy change for electron attachment to other molecules which are part of the ladder were obtained.

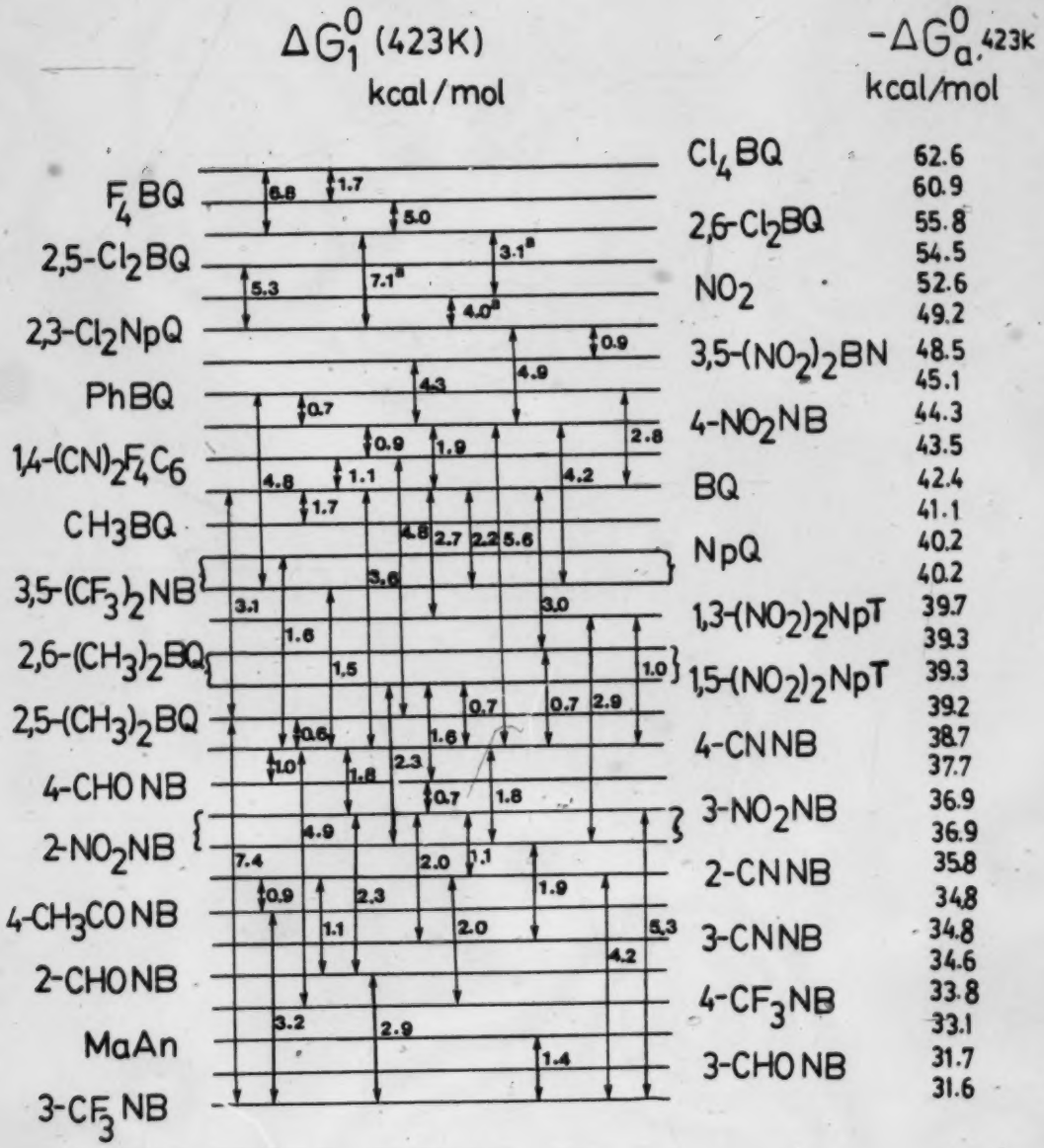

Figure 4.8. Shown are free enrgy changes ΔG_1^0 for all compounds except, perfluoro-compounds obtained in the present investigation. ΔG_a^0 of some reference molecules established in Figure 4.7, are used to obtain ΔG_a^0 for all other molecules which are part of this continuous ladder. All equilibria, unless otherwise indicated are measured at 150°C; (a) 215°C, (b) 80°C.

Figure 4.8 continued.

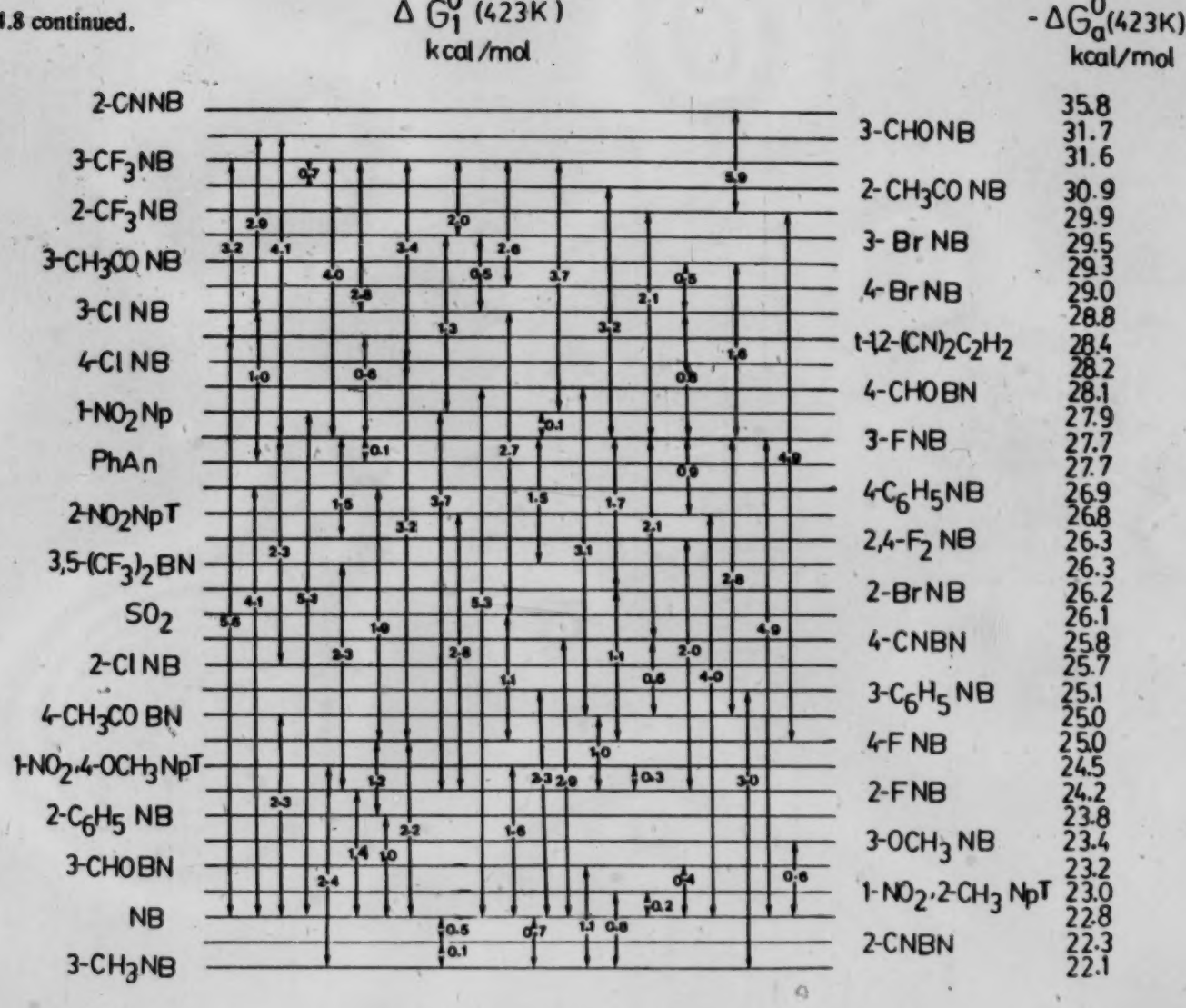

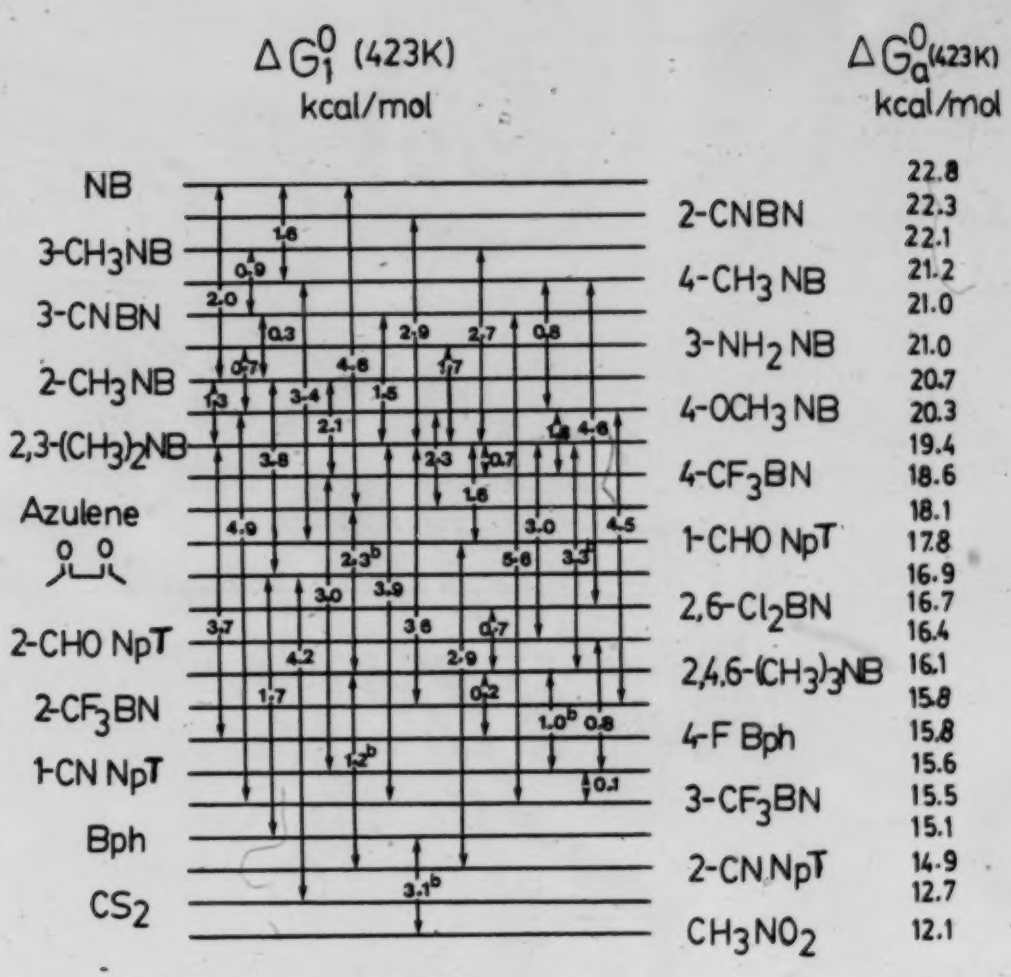

Figure 4.8 continued.

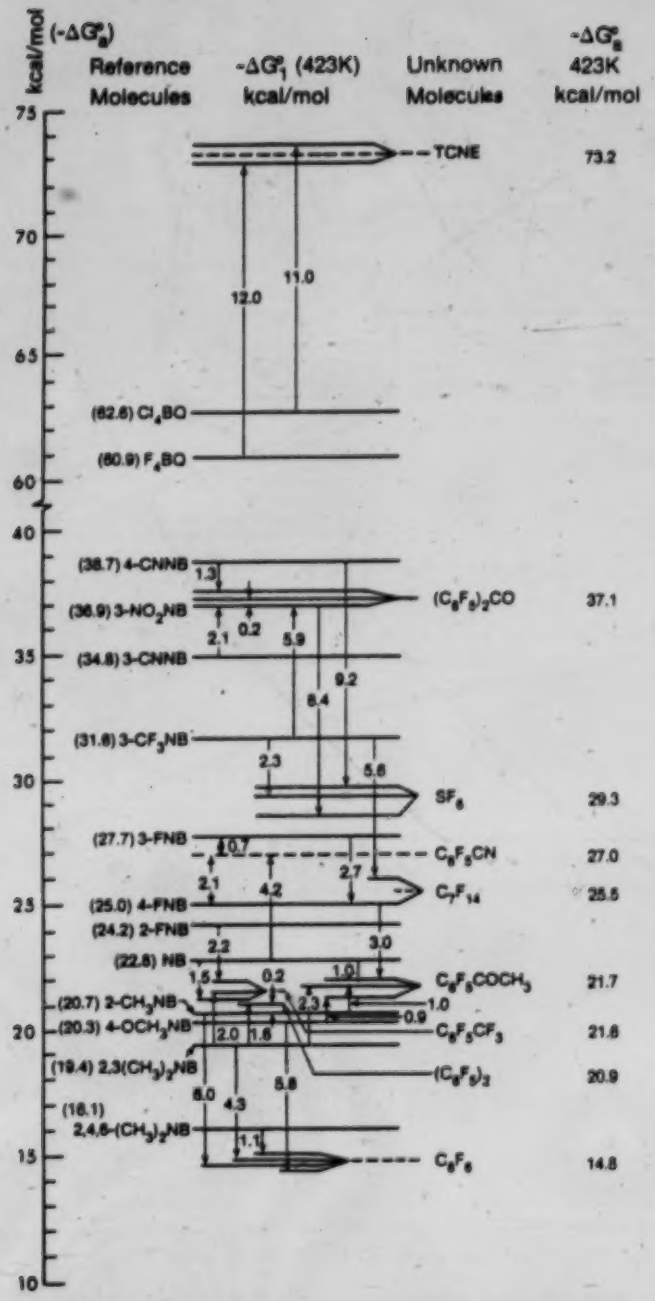

Figure 4.9. Free energy change scale for electron transfer reaction (1.1) involving TCNE and other perfluorocompounds for which internal consistency in free energy changes obtained was not as good as was the case for other molecules studied and shown in Figures 4.7 and 4.8. The ladder is drawn in scale, such that the relatively poorer consistency is visible. These values could also be incorporated in the continuous ladder of Figure 4.8, but was not done.

compounds are clearly visible.

The reason for relatively less consistency obtained and problems encountered in case of perfluoro molecules are discussed in the previous section. However, the reason for obtaining poor consistency in reactions involving TCNE is a different one. TCNE has very high electron affinity, see Figure 4.9 and therefore, no suitable molecule in the appropriate elctron affinity range were available to use as partner A to measure equilibrium constant K_1. The measurements therefore had to be done with tetrafluoro- and tetrachlorobenzoquinone, molecules of highest electron affinity available and the reactions were of very high exothermicity. The Figure 4.10 shows such an unusual experiment between TCNE and F_4BQ^- with an exothermicity of 12.0 kcal/mol. This required a large concentration ratio ([A]/ [B]) as experimentally possible (ratio used ≈ 240), which could be achieved only by using low concentrations of B(=TCNE). The low [B] slows down the achievement of equilibrium (1.1). A larger ion residence time was achieved by using SF_6 as bath gas. It's high mass slows down the diffusion of the ions to the walls and permits to observe ions over longer period (Figure 4.10).

The equilibrium constants K_1 for a given A, B pair can be measured at different temperatures and the enthalpy change, ΔH_1^0 and the entropy change, ΔS_1^0 can be obtained from van't Hoff plots and equation (1.17). The van't Hoff plots obtained from the measurement

$$\Delta G_1^0 = \Delta H_1^0 - T\,\Delta S_1^0 \qquad (1.17)$$

of the temperature dependence of the electron transfer equilibria (1.1) are given in Figures 4.11 through 4.18. The ΔH_1^0 and ΔS_1^0 data deduced from such plots and connected in ΔH_1^0 and ΔS_1^0 ladders are shown in Figures 4.19 through 4.22. ΔG_1^0 measurements were performed with ninety three (93) molecules shown in Figures 4.8 and 4.9. Since the van't Hoff plot determinations are time consuming, van't Hoff plots for some forty eight electron transfer reactions were performed only in the present investigation. The results from van't Hoff plot measurements are given in table 4.1.

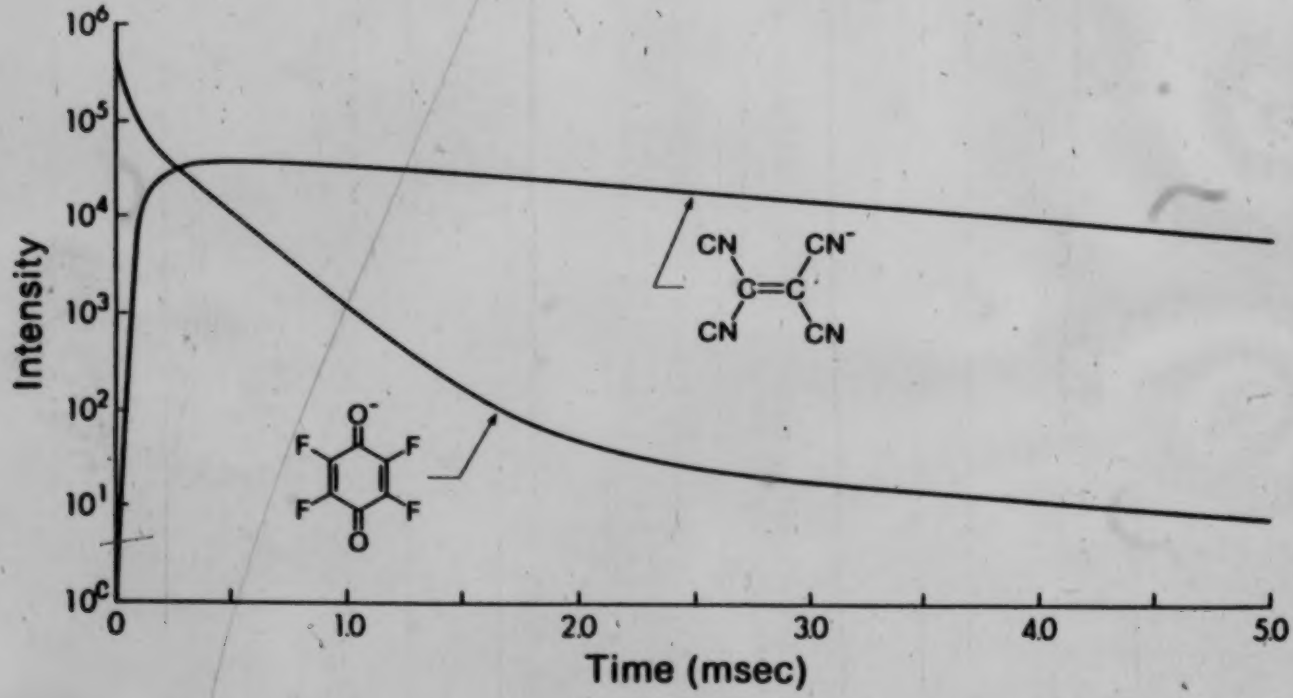

Figure 4.10. Shown are log of ion intensities of $TCNE^-$ and F_4BQ^- obtained after an ionising electron pulse. Initial linear logerithmic decay of fluoranil negative ion is due to the electron transfer to TCNE. TCNE stands for tetracyanoethylene. Reaction reaches equilibrium after ~3.0 ms. SF_6 at 3.4 torr was used as bath gas with 40.5 mtorr of tetrafluorobenzoquinone and 0.17 mtorr of TCNE at 235°C.

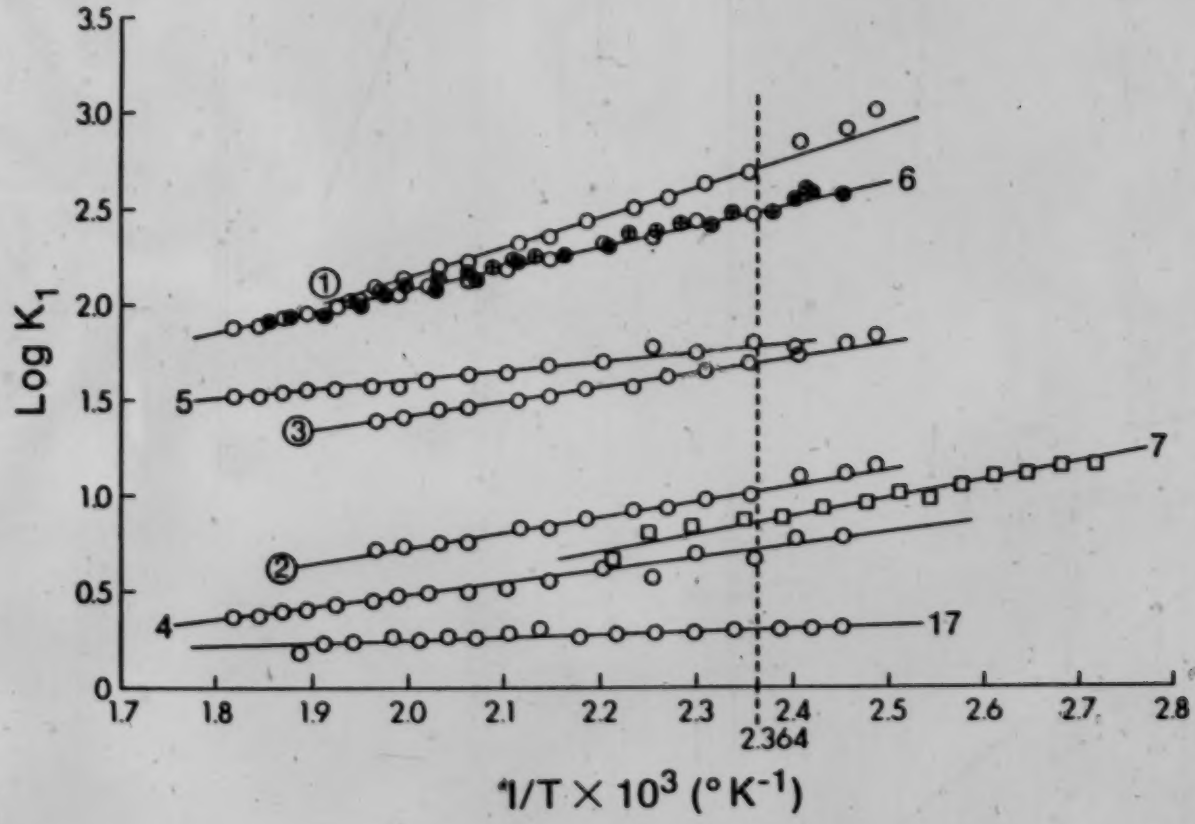

Figure 4.11. van't Hoff plots of equilibrium constants for reaction (1.1): $A^* + B \rightleftharpoons A + B^*$. Numbers beside plots identify reactions given in the Table 4.1. Three sets of experimental points for reaction (6), Table 4.1, illustrate the reproducibility obtained in three measurements separated by two months on the same instrument.

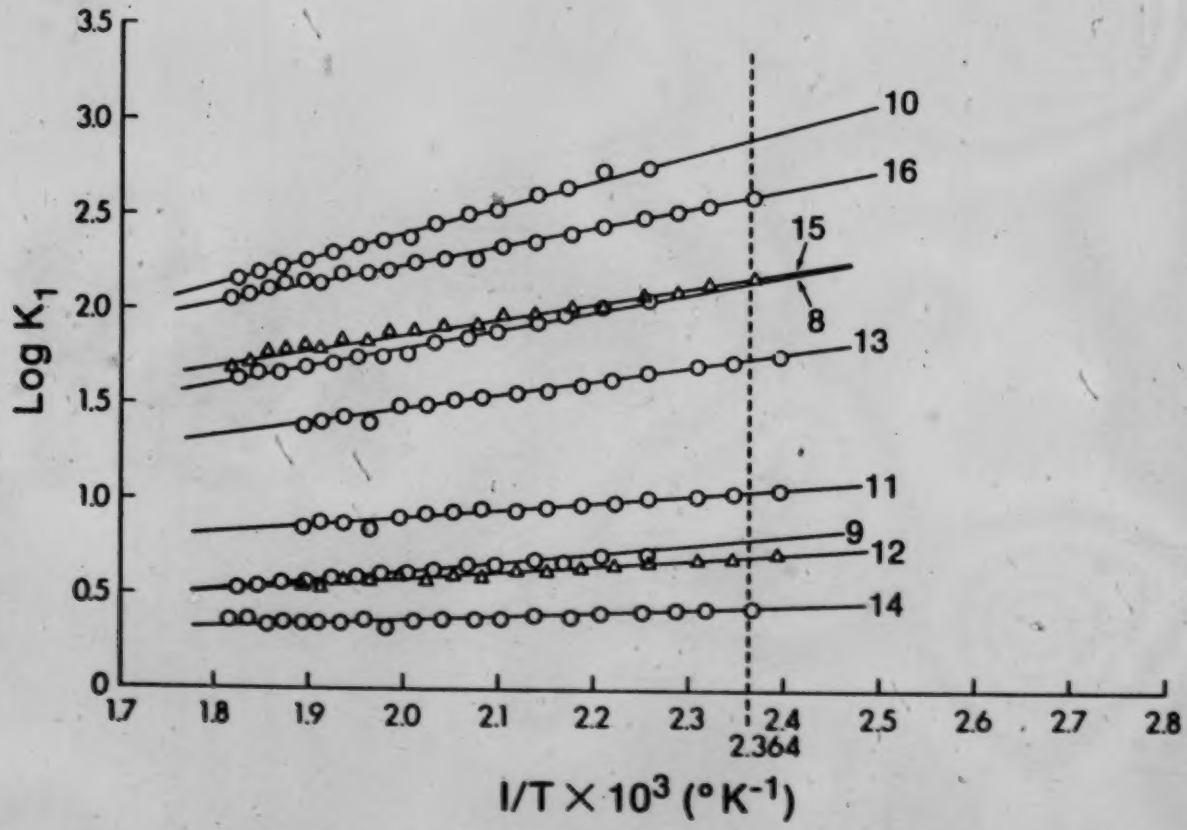

Figure 4.12. van't Hoff plots of equlibrium constants K_1. Numbers beside identify reactions in Table 4.1.

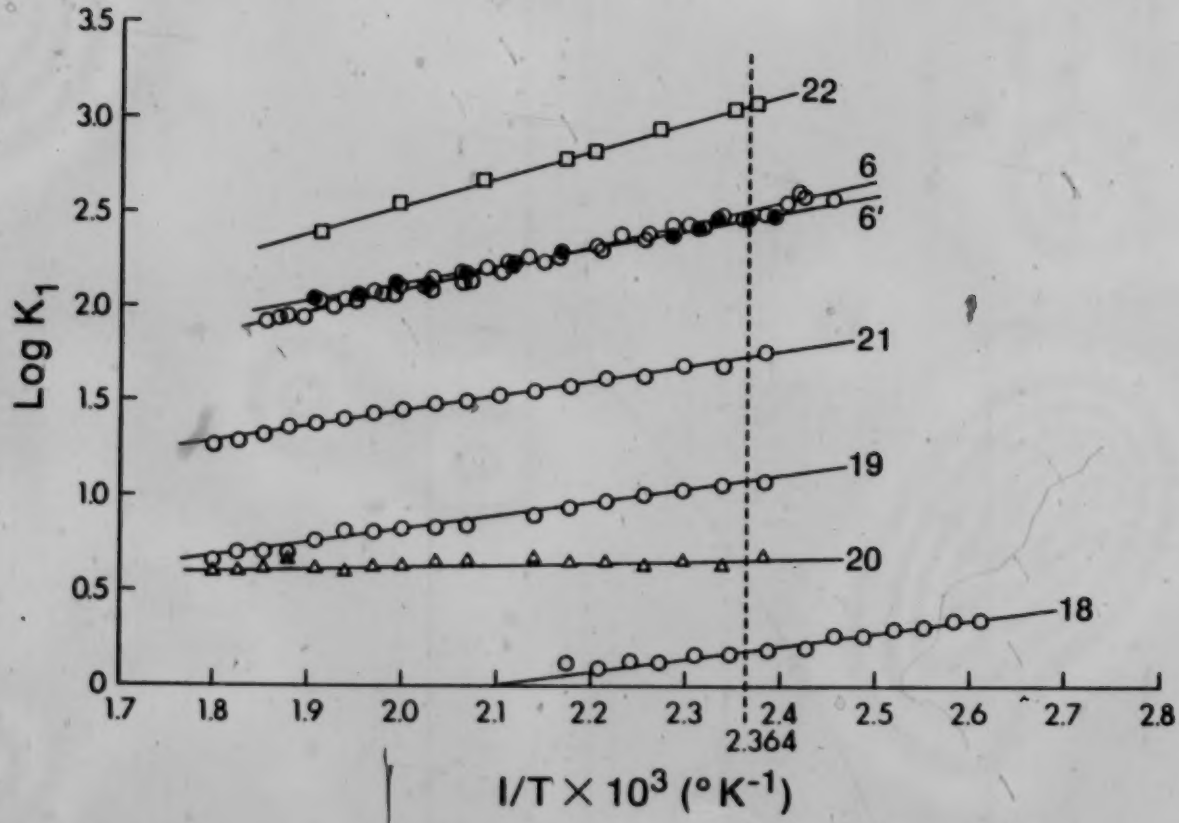

Figure 4.13. van't Hoff plots of equilibrium constants K_1. Numbers beside plots identify the reactions in Table 4.1. As a cross check, reaction 6, Table 4.1 was redetermined by a different investigator with a different instrument of similar design. O, data from instrument on which all other measurements were performed and reported in the present investigation; ●, data from the second instrument by a different investigator.

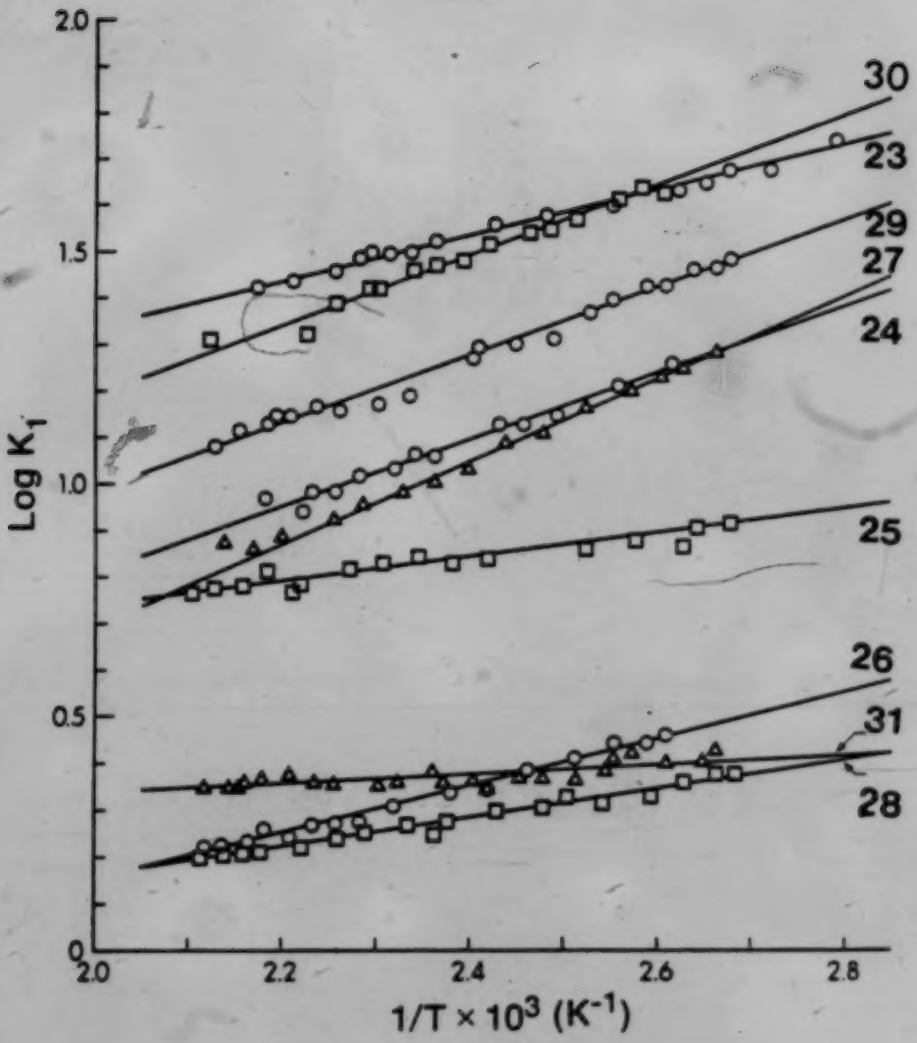

Figure 4.14. van't Hoff plots of equilibrium constants of the electron transfer reaction (1.1). Numbers beside plots identify reactions in Table 4.1.

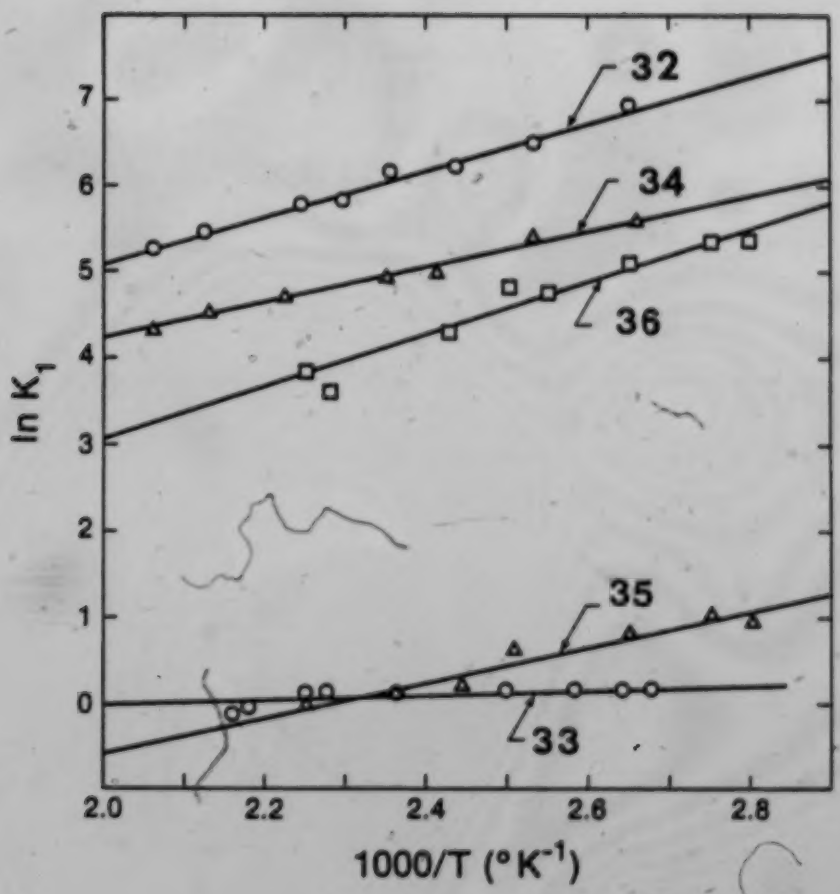

Figure 4.15. van't Hoff plots of equilibrium constants of the electron transfer reaction (1.1). Numbers beside plots identify reactions in Table 4.1.

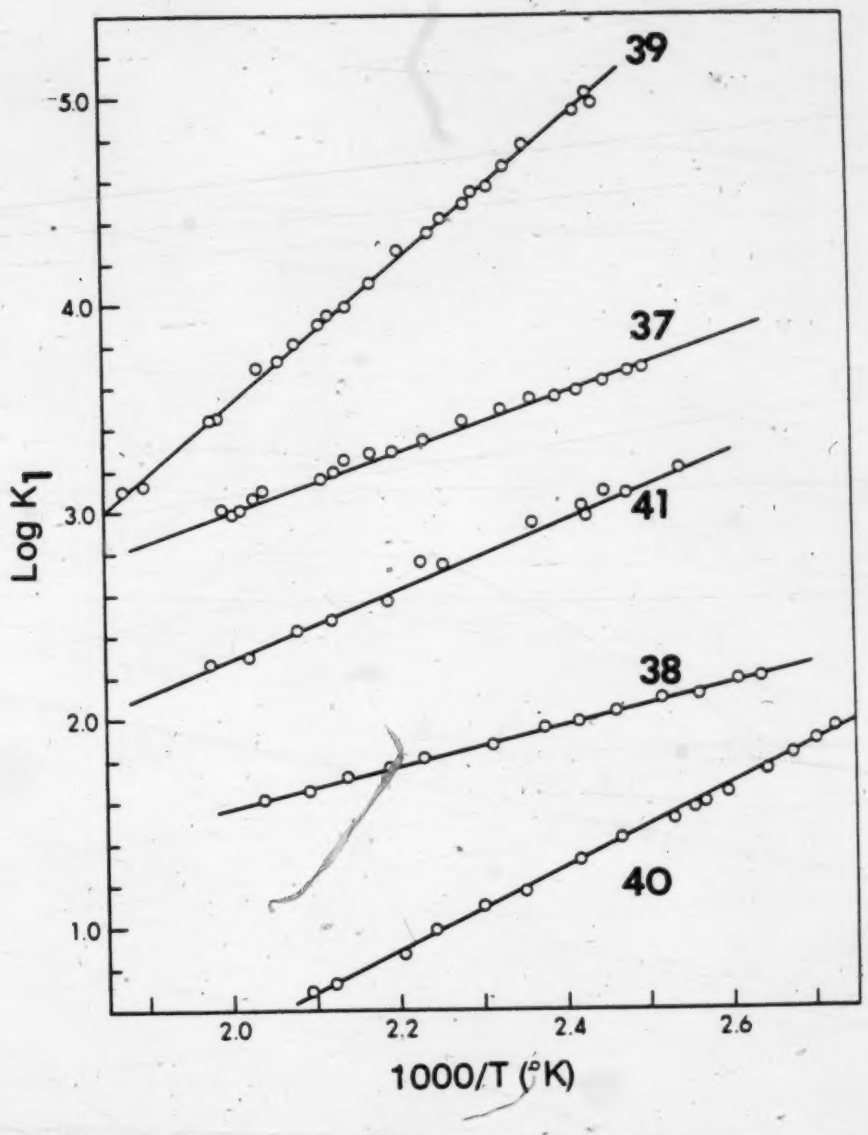

Figure 4.16. van't Hoff plots of equilibrium constants of the electron transfer reaction (1.1). Numbers beside plots identify reactions in Table 4.1.

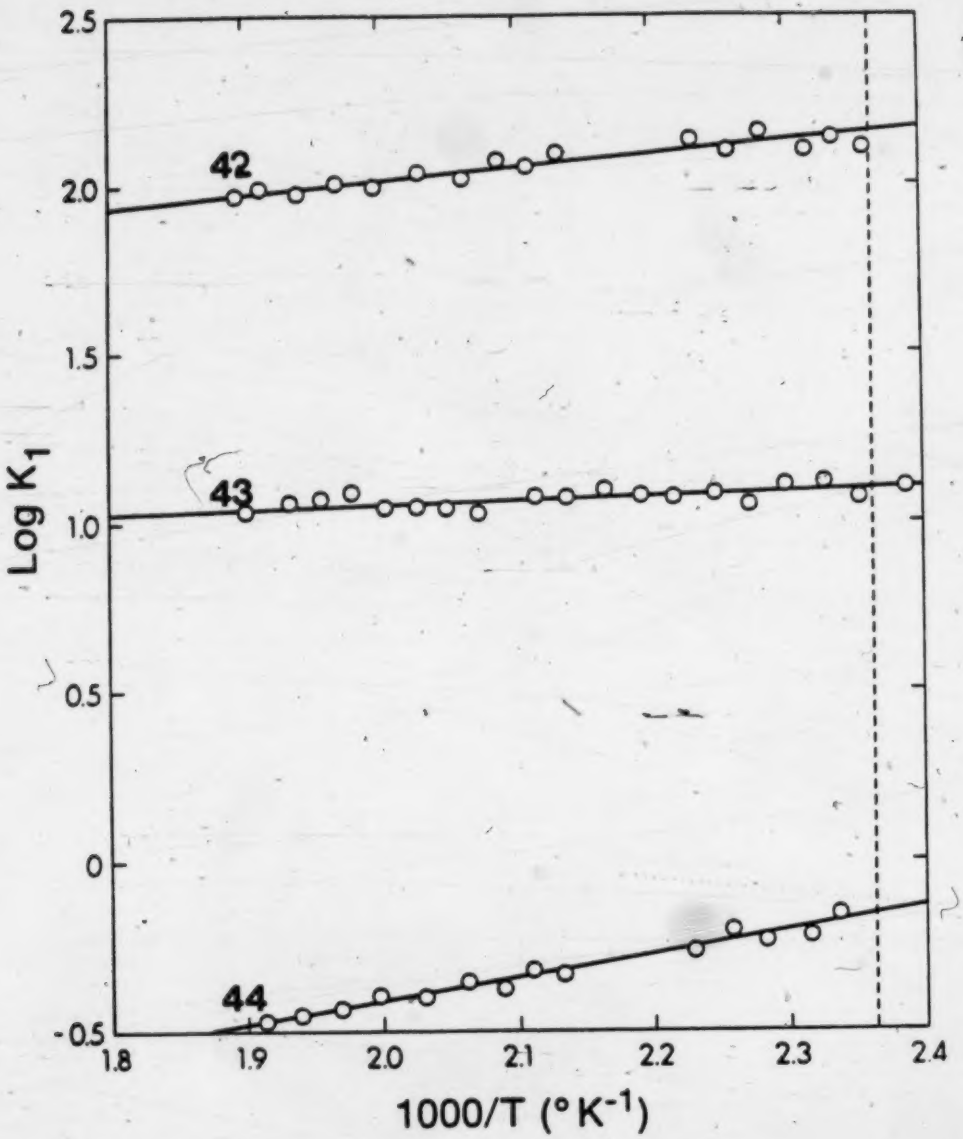

Figure 4.17. van't Hoff plots of equilibrium constants of the electron transfer reaction (1.1). Numbers beside plots identify reactions in Table 4.1.

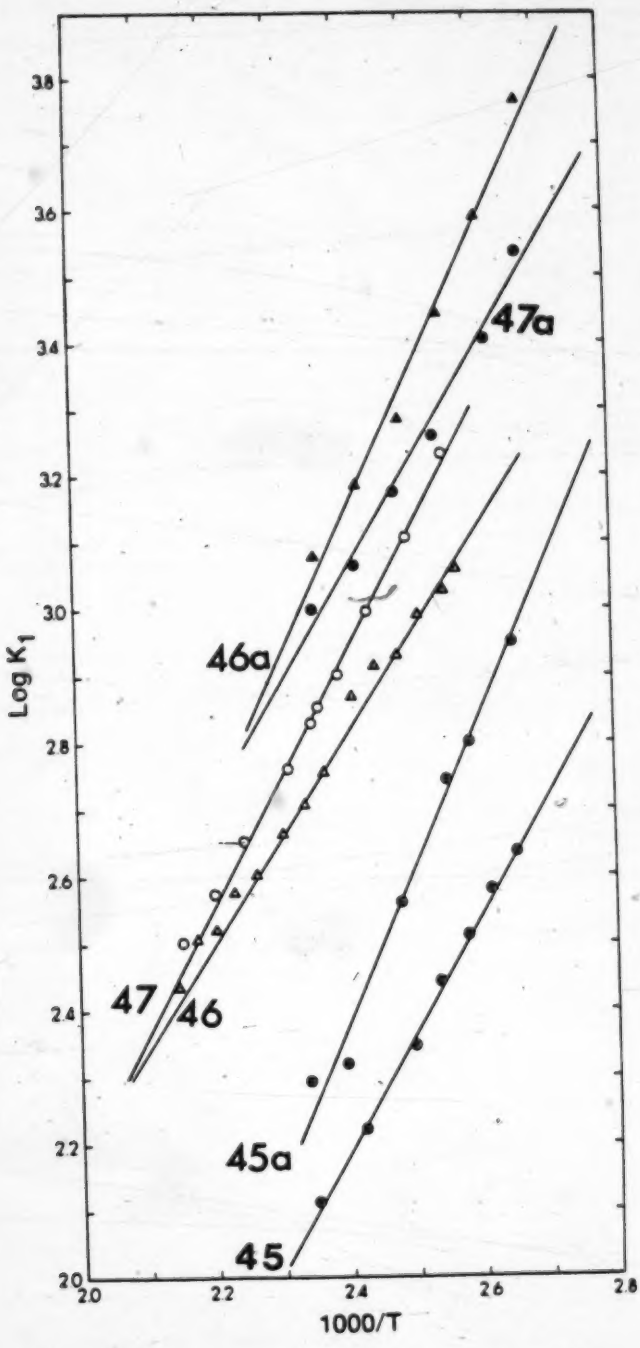

Figure 4.18. van't Hoff plots of equilibrium constants of the electron transfer reaction (1.1). Numbers beside plots identify reactions in Table 4.1. The numbers 45a, 46a and 47a in the figure represent the same reactions 45, 46, and 47 respectively, but are based on experiments with a different instrument of similar design, performed by a different investigator. Agreement between two sets of determinations is much poorer than is commonly obtained with systems not involving C_6F_6 (see text).

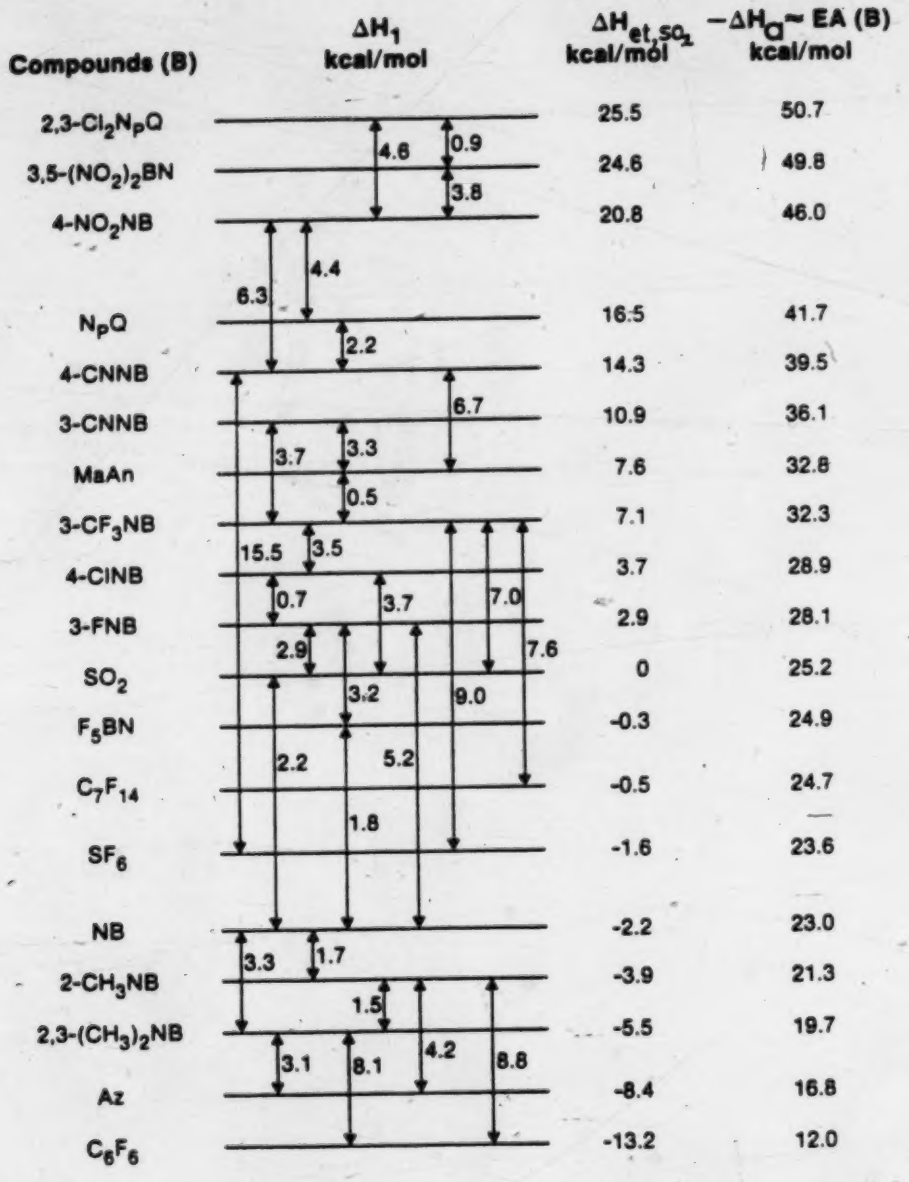

Figure 4.19. Ladder for ΔH_1^0 changes from van't Hoff plots (Table 4.1 and Figures 4.11 to 4.18). $\Delta H^0_{et,SO_2}$ corresponds to reaction $A^- + SO_2 = A + SO_2^-$. $\Delta H_a^0(A)$ is the enthalphy change for the reaction $e + A = A^-$ at 423K.

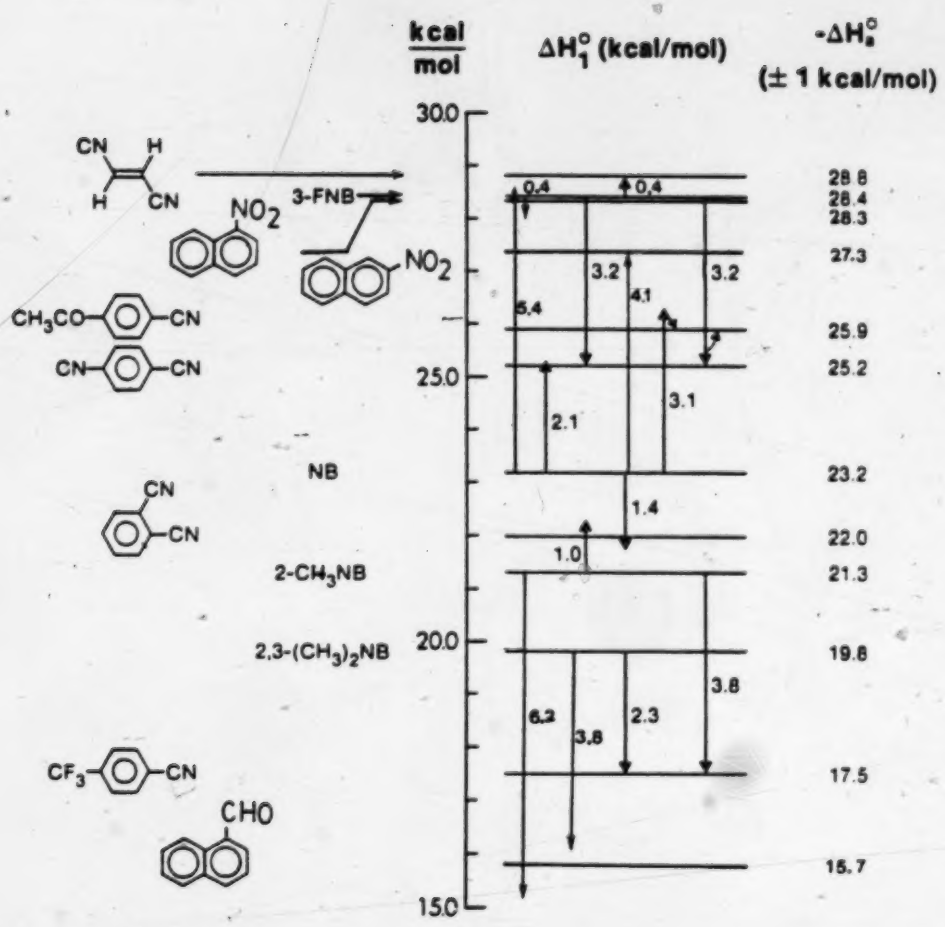

Figure 4.20. An additional ladder for ΔH^0_1 changes obtained from van't Hoff plots (Table 4.1). These results could be incorporated into the Figure 4.19, but was not done so to avoid crowding in the figure.

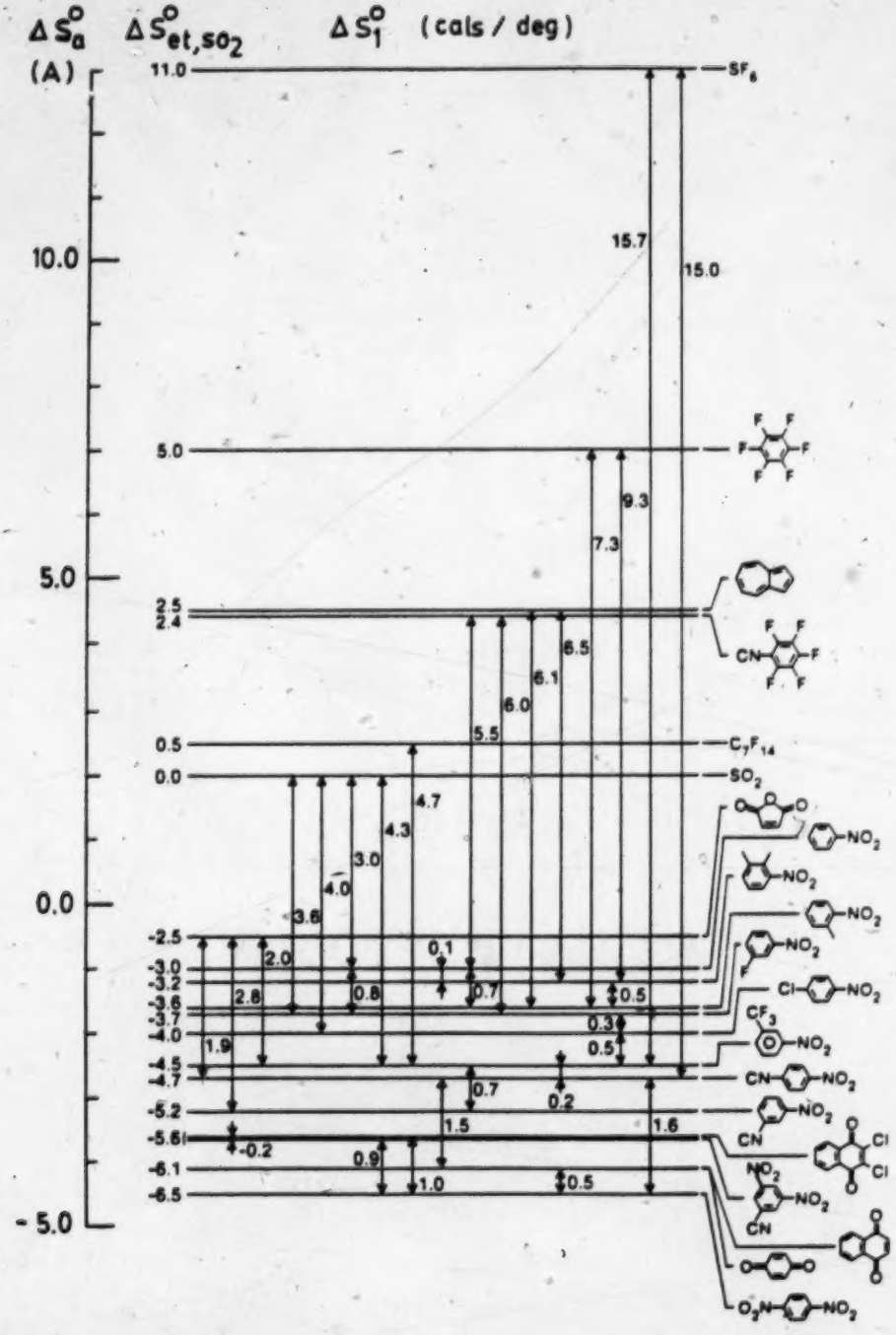

Figure 4.21. Ladder for ΔS^0_1 changes from van't Hoff plots (Table 4.1 and Figures 4.11 to 4.18). $\Delta S^0_{et,SO_2}$ corresponds to reaction $A^- + SO_2 = A + SO_2^-$. $\Delta S^0_a(A)$ is the entropy change for the reaction $e + A = A^-$ at 423K.

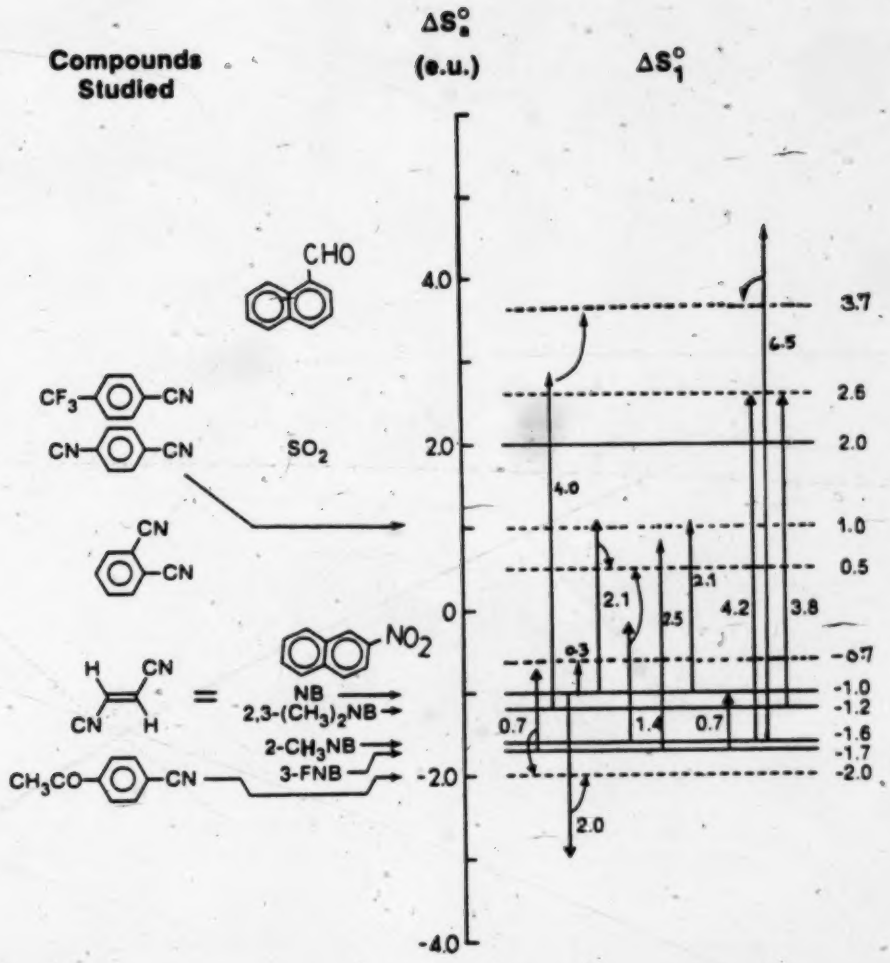

Figure 4.22. An additional ladder for ΔS^0_1 changes obtained from van't Hoff plots (Table 4.1). These results could be incorporated into the Figure 4.21, but was not done so to avoid crowding in the figure.

Table 4.1:[a,b] ΔG^0_1(423K), ΔH^0_1 and ΔS^0_1 values for electron transfer reactions (1.1): $A^- + B = A + B^-$ from van't Hoff plots.

	A[c]	B[c]	$-\Delta G^0_1$(423K)	ΔS^0_1	$-\Delta H^0_1$
1	SO_2	3-CF_3NB	5.3(6.2)	-4.3(-1.4)	7.0(6.8)
2	SO_2	4-ClNB	2.0(3.0)	-4.0(-3.6)	3.7(4.6)
3	4-ClNB	3-CF_3NB	3.3	-0.5	3.5
4	SO_2	3-FNB	1.4	-3.6	2.9
5	NB	SO_2	3.4(2.7)	3.0(3.0)	2.2(1.4)
6	NB	3-FNB	5.0(4.7)	-0.9(1.1)	5.9(4.3)
7	Az	2-CH_3NB	1.7	-6.1	4.2
8	NpQ	4-NO_2NB	4.1	-0.6	4.4
9	4-CNNB	NpQ	1.5	-1.5	2.2
10	4-CNNB	4-NO_2NB	5.6	-1.6	6.3
11	2-CH_3NB	NB	2.0(3.6)	0.7(1.8)	1.7(2.9)
12	2,3-diCH_3NB	2-CH_3NB	1.4	-0.4	1.5
13	2,3-diCH_3NB	NB	3.4	0.1	3.3
14	3,5-diNO_2BN	2,3-diClNpQ	0.9	-0.2	0.9
15	4-NO_2NB	3,5-diNO_2BN	4.2	0.9	3.8
16	4-NO_2NB	2,3-diClNpQ	5.0	1.0	4.6
17	3-FNB	4-ClNB	0.6	-0.3	0.7
18	Az	2,3-diCH_3NB	0.4	-6.5	3.1
19	MaAn	3-CNNB	2.1	-2.8	3.3
20	3-CF_3NB	MaAn	1.3	2.0	0.5
21	3-CF_3NB	3-CNNB	3.3	-0.8	3.7
22	MaAn	4-CNNB	5.9	-1.9	6.7
23	NB	4-CNBN	2.9	2.0	2.1
24	4-CNBN	3-FNB	2.1	-2.5	3.2
25	2-CH_3NB	2-CNBN	1.2	1.4	1.0
26	4-CF_3BN	2,3-diCH_3NB	0.7	-3.8	2.2
27	4-CF_3BN	2-CH_3NB	2.1	-4.2	3.8
28	2-CNBN	NB	0.5	-2.1	1.4
29	NB	4-CH_3COBN	2.3	-2.1	3.3
30	4-CH_3COBN	3-FNB	2.8	-1.0	3.2
31	3-FNB	DCNE	0.7	0.7	0.4
32	NB	1-NO_2NpT	5.1	-0.7	5.4
33	1-NO_2NpT	3-FNB	0.2	-1.8	0.4
34	NB	2-NO_2NpT	4.0	0.3	4.1
35	1-CHONpT	2,3-diCH_3NB	1.6	-3.9	3.8
36	1-CHONpT	2-CH_3NB	2.9	-6.5	6.2

37	3-CF_3NB	4-CNNB	7.0	-0.2	6.8
38	4-CNNB	BQ	3.6	-1.5	4.3
39	SF_6[d]	4-CNNB	9.2	-15.0	15.5
40	SF_6[d]	3-CF_3NB	2.3	-15.7	9.0
41	$CF_3C_6F_{11}$[e]	3-CF_3NB	5.6	-4.7	7.6
42	NB	C_6F_5CN	4.2	5.5	1.8
43	4-FNB	C_6F_5CN	2.1	3.7	0.6
44	C_6F_5CN	3-FNB	0.7	6.0	3.2
45	C_6F_6	2,3-diCH_3NB	4.1(4.3)	-9.3(-14.2)	8.1(10.4)
46	C_6F_6	4-CH_3ONB	5.3(5.8)	-5.0(-4.7)	7.4(7.8)
47	C_6F_6	2-CH_3NB	5.5(6.0)	-7.7(-9.4)	8.8(9.9)
48	C_6F_6	2,4,6,-tri-CH_3NB	1.1	-8.1	4.1

[a]Results from van't Hoff plots from Figures 4.11 to 4.18. Energy values are in kcal/mol and entropy values are in cals/deg; standard state 1.0 atm.

[b]The values in bracketts are obtained to check the present measurements in a different instrument of similar design, performed by a different investigator, in our laboratory.

[c]Abbreviations used are: NB = nitrobenzene, BN = benzonitrile, Az = Azulene, BQ = 1,4-benzoquinone, NpQ = 1,4-Naphthoquinone, MaAn = maleic anhydride, NpT = naphthalene, and DCNE = trans-1,2-dicyanoethylene

[d,e]These measurements were carried out with SF_6 and $CF_3C_6F_{11}$ as bath gas respectively.

The numbers beside the van't Hoff plots (Figures 4.11 to 4.18) identify reactions given in Table 4.1. Three sets of experimental points are shown in Figure 4.11 for reaction 6 in Table 4.1 involving nitrobenzene negative ion, NB^- and 3-FNB. The three sets of data are for measurements performed separated by two months and after the replacement of the slit of the ion source. The reproducibility of the measurements is good. The same reaction was investigated, as a cross check by a different investigator in a different instrument of similar design. The results indicated as 6' are shown in Figure 4.13 together with the data from the present investigation (#6). The second set of data did not show a good degree of internal consistency and the ΔS_1^0 determinations for the same system in the two sets of experiments were found to differ by 1-2 cal/deg with occasionally even larger disagreements. The worst situation is encountered for reactions involving C_6F_6, as shown in Figure 4.18. The plots 45a, 46a, and 47a represent the same reactions 45, 46, and 47 respectively but performed by a different investigator on a different instrument mentioned earlier. The relatively poorer reproducibility observed in Figure 4.18 compared to that generally found for other systems is probably partly due to electron detachment problem and side reactions of C_6F_6 with trace oxygen. The data given in brackets in the Table 4.1 are from the experiments performed as a check by the different investigator from our laboratory.

4.1.3 Electron Affinities and Other Thermochemical Quantities: ΔH_a^0, ΔS_a^0, and ΔG_a^0 for Electron Attachment Reaction

Once the ΔG_1^0, ΔH_1^0, and ΔS_1^0 values are obtained, one can construct the scales of ΔG_1^0, ΔH_1^0, and ΔS_1^0 as shown in Figures 4.7-4.9, 4.19-4.22. The determinations of these quantities are superfluous and lead to multiple thermodynamic cycles, indicating the consistency of the data. For example in Figure 4.7, ΔG_1^0 for electron transfer from 3-CF_3NB^- to 2-CNNB is - 4.2 kcal/mol, that from 2-$CNNB^-$ to 1,3-dinitronitrobenzene is - 1.1 kcal/mol; while a direct measurement from 3-CF_3NB^- to 1,3-dinitronitrobenzene gives - 5.3 kcal/mol {= (- 4.2) + (- 1.1)}. However, consistency in ΔH_1^0 and ΔS_1^0 is not in all cases as good as ΔG_1^0 values, as can be

seen in Figures 4.19, 4.20, 4.21 and 4.22. Multiple cycles show an average consistency for enthalpy changes better than 1.0 kcal/mol and entropy changes better than 2.0 cals/deg.

Absolute electron affinities can be obtained by anchoring the enthalpy (ΔH_1^0) and free energy (ΔG_1^0) scales to the electron affinity of one compound whose absolute electron affinity is established in the literature from other experimental measurements. As pointed out earlier we chose the electron affinity of SO_2 as such standard in the present investigation. The electron affinity of SO_2 has been determined by Hall and coworkers[61] from electron photodetachment measurements. There are several other experimental measurements of the electron affinity of SO_2 from different techniques[49,51,62,64-65] which are within ±0.1 eV to the value 1.097±0.1 eV provided by Hall[61]. In addition to the above fact, SO_2 being a small molecule, vibrational frequencies and geometries of SO_2 and SO_2^- are available from experimental measurements and theoretical calculations, which can be utilized to calculate electron attachment entropy, ΔS_a^0(equation (1.2)) to SO_2 in order to calibrate the ΔS_1^0 ladder. NO_2 could also be used as a standard, but measurements involving NO_2 is complicated by many side reactions as will be discussed in chapter 6. These advantages made SO_2 an unique standard for obtaining absolute thermochemical quantities, such as ΔG_a^0, ΔS_a^0, and ΔH_a^0 for all other molecules from ΔG_1^0, ΔS_1^0, and ΔH_1^0 scales. Data for the vibrational frequencies and geometries of SO_2 and SO_2^- are summarized in Table 4.2.

From ΔG_1^0, ΔS_1^0, and ΔH_1^0 ladders one can evaluate first $\Delta G_{et,SO_2}^0$, $\Delta S_{et,SO_2}^0$, and $\Delta H_{et,SO_2}^0$ changes via equation (4.2) for electron

$$SO_2^- + A = SO_2 + A^- \qquad (4.2)$$

transfer from SO_2^- to compounds A, as shown in Figures 4.7, 4.19, and 4.21. The thermodynamic cycle (4.3) then can be used to connect the enthalpy changes, $\Delta H_{et,SO_2}^0$ at 0 K which corresponds to the exact adiabatic electron affinity difference to the measured ΔH_1^0 values at a given T. To complete the cycle one requires the heat capacities of

Table 4.2 Entropy (ΔS_a^0) and enthalpy (ΔH_a^0) change for reaction: $e + SO_2 = SO_2^-$ at 423K[a]

	SO_2	SO_2^-
O-S-O angle	120° 119°[b]	113.8°[b]
r_{S-O} (A)	1.432 1.416[b]	1.497[b]
ν_1 (cm^{-1})	1150.5, 1361[b]	984.8[c], 1131[b], 961[d]
ν_2	525, 597[b]	495.6[c], 513[b], 436[d]
ν_3	1336, 1561[b]	1040[c], 1232[b], 1047[d]

$\Delta H_a^0 = \Delta H_f^0(SO_2^-) - \Delta H_f^0(SO_2) = -25.3$ kcal/mol at 0 K (Hall, ref. 61)

$\Delta H_a^0(423\ K) = \Delta H_a^0(0\ K) + \Delta H_a^0(vib)_T = (-25.3 + 0.1)$ kcal/mol $= -25.2$ kcal/mol at 423 K

$\Delta S_a^0(SO_2) = S^0(SO_2^-) - S^0(SO_2) = \Delta S_a^0(rot) + \Delta S_a^0(vib) + \Delta S_a^0(spin) = 0.25 + 0.35 + 1.38 = 2.0$ cals/deg.

$\Delta G_a^0(423\ K) = \Delta H_a^0 - T\,\Delta S_a^0 = -26.1$ kcal/mol

[a]Data for SO_2 except where otherwise mentioned, from Herzberg (ref. 107).

[b]Data from SAC-CI calculation due to Hirao (ref. 108)

[c]Data from Milligan (ref. 109) in solution.

[d]Hirao frequencies for SO_2^- reduced by 15%.

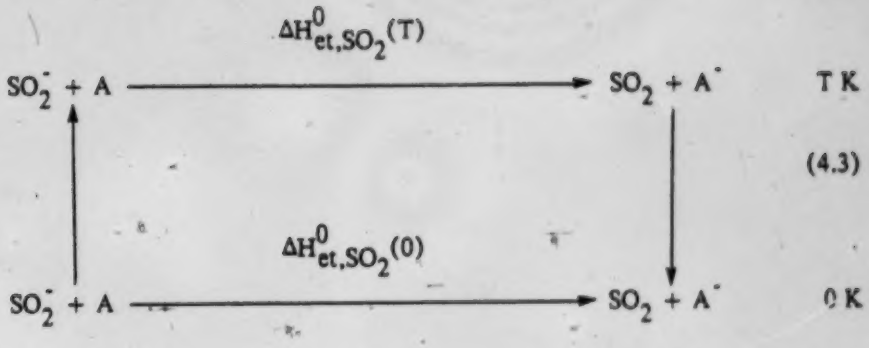

SO_2, SO_2^-, A and $A^\cdot$. In general one expects that the heat capacities of the neutral molecule and the negative ion will be quite similar, such that a cancellation occurs and $\Delta H^0_{et,SO_2}$(0 K) and $\Delta H^0_{et,SO_2}$ (298 K) will differ by less than 1.0 kcal/mol. Heat capacities for most of the negative ions are not available, however, for SO_2 using the data from Table 4.2 one can evaluate the change in electron attachment energy to SO_2, $\delta\Delta H^0_a(SO_2)$ between 0 K and 423 K to be only 0.1 kcal/mol.

This evaluation can be done with the fomal cycle (4.4), to obtain energy for electron detachment from SO_2^-, ΔH^0_d (= - ΔH^0_a).

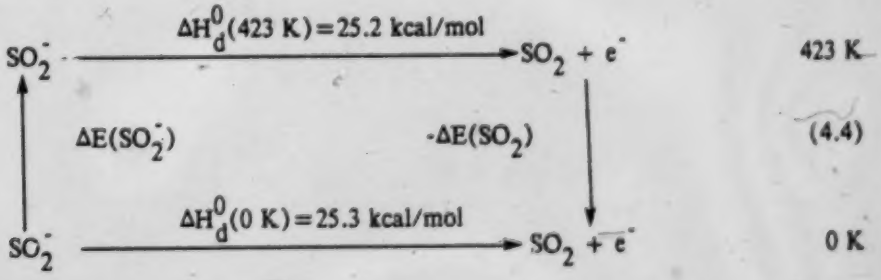

We used the stationary electron convention[110-112], in which the translational thermal energy of the electron is neglected. Stull and Prophet[113] however have used the thermal electron convention. The stationary electron convention is used here, only in order not to add to the

confusion.

From the cycle (4.4) one can deduce equations (4.5).

$$\Delta H_d^0(SO_2)(423\ K) = EA(SO_2) - \Delta E(SO_2^-) + \Delta E(SO_2) \qquad (4.5)$$
$$= EA(SO_2) + \Delta E_{rot}(SO_2) - \Delta E_{rot}(SO_2^-) + \Delta E_{vib}(SO_2)$$
$$- \Delta E_{vib}(SO_2^-) + \Delta E_{trans}(SO_2) - \Delta E_{trans}(SO_2^-)$$

Since $\Delta E_{trans}(SO_2)$ and $\Delta E_{trans}(SO_2^-)$; $\Delta E_{rot}(SO_2)$ and $\Delta E_{rot}(SO_2^-)$ are classical translational (3/2RT) and rotational energies (3/2RT), the values for SO_2 and SO_2^- thus cancel one another and equation (4.5) becomes (4.6).

$$\Delta H_d^0(423\ K) = EA(SO_2) + \delta\Delta E_{vib}(SO_2^- \rightarrow SO_2)(423\ K) \qquad (4.6)$$

For electron attachment to SO_2: $SO_2 + e \rightarrow SO_2^-$, the equation (4.6) can be rewritten as (4.7). The $\delta\Delta E_{vib}$ for electron attachment to SO_2 can be calculated from the available information provided in Table 4.2.

$$\Delta H_a^0(SO_2)(423\ K) = \Delta H_a^0(SO_2)(0\ K) + \delta\Delta E_{vib}(SO_2 \rightarrow SO_2^-) \qquad (4.7)$$

Complete data for SO_2 are available in Herzberg[107]. Geometric information for SO_2^- are available from theoretical calculations due to Hirao[108]. Vibrational frequencies for SO_2^- are available from Milligan[109] obtained in the solution phase. Vibrational frequencies for SO_2^- are also calculated by Hirao[108]. However, they are uniformly too large by 15%, but when reduced by that amount, the frequencies (reduced) are in good agreement with those due to Milligan[109] (see Table 4.2).

By using the table of Einstein functions[114] expressed as a function of ν_0/T, where ν_0 is the fundamental vibrational frequency, the $\Delta S^0_a(vib)(SO_2)$ is calculated to be 0.34 cal/deg. Thus $\delta\Delta E_a(vib)(SO_2)$ = 0.1 kcal/mol at 423 K. Hence $\Delta H^0_a(SO_2)$ for electron attachment to SO_2 at 423 K was evaluated from the EA(SO_2) = 1.097 eV or 25.3 kcal/mol due to Hall[62], which corresponds to - $\Delta H^0_a(SO_2)$ at 0 K. The $\Delta H^0_a(SO_2)$ at 423 K is therefore, - 25.2 kcal/mol according to equation (4.7), see Table 4.2 also. The internal thermal energy change at 423 K is only 0.1 kcal/mol for SO_2 which makes the electron affinity at 0 K essentially identical with $-\Delta H^0_a(SO_2)$ at 423 K and 298 K(room temperature).

The value for $\Delta S^0_a(SO_2) = S^0(SO_2^-) - S^0(SO_2)$ is calculated to be equal to 2.0 cal/deg as shown in Table 4.2 from the evaluation of the rotational and vibrational entropies. The spin multiplicity change on electron capture (SO_2 is singlet, SO_2^- is doublet) is added also, but the spin multiplicity of the free electron is neglected. The ΔS^0_a was evaluated for 423 K but the change of ΔS with temperature is very small in the range 298-423 K. Since $\Delta H^0_a(SO_2)$ and $\Delta S^0_a(SO_2)$ is known, the $\Delta G^0_a(SO_2)$ at 423 K is readily calculated from the relation (1.17) which is equal to - 26.1 kcal/mol (see Table 4.2).

$$\Delta G^0_a = \Delta H^0_a - T\Delta S^0_a \qquad (1.17)$$

Since the spin multiplicity of the free electron is neglected, ΔH^0_a, ΔS^0_a, and ΔG^0_a thus refer actually to the formal change from A to A^-.

From the $\Delta X^0_a(SO_2)$ and $\Delta X^0_{et,SO_2}$ (where X = H, S, or G) one can evaluate absolute thermodynamic quantities for electron attachment to A (reaction (1.2)) with the help of equations (4.8) through (4.11).

$$\Delta X^0_a(A) = \Delta X^0_{et,SO_2} + \Delta X^0_a(SO_2) \qquad (4.8)$$

$$\Delta H^0_a(A) = \Delta H^0_{et,SO_2} + \Delta H^0_a(SO_2) \qquad (4.9)$$

$$\Delta S^0_a(A) = \Delta S^0_{et,SO_2} + \Delta S^0_a(SO_2) \qquad (4.10)$$

$$\Delta G^0_a(A) = \Delta G^0_{et,SO_2} + \Delta G^0_a(SO_2) \qquad (4.11)$$

Figures 4.7, 4.19, and 4.21 show such conversion of ΔG^0_1, ΔS^0_1, and ΔH^0_1 ladders to ΔG^0_a(423 K), ΔS^0_a, and ΔH^0_a values respectively for A molecules. The figures 4.19 and 4.20 (similarly Figures 4.21 and 4.22) could be amalgamated into one ΔH^0 (or ΔS^0) ladder, but in order to avoid crowding a second ladder was constructed. While the first ΔG^0 ladder (Figure 4.7) is constructed to obtain ΔG^0_a for some reference molecules by anchoring with $\Delta G^0_a(SO_2)$ and those ΔG^0_a(reference) values were used in the next ΔG^0 scales to determine ΔG^0_a for all A molecules provided in Figures 4.8 and 4.9 through multiple overlap cyclic measurements.

The thermochmical data thus obtained are given in Table 4.3. $\Delta H^0_a(A)$ and $\Delta S^0_a(A)$ of only 28 molecules are obtained by direct measurement of the van't Hoff plots i.e., the T-dependence of forty eight electron transfer equilibria (1.1). $\Delta S^0_a(NO_2)$ is calculated from the available geometries and vibrational frequencies from Lineberger[89] as is done for SO_2 and the $\Delta H^0_a(NO_2)$ is obtained through equation (1.17). For other molecules entropy of electron attachment is estimated from structural similarities with molecules for which ΔS^0_a is measured directly as indicated in the Table 4.3. Molecules for which estimation was not possible, $\Delta S^0_a(A) = 0$ is assumed, which means that $\Delta H^0_a(A) = \Delta G^0_a(A)$. As shown in Figures 4.21 and 4.22, ΔS^0_a values are generally within ± 3.0 cal/deg with the exception of perfluoro compounds. So the neglect of $\Delta S^0_a(A)$ for some A molecules in Table 4.3 will lead to an error of ± 1.3 kcal/mol or ± 0.05 eV to the EA values.

4.2 Discussion of Results Obtained from Electron Transfer Equilibria Measurements

The electron affinities and other thermochemical quantities such as, ΔH^0_a, ΔS^0_a, and ΔG^0_a(423 K) obtained from electron transfer equilibria measurements in the present investigation are provided in Table 4.3. Also given in Table 4.3 are the available EA values from the literature. As is shown in Table 4.3 in most cases a very good agreement, within ± 0.1 eV,

Table 4.3 Electron affinities and other thermochemical data[a] for electron attachment reaction (1.2): $A + e = A^-$.

Molecules	$\Delta S_a^0 \pm 2.0$ cals/deg	$-\Delta H_a^0$ kcal/mol	$= EA^b$ ±0.1 eV	Literature[c] EA, eV	$-\Delta G_a^0$(423K) kcal/mol
Triatomic					
NO_2	-0.82	53.0	2.30	2.36±0.1(LPD,89); 2.28±0.1(ECT,49); 2.28±0.025(LPD,115); ≥2.5±0.1(CI,42)	52.6
SO_2	2.0	25.2	1.09	1.097±0.036(PES,61); 1.05(ECT,51); 0.99±0.1(ECT,49); ≤1.0±0.1(PD,62)	26.1
CS_2	2.0[d]	11.8	0.51	0.50±0.2(ECT,49); 1.0±0.2(CI,43) 0.62±0.2(CI,116)	12.7
Polyatomic					
Nitromethane	2.0[d]	11.2	0.48	0.44±0.1(CI,44); 0.45±0.1(ECD,30)	12.1
trans-1,2-dicyanoethylene	-1.0	28.8	1.24		28.4
2,3-butanedione	2.0[d]	16.0	0.69	0.63± .05(ECD,30)	16.9
Tetracyanoethylene[e]	0.0[d]	73.0	3.17	2.3±0.3(PD,117); 2.9±0.1(CTS,29); 2.9(M,66)	73.0
Substituted benzenes					
2,4-difluoronitrobenzene	-1.7[d]	27.0	1.17		26.3
2-bromonitrobenzene	-1.6[d]	26.8	1.16(18)		26.2
3-bromonitrobenzene	-1.7[d]	30.2	1.32(21)		29.5

4-bromonitrobenzene	-2.0[d]	29.9	1.29(10)		29.0
2-chloronitrobenzene	-1.6[d]	26.3	1.14(17)		25.7
3-chloronitrobenzene	-1.7[d]	29.5	1.28(47)		28.8
4-chloronitrobenzene	-2.0	29.0	1.26(14)		28.2
2-fluoronitrobenzene	-1.6[d]	24.8	1.07(17)		24.2
3-fluoronitrobenzene	-1.7	28.4	1.23(28)		27.7
4-fluoronitrobenzene	-2.0[d]	25.8	1.12(10)		25.0
2-dinitrobenzene	-3.2[d]	38.2	1.65(463)	1.66(HWP,29); 1.06(CTS,29)	36.9
3-dinitrobenzene	-3.2[d]	38.2	1.65(537)		36.9
4-dinitrobenzene	-4.5	46.2	2.00(421)		44.3
Nitrobenzene	-1.0	23.2	1.01(40)	>0.8±0.2(ECD,30); ≥0.7±0.2(ECT,50)	22.8
3-nitroaniline	-2.0[d]	21.9	0.95(21)		21.0
2,6-dichlorobenzonitrile	+1.4[d]	16.1	0.72		16.7
3,5-dinitrobenzonitrile	-3.5	49.9	2.16		48.5
2-(α,α,α-trifluoromethyl)-nitrobenzene	-2.0[d]	30.8	1.33(200)		29.9
3-(α,α,α-trifluoromethyl)-nitrobenzene	-2.5	32.6	1.41(187)		31.6
4-(α,α,α-trifluoromethyl)-nitrobenzene	-2.5[d]	34.9	1.51(143)		33.8
2-nitrobenzonitrile	-3.2	37.1	1.61(209)		35.8
3-nitrobenzonitrile	-3.2[d]	36.1	1.56(315)		34.8
4-nitrobenzonitrile	-2.7	39.5	1.72(205)		38.7
2-nitrobenzaldehyde	-2.0[d]	35.5	1.54(395)		34.6
3-nitrobenzaldehyde	-2.0[d]	32.6	1.41(205)		31.7
4-nitrobenzaldehyde	-2.0[d]	38.6	1.67(47)		37.7
2-nitrotoluene	-1.6	21.3	0.92		20.7
3-nitrotoluene	-1.7[d]	22.8	0.99		22.1
4-nitrotoluene	-2.0[d]	22.0	0.95		21.2
3-methoxynitrobenzene	-1.7[d]	24.1	1.04		23.4
4-methoxynitrobenzene	-2.0[d]	21.1	0.91		20.3
3,5-di(α,α,α-trifluoromethyl)-					

nitrobenzene	-2.5[d]	41.2	1.79		40.2
2-(α,α,atrifluoromethyl)-benzonitrile	0.5[d]	16.1	0.70		15.8
3-(α,α,atrifluoromethyl)-benzonitrile	0.0[d]	15.5	0.67		15.5
4-(α,α,atrifluoromethyl)-benzonitrile	2.6	17.5	0.76		18.6
2-cyanobenzonitrile	0.5	22.0	0.95	1.11(M,66); 0.95(HWP,29)	22.3
3-cyanobenzonitrile	0.0	21.0	0.91	0.90(HWP,29)	21.0
4-cyanobenzonitrile	1.0	25.4	1.10	1.10(HWP,29); 1.07(CTS,29)	25.8
3-cyanobenzaldehyde	0.0	23.2	1.00		23.2
4-cyanobenzaldehyde	0.0	28.1	1.22		28.1
2-nitroacetophenone	-2.0[d]	31.8	1.38		30.9
3-nitroacetophenone	-2.0[d]	30.2	1.31		29.3
4-nitroacetophenone	-2.0[d]	35.7	1.55		34.8
2,3-dimethylnitrobenzene	-1.1	19.8	0.86		19.4
3,5-di(α,α,atrifluoromethyl)-benzonitrile	0.0	26.3	1.14		26.3
4-cyanoacetophenone	-2.0[d]	25.9	1.13		25.0
2,4,6-trimethylnitrobenzene	-1.1	16.3	0.70		16.1
2-nitrobiphenyl	-2.0[d]	24.7	1.17		23.8
3-nitrobiphenyl	-2.0[d]	26.0	1.13		25.1
4-nitrobiphenyl	-2.0[d]	27.8	1.20		26.9
4-fluorobenzophenone	+2.0[d]	14.9	0.64		15.8
Benzophenone	2.0	14.4	0.62	0.64±0.5(ECD,30)	15.3
Perfluorocompounds					
Hexafluorobenzene	7.4	12.0	0.52(12)	≥1.8±0.3(ECT,50); 1.2(M,67)	14.8
Octafluorotoluene	0.0	21.6	0.94(12.2)	≥1.7±0.3(ECT,50)	21.6
Pentafluorobenzonitrile	4.4	25.0	1.09(17)		27.0

Pentafluoroacetophenone	0.0[d]	21.7	0.94		21.7
1,4-dicyanotetrafluorobenzene	4.4[d]	41.8	1.81		43.5
Decafluorobiphenyl	0.0[d]	20.9	0.91		20.9
Decafluorobenzophenone	0.0[d]	37.1	1.61		37.1
Sulfur hexafluoride	+13.0	23.7	1.03	0.75±0.1(CI,118); >0.6±0.1(ECT,59); 0.54±0.1(CI,119); 1.0±0.2(KB,59)	29.3
Perfluoromethyl-cyclohexane	+2.5	24.9	1.08(793)		26.0
Azulene and substituted naphthalenes					
Azulene	4.9	16.0	0.69	0.66(ECD,120)	18.0
1-nitronaphthalene	-0.9	28.3	1.23		27.9
2-nitronaphthalene	-0.7	27.3	1.18		26.8
1,3-dinitronaphthalene	-3.2[d]	41.1	1.78		39.7
1,5-dinitronaphthalene	-3.2[d]	40.7	1.76		39.3
1-naphthonitrile	0.0	15.6	0.68		15.6
2-naphthonitrile	0.0	14.9	0.65		14.9
1-naphthaldehyde	3.7	15.7	0.68(15)	0.68±0.025(ECD,33)	17.8
2-naphthaldehyde	3.7[d]	14.8	0.64(7.6)	0.62±0.015(ECD,33)	16.4
2-methyl,1-nitronaphthalene	-1.6	23.7	1.03		23.0
4-methoxy,1-nitronaphthalene	-2.0[d]	25.4	1.10		24.5
Benzo- and naphthoquinones					
Tetrachloro-p-benzoquinone	-3.5[d]	64.0	2.78	2.76±0.2(CI,46); 2.48(CTS,29); 2.50(HWP,29)	62.6
Tetrafluoro-p-benzoquinone	-3.5[d]	62.3	2.70	2.92±0.2(CI,46); 2.45(HWP,29)	60.9
2,6-dichloro-p-benzoquinone	-3.5[d]	57.2	2.48		55.8

p-benzoquinone	-4.0	44.1	1.91	1.89±0.2(CI,46); 1.83(CTS,29); 1.98(HWP,29)	42.4
2-methyl-p-benzoquinone	-4.0[d]	42.7	1.85	1.74(CTS,29); 1.91(HWP,29)	41.1
2,6-dimethyl-p-benzoquinone	-4.0[d]	41.0	1.78		39.3
2,5-dimethyl-p-benzoquinone	-4.0[d]	40.9	1.77		39.2
2,3-dichloronaphthoquinone	-3.5[d]	50.6	2.19	2.00(CTS,29); 2.04(HWP,29)	49.2
1,4-Naphthoquinone	-4.0	41.8	1.81	1.71(CTS,29); 1.78(HWP,29)	40.2
Cyclic unsaturated anhydrides					
Maleic anhydride	-0.4	33.2	1.44	1.39±0.2(CI,45)	33.1
Phthalic anhydride	-0.4[d]	27.9	1.21	1.30(CTS,29); 1.18(HWP,29)	27.8

[a]Free energy, enthalpy, and entropy changes for electron attachment reaction (1.2) are from Figures 4.8, 4.9, 4.19, 4.20, 4.21 and 4.22, except otherwise noted.

[b]The values in brackets are autodetachment lifetimes of the negative ions in μs, after capture of near thermal electrons in the absence of third body stabilization, from Christophorou et al. (ref. 25). For sulfur hexafluoride the autodetachment lifetime ranges (see ref. 25) from 25μs to "very long" (>ms).

[c]The notation in the brackets beside literature electron affinity values indicate the method by which the electron affinity values were obtained and the numbers in the bracket indicate the literature from which the value is taken. Notations used are: CTS, charge transfer spectroscopic measurements in solution; HWP, polarographic half wave potential measurements in solution; ECT, endothermic charge transfer method; CI, alkali beam collisional ionisation method; LPD, laser photodetachment method; PES, photoelectron spectrocopic method; ECD, electron capture detector technique; KB, kinetic bracketting method.

[d]Entropy values are not determined experimentally, however, they are estimated from structural similarities with molecules for which entropy change on electron attachment were measured through electron transfer equilibria measurements.

[e]The uncertainty in the EA of tetracyanoethylene in the present measurement is estimated to be ±0.2 eV, while other values are within ±0.1 eV.

between the present results and the literature values exists. Cases where major disagreement occurred will be discussed in the subsection 4.2.2.

The following points will be discussed in this section based on the results provided in Table 4.3. They are: (i) comparison of relative electron affinities reported by McIver[79-80], obtained from electron transfer equilibria measurements by ICR spectrometer with those from the present studies, (ii) structure and stabilities of radical anions, effect of substituents on the electron affinity of aromatic systems, (iii) comparison of gas phase electron affinities with those obtained in the condensed phase, and (iv) entropy changes on electron attachment.

4.2.1 Comparison of Relative EAs Obtained in the Present Investigation with Those Reported by Fukuda and McIver

Fukuda and McIver reported recently an extensive measurement of the relative electron affinities based on ΔG_1^0 obtained from electron transfer equilibria measurements with the help of a pulsed ICR spectrometer. The compounds for which the relative electron affinities reported[79-80] are substituted nitrobenzenes, substituted benzo- and naphthoquinones, benzophenones and SO_2. In order to obtain a comparison, Fukuda's results i.e., ΔG_1^0 values were converted to $\Delta G^0_{et,SO_2}$. Then anchoring $\Delta G^0_{et,SO_2}$ values to $-\Delta G^0_a(SO_2) = 26.1$ kcal/mol from Table 4.2, $\Delta G^0_a(A)$ for all molecules for which ΔG_1^0 measurements were reported by Fukuda[79-80] were obtained. As mentioned earlier no temperature dependence of electron transfer equilibria was reported by Fukuda et al., hence only electron attachment free energy change $\Delta G^0_a(A)$ and not the electron affinities can be compared with the present results. Such comparisons are shown in Figures 4.23 and 4.24. $\Delta G^0_a(A)$ for all substituted nitrobenzenes which overlapped due to the measurements obtained from both the laboratories are shown in Figure 4.23. A very good agreement (within ± 0.2 kcal/mol) exists between the results obtained in the present study and those of Fukuda and McIver[79-80]. A similar good agreement is reflected in Figure 4.24 where the ΔG^0_a for benzo- and naphthoquinones are compared. The only serious disagreement occurred for tetrafluofo-p-benzoquinone for which Fukuda's[79-80]

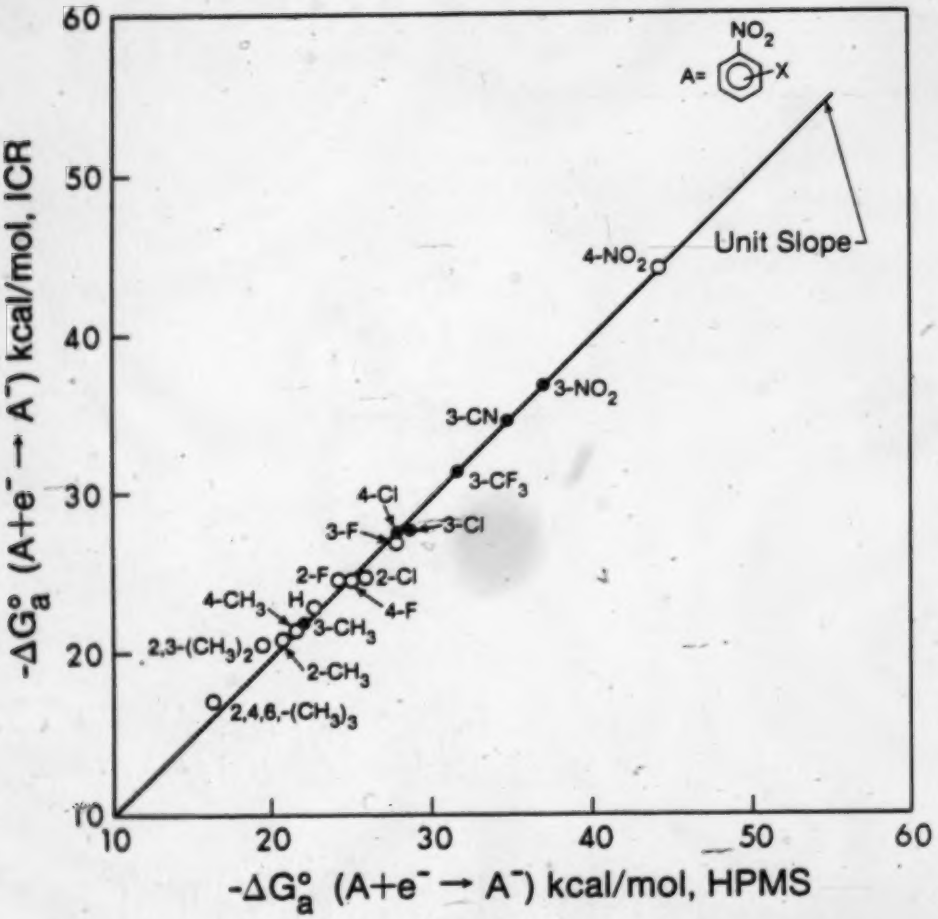

Figure 4.23. Comparison of ΔG_a^0 values for the reaction A + e = A^- from the present investigation (Table 4.3) with those reported by Fukuda and McIver (ref. 78-80), measured with the help of a pulsed ICR spectrometer, where A are substituted nitrobenzenes.

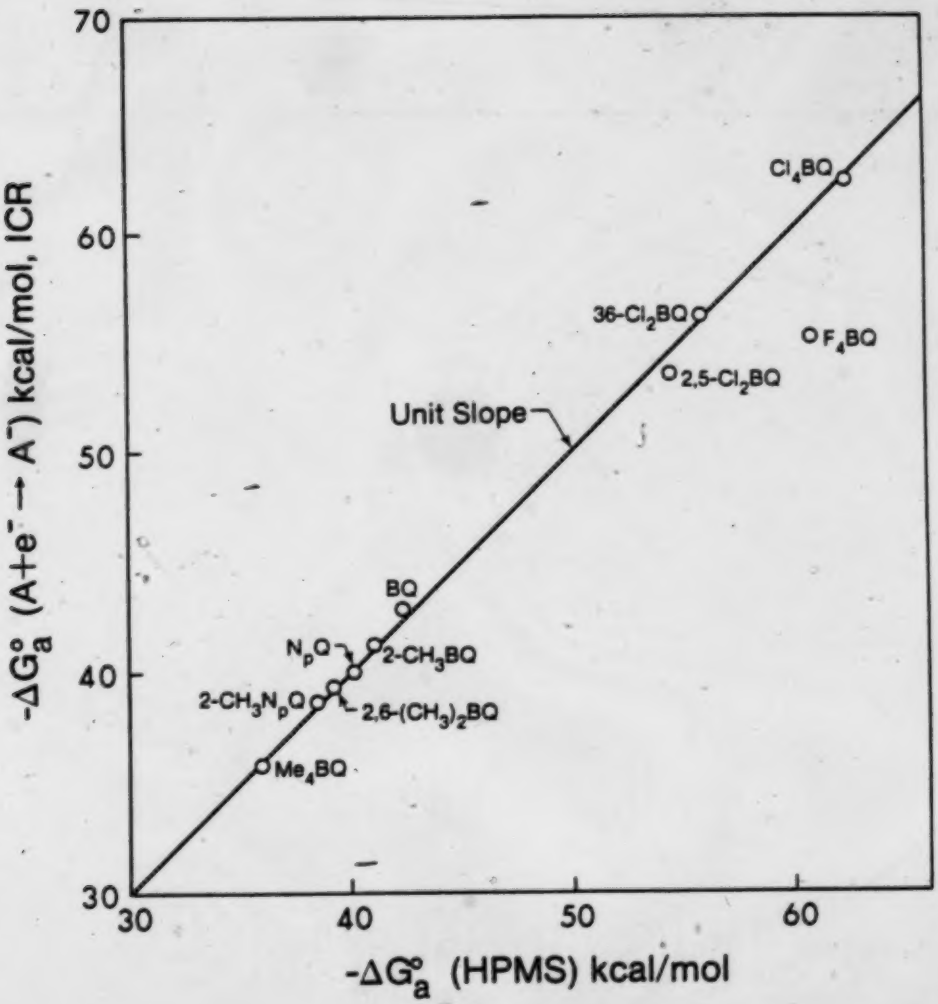

Figure 4.24. Comparison of $\Delta G_a^0(A)$, where A are substituted benzo- and naphthoquinones obtained in the present investigation, with those reported by Fukuda and McIver (ref. 78-80).

value is 5.7 kcal/mol lower than the value obtained in the present work (Fig. 4.24). The reason for such disagreement is not clear.

4.2.2 Electron Affinities. Structure and Stabilities of Radical Anions. Effects of Substituents on Electron Affinities

As shown in Table 4.3, the electron affinities of the majority of molecules are measured for the first time in the present investigation. Since the EAs of molecules with variety of substitutents are available, this offered an opportunity to explore the effect of substituents on the electron affinity of molecules or on the stability of radical anions for the first time. These effects involving various groups of compounds will be discussed in various subsections in this chapter.

(i) Substituted Aromatic Compounds

Aromatic radical anions being the species formed in the first stage of the Birch reduction[72] by alkali metals and alcohols in liquid ammonia or similar solvents (equation (4.12)) are of particular interest to experimental organic chemists.

$$C_6H_5X \underset{-e}{\overset{+e}{\rightleftharpoons}} C_6H_5X^- \xrightarrow{H^+} C_6H_6X \underset{-e}{\overset{+e}{\rightleftharpoons}} C_6H_6X^- \rightarrow \text{and so on.} \qquad (4.12)$$

Addition of an electron to benzene, the precursor of all aromatic hydrocarbons, is of interest to theoretical chemists as a typical Jahn-Teller situation[121-122]. Examination of π (Huckel) molecular orbitals of benzene shows that, in the benzene negative ion, the extra electron can be accommodated in either of the degenerate e_{2u} orbitals. The ion distorts from D_{6h} to D_{2h} symmetry and the degenerate pair of e_{2u} orbitals is split into nondegenerate a_u and b_{1u} orbitals, with the electronic configurations ^2A_u and $^2B_{1u}$ respectively. Benzene negative ion in gas phase is metastable and appears to be short lived resonance state lying about 1.1 eV above

neutral benzene and decays by ejecting the extra electron into the continuum[123]. This suggests that adiabatic electron affinity of benzene in gas phase is negative and electron transmission spectroscopic studies provide[123-124] EA = -1.15 eV for benzene. However,the presence of strong electron withdrawing substituents, such as, CF_3, CHO, CN, and NO_2 etc. in benzene or other polycyclic aromatic systems lowers the energy of the π^* orbital, the singly occupied molecular orbital or SOMO in radical anion, such that, with the presence of some electron withdrawing substituents, electron affinity becomes positive. Electron affinities of some monosubstituted benzenes were determined and reported in the literature; for example, benzonitrile (EA = 0.24 eV)[33], benzaldehyde (EA = 0.43 eV)[33], and nitrobenzene (EA = 1.0 eV, present investigation). Electron affinity also increases with the increase of number of rings. In unsubstituted benzene, naphthalene, and anthracene, HMO predicts[125] an increase of electron affinity with the extension of the aromatic system. Thus EA(benzene) = -1.15 eV[123-124], EA(naphthalene) = -0.15 eV[124] and EA(anthracene) = 0.60 eV[126]. These values are obtained from experimental measurements and are in line with the theoretical predictions[125].

Radom[122] investigated radical anions, $C_6H_5X^-$ of a set of substituted benzenes with substituents X = H, CH_3, COO^-, CF_3, CN, $CH{=}CH_2$, COOH, NO_2, CHO, F, OH, OCH_3 by ab initio molecular orbital theory using STO-3G basis set. Radom pointed out that[122] electron withdrawing substitutents like CN, CHO, NO_2 have preference for the $2b_{1u}\pi^*$ orbital as SOMO with ^2B ground state, while π donating substituents (X = F, OH, NH_2, OCH_3) prefer $1a_u\pi^*$ orbital i.e., ^2A ground state. These observations can be easily understood in terms of the nodal properties (scheme 4.1) of the SOMO in the ^2A and ^2B states.

Scheme 4.1

^2B ^2A

In the former SOMO has a node, and hence zero electron density, on the carbon adjacent to the substituent and is therefore, favored by the π-electron donor substituents. The SOMO of the ^2B state, on the other hand, has a large coefficient at the ipso carbon, thus a good position for π-electron transfer to π-electron acceptors.

Shown in Figure 4.25 is a comparison of effects of substituents (X = H, CHO, CN, NO_2) on the electron affinity of different group of compounds. The various groups of compounds shown are singly substituted benzenes, C_6H_5X; para substituted nitrobenzenes, $4\text{-}NO_2C_6H_4X$; substituted naphthalenes in position 1- and 2-, $XC_{10}H_7$ and substituted anthracenes, $9\text{-}XC_{14}H_9$. The electron affinities of these compounds are then plotted (Figure 4.25) against σ_p^-, the Hammett substituent constants deduced by Taft et al.[127] based on the gas phase phenol acidities. Also plotted in Figure 4.25 are the gas phase acidities of substituted phenols[127]. Electron affinities of nitrobenzene NB, 4-XNB, 4-X benzonitriles 4-XBN and 1- and 2- substituted naphthalenes are from the present investigation, while electron affinities of anthracenes are from Heinis[126], benzene and naphthalene from Jordan[123-124] and benzonitrile and benzaldehyde are from Chen[33].

The following interesting observations are obtained from the Figure 4.25. First, the increase of electron affinity due to electron withdrawing substituents X, in other words, the slope ρ in EA vs. σ_p^- plot, decreases in the series benzene, naphthalene and anthrecene. Similarly the ρ values decrease from monosubstituted benzenes to 4-XBN to 4-XNB. The trend in the ρ values obtained in the Figure 4.25 can be rationalized in terms of the availability of the

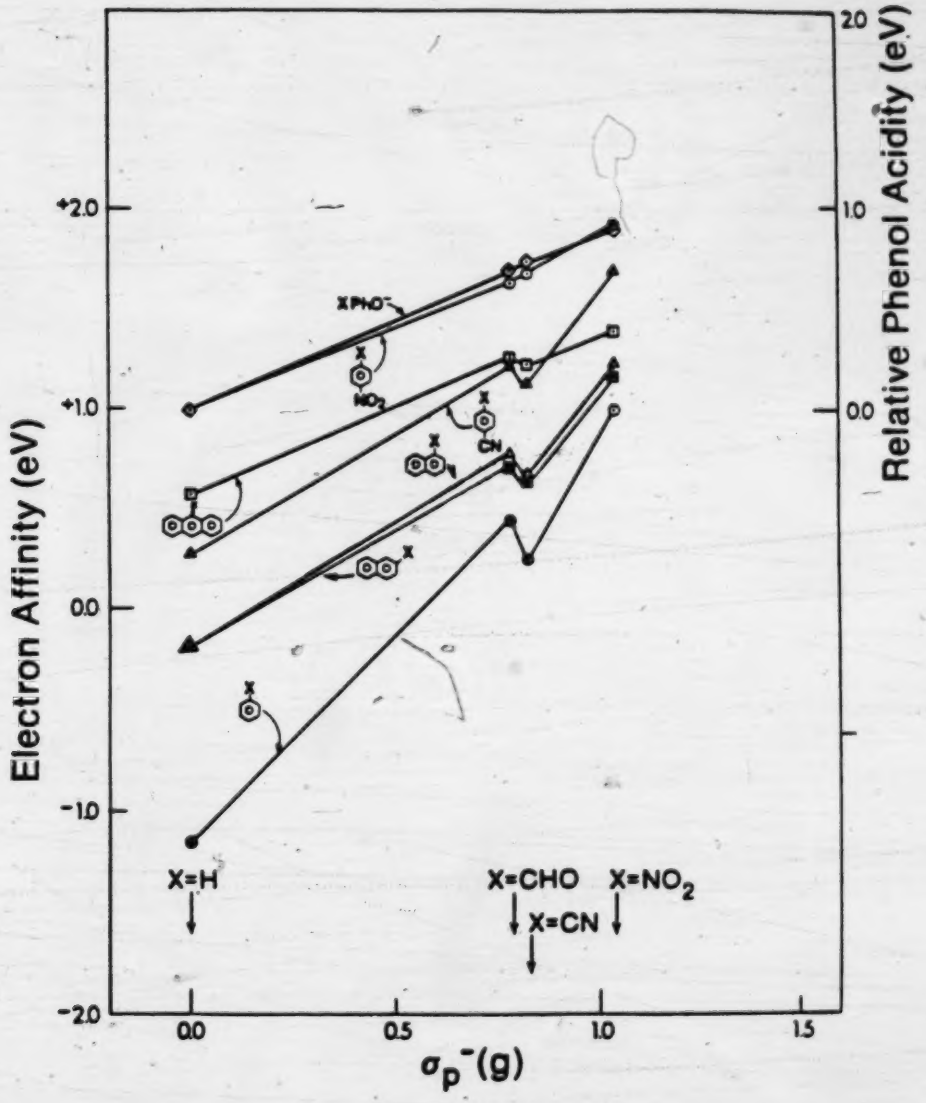

Figure 4.25 Electron affinities of benzenes, naphthalenes, anthracenes, cyanobenzenes, and nitrobenzenes with various substituents, X (= H, CHO, CN and NO_2^-) versus Hammet substituent constants $\sigma_p^-(g)$ based on gas phase acidities of phenols due to Taft (ref. 127). The free energy change for the proton transfer reaction $PhO^- + X\text{-}PhOH = PhOH + X\text{-}PhO^-$ is also shown on the right side of the ordinate. Electron affinities of benzaldehyde and benzonitrile are from Wentworth (ref. 33), benzene and naphthalene from Jordan (ref. 124), anthracenes are from Heinis (ref. 126). All other values are from present investigation.

electron density in the SOMO for substituents, X to operate on. As one goes from benzene to naphthalene to anthracene, conjugation of the SOMO in the corresponding radical anion system increases, involving more atoms, covering larger areas. Thus the electron density in the SOMO becomes less and less available to feed electron withdrawing substituents. Therefore, the slope ρ is the largest for monosubstituted benzenes and is the smallest for substituted anthracenes. The same argument holds for the systems X-benzenes, 4-XBN, and 4-XNB. CN and NO_2 being electron withdrawing substituents make the availability of SOMO electron density less and less for oncoming substituents. Radom's[122] calculations of π-electron densities of some monosubstituted benzene radical anions $PhX^{\cdot}$ show that in $BN^{\cdot}$ about 0.16e of the charge is located on the CN group, while in $NB^{\cdot}$ 0.46e of the charge is on the NO_2 group. This explains why ρ decreases in the series Bz, BN, NB.

A second interesting point to be noted from the Figure 4.25 is the reversal of the substituent effect between the CHO and CN group. As the electron affinity of the parent molecule is increased, i.e., if we go from Bz to naphthalene etc., the difference between the stabilization effect of CHO and CN is also decreased and at one point, in case of 4-XNB, a series with highest electron affinities in Figure 4.25 a reversal of the substituent effect took place.

As pointed out earlier from the STO-3G calculation due to Radom[122] that SOMO stabilizing substituents such as CHO, CN, NO_2 lead to preference for the $2b_{1u}\pi^{*}$ orbital (as SOMO) since this orbital can much better provide π-type electrons to feed the π-electron withdrawing substituents and also helps nearby electron charge to interact with the dipole of X (field effect). The calculations of Radom also predict[122] for the benzoanions $PhX^{\cdot}$, a higher electron density on X=CHO (0.528e) relative to X=CN (0.16e). The separation by Taft and coworkers[127] of the substituent effects, based on gas phase phenol acidities and calculations assigns a large electron withdrawing R effect (-9.2 kcal/mol) and a small electron withdrawing I/F effect (-6.6 kcal/mol) to CHO while for CN the opposite assignment of a small R effect (-4.5 kcal/mol) and a large I/F effect (-12.1 kcal/mol) is made. The larger R effect for CHO is parallel to the Radom-calculated larger SOMO π-density for the CHO group in $PhCHO^{\cdot}$

compared to CN in $PhCN^{\cdot-}$.

The observation that the CHO substitutent has a stronger stablizing effect relative to CN in the radical anions of large SOMO π-electron density in the ring and the reversal of the effect as the density is decreased (Figure 4.25), indicates that the π-withdrawl (R-effect) is much more strongly attenuated than the inductive/field effect with the decrease of the electron density in the SOMO.

A comparison between the effect of a large variety of substituents X in position 2-, 3-, and 4- on the electron affinity of cyanobenzenes XBN and nitrobenzenes XNB is given in Figure 4.26. Two interesting observations are reflected from Figure 4.26. First, any substituent X always increases the electron affinity of XBN more than it does for XNB. This is in line with the higher SOMO π-density in benzonitrile negative ion $XBN^{\cdot-}$ compared to $XNB^{\cdot-}$ available for the substituent X to operate on. Secondly, the substituents such as CF_3, CN etc. which have a strong field effect and small resonance effect fall close to the unit slope line i.e., for these substituents the reduced SOMO density of the NB ring relative to the BN ring is of less consequence, while the strongly π-withdrawing substituents like CHO and NO_2 are displaced further to the right. This means that in XNB these two substituents produce a smaller electron affinity increase compared to that in XBN. These trends are in agreement with the observations in Figure 4.25 and the discussions given earlier.

Also given in Table 4.3 and Figure 4.25 are the electron affinities of some substituted naphthalenes. Since the electron affinity of naphthalene is negative[124], its electron affinity could not be determined in the present investigation. Only the electron affinities of six monosubstituted naphthalenes with strong electron withdrawing substituents (such as, CHO, CN, NO_2) and four disubstituted naphthalenes were determined. It may be noted that for all three substituents X, 2-$XC_{10}H_7$ has lower electron affinity than 1-$XC_{10}H_7$ (Figure 4.25 and Table 4.3). Except for 1- and 2-naphthaldehyde there are no experimental electron affinities reported in the literature for substituted naphthalenes. The literature values[23] EA(1-naphthaldehyde) = 0.68 eV and EA(2-naphthaldehyde) = 0.62 eV are in good agreement with the results obtained in the present investigation 0.68 and 0.64 eV respectively

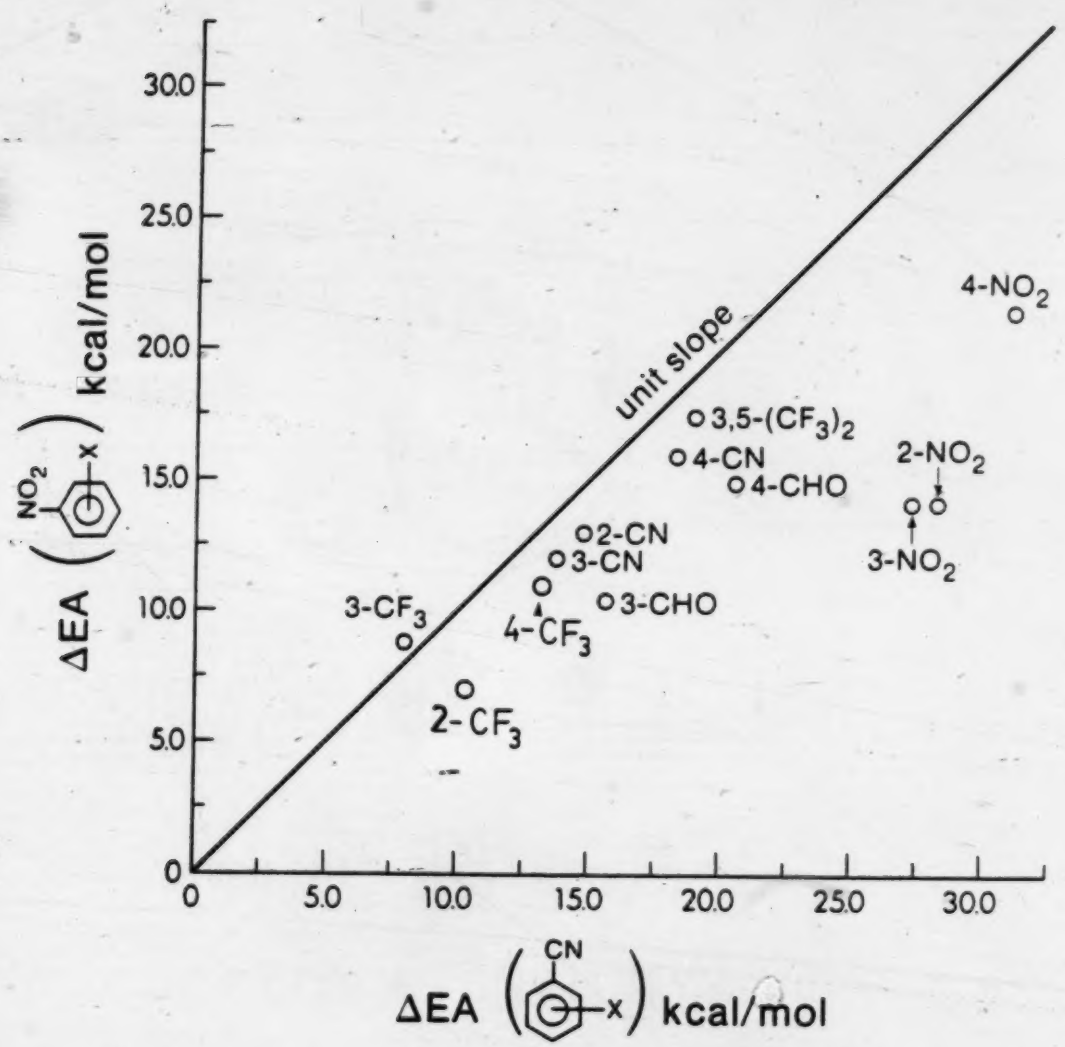

Figure 4.26. Relative electron affinities. Substituted cyanobenzenes versus substituted nitrobenzenes from Table 4.3.

(see Table 4.3).

We now examine the dependence of the substitution site on the electron affinity of naphthalene. Let us consider nitronaphthalene, for example. It is well known that NO_2 is a strong electron withdrawing substituent. The presence of NO_2 in either position (position 1- and 2-) leaves the ring partially positively charged and the NO_2 group partially negatively charged. The partial positive charge in the ring can be distributed to 5 different positions in both the isomers. In the 1-X isomer two structures out of five exist having an intact benzene ring in each (structures I and II in scheme 4.2 below), whereas only one structure, (III) is possible in the 2-NO_2 isomer. This means that electron withdrawing substitutents would stabilize position 1- more than position 2-.

Scheme 4.2

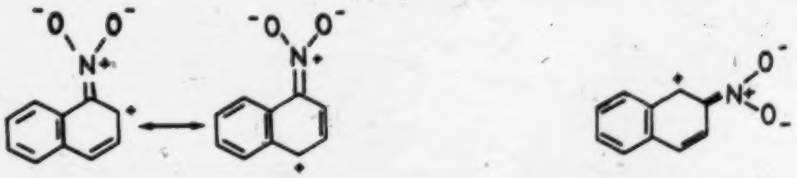

I II III

The order of stability in the monosubstituted naphthalene negative ion is also expected to be the same.

Hamano and Kondo[128] calculated the π-spin densities ρ_p at various substituent site p of naphthalene and other π-conjugated negative ions. ρ_p values calculated by the unrestricted Hartree Fock method (UHF) show that ρ_1 (=0.233e) is higher than ρ_2 (=0.042e). Therefore, electron withdrawing substituents will stablize position 1- more, where the electron density is higher than position 2-. That is the electron affinity of 1-X naphthalene will be higher than that of 2-X naphthalene for X = electron withdrawing substituents. This prediction is in accord with the experimental electron affinity values (Table 4.3) obtained for substituted naphthalenes in the present investigation. Shown in Figure 4.27 is a plot of the net charge density $\delta_{net}(p)$ at the site p of neutral naphthalene against the electron affinities of isomeric monosubstituted

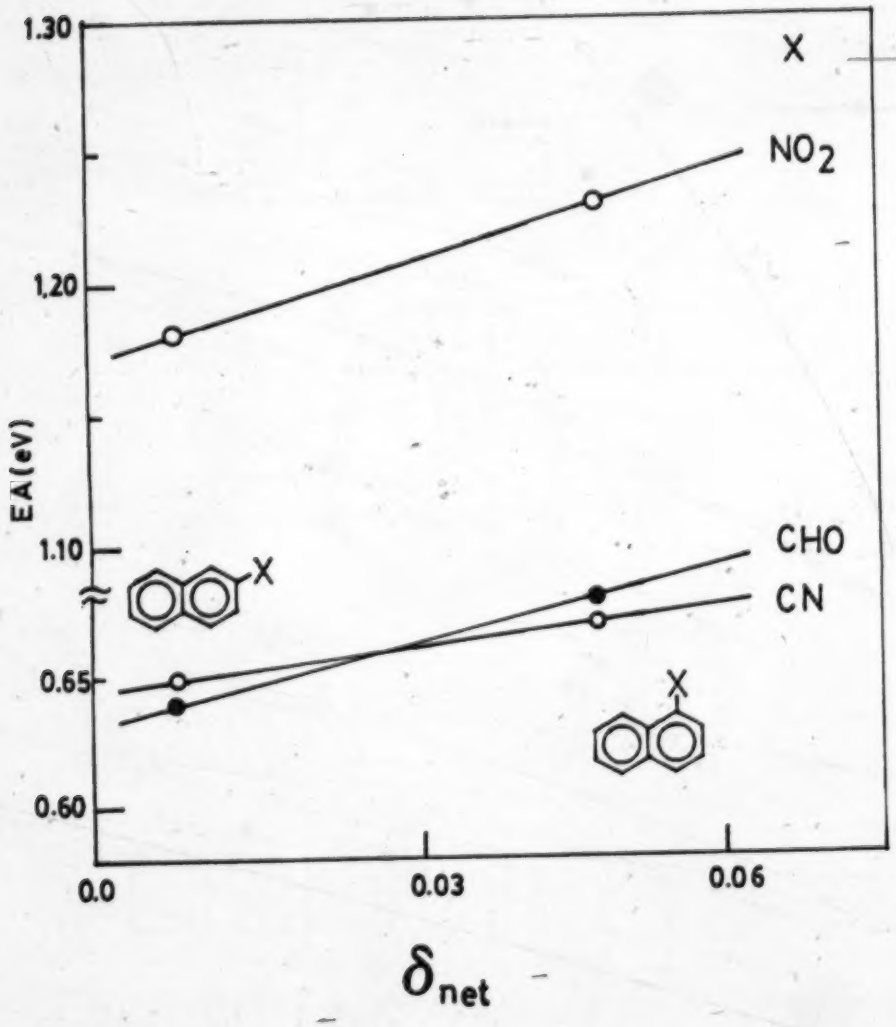

Figure 4.27. Plot of net charge distribution in position 1 and 2 of naphthalene against the electron affinities of substituted naphthalene.

naphthalenes, $XC_{10}H_7$; where X = CHO, CN, NO_2. The slope of the line in Figure 4.27 is highest for X=NO_2 and is lowest for X=CN. This means that, the relative stabilization of position 1- in monosubstituted naphthalene negative ion, where the electron density is higher compared to that in position 2-, is related to the π-withdrawing effect of the substituent, X.

(ii) Effect of Substituents on the Electron Affinity of Nitrobenzenes. Separation of Field and Resonance Effects

So far we have discussed only the effects of strong electron withdrawing substituents, such as, CHO, CN, and NO_2. In this subsection we will discuss the effect of twelve (12) substituents at different positions in 25 substituted nitrobenzenes, XNB. Shown in Figure 4.28 is the effect of substituents, X, on the electron affinity of nitrobenzenes X-NB versus the effect of the same substituents on the gas phase acidity of phenols, X-PhOH. The increasing gas phase acidity of the phenols X-PhOH is represented by the free energy change for the reaction (4.13).

$$PhO^- + X\text{-}PhOH = PhOH + X\text{-}PhO^- \qquad (4.13)$$

The electron affinities are the present results from Table 4.3 and gas phase acidities are from Taft[127]. The relationship observed in Figure 4.28 is quite remarkable. Not only the observed substituent order is practically the same in both cases but also the slope of the correlation is very close to unity, i.e., the substituent effect is also nearly of exactly the same magnitude for the two systems.

As pointed out earlier the extra electron in nitrobenzene radical anion is in a π^* type orbital (SOMO) which extends over the NO_2 group and the aromatic ring and predicts larger densities in position ortho and para to the nitro group. This electronic charge distribution is very similar to that of phenoxide anions, X-PhO^- and this similarity largely explains the correlation betwen substituent effects observed in Figure 4.28. However, the electron affinities of ortho substituted compounds are relatively lower compared to their counter part phenol

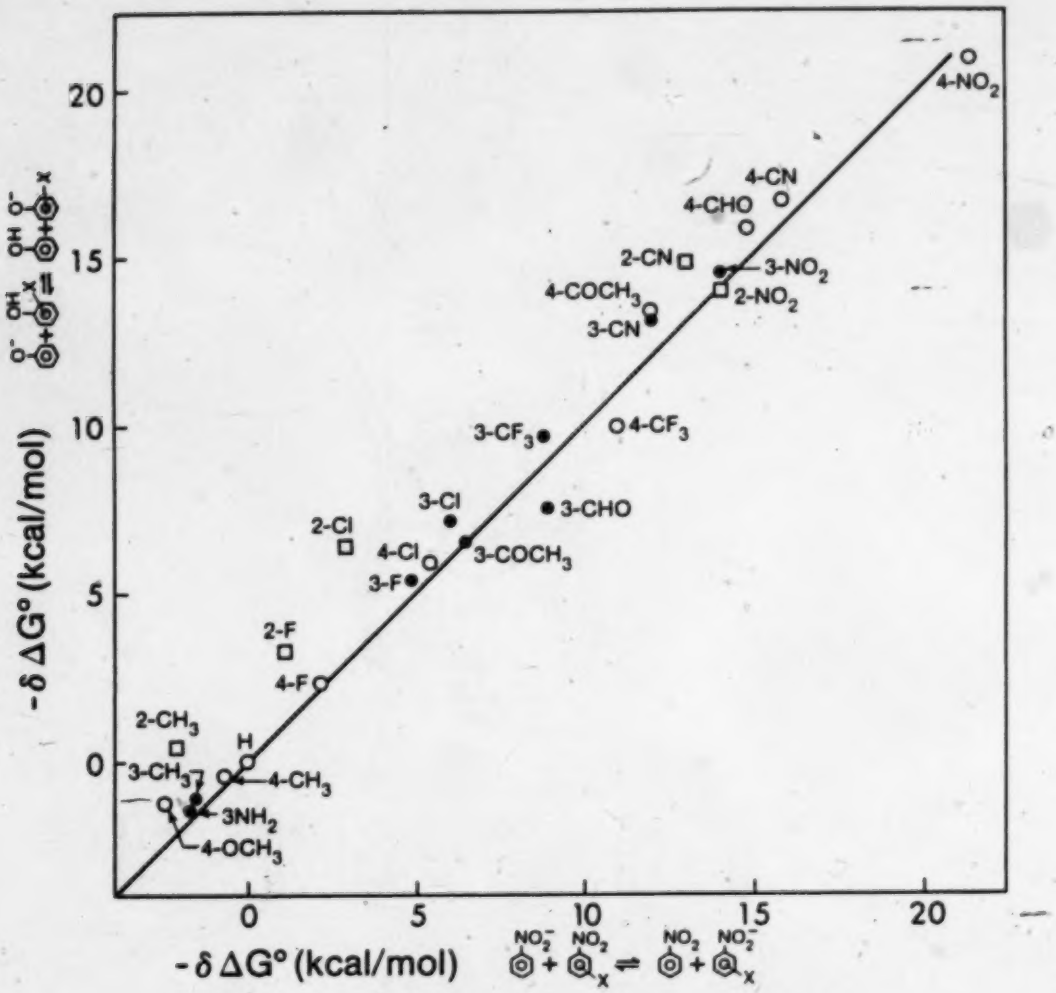

Figure 4.28. Comparison of relative electron affinities of substituted X-NB, EA(X-NB) - EA(NB), with relative gas phase acidities of substituted phenols X-PhOH, D(XPhO-H) - D(PhO-H). The near unit slope demonstrates similarity of electronic effects of substituents on the nitrobenzene radical anion and the phenoxy anion.

acidities. Destabilization in the ortho position could be due to sterically caused out-of-plane bending or twisting of the hetero groups, which reduces π-conjugation with the ring.

Given in Table 4.4 are the net substituent effects (kcal/mol) on the stability of nitrobenzene radical anion, in other words, these are the increases or decreases in electron affinities of nitrobenzene due to the presence of substituents. The following discussions about substituent effects will be based on the $\delta\Delta G^0_a$ ($=\{\Delta G^0_a(X\text{-}NB) - \Delta G^0_a(NB)\}$), since van't Hoff plots for all nitrobenzenes are not obtained. Further, ΔG^0_a values are more accurate (± 0.2 kcal/mol) than ΔH^0_a (± 1.0 kcal/mol) values. The values given in Table 4.4 for substituent effects can be separated into contributions from the field/inductive (F) effects and π/π^* delocalization (resonance, R) effects. Taft et al.[127] separated the substituent effects in phenol acidities using a procedure of Taft and Lewis[129]. Adopting a similar procedure we attempted to separate substituent effects into F and R. The method of Taft and Lewis[129] assumes that: (i) the effect of the polarizability, P of the substituents may be neglected, because of the large distances involved, for meta and para substituted compounds; (ii) the field/inductive effects, F are proportional between the meta and para positions, i.e., $F^m = kF^p$, where k is the proportionality constant, whose value is near unity; (iii) the resonance effects, R for a given substituent are attenuated by a constant factor at the non conjugating meta position compared to the conjugated para position, i.e., $R^m = \alpha R^p$, where α is a reaction series constant, having values between 0.1 to 0.6. Thus $\delta\Delta G^0 = F + P + R \simeq F + R$ leads to the following equations.

$$\delta\Delta G^0_m = F^m + R^m = kF^p + \alpha R^p \qquad (4.14)$$

$$\delta\Delta G^0_p = F^p + R^p \qquad (4.15)$$

Eliminating R^p from equations (4.14) and (4.15), equations (4.16) to (4.18) were obtained.

$$\delta\Delta G^0_m - \alpha\delta\Delta G^0_p = (k - \alpha)F^p \qquad (4.16)$$

Table 4.4: Relative electron affinities[a] of substituted nitrobenzenes in kcal/mol.

Substituents	para	meta	ortho
NH_2		-1.8	
CH_3	-1.6	-0.7	-2.1
H	0.0	0.0	0.0
OCH_3	-2.5	0.6	
C_6H_5	4.1	2.3	1.0
F	2.2	4.9	1.4
Cl	5.4	6.0	2.9
Br	6.2	6.7	3.4
CF_3	11.0	8.8	7.1
CH_3CO	12.0	6.5	8.1
CHO	14.9	8.9	11.8
CN	15.9	12.0	13.0
NO_2	21.5	14.1	14.1

[a]Relative electron affinities represent the negative of the free energy change for the reaction: $NB^{\cdot} + X\text{-}NB = NB + X\text{-}NB^{\cdot}$. NB stands for nitrobenzene.

$$\text{or,} \quad F^p = (\delta\Delta G^0_m - a\delta\Delta G^0_p) / (k - a) \qquad (4.17)$$

$$\text{and} \quad R^p = \delta\Delta G^0_p - F^p$$

$$= (k\delta\Delta G^0_p - \delta\Delta G^0_m) / (k - a) \qquad (4.18)$$

Taft[127] obtained the best separation of F and R values from the experimental gas phase results of phenol acidities, using k = 1.00 and a = 0.2 for +R substitutents and 0.6 for -R substitutents. Since, the effect of substituents on the electron affinity of nitrobenzene correlate very well with the effect of substituents on phenol acidities for the same substituent in the same position (Figure 4.28), the same values for k and a were used in the present study to separate F and R from the effects of substituents on the electron affinity of NB. The results thus obtained are given in Table 4.5. The separated R values for electron affinity change are compared with the R values for phenol acidities separated by Taft[127] in Table 4.6 and comparison of F values are given in Table 4.7. In general both F and R values for EAs of NBs are in good agreement ($\pm$ 1.5 kcal/mol) with those of phenol acidities. The differences observed for F and R values in two systems i.e., in X-NB and X-PhOH are probably the consequences of the different nature of molecular orbitals involved. In the former (X-NB) it is a π^* orbital (SOMO) while in the latter it is a bonding π orbital (HOMO). Further we have assumed same values for k and a as were used by Taft et al. These values which were used for separating substituents effect on gas phase phenol acidity may not necessarily be the same for substituents effects on the electron affinity of nitrobenzenes. More studies including theoretical calculations will lead to information which will allow a better separation of substituents effect on electron affinities into F and R values.

Since no Hammett substituent coefficients are available in the literature for radical anions, an attempt is made to test the dependence of $\delta\Delta G^0$(EA) of substituted nitrobenzenes with σ_m, σ_p^- the substituent constants for phenol acidity in gas phase due to Taft[127]. Plotted in Figure 4.29 are relative electron affinities of substituted nitrobenzenes against Hammett

Table 4.5: Separation of field effect (F) and resonance effect (R) of substituents on the electron affinity of nitrobenzene.

Substitutents	Position	$\delta\Delta G^0$ kcal/mol	F (g) kcal/mol	R (g) kcal/mol
CH_3	para	1.6	-0.4	2.0
	meta	0.7	-0.4	1.1
H		0.0	0.0	0.0
OCH_3	para	2.5	-5.3	7.8
	meta	-0.6	-5.3	4.7
F	para	-2.2	-9.0	6.8
	meta	-4.9	-9.0	4.1
Cl	para	-5.4	-6.9	1.5
	meta	-6.0	-6.9	0.9
Br	para	-6.2	-7.2	1.0
	meta	-6.6	-7.2	0.6
CF_3	para	-11.0	-8.3	-2.7
	meta	-8.8	-8.3	-0.5
CH_3CO	para	-12.0	-5.1	-6.9
	meta	-6.5	-5.1	-1.4
CHO	para	-14.9	-7.4	-7.5
	meta	-8.9	-7.4	-1.5
CN	para	-15.9	-11.0	-4.9
	meta	-12.0	-11.0	-1.0
NO_2	para	-21.5	-12.3	-9.2
	meta	-14.1	-12.3	-1.8

Table 4.6: Comparison[a] of resonance effects R (g) of various substituents on the electron affinity(EA) of nitrobenzene with those on the gas phase phenol acidity.

Substituents	Position	R (EA) kcal/mol	R (Phenol acidity) kcal/mol	Difference kcal/mol
H		0.0	0.0	0.0
CH_3	para	2.0	1.8	+0.2
	meta	1.1	1.1	0.0
OCH_3	para	7.8	5.8	+2.0
	meta	4.7	3.4	+1.3
F	para	6.8	7.5	-0.6
	meta	4.1	4.5	-0.4
Cl	para	1.5	3.1	-1.6
	meta	0.9	2.1	-1.2
CF_3	para	-2.7	-2.9	+0.2
	meta	-0.5	-0.6	+0.1
CN	para	-4.9	-4.5	-0.4
	meta	-1.0	-0.9	-0.1
$COCH_3$	para	-6.9	-8.5	+1.6
	meta	-1.4	-1.6	+0.2
CHO	para	-7.5	-9.2	+1.7
	meta	-1.5	-1.9	+0.4
NO_2	para	-9.2	-8.1	-1.1
	meta	-1.8	-1.6	-0.2

[a]Gas phase phenol acidities are from Taft (ref. 127); electron affinities are from the present investigation (Table 4.3).

Table 4.7: Comparison[a] of the field effect, F of various substituents on the electron affinity of nitrobenzene with that on the gas phase acidity of phenol for the same substituent.

Substituents	F (EA) kcal/mol	F (phenol acidity) kcal/mol	Differences kcal/mol
H	0.0	0.0	0.0
OCH_3	-5.3	-4.5	-0.8
CH_3CO	-5.1	-4.8	-0.3
CHO	-6.6	-7.4	+0.8
CF_3	-8.3	-9.0	+0.7
Cl	-6.9	-9.0	+2.1
F	-9.0	9.8	+0.8
CN	-11.0	-12.1	+1.1
NO_2	-12.3	-12.8	+0.5

[a]Electron affinities are from present investigation, Table 4.3 and gas phase phenol acidities are from Taft (ref.127).

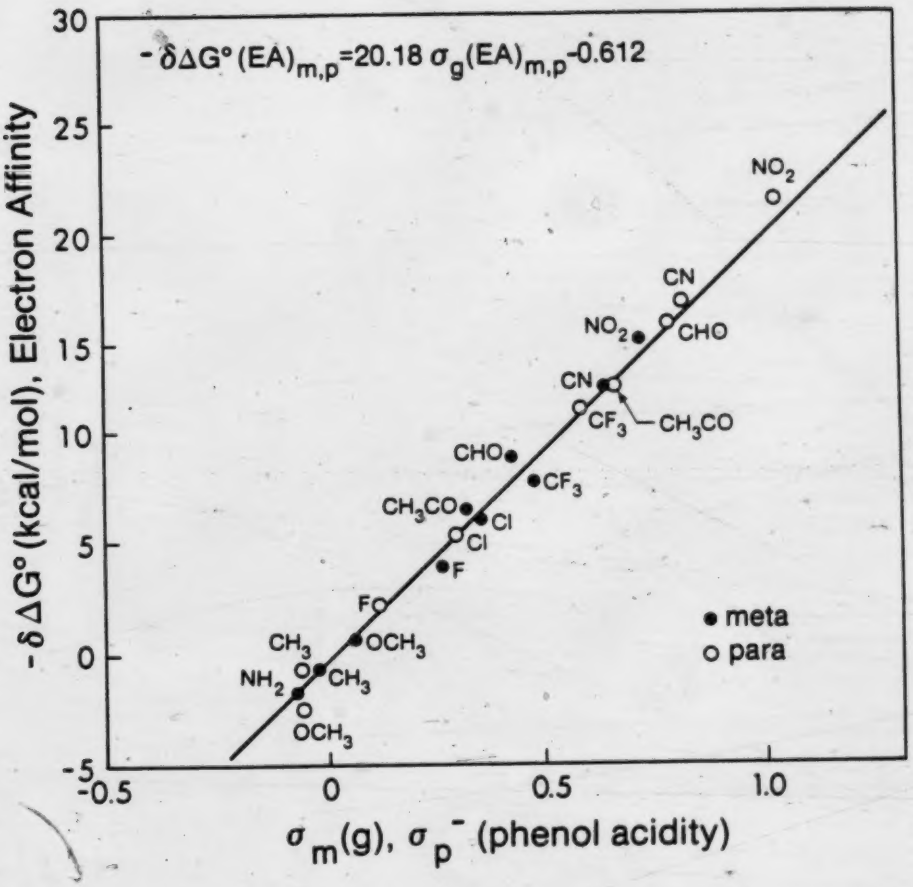

Figure 4.29. Plot of relative electron affinities of substituted nitrobenzenes X-NB, EA(XNB) - EA(NB), versus Hammett substituent constants for gas phase phenol acidities due to Taft (ref. 127).

coefficients due to Wepester[130] (σ_m^n, σ_p^- corrected for gas phase acidities of phenols by Taft[127] $\sigma_m(g)$, σ_p^-). A good correlation is obtained, which is obvious from the previous discussions. By fitting the data from Table 4.5, plotted in Figure 4.29 one obtains the relationship (4.19),

$$- \delta\Delta G_g^0(EA) = 20.18\ \sigma_g - 0.612 \text{ (in kcal/mol)} \qquad (4.19)$$

while Taft[127] obtained equation (4.20) for phenol acidities in gas phase. Substituent constants in both equations (4.19) and (4.20) are those of phenol acidities due to Taft.

$$- \delta\Delta G_g^0(\text{phenol acidity}) = 20.0\ \sigma_g \qquad (4.20)$$

Thus based on the observed relationship (4.19) Hammett coefficients, σ, are deduced for the substituent effects on the electron affinities of nitrobenzenes, X-NB. These results along with Taft's[127] parameters are given in Table 4.8. To our knowledge this is the first detailed study of the substituent effects on the stability of radical anions or the EA of the corresponding neutral molecule on the basis of experimental results. More rigorous studies including theoretical calculations with higher basis sets will provide information for better understanding of the substituent effects in order to deduce substituent constants for the stability of radical anions. The preliminary results presented here would encourage such efforts.

(iii) Benzo- and Naphthoquinones

Quinones belong to an extremely interesting group of compounds in bio-, organic and theoretical chemistry. Quinones occur as essential components in the membrane bound mitocondrial, photosynthetic and bacterial electron transport chains[24]. They act as a lyophilic electronic connectors between the large multiprotein donors and acceptors[26]. Quinones especially parabenzoquinone (pBQ) has been the starting material[131] for the synthesis of many

Table 4.8: Hammett type substituent constants[a,b]

Substitutents	σ_m(g), Ph. A.	σ_m(g); EA.	σ_p^-(g), Ph. A.	σ_p^-(g), EA.
NH_2	-0.07	-0.06	-0.17	
CH_3	-0.02	-0.004	-0.06	-0.05
OCH_3	0.06	0.06	-0.06	-0.09
H	0.00	0.00	0.00	0.00
F	0.27	0.27	0.12	0.14
Cl	0.36	0.33	0.30	0.30
Br		0.36		0.34
C_6H_5		0.14		0.23
CF_3	0.48	0.47	0.59	0.58
$COCH_3$	0.33	0.35	0.66	0.63
CHO	0.43	0.47	0.79	0.77
CN	0.65	0.63	0.83	0.82
NO_2	0.72	0.73	1.04	1.10

[a]Ph. A. stands for gas phase phenol acidities. Substituent constants for gas phase phenol acidities are from Taft (ref. 127).

[b]Substituent constants based on gas phase electron affinities of substituted nitrobenzenes are deduced by using the equation 4.19.

steroids, estrone and terramycin, among others.

Although pBQ has a large positive electron affinity (Table 4.3), it does not attach thermal electrons in a high pressure mass spectrometric ion-source, as is often the case for polyatomic systems of high electron affinity. However, pBQ^- can be formed by exothermic electron transfer reaction. The detection of very low thermal electron attachment to BQ is reported earlier by Cooper et al.[45], observed in a collisional ionisation MS and Collins et al.[132] in a TOF mass spectrometer. The existence of very low thermal electron attachment cross section to pBQ leads to the suggestion that, there is very small Frank Condon overlap between the ground states of the neutral molecule, pBQ and the negative ion. However, attachment of 2.1 eV electrons to pBQ is 100 times more efficient[132] than those of thermal electrons. According to Collins et al.[132] pBQ^- is formed by an electron excited feshbach resonance at 2.1 eV, with the capture of an electron in the field of the lowest triplet state T_1, resulting from an $n \rightarrow \pi^*$ transition at 2.31 eV.

The electron affinities and other thermochemical quantities for electron attachment to quinones, reaction (1.2), obtained in the present investigation are given in Table 4.3. For benzoquinone, there are a number of electron affinity values available in the literature[21] ranging from 0.4 eV to 2.1 eV. The only value obtained in the gas phase is 1.89 ± 0.2 eV due to Cooper et al.[45] from Cs-beam collisional ionisation experiments. This value is in good agreement with the result obtained in the present study, EA(pBQ) = 1.91 eV (see Table 4.3).

Cooper et al.[46] also reported the determination of EAs of tetrafluorobenzoquinone, F_4BQ; tetrachlorobenzoquinone, Cl_4BQ; and Br_4BQ by alkali atom collisional ionisation technique. The electron affinities obtained are[46] 2.92±0.2 eV, 2.76±0.2 eV and 2.44±0.2 eV respectively, i.e., an order of decreasing EA from tetrafluoro to tetrabromo benzoquinone. In contrast the EA of Cl_4BQ (=2.78 eV) is observed to be higher than that of F_4BQ (=2.70 eV) in the present investigation, Table 4.3. However, EA of Br_4BQ was not determined in the present investigation.

It is a well known fact that Cl substitution stabilizes negative ions more than F substitution does (see EAs of various F and Cl substituted compounds in Table 4.3). Therefore,

EA of Cl_4BQ should be higher than that of F_4BQ. Electron affinities deduced from half wave reduction potential values and charge transfer spectroscopic measurements in solution, by Chen and Wentworth[29] also shows EA(tetrafluorobenzoquinone) < EA(tetrachlorobenzoquinone).

It is interesting to note that the electron affinity (Table 4.3) of benzoquinone, pBQ (1.9 eV) is higher than 1,4-naphthoquinone, 1,4-NpQ (1.8 eV) (see Table 4.3) and 9,10-anthraquinone, 9,10-AnQ has the lowest electron affinity (1.6 eV)[133]. The same order of decreasing electron affinity on ring expansion of quinones was also reported by Kunni and Kuroda[134] from semi empirical calculations based on Pariser-Parr-Pople approximation, and by Chen and Wentworth[29] deduced from the solution phase half wave reduction potentials. In contrast, as discussed in the previous section 4.2.2, electron affinity increases on ring expansion in hydrocarbon systems, such that EA(Benzene) < EA(naphthalene) < EA(anthracene).

One can explain the observation that the EA(pBQ) > EA(1,4-NpQ) > EA(9,10-AnQ) with the help of a simple approach[125b], based on the charge delocalization energies between quinone molecule and the semiquinone radical anion. In this simple approach the π-energy of the radical anion (semiquinone) is taken as that of the parent accene i.e., the conjugation of a phenoxy oxygen with the aromatic ring is ignored. Further, the quinone carbonyl group is treated as a double bond. Thus from simple HMO calculation[125b] formation of pBQ^- from pBQ scheme 4.3 from nonbenzoid structure to a benzoid Kekule's

scheme 4.3

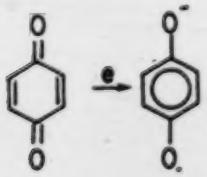

$\Delta DE/\beta = +0.08$

scheme 4.4

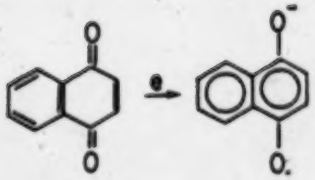

$\Delta DE/\beta = -0.12$

scheme 4.5

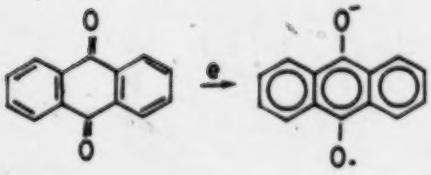

$\Delta DE/\beta = -0.37$

structure leads to the charge delocalization energy ΔDE (in β unit) = 0.08; while those for formation of 1,4-NpQ$^{\cdot}$ and 9,10-AnQ$^{\cdot}$ from 1,4-NpQ and 9,10-AnQ respectively (schemes 4.4 and 4.5) are -0.12 and -0.37. The above observation is the result of the fact that in pBQ/pBQ$^{\cdot}$ system 4 double bonds between carbonyl carbon and sp^2-carbons are converted to aromatic bonds. In 1,4-NpQ/1,4-NpQ$^{\cdot}$ system 3 double bonds are converted to aromatic bonds, while in 9,10-AnQ/9,10-AnQ$^{\cdot}$ system 2 double bonds are converted to aromatic bonds. Of course a closer approximation to π-energy could be obtained by including suitable values for the oxygen parameters. The above approach is an oversimplification of the real situation.

Unfortunately no modern theoretical calculation is available on the negative ions of quinones. A relatively recent SCF MO calculation with the help of STO-3G basis set on the neutral benzoquinone and naphthoquinone shows that[131] the LUMO, π^{*}_{cc} of benzoquinone, is heavily concentrated on the C=C double bond and is lowered in energy to a large extent, because it has correct symmetry to have substantial interaction (mixing) with π^{*}_{co} orbital. This is probably why quinones have large electron affinity compared to their parent hydrocarbons. It is also shown that[131] upon monosubstitution the symmetry of the LUMO is reduced. It is possible that the LUMO (π^{*}_{cc}) of naphthoquinone does not retain the correct symmetry as is

present in the pBQ to have substantial mixing with the π^*_{CO} orbitals. Therefore, the LUMO of naphthoquinone is of higher energy than benzoquinone and it is expected that the order of SOMO energies in benzo- and naphthoquinone anions will be the same as is shown[131] for LUMO energies in benzo- and naphthoquinone. That is EA(pBQ) > EA(1,4-NpQ).

The effect of substituents on the EA of benzo- and naphthoquinone are shown in Table 4.3 and Figure 4.8. As was observed earlier in case of aromatic hydrocarbons, that the Cl substitution (for H) increases the electron affinity while CH_3 substitution decreases the electron affinity, the effects of Cl and CH_3 substitution in quinone systems are also similar. Shown in Figure 4.30 is the effect of number of Cl and CH_3 substitutions on the electron affinity of pBQ. The EA of Me_4BQ is from Heinis[133], other values in Figure 4.30 are from the present investigation, Table 4.3. It is interesting to note that there is no saturation for Me substitution on the EA of pBQ. The decrease of electron affinity for each Me substitution is ~1.7 kcal/mol. The same is observed for the first Me substitution to 1,4-NpQ[133]. However, the electron affinities of other Me substituted naphthoquinones were not investigated. In contrast Cl substitutions show a gradual decrease in the EA increase with the increase of the number of Cl groups being substituted, as shown in Figure 4.30. This is not surprising. Since Cl substitutions increase EA and thus lower the SOMO electron density of the radical anion, by electron withdrawing through F/I effect, they make the SOMO electron density lesser and lesser available for on-coming Cl substitution. Therefore, the decrease in the relative EA increase with the increase of number in Cl groups is in qualitative agreement with the decrease in SOMO electron density with increased Cl substitution.

(iv) Hexafluorobenzene, C_6F_6; Substituted Perfluorobenzenes, C_6F_5X; SF_6 and $CF_3C_6F_{11}$

The interest in the EA of C_6F_6 and the negative ion state of $C_6F_6^-$ is of two fold. First the EA values available from experimental measurements, until recently, in the literature[50,67] gave enormously higher electron affinity for C_6F_6, than the value one could deduce from the six F substitutions to benzene. The more recent determination, from endothermic charge

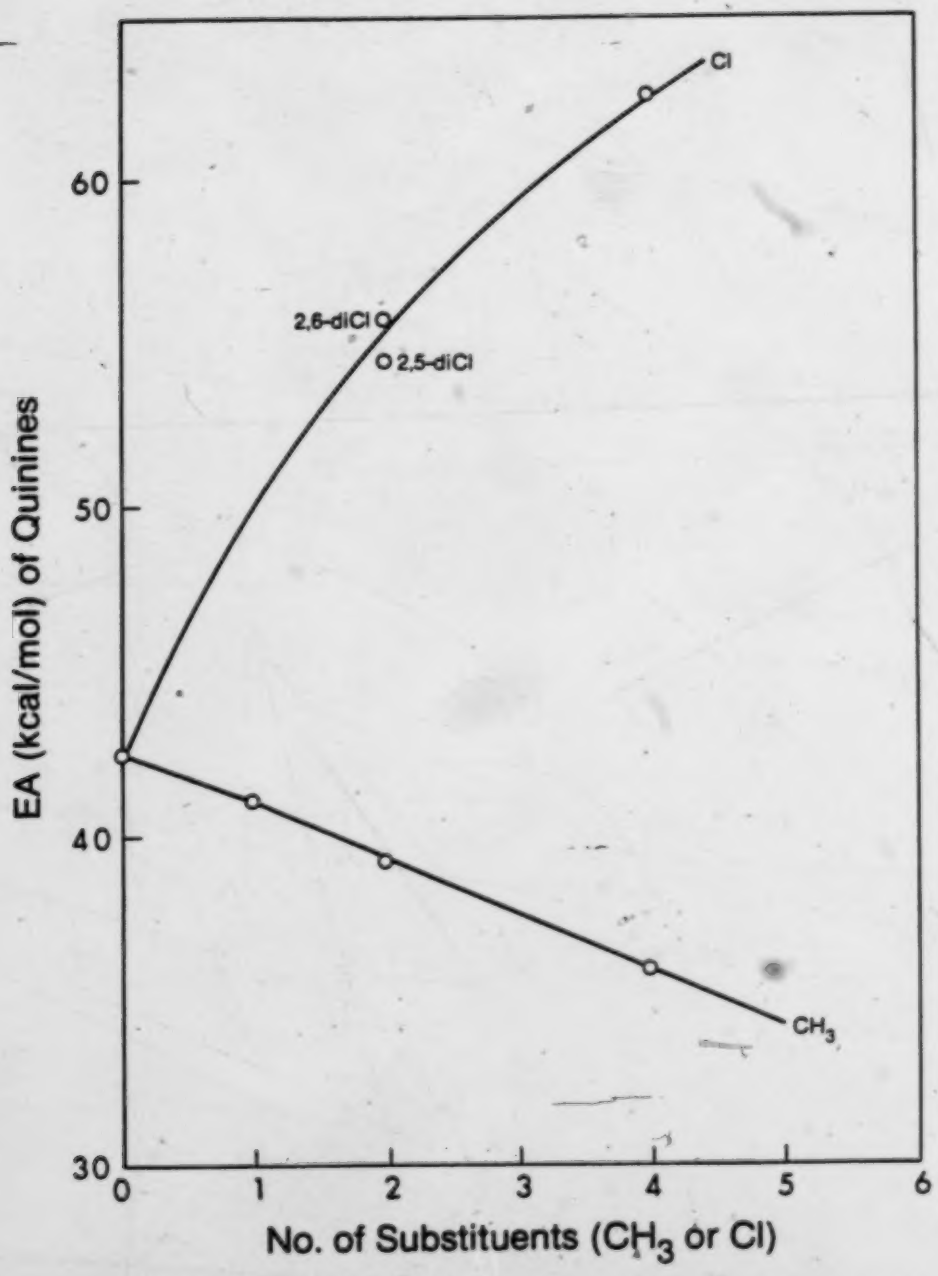

Figure 4.30. Plot of electron affinities of CH_3 and Cl substituted benzoquinones versus number of substituents. The results show that there is no saturation effect for increased number of CH_3 substitution to p-benzoquinone on the electron affinity. However, the increase of electron affinity due to subsequent Cl substitution decreases with the increase of the number of Cl being substituted.

transfer method gives EA(C_6F_6) ≥ 1.8 eV[50]. Second, the nature of singly occupied MO in $C_6F_6^{\cdot}$ has been a debatable topic[134-139]; whether the extra electron lies in a π^*-orbital or in a σ^*-orbital; the later being in line with the perfluoro effect[140].

Studies of photoelectron spectra and the energies of occupied MOs of unsaturated and aromatic compounds have indicated that perfluoro substitution decreases the energy of π-orbitals only slightly, but lowers the energy of σ-type orbitals significantly[140]. The perfluoro effect can be understood from the well known substituent effects. The F atom is strongly electron withdrawing by field/inductive effect and weakly electon pair donating (π donation). Thus, fluorine substitution can be expected to be strongly stabilizing to σ-type orbitals, while the combined field effect and the opposing π-donation can have only moderately net stabilizing effect on π-type orbitals.

Electron transmission spectroscopic measurements in gas phase have shown that[123-124] EA(Bz) = -1.15 eV and EA(F-Bz) = -0.89 eV, which means that a fluorine substitution in benzene increases the EA by 0.26 eV or 6.0 kcal/mol. Radom also observed[123,124] an electron affinity increase of 6.0 kcal/mol for first fluorine substitution to Bz from ab initio MO calculation. Increased fluorine substitution in Bz increases the electron affinity[135,137] such that at some high fluorine content the EA becomes positive. Stable $C_6F_6^{\cdot}$ have been observed in gas phase. By assuming that each fluorine substitution increases the electron affinity by same amount (0.26 eV), so that six F would increase by 1.56 eV i.e., from EA(Bz) = -1.15 eV to EA(C_6F_6) ≈ 0.41 eV. In fact, if F substitutions show saturation on increased substitution, EA of C_6F_6 will be even lower. The literature values for EA(C_6F_6) ≥ 1.8 eV[50] and =1.2 eV[67] are therefore much higher than expected.

The electron affinities obtained in the present investigation for C_6F_6 and other substituted perfluorobenzenes are given in Table 4.3. Briefly the EAs are: C_6F_6, 0.52 eV; $C_6F_5CF_3$, 0.94 eV; $C_6F_5COCH_3$, 0.94 eV; $(C_6F_5)_2$, 0.91 eV; C_6F_5CN, 1.1 eV; $(C_6F_5)_2CO$, 1.61 eV; 1,4-$(CN)_2C_6F_4$, 1.89 eV. The determinations for C_6F_6 and C_6F_5CN are based on the determination of the temperature dependence of K_1 and ΔH_a^0 and ΔS_a^0 are deduced from the van't Hoff plots. For other compounds an assumption $\Delta G_a^0 \approx \Delta H_a^0$ was made. The electron

affinity for C_6F_6 (EA=0.52 eV) obtained in the present investigation is much lower than the $EA(C_6F_6) \geq 1.8$ eV[50]. A similar large difference is observed for perfluorotoluene $EA(C_6F_5CF_3) \geq 1.7$ eV[50].

The electron affinities of other C_6F_5X compounds given in the previous paragraph (see Table 4.3) are also much lower than $EA(C_6F_6) \geq 1.8$ eV due to Lifshitz[50]. There are two strong evidences for *low* EA of C_6F_6 obtained in the present study.

First, the increase of EA in C_6F_5X due to replacement of F by X from C_6F_6 is in accord with the qualitative prediction of substituent effects. Shown in Table 4.9 is a comparison of ΔG^0_a values to substituted nitrobenzenes, X-NB and substituted perfluorobenzenes, X-C_6F_5. The extra electron in NB^- is in a π^*-type orbital extending over the aromatic ring and the NO_2 group. Electron withdrawing substituents increase the electron affinity relative to NB (Table 4.3 and discussions in previous sections). It is expected that such substituents will also increase the electron affinity relative to C_6F_6. Since the negative charge in NB^- is probably more delocalized than in $C_6F_6^-$, one might expect a larger substituent effect for the perfluoro benzenes, for H being replaced by X. However, since the change from C_6F_6 to C_6F_5X involves the substitution of X for F, the effect will be smaller compared to what was expected for H being replaced by F. Therefore, the increase in EA for NB to XNB might be expected to be similar to that for C_6F_6 and C_6F_5X. This is what is observed in Table 4.9. Since EAs of all C_6F_5X compounds obtained in the present investigation cannot be wrong, the observed substituent effect strongly supports $EA(C_6F_6) = 0.52$ eV.

Secondly, $C_6F_6^-$ is observed to show thermal electron detachment at 150°C. Thermal electron detachment is the reverse process (d) of electron attachment, reaction (1.2).

$$A + e^- \underset{d}{\overset{a}{\rightleftharpoons}} A^- \qquad (1.2)$$

The electron detachment energy $\Delta H^0_d = -\Delta H^0_a$ obtained for C_6F_6 is 0.52 eV (Table 4.3) is a

Table 4.9: Effect of substituents,[a,b] X on the electron affinity of NB and hexafluorobenzene.

Substituents, X	X-NB	X-C_6F_5
H or F	22.8	14.8
4-CN	38.7 (15.9)	27.0 (12.2)
3-CN	34.8 (12.0)	
3-CF_3	31.6 (6.8)	21.6 (6.8)
3-$COCH_3$	29.3 (6.5)	21.7 (6.9)

[a]All values relate to $-\Delta G^0_a(A) = EA\ (A)$ in kcal/mol, where A are the substituted nitrobenzenes, X-NB and perfluorobenzenes, X-C_6F_5.

[b]The values in parenthesis give the difference $\Delta G^0_a(NB) - \Delta G^0_a(X\text{-NB})$ in the middle column and $\Delta G^0_a(\text{hexafluorobenzene}) - \Delta G^0_a(X\text{-pentafluorobenzene})$ in the right most column.

very small value and thermal electron detachment from $C_6F_6^-$ can be expected at temperatures above +150°C. A detailed study of the thermal electron detachment rates for detachment from azulene negative ion will be discussed in the next chapter, chapter 5.

The time dependence of $C_6F_6^-$ observed in experiments where only C_6F_6 and the carrier gas were present in the ion-source is shown in Figure 4.31. At short times $C_6F_6^-$ is by far the major ion. It's intensity decreases with time more rapidly (k_d = 4300/s) than the decrease expected due to diffusion to the wall. The k_d due to diffusion expected at this temperature is 1100/s. Material balance considerations show that conversion of $C_6F_6^-$ by ion molecule reactions into other ions observed: m/z= 310($C_{10}F_{10}^-$), 205($C_6F_6.F^-$), 183($C_6F_5O^-$) and other minor ions not shown in Figure 4.31 are only a minor sink for $C_6F_6^-$. This means that the major sink must be thermal electron detachment. This supposition is confirmed by the unusual shape of the intensity curves observed in Figure 4.31. The linear logarithmic decay of $C_6F_6^-$ quite suddenly converts to a much larger slope at residence times of ~1.2 ms. In the same region the intensity of other negative ions is observed to increase suddenly. This unusual shape of the intensity curve could be explained as due to breakdown of the positive space charge field at low electron detachment rates. The detached electrons are then captured by other molecules and radicals in the source and therefore, the increase of intensity of other ions is observed. Thus, the results in Figure 4.31 positively identify the occurrence of electron detachment from $C_6F_6^-$ at T > 150°C. These results show an independent confirmation of the low electron affinity of C_6F_6 deduced from electron transfer equilibria measurements (Table 4.3). If C_6F_6 has a high electron affinity in the 1.8 eV range[50], thermal electron detachment would have been observed only at temperatures several hundreds of degrees higher than 150°C.

Some structural information on $C_6F_6^-$ are available from ESR measurements in solution and from theoretical calculations. Symons[136] on the basis of ESR coupling constant magnitudes, has suggested that $C_6F_6^-$ has a highly distorted structure, the carbon skeleton being simililar to the chair form of cyclohexane. It was also suggested that the extra electron resides in a σ^*-type orbital in line with the perfluoro effect and earlier arguments of Yim and Wood[139] on the the basis of ESR hyperfine coupling constant magnitudes. It is to be pointed out that the

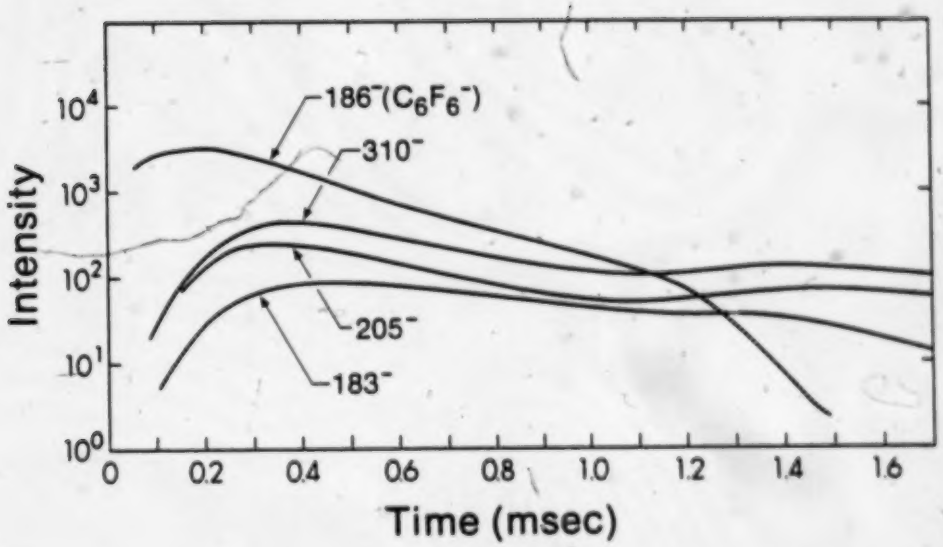

Figure 4.31. Time dependence of intensities of major ions observed after electron pulse with methane, 3.0 torr and C_6F_6, 1.8 mtorr at 149°C. The major $C_6F_6^-$ ion decreases more rapidly than expected, since diffusion to the wall and conversion to other minor ions are the only minor ion-loss mechanisms. The major cause for decrease is thermal electron detachment. Due to rapid loss of electrons to the wall, weak positive space charge is present which traps the negative ions. At 1.2 ms this field collapses since the production of the electrons by detachment is insufficient to maintain the field.

theoretical calculations (INDO) by Yim and Wood[139] on the various σ-states of perfluoro benzenes showed that the σ-states are all higher in energy and there is no *clear* trend in the energy differences which would indicate the likelihood of a π^*-σ^* cross over. This indicates that SOMO in $C_6F_6^-$ may be a π^*-type orbital rather than a σ^*-type. A more recent and detailed theoretical examination by Schegoleva[138] suggests a structure for $C_6F_6^-$ that leads to better agreement with the coupling constants. This is a planar carbon structure containing out-of-plane C-F bonds in which the π^* component prevails[138].

The present investigation suggests that the extra electron in the perfluoro negative ions investigated is almost certainly in the π^*-type orbital. The consistency in the trend observed in the Table 4.9 for substituent effects in X-C_6F_5 and X-NB indicates that the extra electron for all compounds involved including $C_6F_6^-$ is in a predominantly π^*-like orbital. This is in agreement with the theoretical prediction of Schegoleva[138] and INDO calculation of Yim[139] for $C_6F_6^-$.

Electron affinity of SF_6, $EA(SF_6)$ = 1.03 eV obtained in the present investigation is in good agreement with the result of 1.0±0.2 eV due to Streit[59] obtained from exothermic electron transfer kinetic bracketing method. However, electron affinities obtained for SF_6 from endothermic charge transfer method by Lifshitz et al.[50] $EA(SF_6) \geq 0.6$ eV and from alkali beam collisional ionisation method by Compton et al.[44] $EA(SF_6)$ = 0.46±0.2 eV are much lower than the present value. The reasons for the discrepancies between the present result and those from beam methods[45,50] have been discussed in the chapter 3 and therefore, will not be repeated, here.

The EA for $CF_3C_6F_{11}$ is found in the present study to be 1.08 eV (see Table 4.3). This is the first EA value reported for $CF_3C_6F_{11}$. The large electron capture cross section of the neutral molecules and the great stability of negative ions, make this and other perfluoro alkanes and cycloalkanes rather unique electron scavengers. While SF_6 has similar properties, the SF_6 neutral is probably chemically less stable. Lovelock and Ferber[34b] have proposed the use of branched perfluoro compounds like $CF_3C_6F_{11}$ as "exotic tracers for atmospheric studies" because of their high sensitivity for detection with the electon capture detector, their high

stability against thermal and environmental degradation and low toxicity. The determination of electron affinity of $CF_3C_6F_{11}$ in the present investigation represents one more step towards the characterization of this interesting group of negative ions.

(v) Unsaturated Cyclic Anhydrides

Also given in Table 4.3 are the electron affinities of maleic anhydride, MaAn and phthalic anhydride, PhAn. These compounds are conjugated dicarbonyl compounds of structures I and II respectively as shown below.

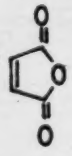

I (MaAn)

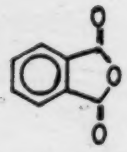

II (PhAn)

The capability of these compounds to capture thermal electrons to form radical anions is known long since and the electron attachment cross section of these compounds as a function of electron energy is determined[141-142]. It is reported that[141-142], these compounds attach thermal electrons to form negative ions with long autodetachment life time and the determination of EA of MaAn(I) is reported (EA(MaAn)=1.4 eV)[143] from Cs-beam collisional ionisation threshold measurement. Chen and Wentworth[29] deduced the EAs of some substituted conjugated dicarbonyl compounds with various heteroatoms, such as, O, NH, etc. in the ring, from experimental values of charge-transfer energies and half wave reduction potentials in solution. The reported values[29] are, MaAn: 1.33, 1.65 eV; PhAn: 1.30, 1.18 eV; obtained respectively from the charge-transfer spectral studies and polarographic half wave potential measurements. The electron affinity values obtained for MaAn and PhAn in the present investigation are 1.44 and 1.21 eV respectively (Table 4.3). These values are in good agreement with other experimental results given in Table 4.3.

An interesting similarity these compounds have with quinones is that the EA decreases with ring expansion, i.e., EA(MaAn) > EA(PhAn) in contrast to aromatic hydrocarbons,

where the EA increases on ring expansion[123-124], such that EA(Bz) > EA(Naphthalene). No modern theoretical calculations are available on the radical anions of this group of compounds. A recent investigation from electron transmission spectroscopic study and theoretical calculations due to Modelli et al.[144] showed that in the unsaturated conjugated diketonic compounds, the ethylinic π^*_{cc} MO belonging to the a_2 symmetry of the C_{2v} point group interacts with the out-of-phase combination, π^{*-}_{co} of the two π^*_{co} MOs. It is the interaction of the π^*_{cc} MO with π^{*-}_{co} MO, which leads to the formation of the energetically lower, LUMO, the π^*_1 orbital. It is also shown that[144] the trend in the LUMO's should follow the same in the SOMO's of the radical anions.

The reason for decreasing electron affinity on ring expansion is not clear. It is possible that, the π^*_{cc} orbital in PhAn does not have the correct symmetry, present in maleic anhydride, MaAn. This means that the interaction between π^*_{cc} orbital with π^{*-}_{co} orbital will be less in PhAn compared to that in MaAn. Therefore, $E_{LUMO}(MaAn) < E_{LUMO}(PhAn)$.

(vi) Tetracyanoethylene, TCNE

Electron affinity of tetracyanoethylene, TCNE is important to spectroscopist and others, who deal with charge transfer complexes[19], because it is known to have high electron affinity and therefore, is a strong π-charge transfer acceptor. For TCNE there are two experimental gas phase literature values, one of Lyons and Palmer[117] 2.3±0.3 eV, the other due to Page[66], 2.9 eV and two indirect values 2.9 and 2.8 eV based on Chen and Wentworth's[29] correlation. The later three values are close to the present result of 3.1±0.2 eV. The significantly lower value of Lyons[117] is based on electron photodetachment from $TCNE^-$ negative ion and might have been considered as the most reliable of the literature data. However, examination of the experimental results and the interpretation of Lyons[117] reveal significant problems. The photodetachment curve obtained had no visible structure above the onset which occurred at 2.0 eV. The first report of Lyons[145] gave an EA of 2.0 eV. A calibration to relative values from charge transfer spectra[146] shows that this value is too low and Lyons reinterpreted the onset curve[117]. Making the reasonable assumption that the major

geometry change on formation of the negative ion corresponds to a stretch of the central C=C bond, Lyons and Palmer[117] fitted the curve to a progression of vibrational transitions involving this stretch. The fit indicates some 0.4 eV contribution due to the vibrational excitation present in the ion. This assignment moves the EA by 0.4 eV above the threshold i.e., to 2.4 eV. The analysis, while plausible, need not be correct. The present 3.1 eV result indicates a much larger shift due to excitation of the negative ion.

The value of 2.9 eV due to Page[66], which is close to the present result was obtained by the Magnetron method. This method is not reliable[147-148]. The major problem is the absence of identification of the negative ion i.e., the nature of the negative ion is deduced on the basis of the reagents added. Often other ions than those assumed to be present are found to be dominant[148]. It is interesting to note that mass spectral analysis for the case of TCNE has shown[148] that the dominant ion is $TCNE^-$. This fact lends support to the determination by Page.

The uncertainty of the present determination for TCNE given as ±0.2 eV, see Table 4.3, is larger than usual ±0.1 eV. The larger error was assumed in order to take into account the very large ΔG_1^0 value of the equilibrium constant invoved in the determinations and the slow electron transfer kinetics, see Figure 4.10. However, the results in Figure 4.10 clearly demonstrate that tetracyanoethylene has an EA many kcal/mol above that of the reference compound tetrafluorobenzoquinone, EA = 2.70 eV, a compound with higher electron affinity than 2.3 eV, the result of Lyons[117] for TCNE.

4.2.3 Comparison of EAs from Gas Phase ET-Equilibria Obtained in the Present Study with those Deduced from the Measurements in Solution

A comparison of the present results with EAs derived from polarographic half wave potentials ($E_{1/2}$) and energy of charge transfer absorption band (E_{CT}) measured in solution is also given in the Table 4.3 and Figure 4.32. These solution derived electron affinities are from Chen and Wentworth[29] who, following Briegleb[18], Peover[149], Batley and Lyons[146] obtained

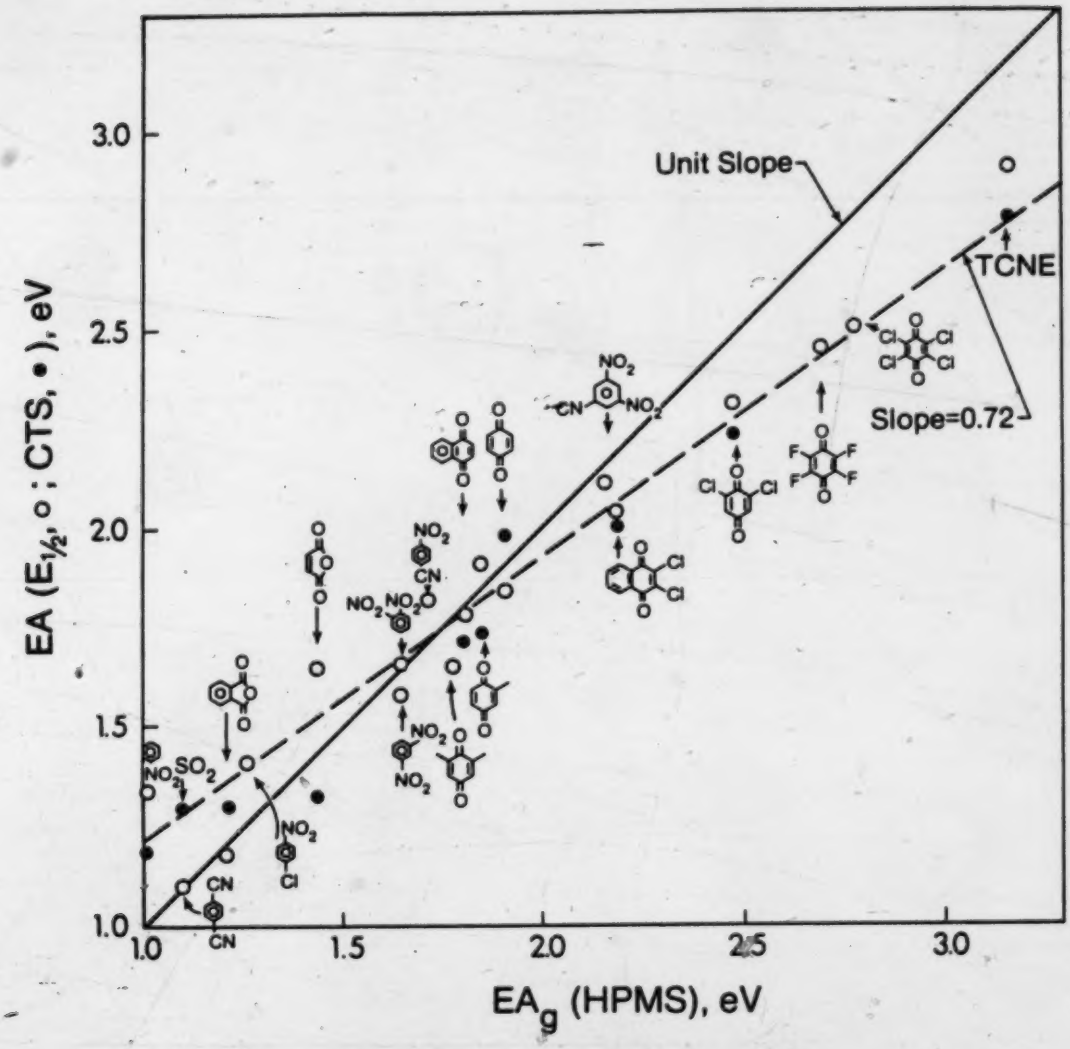

Figure 4.32. Comparison of electron affinities from the present work (Table 4.3) with electron affinities measured in solution. O, EA from polarographic half wave reduction potential measurements; ●, EA from charge transfer spectra in solution. The solid line corresponds to the slope of unity, i.e., complete agreement with the present results. The dashed line is the approximate representation of the solution data (slope = 0.72).

the data by adjusting the constant $C_{1/2}$ and C_{CT} in the equation (4.21) and (4.22) so as to obtain a best fit with avilable gas phase electron affinities.

$$E_{1/2} = EA - \Delta G_s^0 - \text{const} = EA - C_{1/2} \quad (4.21)$$

$$E_{CT} = IP - EA + \Delta G_s^0 + C = IP - EA + C_{CT} \quad (4.22)$$

$$\Delta G_s^0 = \Delta G_s^0(A^-) - \Delta G_s^0(A) \quad (4.23)$$

Examining the resulting electron affinities in Figure 4.32, one finds fair agreement with the present results. The solution-derived EAs are generally somewhat higher for compounds with low electron affinity and lower for compounds with high electron affinities which leads to a slope less than unity (slope = 0.72). The solution EA depends on the assumption that the solvation energy difference ΔG_s^0 given by equation (4.23), where $\Delta G_s^0(X)$ is the solvation free energy of the species X, is constant for all compounds. Since the solvation of A^- is more exothermic than that of A, ΔG_s^0 is negative. Higher electron affinities for compounds present in Figure 4.32 is largely achieved through more extensive conjugation and increased number of electron withdrawing substituents. Both factors disperse the negative charge in A^- over a larger number of atoms. It is well known that such charge delocalization leads to a decrease of the solvation exothermicity of A^-. Since the solvation energy of the ion is dominant over that of the neutral, this should lead to an increase in ΔG_s^0 with increasing EA, i.e., decrease in the absolute value $|\Delta G_s^0|$. This increase is not taken into account in the one constant parameter equations (4.21) and (4.22) and it is probably this neglect of the change of the solvation energy that leads to the less than unit-slope observed in Figure 4.32. Peover[149], who produced most of the half wave potential data used in Figure 4.32, did the measurements in dipolar aprotic solvents such as acetonitrile. The solvation of negative ions with charge dispersion in the ion is known[150] to decrease least in such solvents. Solvation of negative ions in protic solvents decreases much more with the charge dispersal, and had such solution data been used, a much smaller slope i.e., a much larger deviation from unit slope in Figure 4.32 would have been observed.

The interaction of charge delocalized anions A^- with various protic and aprotic solvent molecules and the trend in solvation energies of A^- in the bulk solution will be discussed in more detail in chapter 6.

4.2.4 Autodetachment Lifetimes of Negative Ions and the Electron Affinities of Neutral Molecules

Also given in Table 4.3 (column 4 in bracket, in μs) are the autodetachment lifetimes of the negative ions, after capture of near thermal electrons in the absence of third body stabilization. The lifetimes, from experimental measurements by various authors using the time of flight mass spectrometer or electron swarm experiments, were collected by Christophorou[25] (Table VII, ref. 25). The lifetimes increase with electron affinity, from tens of microseconds for compounds with low electron affinities to hundreds of microseconds for compounds of high EA. Christophorou[25] have applied unimolecular kinetics statistical theory using essentially RRKM[151] formalism, to the special case of the chemically activated autodetachment process. Expressions with various levels of approximations were obtained. These predict an increase of lifetimes with increasing EA and internal degrees of freedom of A, however, the predictions are only in qualitative agreement with experiment. It is not clear whether the quantitative failure of the theory was due to the approximations used or unapplicability of the statistical theory. Christophorou et al. was lacking reliable experimental data on electron affinities and other basic information on the properties of the anions. The present electron affinities and results from the electron transfer kinetics can be of significant benefit. For example, the particularly simple expression (4.24) was obtained by Christophorou et al.[25] for the (relative) lifetimes τ of substituted nitrobenzene anions, where N is the number of internal degrees of freedom in the molecule.

$$\tau \propto (EA)^{N-1} \qquad (4.24)$$

While a fair linear correlation was obtained between $\tau^{-(N-1)}$ and EA values (actually $E_{1/2}$ values due to lack of EA data at that time) there are some unexplained features. Thus the experimentally measured life times of dinitrobenzene negative ions increase in the order para, meta while the electron affinities increase in the opposite order and the same is true for corresponding cyanobenzenes. Equation (4.24) applied to a given pair of isomers for which N is assumed to be constant predicts a higher τ for the higher EA compounds i.e., the para isomer. This discrepancy can be resolved when one considers the situation in greater detail. As will be shown below, the greater EA of the para nitro isomer is due to π-electron pair withdrawl by the substituent. This decreases the negative charge near the nitro group which carries much of the excess negative charge, and a stabilization of the negative ion results. An equivalent stabilization is not possible in the meta isomer. However, the π-electron withdrawal forms a partial double bond between the substituents and the aromatic carbons and this introduces additional hindrance for rotation around that bond. A significant reduction of the density of states of the anion may be expected due to loss of rotation and this results in a decrease of the lifetime for autodetachment. This change of density of states is not taken into account by the simple expression (4.24).

The kinetics measurements of electron transfer reactions (1.1) described in the preceeding chapter (3) showed that perfluorocycloalkanes behaved anomalously, and a suggested possible cause for this behavior was an extremely large geometry change between A and A^-. Such large changes, if true, will also have to be taken into account in the evaluation of the negative ion lifetimes of perfluorinated negative ions. Christophorou's lifetime evaluations of the negative ions of perfluorinated compounds[25] did not include such considerations.

4.3 Entropy Changes on Electron Attachment

Given in Figures 4.21, 4.22 and Table 4.3 are the entropy changes on electron attachment, ΔS_a^0. All values in Figures 4.21 and 4.22 are obtained from direct measurement of

the temperature dependence of the electron transfer equilibria (1.1) through van't Hoff plots. ΔS_a^0 for SO_2 and NO_2 are calculated from available vibrational frequencies and geometries of the neutral molecule and the negative ion. Other values for ΔS_a^0 in Table 4.3 are estimated.

The results of entropy change $[S^0(A^-) - S^0(A)]$ shows that the substituted nitrobenzenes and quinones have negative values for ΔS_a^0 i.e., these compounds experience a decrease of entropy on becoming negative ions. Since all resulting negative ions are doublet, while the neutral molecules are singlet, the $[S^0(A^-) - S^0(A)]$ value for the multiplicity change is 1.4 cals/deg. The observed overall decrease in entropy for these compounds must be due to stiffening of vibrations in the negative ions. The $-\Delta S_a^0$ is seen to increase with increasing electron affinities of the nitrobenzenes and quinones. Increase of electron affinity is achieved by increased substitution with electron-withdrawing groups. As mentioned earlier, the extra electron in the nitrobenzene radical anion is in a π^*-type orbital which extends over the nitro group and the aromatic ring. The presence of the electron in NB^- may lead to a stiffening of the internal rotation of the nitro group relative to the phenyl group. The rotational barrier in nitrobenzene is known to be 6.0 kcal/mol[152]. From the reduced moment of inertia one can evaluate[153] the entropy for restricted rotation $S^0(rest.) = 4.2$ cal/deg.

The presence of an additional electron in NB^- may double or triple the internal barrier and this would lead to a loss of 1.0 to 2.0 cals/deg in this rotation. Additional stiffening may occur in the C-N and N-O bonds, and the ring bending vibrations of NB^-. These combined effects may be responsible for the observed negative ΔS_a^0 of the nitrobenzenes.

Quinones also show negative entropy changes on electron attachment. Of the 30 vibrations of benzoquinone there are some five CO bending modes[154] ranging from 240 to 500 cm^{-1}. A stiffening of these modes in the presence of the extra electron in benzoquinone negative ion can be expected. This would lead to a loss of entropy by a few cals/deg.

The entropy change ΔS_a^0 for electron attachment to C_6F_6 was found to be 7.4 cals/deg (see Table 4.3). When 1.4 cals/deg is subtracted, there remains 6.0 cals/deg. This change could be due to loosening of the vibrational frequencies in $C_6F_6^-$ and/or to a decrease of symmetry from C_6F_6 to $C_6F_6^-$. The kinetic data (Table 3.3) showed that electron transfer from $C_6F_6^-$

occurs with near 100% efficiency, even when the reaction is near thermoneutral. This result indicates that the energy difference between the $C_6F_6^-$ obtained by a vertical transition from C_6F_6 and the ground state geometry of $C_6F_6^-$ is not large. This conclusion is drawn from the fact that the the energy barrier for electron transfer reactions from SF_6^- obtained by a vertical transition from SF_6 and the ground state geometry of SF_6^- is large, due to the poor Frank-Condon overlap caused by the geometry change on formation of the SF_6^- from SF_6. Thus the observed positive $\Delta S_a^0(C_6F_6)$ is compatible with a change of soft vibrations and/or a change of symmetry number, since these two changes need not lead to a large energy change in the vertical transition. C_6F_6 is highly symmetric, with symmetry number $\sigma = 12$. Thus loss of symmetry in $C_6F_6^-$ ($\sigma = 1$ or 2) will lead to a ΔS_a^0(rot,sym) $\approx$ 5 cals/deg. Either the softening of vibrations in $C_6F_6^-$ or the change in symmetry number may be sufficient to lead to the observed $\Delta S_a^0(C_6F_6)$.

The entropy change on electron attachment to SF_6, $\Delta S_a^0(SF_6)$ is measured to be +13.0 cals/deg (see Table 4.3). Only a rough analysis of $\Delta S_a^0(SF_6)$ is possible since the vibrational frequencies and the symmetry of SF_6^- are not known. The theoretical calculation of Hay[98] predicts 844 cm^{-1} for the symmetric stretch in SF_6 and 652 cm^{-1} for that in SF_6^-. This corresponds to a 77% decrease in vibrational frequencies of the negative ion. To estimate the other frequencies in SF_6^- one can take the available[107] experimental six stretching and nine bending vibrations of SF_6 and reduce them to 77%. The vibrational entropy change ΔS_a^0(vib) $\approx$ 6.5 cals/deg can be evaluated from these frequencies. The increased moments of inertia in SF_6^- due to the larger S-F distance lead to the value ΔS_a^0(rot) = 1.1 cals/deg. The sum of these changes gives $\Delta S_a^0(SF_6)$ = 7.6 cals/deg, which is smaller than 13.0 cals/deg obtained in the present investigation from the study of the temperature dependence of the electron transfer equilibria (1.1). Unfortunately no good theoretical calculations on SF_6 and SF_6^- are available, such that a good estimation of $\Delta S_a^0(SF_6)$ can be made.

It is also possible that the structure of SF_6^- is different. Hay[98] assumed that the octahedral symmetry of SF_6 is retained in SF_6^- and there is no Jahn-Teller distortion, but did not investigate structures of lower symmetries. A low symmetry structure resembling SF_5....F^-

has been proposed by Brauman[91a]. Lifetime calculations of $(SF_6^-)^*$ were more compatible with such a structure than with the regular octahedron. The softer frequencies and lower symmetries used by Brauman[91a] for this structure probably lead to a ΔS^0_a much closer to 13.0 cals/deg. Unfortunately Brauman's calculations were based on $EA(SF_6) = 0.54$ eV[119], a value much lower than the 1.03 eV supported by the present investigation (Table 4.3).

Modern ab initio MO calculations for SF_6, SF_6^-, C_6F_6, $C_6F_6^-$, and other compounds discussed above can provide useful information on the geometry and vibrational frequency changes. The present stimulating results should encourage such efforts.

5. THERMAL ELECTRON DETACHMENT RATE CONSTANTS. THE ELECTRON DETACHMENT FROM AZULENE NEGATIVE ION

5.1 Introduction

The measurements and results presented in the chapter are also part of the collaborative works done by this author with Dr. E. P. Grimsrud, who spent his 1984/85 sabbatical leave in our laboratory, when this project was undertaken.

In the course of our continued investigations on kinetics and equilibria of electron transfer reactions (5.1), we had noticed in high temperature runs involving compounds of low electron affinity that the decreases of the negative ion concentrations with time were attributed to thermal electron detachment d, (equation (5.2))

$$A^- + B = A + B^- \qquad (5.1)$$

$$A^- \underset{a}{\overset{d}{\rightleftharpoons}} A + e \qquad (5.2)$$

These observations led to the idea that measurements of the electron detachment rate constant, k_d, based on the observation of the decay of A^- with time would be possible with our apparatus. In order to prevent interference from electron (re)attachment by equation (5.2)a, the presence of an electron scavenger (Sv) would be necessary. The electron scavenger should have a high electron affinity, EA, so that it does not detach electrons. Furthermore, Sv or Sv^- should not react with A or A^-. In order to test the feasibility of the detachment measurements, azulene, EA(Az) = 16.0 kcal/mol (Table 4.3) was selected as the subject of the measurement and perfluoromethyl cyclohexane C_7F_{14}, EA = 24.9 kcal/mol (Table 4.3), as the scavenger. SF_6 has been commonly used as an electron scavenger and probably it would have worked also in the present experiments. The choice of C_7F_{14} was made on the basis that this compound was

found to be somewhat less reactive[34b] than SF_6 towards electron transfer.

To our knowledge, direct determination of the thermal electron detachment rates (d) from polyatomic ions have not been reported previously. Pack and Phelps[155] have measured detachment rates from the diatomic O_2^-. These were based on observations of electron current waveforms in drift tube experiments. Azulene is a suitable choice also because the thermal electron attachment rate constant k_a for this compound is available from electron swarm experiments performed by Christophorou et al.[132]. Therefore, the equilibrium constant for electron detachment and attachment given in equation (5.2) can be evaluated from k_a, once k_d has been determined. Furthermore, K can be evaluated from statistical mechanics using the known EA of Az and the known entropy change $S^0(Az^-) - S^0(Az)$. The $\Delta H_a^0(Az)$ and $\Delta S_a^0(Az)$ are given in Table 4.3 obtained from electron transfer equilibria measurements. Comparison of two independent determinations represents a fundamental test of the consistency of all the data, equations and assumptions.

The measurements of electron attachment/detachment rate constants are performed with the same instrument used for other measurements in the present investigation. The determination of rate constants follows the same procedure discussed in chapter 3.

5.2 Measurements and Results: Reaction Mechanisms and Determination of Thermal Detachment Rate Constant

The key experiments demonstrating the nature of the measurements are given in Figs. 5.1 to 5.7. The pertinent reactions are shown in mechanism (5.3).

$$Az + e \underset{d}{\overset{a}{\rightleftharpoons}} Az^- \qquad (5.3)$$

$$Sv + e \xrightarrow{s} Sv^-$$

$$Az^- + Sv \xrightarrow{tr} Az + Sv^-$$

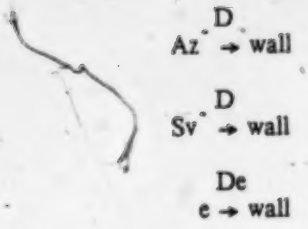

Both Az and the scavenger Sv (C_7F_{14}) capture secondary electrons produced by the electron pulse and form the negative ions Az^- and Sv^-, Figure 5.1. Az^- particularly at the higher temperatures, is seen to decrease rapidly with time. It will be shown that the high temperature decrease is due almost exclusively to thermal electron detachment (d) and Az^- decay curves like those in the high temperature runs of Fig. 5.1 can be used to determine k_d and its temperature dependence. The slopes obtained from the linear sections of the log[Az^-] versus time plots (Figure 5.1) lead to the (observed) Az^- loss frequencies $\nu_0(s^{-1})$.

Since Az^- is also lost by diffusion to the wall, the reactive loss of Az^- is given by (5.4). The diffusion coefficients for Az^- and Sv^- are expected to be very similar.

$$\nu(Az^-) = \nu_0(Az^-) + \nu_D \tag{5.4}$$

$$\nu_D(Az^-) \simeq \nu_D(Sv^-) \tag{5.5}$$

The reason for such an expectation is the following. Lindinger and Albritton[156], have shown that the zero field mobilities and thus the diffusion coefficients for a large variety of ions in argon follow the Langevin mobility expression. This means that the diffusion coefficients ratio of the two different ions like Az^- and Sv^- in the same gas (CH_4) will be given by[156],

$$D(Az^-)/D(Sv^-) = (\mu_{Sv}/\mu_{Az})$$

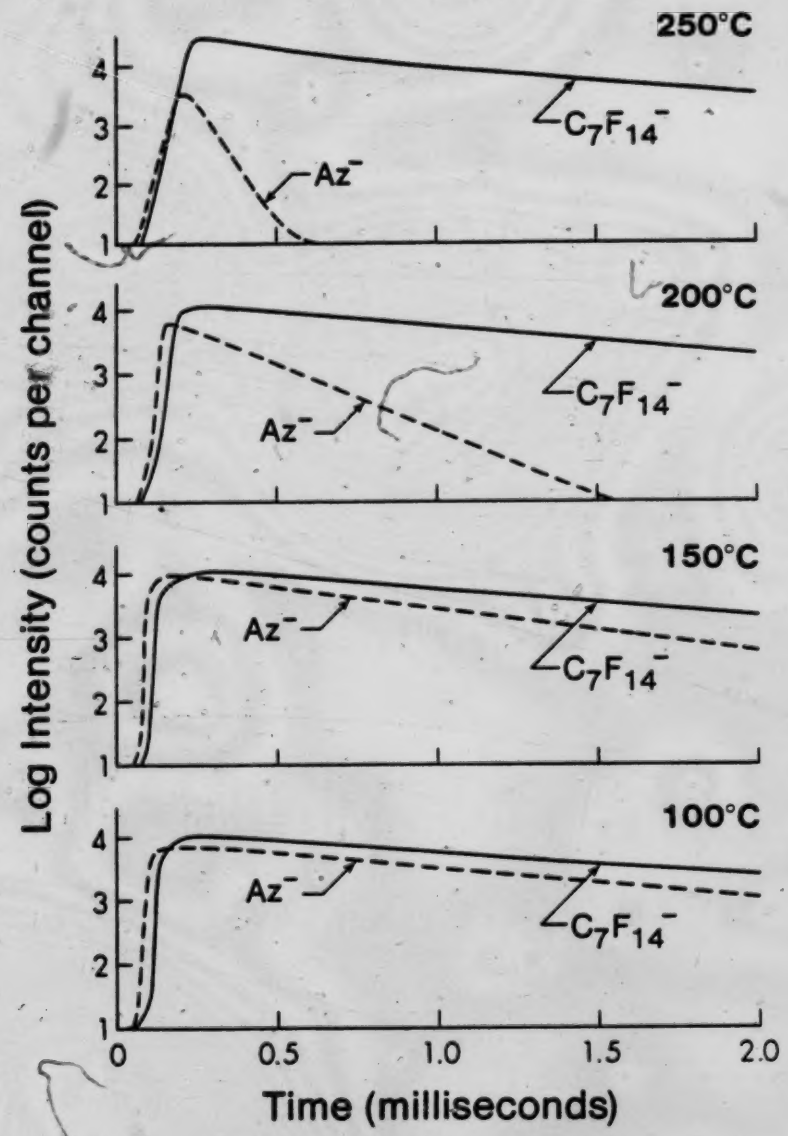

Figure 5.1 Observed ion intensities for azulene negative ion Az^- and perfluoromethylcyclohexane negative ion $C_7F_{14}^-$. All runs were made with the composition: carrier gas methane 4.0 torr, azulene 2.2 mtorr and perfluoromethylcyclohexane 0.7 mtorr. Slopes of linear sections of log[Az^-] vs. t plots lead to the observed pseudo first order rate constant $\nu_0(Az^-)$. At the low temperature 100°C, $\nu_0(Az^-)$ is mostly due to the (slow) direct electron transfer to the electron scavenger, $\nu_{tr}(Az^-)$, and to diffusion to the wall $\nu_D(Az^-)$. At the high temperatures 175-250°C the loss of azulene negative ion is almost exclusively due to thermal electron detachment (d): $Az^- \rightarrow Az + e$.

where μ is the reduced mass involving the molecular mass of the gas molecule and that of the respective ion. Due the much larger mass of the ions relative to that of CH_4, the above diffusion coefficients and the corresponding k_D for the heavy ions can be assumed to be identical. In the present investigation we have assumed $D(Az^-) \simeq D(Sv^-)$, equation (5.5), and used experimentally measured $\nu_D(Sv^-)$ obtained in runs with same major gas composition, pressure and temperature, but without Az, to evaluate $\nu_D(Sv^-)$. In such runs, the observed log[Sv^-] vs time is linear, Figure 5.6A, and the slope provides $\nu_D(Sv^-)$. The experimentally determined $\nu_D(Sv^-)$ and its temperature dependence is given in Table 5.1.

The ideal electron scavenger should not react with Az^-. Unfortunately, C_7F_{14} is not ideal in sofar as it accepts electron from Az^-. However, the electron transfer (tr) reaction is very slow and essentially temperature independent. This is demonstrated in Figure 5.2 where $\nu(Az^-)$ is plotted vs. temperature. In these runs a constant pressure of Sv was used. From 30 to about 130°C, $\nu(Az^-)$ is seen to be approximately constant. Above this temperature a rapid increase is observed. Evidently, the constant $\nu(Az^-)$ at low temperature is due to electron transfer alone, $\nu_{tr}(Az^-) = k_{tr}[Sv]$, while at the higher temperatures there is a rapid onset of electron detachment. A confirmation that $\nu(Az^-) = \nu_{tr}$ in the low temperature range is given in Figure 5.3. The plot of $\nu(Az^-)$ versus Sv concentration goes through the origin as required by the relationship. The k_{tr} determined from the straight line extrapolation in Fig. 5.2 to higher temperatures can be used to obtain values for k_{tr} at higher temperatures, where transfer and detachment occur. The k_{tr} data are given in Table 5.1.

The rates of Az^- and electron (e) formation based on the mechanism (5.3) are shown in equations (5.6) and (5.7). The equations are valid for reaction times longer than ~0.2 ms i.e., past the initial electron capture regime.

$$-d[Az^-]/dt = (k_d + k_D + k_{tr}[Sv])[Az^-] - k_a[Az][e] \quad (5.6)$$

$$d[e]/dt = k_d[Az^-] - (k_a[Az] + k_s[Sv] + k_{De})[e] \quad (5.7)$$

For steady state concentration of electron, $d[e]/dt = 0$, thus

$$[e] \simeq k_d[Az^-]L \quad (5.8)$$

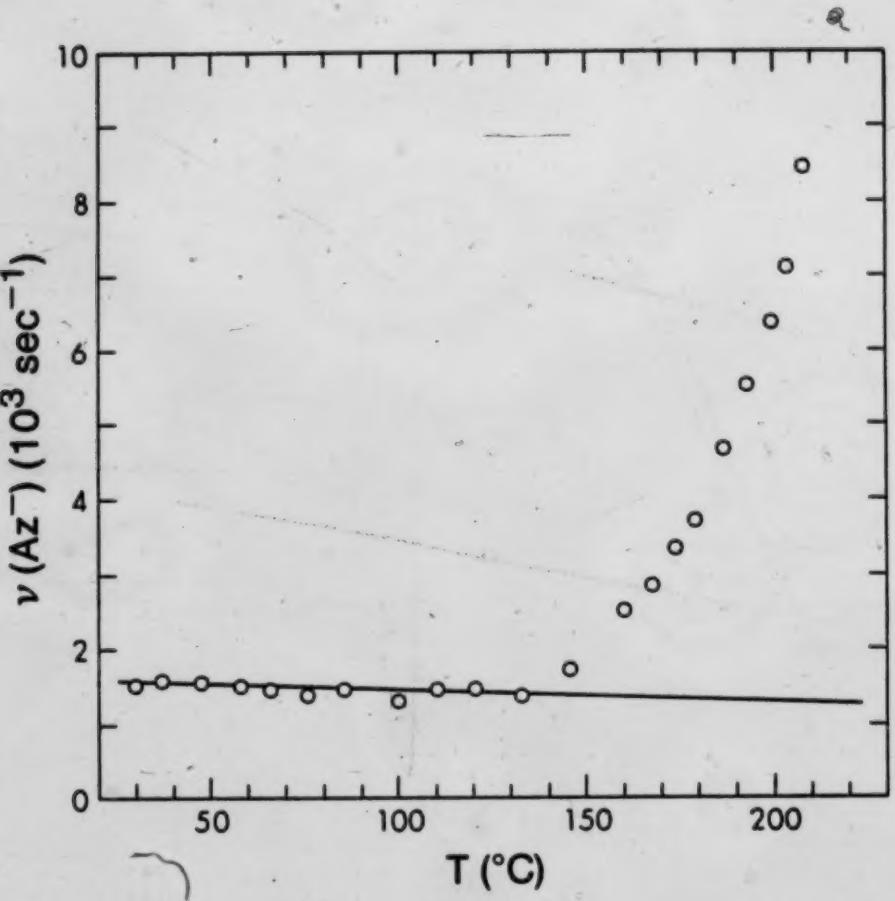

Figure 5.2. Plot of $\nu(Az^-)$, obtained after correction for the diffusional loss versus temperature. $\nu(Az^-)$ is the reaction frequency for loss of Az^- by electron detachment and electron transfer. Constant $\nu(Az^-)$ from 30 to ~130°C is only due to electron transfer tr. (see Figure 5.3). The rapid increase of $\nu(Az^-)$ above 150°C is due to thermal electron detachment from Az^-. Methane 4.0 torr, azulene 1.9 mtorr, electron scavenger 7.3 mtorr.

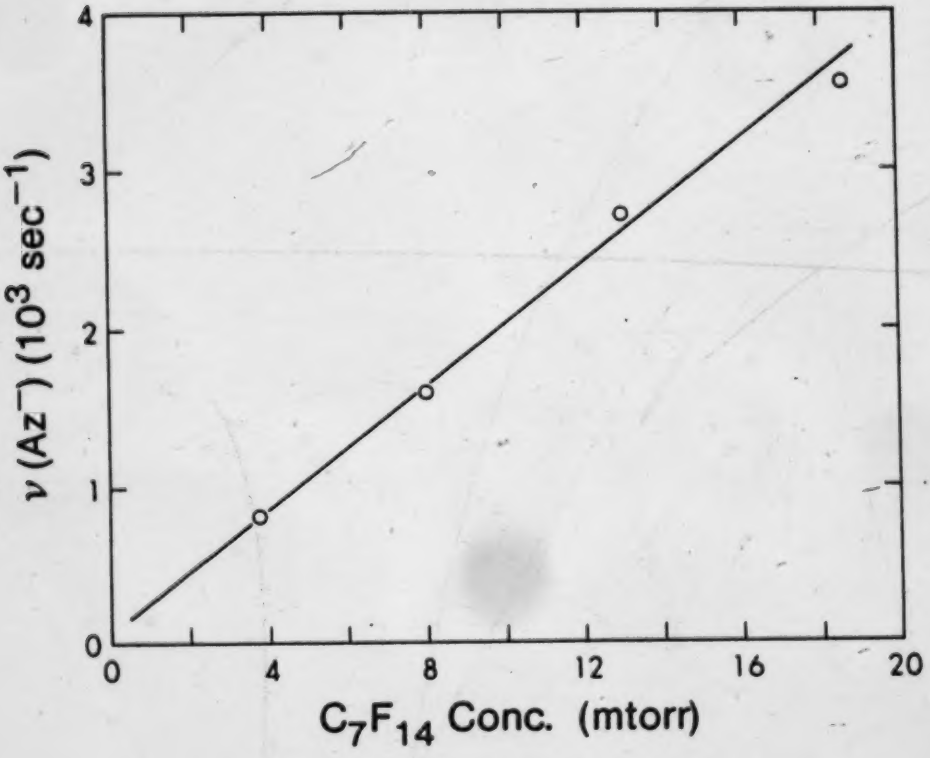

Figure 5.3 Plot of $\nu(Az^-)$, after correction for diffusional loss; versus pressure of perfluoromethylcyclohexane at constant temperature 35°C. Proportionality of $\nu(Az^-)$ with the scavenger pressure, demonstrate that at this low temperature $\nu(Az^-) = k_{tr}[C_7F_{14}]$ i.e., electron loss due to detachment can be completely discounted.

Table 5.1: Kinetic data[a].

Reaction	Symbol and magnitude of rate constant	Source of data
$Az^- \rightarrow$ Wall	$\nu_D = k_D = (1.84 \times 10^{-2} T^2/p)\ (s^{-1})$[b]	present work and
$Sv^- \rightarrow$ Wall	$\nu_D = k_D = (1.84 \times 10^{-2} T^2/p)\ (s^{-1})$[b]	Fig. 5.6A, ref. 156
$e \rightarrow$ Wall	$\nu_{De} = k_{De}\ (1.6 \times 10^7/p(\text{torr, methane})\ s^{-1})$	Ref. 158-159.
$Az^- + Sv = Az + Sv^-$	$k_{tr} = 2.9 \times 10^{-13} T^{0.554}$ (cc particle^{-1} s^{-1})	Present work, Fig. 5.2-5.3.
$Az^- \rightarrow Az + e$	$k_d = 1.14 \times 10^{11} \exp[-15.7\ (\text{kcal/mol})/RT]\ s^{-1}$	Present work, Fig. 5.5
	$k_d = 2.49 \times 10^6 T^{3/2} \exp[-14.5\ (\text{kcal/mol})/RT]\ (s)^{-1}$	
$e + Az \rightarrow Az^-$	$k_a(Az) = 4 \times 10^{-8}$ (cc particle^{-1} s^{-1})	Christophorou[25,132]
$e + Sv \rightarrow Sv^-$	$k_S = 14 \times 10^{-8}$ (cc particle^{-1} s^{-1})	Christophorou[25,132]

[a] $Sv = C_7F_{14}$.

[b] major gas methane, p in torr.

where,

$$L = 1/(k_a[Az] + k_s[Sv] + k_{De})$$

$$-d[Az^-]/dt = (k_d + k_D + k_{tr}[Sv] - k_a k_d[Az]L)\,[Az^-] \quad (5.9)$$

$$\nu(Az^-) = k_{tr}[Sv] + k_d N \quad (5.10)$$

$$N = 1 - k_a[Az] / (k_a[Az] + k_s[Sv] + k_{De})$$

$$= 1 - k_a[Az]L \quad (5.11)$$

$$\nu_N(Az^-) = \nu(Az^-) - k_{tr}[Sv] = k_d N \quad (5.12)$$

Since all the rate terms involving $[Az^-]$ and [e] are first order, the exact integration of (5.6) and (5.7) predicting the time dependence of $[Az^-]$ and [e] is possible. The integrated equations are available[157]. The expressions are lengthy so that the importance of the individual terms is difficult to assess. The experimental conditions, see rate data in Table 5.1, are such that the rate of production of electrons by detachment (d) is slow compared to the removal of electrons by diffusion (De), attachment (a) and scavenging (s). This condition justifies the application of the steady state assumption to the rate of change in [e], equation (5.7). With this assumption one obtains (5.8) to (5.12). Equation (5.8) predicts that the rate of Az^- disappearance is first order in $[Az^-]$, as observed in the experiments, Figure 5.1.

The factor N (equation (5.12)) gives the net electron loss from Az^- i.e., the fraction of electrons formed by detachment from Az^- and not recaptured by Az. At very high Sv concentration N = 1 and $\nu_N(Az^-) = k_d$.

Plots of $\nu_N(Az^-)$, obtained from the experimentally determined $\nu(Az^-)$ and $\nu_{tr}(Az^-)$ (equation (5.12)), versus [Sv] are shown in Figure 5.4. Also given in Figure 5.4 are values of N calculated with equation (5.11) using available values[25,158] for k_a, k_s, and k_{De}, see Table 5.1. An estimate for the rate constant of electron loss by free diffusion (k_{De}) could be obtained by using the expressions given in McDanial[158]. Λ is obtained from Fig. 10-10-3 of ref. 158. For the present roughly spherical ion-source of diameter ~1.0 cm, Λ = 0.16 cm. The diffusion coefficient De in methane was determined by applying Einstein equation [eq. (10-2-5)][158] to electron mobility data reported by Hurst et al.[159]. The electron attachment rate constants, k_a

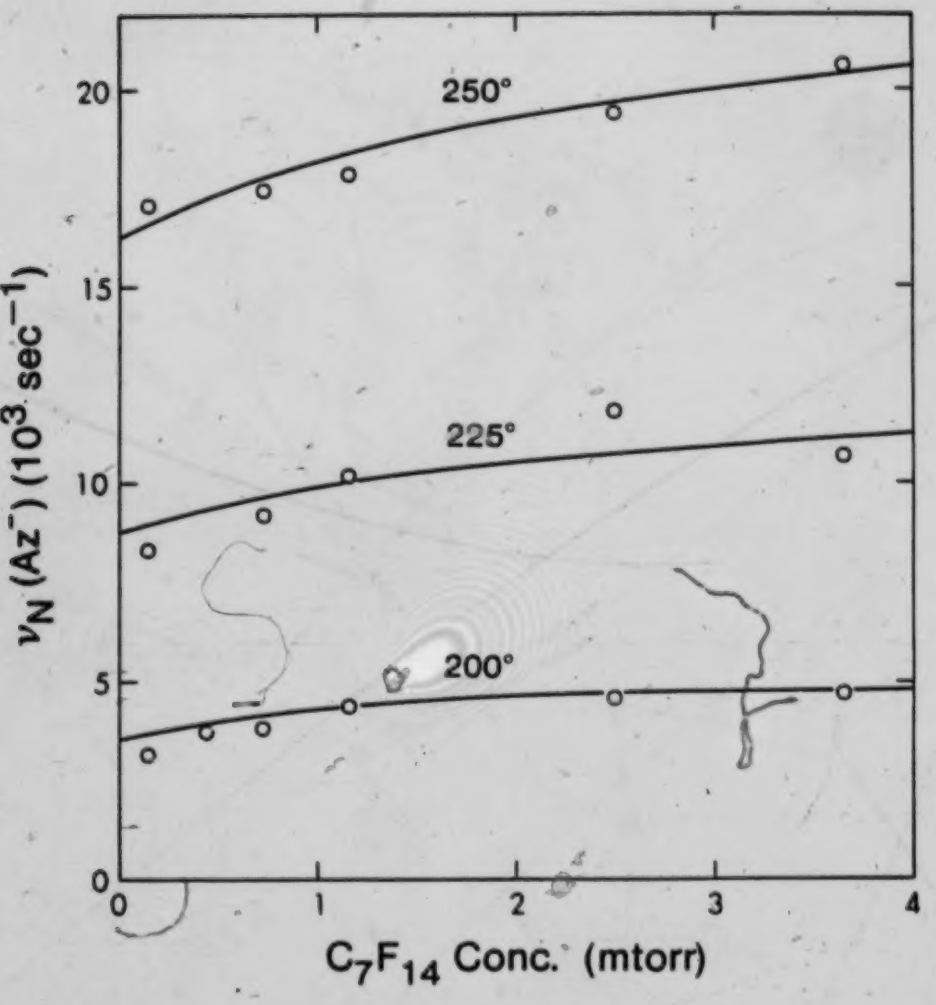

Figure 5.4. Plot of experimental points for $\nu_N(Az^-) = \nu(Az^-) - \nu_{tr}(Az^-)$ versus pressure of electron scavenger. At high scavenger concentrations none of the detached electrons from Az^- are recaptured by Az. Methane = 4.0 torr, Az = 2.2 mtorr in all experiments.

and k_s are from Christophorou[25,132]. The diffusion rate constant k_{De} for thermal electrons in methane was evaluated on basis of literature data as explained above. Since k_a, k_s, and k_{De} are approximately temperature independent[25,132,158], the same values for N should apply to the three temperature runs shown in Figure 5.4. The solid curves given in the Figure were obtained by multiplying N with a chosen constant factor at each temperature such that, a fit to the experimental data points at this temperature is obtained. The fits obtained are very good. It follows from (5.12) that the constant factor equals k_d at the respective temperature. The k_d's obtained in this manner are high temperature points in the Arrhenius plot of k_d shown in Fig. 5.5. The k_d used in plot of Fig. 5.5 for the lower temperatures were obtained by a slightly different procedure. At lower temperatures it is possible to make measurements of $\nu_N(Az^-)$ at higher scavenger concentrations where $N \simeq 1$ and the ν_N obtained at highest scavenger concentration were taken as k_d, see Figure 2.2. At high [Sv], the initial formation of Az^- is small because Sv scavenges the initial electrons. This makes the measurements of $\nu(Az^-)$, at high [Sv], particularly difficult at high temperatures where Az^- is disappearing very rapidly (Figure 5.1).

The results from the Arrhenius plot of k_d are discussed in the next section. Here we consider two additional points of interest. The results in Fig. 5.4 demonstrate that diffusion to the wall is a major loss route for the electrons. Thus an N as large as 0.7 is predicted in the complete absence of scavenger. One might conclude, that approximate determinations of k_d could have been obtained even without scavenger. Experiments performed under such conditions, Fig. 5.6, demonstrates that the scavenger fulfils an additional important role.

The plot in Figure 5.6a illustrates the behavior when only an electron capturing compound (C_7F_{14}) which does not react further is present. The ionising electron pulse (~30 μs) produces more than 20 secondary electrons for each primary electron. A good fraction of these is probably captured by C_7F_{14}, but some electrons diffuse rapidly to the wall. The resulting weak positive space charge traps the negative ions and induces positive ion-electron ambipolar diffusion over a short period of time (0.1 ms). The negative ions ($C_7F_{14}^-$) emerge after the collapse of the positive field, which terminates the electron ambipolar diffusion (Fig.5.6a).

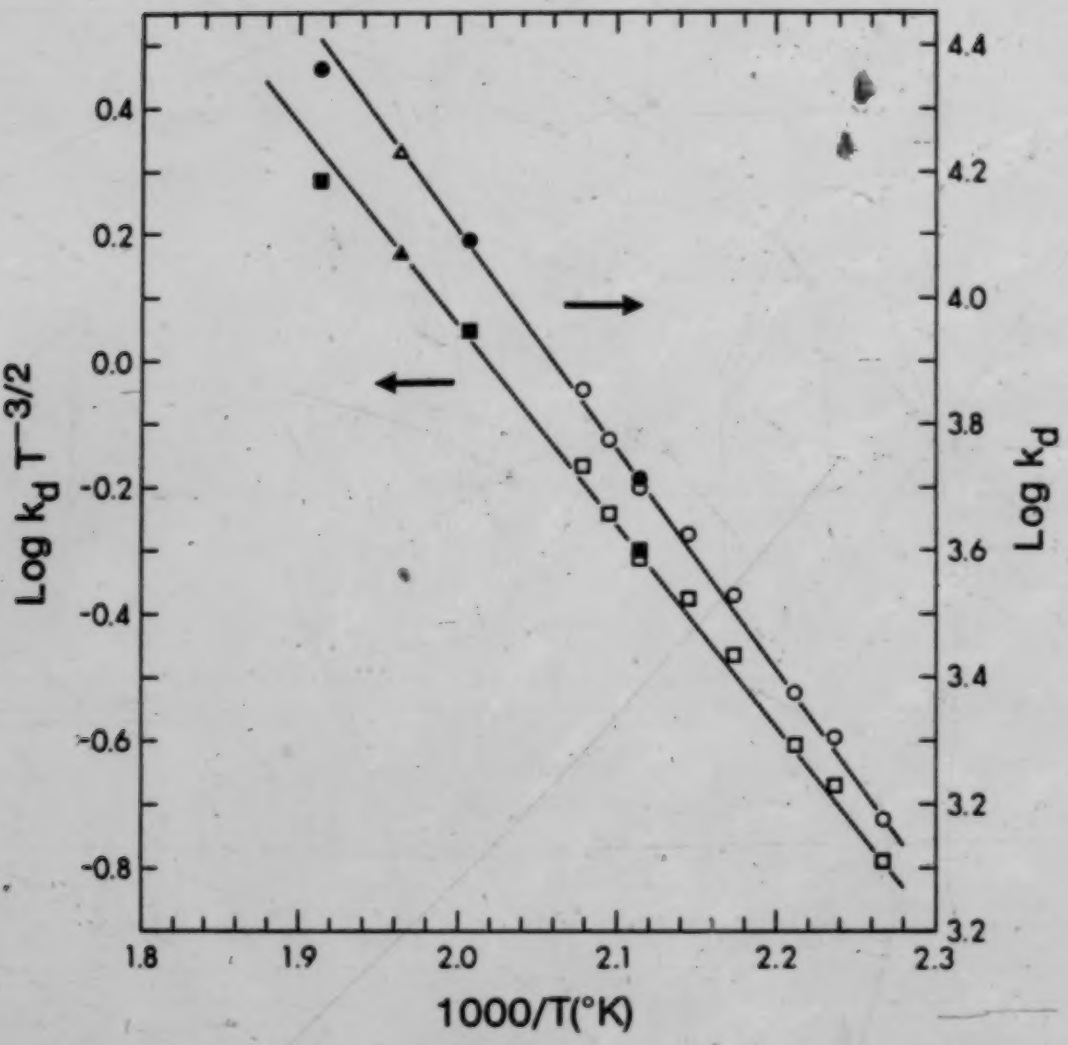

Figure 5.5. Arrhenius plots of rate constant k_d for electron detachment from azulene negative ion. Right hand plot lead to: $k_d = 1.14 \times 10^{11}$ (s^{-1}) exp(-15.7(kcal/mol)/RT). The left hand plot leads to $k_d = 2.5 \times 10^{6}$ (s^{-1})$T^{3/2}$exp(-14.5 (kcal/mol)/RT).

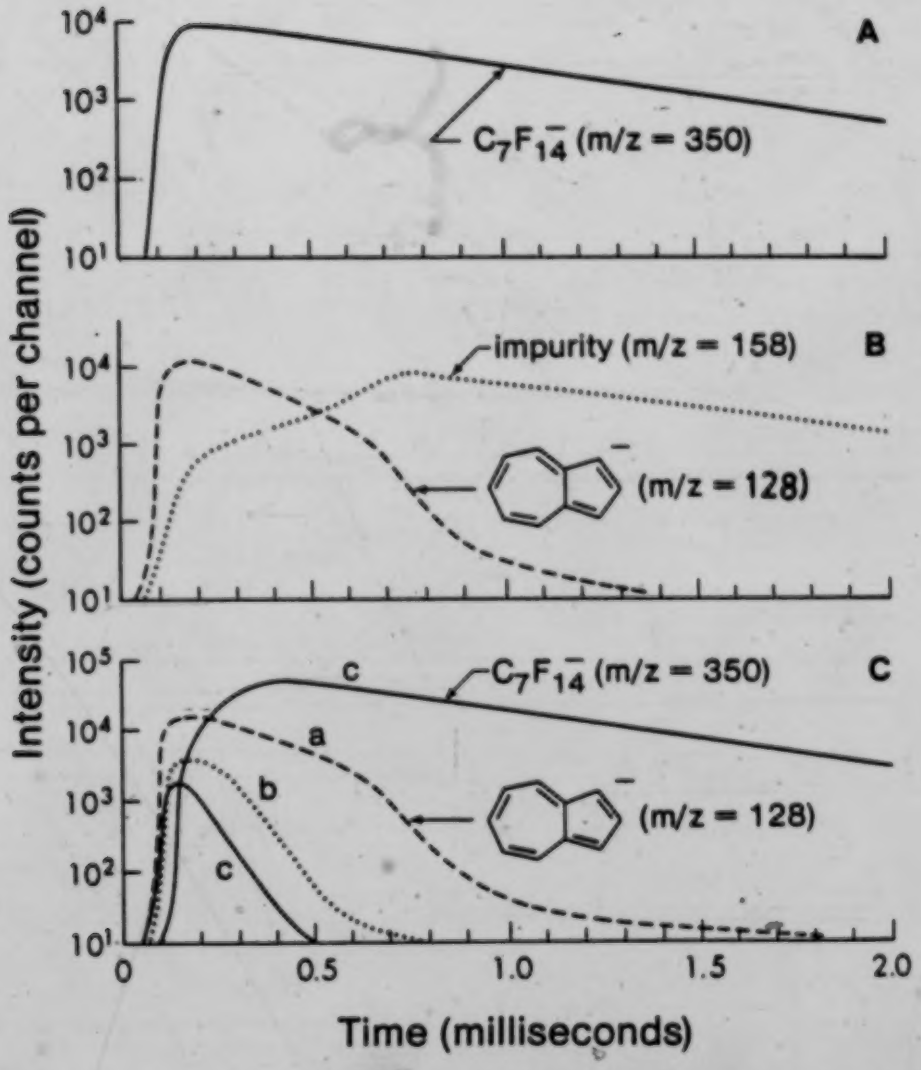

Figure 5.6. Time dependence of ions after ~60 μs ionising electron pulse. All runs are with 3.2 torr methane and at 250°C. (A) only Sv = C_7F_{14} (1.5 mtorr) is present. Decrease of ion intensity due to diffusion of perfluoromethylcyclohexane negative ion to wall. (B) Only azulene (2.2 mtorr) is present. Electrons released by detachment from Az^- are partially trapped by positive space charge which collapses after ~700 μs. (C) Azulene (2.2 mtorr) in all runs with (a) 0.0 mtorr Sv; (b) 2.3 mtorr Sv; (c) 1.5 mtorr Sv is present. The Sv^- signal was essentially identical under conditions (b) and (c).

Between ~0.2 ms and 2.0 ms a very slow decrease of $C_7F_{14}^-$ due to positive-negative ion ambipolar diffusion and free diffusion is observed. In Fig. 5.6b, C_7F_{14} is replaced with azulene which is known to thermally detach electrons. The events in the initial ~0.1 ms are similar to those in Fig. 5.6a. However, because Az^- detaches captured electrons and thus maintains a supply of free electrons, the weak positive space charge and ambipolar positive ion-electron diffusion are maintained for much longer time (~0.6 ms, Fig. 5.6b). In that time period the detaching Az^- decreases more slowly, because it recaptures electrons whose concentration is relatively high due to the slow electron ambipolar diffusion. After collapse of the positive field (0.6 ms) the electrons diffuse more rapidly to the wall, whose concentration decreases and this results in a more rapid loss of Az^- due to the increased net detachment.

The observations based on the Fig. 5.6b are complicated by the presence of a trace impurity contained in azulene. The impurity ion, formed by electron capture and electron transfer from Az^-, does not thermally detach electrons. Its formation aids in the collapse of the positive field. Noticeable is the increase of intensity of this ion on collapse of the positive field (~0.6 ms).

The curves in Fig. 5.6c illustrate the effect of addition of C_7F_{14} to the azulene reaction mixture. At sufficiently high C_7F_{14} concentrations linear plots are obtained which lead to $\nu_0(Az^-)$ used in the measurements of detachment. Under this condition, sufficient electrons are scavenged by C_7F_{14}, the positive trapping field is collapsed and there is free diffusion of the electrons to the wall.

When a molecule like Az or C_7F_{14} or A in general captures thermal electrons, an excited negative ion $(A^-)^*$ is formed. $(A^-)^*$ may detach the electron or be stabilized (quenched) by third body collisions as shown in scheme (5.13), where τ is the lifetime for detachment from $(A^-)^*$.

$$e + A \underset{1/\tau}{\overset{k_a'}{\rightleftharpoons}} (A^-)^* \xrightarrow{k_q[M]} A^- \qquad (5.13)$$

$$e + A \underset{k_d}{\overset{k_a}{\rightleftharpoons}} A^- \qquad (5.14)$$

As dicussed earlier, it can be shown that at high pressures of M, where $k_q[M] >> 1/\tau$ such that $(A^-)^*$ are collisionally stablized, $k_a' = k_a$ and the overall rate in (5.13) becomes second order, $k_a[A][e]$, as shown in (5.14). The reverse of (5.13) is then first order, $k_d[A^-]$. In the preceding treatment of the Az^- data we assumed that the present experiments were falling in this high pressure regime. Since $\tau(Az^-)^* \simeq 7\ \mu s$[25], there will be some 700 collisions of $(Az^-)^*$ with methane within the lifetime of $(Az^-)^*$ at the 4.0 torr of methane used. This result indicates that all the $(Az^-)^*$ formed by attachment will be stabilized, i.e., (5.13) will be at the high pressure limit. The results shown in Fig. 5.7 provide an experimental confirmation that this is the case. It is seen that the experimentally determined ν_N and k_d are independent of the total pressure. This demonstrates that the detachment reaction is first order for the experimental conditions used.

5.3 Discussion of Thermal Detachment Rate Constants and Electron Attachment-Detachment Equilibria

The Arrhenius activation energy derived from the plot in Figure 5.5 is 15.7±1.0 kcal/mol. The electron affinity of azulene obtained from the determinations of electron transfer equilibria measurements is 16.0 kcal/mol, Table 4.3. Thus, the detachment Arrhenius activation energy from Fig. 5.5 is very close to the EA of azulene.

The equilibrium constant K for the thermal electron attachment-detachment equilibria can be expressed by equation (5.14a), the Q's are the respective partition functions, per unit volume and m is the mass of the electron.

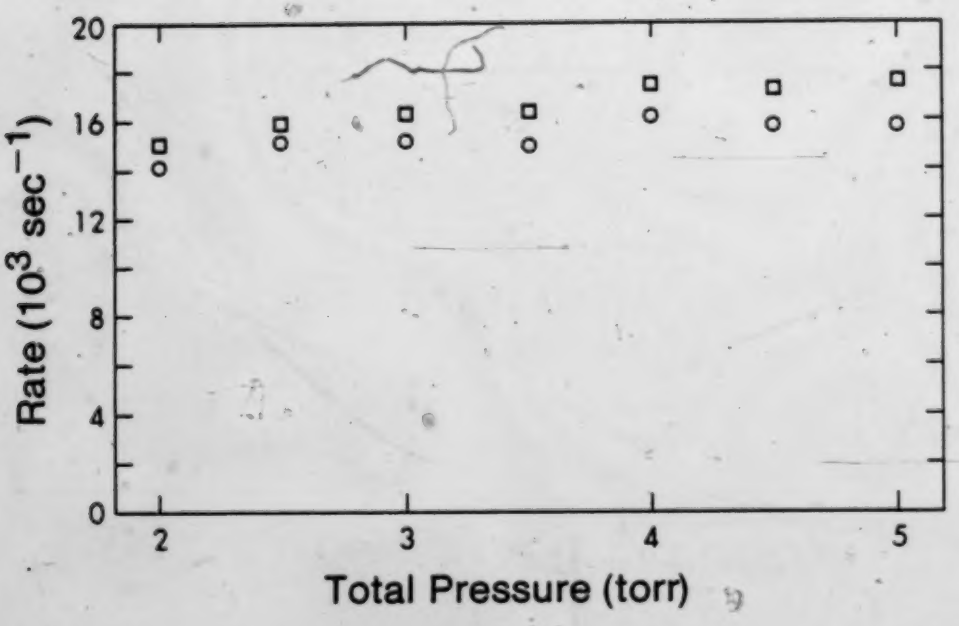

Figure 5.7. Dependence of electron detachment rate constants on total pressure: □ k_d; ν_N: ○. Temperature = 236°C, constant pressure ratio of methane : Az : Sv = 10000 : 2.4 : 5.0.

$$e + A \underset{k_d}{\overset{k_a}{\rightleftharpoons}} A^- \qquad (5.14)$$

$$K = k_a/k_d = (Q_{A^-}/Q_A Q_e) \exp [EA(A)/RT] \qquad (a)$$

$$K(A) = \left[\frac{Q_{A^-}/Q_A}{2(2\pi mkT/h^2)^{3/2}} \right] \exp [EA(A)/RT] \qquad (b)$$

$$Q_{A^-} / Q_A = \exp [\Delta S^0(A^-)/R] \qquad (c)$$

$$\Delta S^0(A^-) = S^0(A^-) - S^0(A) \qquad (d)$$

$$K = 2.07 \times 10^{-16} T^{3/2} \exp[\Delta S^0(A^-)/R + EA(A)/RT] \qquad (e)$$

(stand. state 1 particle cm^{-3})

Since the electron when in a box of laboratory dimension, obeys Boltzman statistics, Q_e is given by the translational partition function of a particle in a box with unit distance and degeneracy of 2. This expression is used in the denominator of equation (5.14)b. The form (5.14)c is useful since $\Delta S^0(A^-)$ values, defined in (5.14)d are available from experimental determinations (Table 4.3, Figure 4.21). Some such values together with the corresponding electron affinities are given in Table 5.2. For azulene $\Delta S^0(Az^-) = 4.4$ cals/deg and EA(Az) = 16.0 kcal/mol. With these data the equilibrium constant K(Az) can be evaluated at any temperature from equation (5.14)e.

Christophorou[25,132] has determined values for k_a of azulene and many other compounds. Some of these values for k_a are given in Table 5.2. For azulene $k_a = 4 \times 10^{-8}$ cm^3 $particle^{-1}$ s^{-1} at 500 K. The value of K(Az) at that temperature is 1.7×10^{-12} (cm^3 $particle^{-1}$).

$$k_d = k_a/K \qquad (5.15)$$

With equation (5.15) one evaluates $k_d(Az) = 2.4 \times 10^4$ s^{-1} (488 K). The value, $k_d(Az)^- = 1.3$

Table 5.2: Thermal electron detachment rate constants[a].

Compound A	EA(A)[b] kcal/mol	ΔS_a^{0}[b] cal/deg	K(500K)[c]	k_a[d]	k_d(500K) s^{-1}
Azulene	16.0	+4.4	1.76×10^{-12}	4×10^{-8}	2.4×10^{4} (1.3×10^{4})[e]
$PhNO_2$	23.2	-1.0	1.9×10^{-10}	7×10^{-10}	4.0
SF_6	23.7	+13.0	3.8×10^{-7}	3×10^{-7}	0.8
C_7F_{14}	24.9	+2.5	6.1×10^{-9}	1×10^{-7}	16.0

[a]Evaluated from $k_d = K/k_a$.

[b]From Table 4.3.

[c]Equilibrium constant evaluated from eqn. (5.12) and EA(A) and ΔS_a^0. Unit of K is (cc particle^{-1}).

[d]From Christophorou (ref. 25, 132), units (cc particle^{-1} s^{-1}).

[e]Experimental value from Fig. 5.5.

x 10^4 s^{-1} was obtained from the present detachment measurements (Fig. 5.5). The agreement is within a factor of 2, which is good considering the ±1 kcal/mol uncertainty of the electron affinity and the uncertainties in the k_d experimental determination.

Experimental determinations[25,132] of attachment rate constants $k_a(A)$, where A are various electron capturing agents, indicate that these are temperature independent, as long as the temperature change is not very large. Assuming that $k_a(Az)$ is temperature independent in the temperature range used in the Arrhenius plot (Fig. 5.5), application of (5.14)e and (5.15) leads to (5.16).

$$k_d(s^{-1}) = (4.8 \times 10^{15} T^{3/2} \times k_a) \exp -[\Delta S^0(A^-)/R + EA(A)/RT] \qquad (5.16)$$

Assuming that the $\Delta S^0(A^-)$ is temperature independent, one should obtain a more accurate EA(A) not from the direct $\ln k_d$ vs. 1/T plot, but from a $\ln(k_d T^{-3/2})$ vs. 1/T plot. Such a plot is given in Fig. 5.5.

Earlier determination of EA(Az) based on the electron capture detector technique[34a], with which the temperature dependence of a quantity proportional to the equilibrium constant K for the electron attachment-detachment, (eqn. (5.14)), is determined, gives values (for EA(Az)) of 13.5 to 15.1 kcal/mol[34a] and 13.8 kcal/mol[160]. These treatments used slopes from van't Hoff plots which were corrected for the $T^{3/2}$ dependence of the equilibrium constant. For a temperature dependent k_a, this approach is equivalent to $\ln k_d T^{-3/2}$ vs. 1/T plot. Thus the lower EA(Az) =14.5 kcal/mol (Fig. 5.5) obtained from this type of plot is in relatively good agreement with the electron capture results[34a,160]. Since the opposing temperature effect of the $\Delta S^0(Az^-)$ is expected to be smaller than the $T^{3/2}$ dependence, the average between the $T^{3/2}$ corrected activation energy (14.5 kcal/mol) (Fig. 5.5) and the electron affinity, EA(Az) = 16.0 kcal/mol from electron transfer equilibria measurments (Table 4.3) are considered to provide the best choice for the electron affinity of azulene and this value is EA(Az) = 15.3 kcal/mol or 0.66 eV.

6. BINDING ENERGIES OF ION-NEUTRAL COMPLEXES INVOLVING CHARGE DELOCALIZED NEGATIVE IONS

6.1 Introduction

The study of the properties of ion-molecule clusters can provide information on ion-solvation, ion-ligand complexes and ion-molecule reaction complexes, i.e., systems of importance in chemistry of ions in the condensed phase. A continuing effort from this laboratory[147,161] has been to try to show some of the major features of ionic solvation in condensed phase which can be explained on the basis of interactions of the ion with small number of solvent molecules. The present investigation is an extension of such efforts.

Negative ions represent one half of the ion population in condensed phases and are obviously important. Furthermore, in organic reactions carried out by ions, negative ions turn out to be much more important than positive ions, a fact well known to synthetic organic chemists. A particularly advantageous combination for synthetic work in the condensed phase involves negative ions and dipolar aprotic solvents like acetonitrile, MeCN; dimethylformamide, DMF; dimethylsulfoxide, DMSO etc. The advantage of this combination can be illustrated by examining reaction (6.1).

$$Cl^- + CH_3Br \rightarrow [\, Cl \cdot \overset{H}{\underset{H}{\overset{|}{\underset{/\quad\backslash}{C}}}} \cdot Br \,]^- \rightarrow ClCH_3 + Br^- \qquad (6.1)$$

The activation energy $E^{\ddagger}$, is smaller in dipolar aprotic solvents and the rates of (6.1) are many orders of magnitude faster than is the case for protic solvents[162]. Determinations of the

reaction coordinate of (6.1) in the gas phase[100-103] show that the energy of the transition state, shown in brackets above, is slightly lower than that of the reactants and this means that $E^{\ddagger}$ in solution is entirely due to the less favorable solvation of the reactants. Since the solvation terms of the ions are dominant, $E^{\ddagger}$ in solution is due largely to the difference of the solvation energy of the larger transition state negative ion relative to the smaller ionic reactant (Cl^-). The smaller $E^{\ddagger}$ observed in the dipolar aprotic solvents thus shows that the solvation energy in these solvents decreases less with increase of negative ion size than is the case for protic solvents[150].

Measured solvation energies of the ions $X^- = Cl^-, Br^-, I^-$ in liquid protic H_2O, MeOH, acetic acid and dipolar aprotic solvents such as, MeCN, DMSO, DMF are found to decrease faster from Cl^- to I^-, i.e., with increasing ionic radius, for the protic solvents relative to the dipolar aprotic solvents[150], in agreement with the expectations based on the reaction rate observations. Gas phase ion-cluster bond energies obtained from measurements of the ion equilibria between $X^- = Cl^-, Br^-, I^-$ and protic solvent, Sl = HOH and aprotic solvent molecules Sl = MeCN, DMSO, Me_2CO showed[150,163] that the bond energies between X^- and one of four solvent molecules: $X^-.Sl$ or $X^-.(Sl)_n$ decrease faster with increasing ion size, i.e., from Cl^- to I^- for protic relative to aprotic solvent molecules. The different behavior of the two types of Sl towards negative ions with increasing radius was attributed[150] to the different location of the dipole in the protic and dipolar aprotic Sl. In aprotic solvent the dipole is located on one end of the molecules viz $H_3C\text{-}C^{+}\equiv N$, such that the attractive approach of a positive ion is favored, while a negative ion cannot come close to the dipole due to the steric interference of the alkyl group. These relationships were also confirmed by theoretical calculations[150,164].

More commonly the reactant and product ions are not spherical monoatomic ions like Cl^- and Br^- in reaction (6.1) but organic anions and particularly organic anions with π-conjugation leading to extensive delocalization of the negative charge over a large part of the molecule (ion).

In the present work, measurements of binding energies of some 20 radical anions, two phenoxide anions and protic and aprotic solvent moleculules, which represents an extension of the analysis to delocalized ions and protic and dipolar aprotic solvent molecules, are presented.

In addition to the binding energies of charge delocalized anions, A^- with protic and aprotic solvent molecules Sl, mentioned above; binding energies of charge delocalized anions A^- to A and B, where A and B are various substituted nitrobenzenes, quinones, perfluoro molecules etc. will also be discussed. The binding energies in adducts involving perfluorinated molecules are of special interest, not only because binding energies in some adducts $A^-.B$, such as $A^-.SF_6$ are unusually weak compared to others, $A^-.C_6F_6$, for example but also the binding energies in $A.B^-$ and $A^-.B$ play an important role in interpreting the features of kinetics of some slow gas phase ion-molecule reactions, especially electron transfer reactions (1.1) as discussed in chapter 3. On basis of the binding energies possible structures for $A^-.B$ and $A.B^-$ will be provided.

6.2 Bonding of Charge Delocalized Anions to Protic and Dipolar Aprotic Solvent Molecules

6.2.1 Measurements and Results

The bond energies of A^- to Sl, where Sl are solvent molecules were determined by measuring the equilibria (6.2).

$$A^- + Sl = A^-.Sl \qquad (6.2)$$

The time dependence of the ion intensities in a typical experiment used for this purpose is shown in Figure 6.1 and is similar to those shown in Figure 3.7 earlier in chapter 3. Ions like A^- and $A^-.Sl$ after having reached equilibrium and thus achieved a constant intensity ratio $[A^-.Sl]/[A^-]$ with time, maintain (in the logarithmic plot used) a constant vertical distance. Inspection of the Figure shows that equilibria (6.2) are achieved very early in the measurement, which means that the forward and reverse rates of reaction (6.2) are fast under the conditions of the experiment. The equilibrium constant K_{ad} for the formation of adducts, are evaluated from the observed ion-intensities and lead to ΔG^0_{ad} values as shown in equation (6.3).

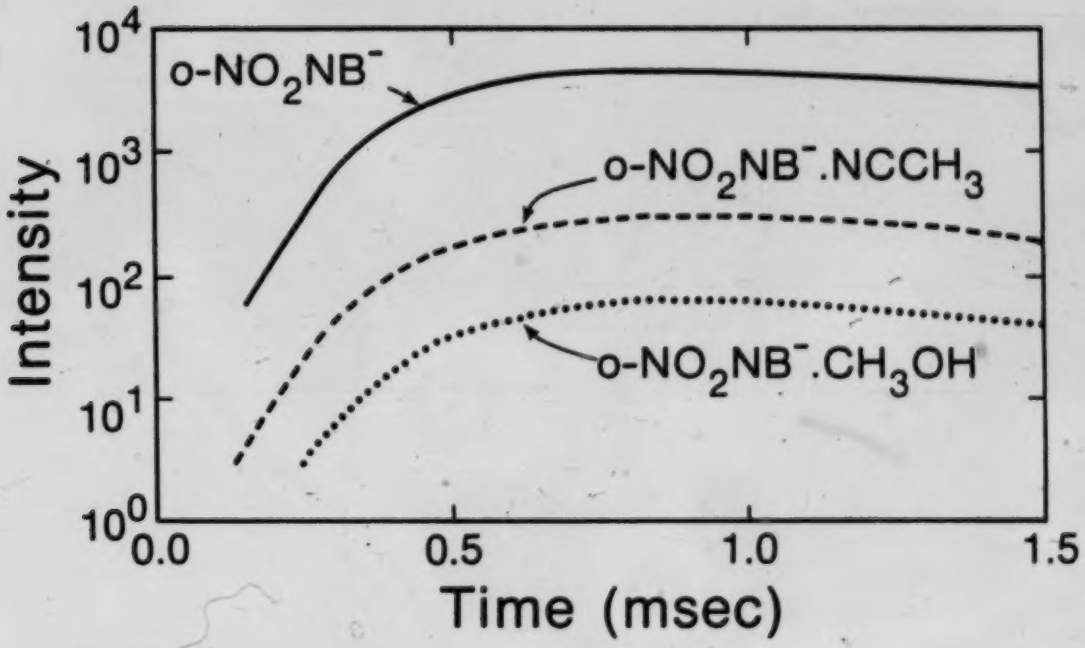

Figure 6.1. Ion intensities observed after electron pulse. Ion source pressures are: 2.8 torr methane; 0.02 mtorr 1,2-dinitirobenzene; 93 mtorr MeOH and 36 mtorr MeCN at 70°C. Adduct equilibria $A^- + Sl = A^-.Sl$ are achieved rapidly, ratio of $[A^-.Sl]/[A^-]$ appears as constant due to the constant vertical distance between respective ion intensities. Sl stands for solvent molecule.

$$K_{ad} = [A^{-}.Sl] / ([A^{-}][Sl]) \quad (6.3)$$

$$\Delta G^{0}_{ad} = - RT\ln K_{ad}$$

$$\Delta G^{0}_{ad} = \Delta H^{0}_{ad} - T\Delta S^{0}_{ad}$$

The results in the figure also demonstrate that for A = 1,3-dinitrobenzene, the A^{-}.MeCN adduct has much greater stability than A^{-}.MeOH.

In all equilibria measurements it was established that K_{ad} remains invariant as the partial pressure of A and Sl is changed, by a factor of 2 or 3, see Figure 6.2. The ΔG^{0}_{ad} values obtained with ~30 different A^{-} ions mostly substituted nitrobenzenes, XNB^{-}, some substituted quinones, azulene and maleic anhydride, with five solvent molecules: MeOH, MeCN, DMSO, DMF and tetrahydrofuran (THF) are given in Table 6.1.

The temperature dependence of the equilibrium constants K_{ad} for some of the equilibria were determined also and ΔH^{0}_{ad} and ΔS^{0}_{ad} values obtained from the van't Hoff plots are shown in Figure 6.3. These values are summarized in Table 6.2.

A plot of the binding energies in A^{-}.Sl versus the electron affinities of A is given in Figure 6.4. The electron affinities used are from the present investigation, Table 4.3.

The ΔG^{0}_{ad}, ΔH^{0}_{ad}, and ΔS^{0}_{ad} values obtained from the van't Hoff plots for equilibria (6.2) and given in Table 6.2 do not show a clear trend. One would have expected that for different A^{-} as $-\Delta G^{0}_{ad}$ decreases, so would also $-\Delta H^{0}_{ad}$ with ΔS^{0}_{ad} changing little, but the data indicate that a decrease in the binding free energy $-\Delta G^{0}_{ad}$ is not so much due to a decrease of $-\Delta H^{0}_{ad}$ but to a decrease of the adverse entropy change $-\Delta S^{0}_{ad}$. Considering that the van't Hoff plots could be measured only over a relatively narrow temperature range, the separation of the ΔG^{0}_{ad} into ΔH^{0}_{ad} and ΔS^{0}_{ad} terms might not be entirely reliable. For this reason, and also because ΔG^{0}_{ad} data in Table 6.1 are much more comprehensive, we will discuss the results only on the basis of the ΔG^{0}_{ad} data. The discussion will tacitly assume that the ΔG^{0}_{ad} values are largely due to ΔH^{0}_{ad} changes. A better understanding of the actual changes and the meaning of ΔS^{0}_{ad} values is possible when more measurements and theoretical calculations for the A^{-}.Sl

Table 6.1: Thermochemical data[a], ΔG^0_{ad} for the reaction (6.2): $A^{\cdot} + Sl = A^{\cdot}.Sl$ at 70°C.

A[b]	EA	MeOH	MeCN	DMSO	DMF	THF[c]
$\mu_D \rightarrow$	kcal/mol	1.4 D	4.0 D	4.1 D	3.9 D	1.6 D
2,3-diMeNB	19.4	6.3				
3-OCH_3NB	23.4	6.1			5.9	
4-OCH_3NB	20.3	6.5	6.5	8.4	6.2	
2-MeNB	20.7	6.5				3.1(2.2)
3-MeNB	22.1	6.3			6.2	3.0(2.1)
4-MeNB	21.2	6.4	6.7	8.6	6.3	3.1(2.2)
NB	22.8	6.3	6.6	8.6	6.2	3.2(2.3)
2-FNB	24.2	5.8	6.1	7.9	5.9	3.2(2.4)
3-FNB	27.7	5.6	6.0	7.8	5.6	2.8(1.9)
4-FNB	25.0	6.0	6.3	8.2	5.9	2.9(2.1)
2-ClNB	25.7	5.4	6.1	7.8		
3-ClNB	28.8	5.4	5.7	7.5		
4-ClNB	28.2	5.6	5.9	7.6		
3-CF_3NB	31.6	4.9	5.3	7.1	4.8	
MaAn	27.8	4.7	5.5	6.7		
2-CNNB	35.8	4.5	5.3	6.8	4.8	3.7(2.8)
3-CNNB	34.8	4.7	5.1	6.6	4.5	2.1(1.2)
4-CNNB	38.7	4.1	4.5	6.0	3.9	1.4(0.5)
2-NO_2NB	36.9	3.3	4.8	6.2	4.5	
3-NO_2NB	36.9	3.8	4.3	5.9		
4-NO_2NB	44.3	2.3	3.2	4.4	2.5	
1,4-NpQ	40.2	5.5	4.8	6.2	4.3	
p-BQ	42.4	4.6	4.2	5.7		
2,3-diClNpQ	49.2	<1.5	<1.5			
F_4BQ	60.9	3.0	3.4	4.5	2.7	
4-NO_2 phenoxide[d]	~80.4	5.0	5.7	5.9		
2-NO_2 phenoxide	~68.3	5.8	6.4	7.4		

[a] ΔG^0_{ad} values are in kcal/mol. EA is the free energy change for the process: $A^{\cdot} \rightarrow A + e$ from Table 4.3.

[b] NB stands for nitrobenzene, MaAn for maleic anhydride, p-BQ for 1,4-benzoquinone, 1,4-NpQ for 1,4-naphthoquinone. μ_D is dipole moment of solvents, Sl given in debye unit.

[c] The $-\Delta G^0_{ad}$ values are measured at 35°C, while the values given in brackets are corrected free energy change at 70°C assuming $\Delta S^0_{ad} = -25.0$ cal/deg.

[d] Estimated electron affinity from EA(phenoxide) = 54.4 kcal/mol (see Brauman et al., J. Am. Chem. Soc., 1975, 97, 1160. The difference of acidity between phenol and 4-nitro phenol = 26.0 kcal/mol, 2-nitro phenol = 13.9 kcal/mol from Kebarle (ref.14).

Table 6.2: Thermochemical results for A^- + Sl = $A^-.Sl$[a,b] from van't Hoff plots.

	A^-	$-\Delta G^0_{ad}$(343K) (kcal/mol)	$-\Delta H^0_{ad}$ (kcal/mol)	ΔS^0_{ad} (cal/deg)
			Sl = MeOH	
1	4-OCH_3NB^-	6.5(6.1)	13.7(14.9)	-21.1(-25.7)
2	3-FNB^-	5.6	15.8	-29.8
3	3-CF_3NB^-	4.9(4.8)	14.6(14.6)	-28.1(-28.7)
4	4-$CNNB^-$	4.1	13.9	-28.6
			Sl = MeCN	
5	4-OCH_3NB^-	6.6(6.5)	13.8(14.2)	-23.0(-22.3)
6	3-CF_3NB^-	5.4(4.9)	13.3(13.3)	-23.2(-23.4)
7	4-$CNNB^-$	4.1	13.9	-25.8
			Sl = DMSO	
8	4-OCH_3NB^-	8.4	16.3	-22.5
9	3-CF_3NB^-	7.1	14.6	-22.3
10	4-$CNNB^-$	6.1	16.0	-33.6

[a]The values in brackets are obtained for a second experiment under identical conditions involving the same compounds.

[b]NB stands for nitrobenzene.

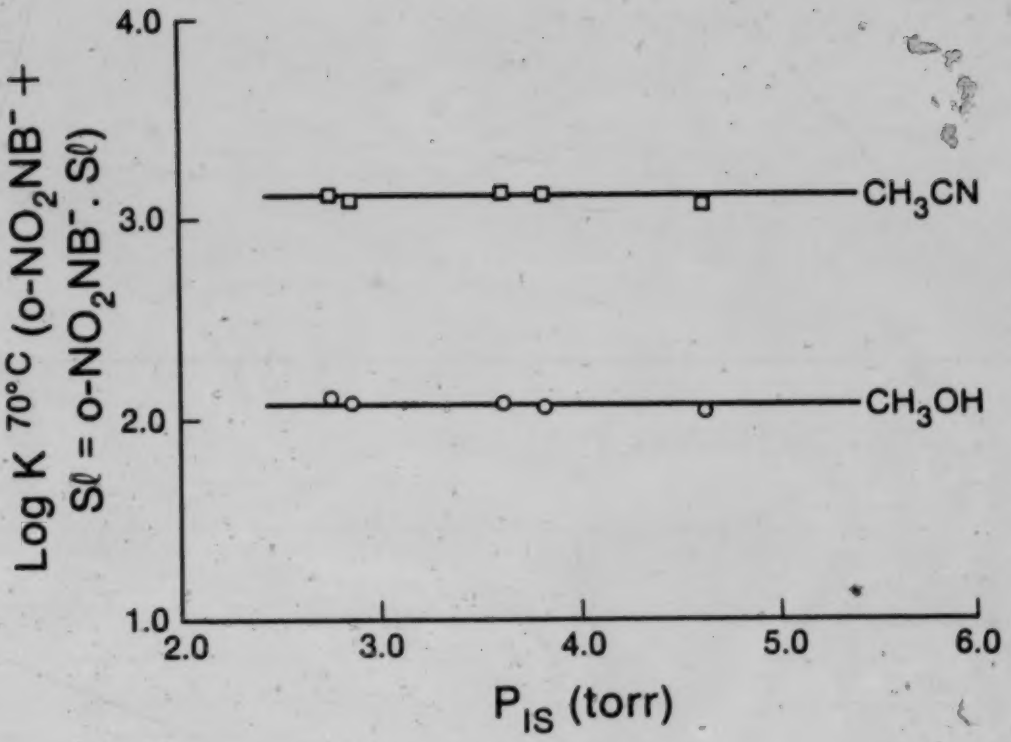

Figure 6.2. Plot showing invarience of adduct forming equilibrium constant K_{ad} for A^- + Sl ⇌ A^-.Sl with increase of total ion source pressure at constant partial pressure ratios.

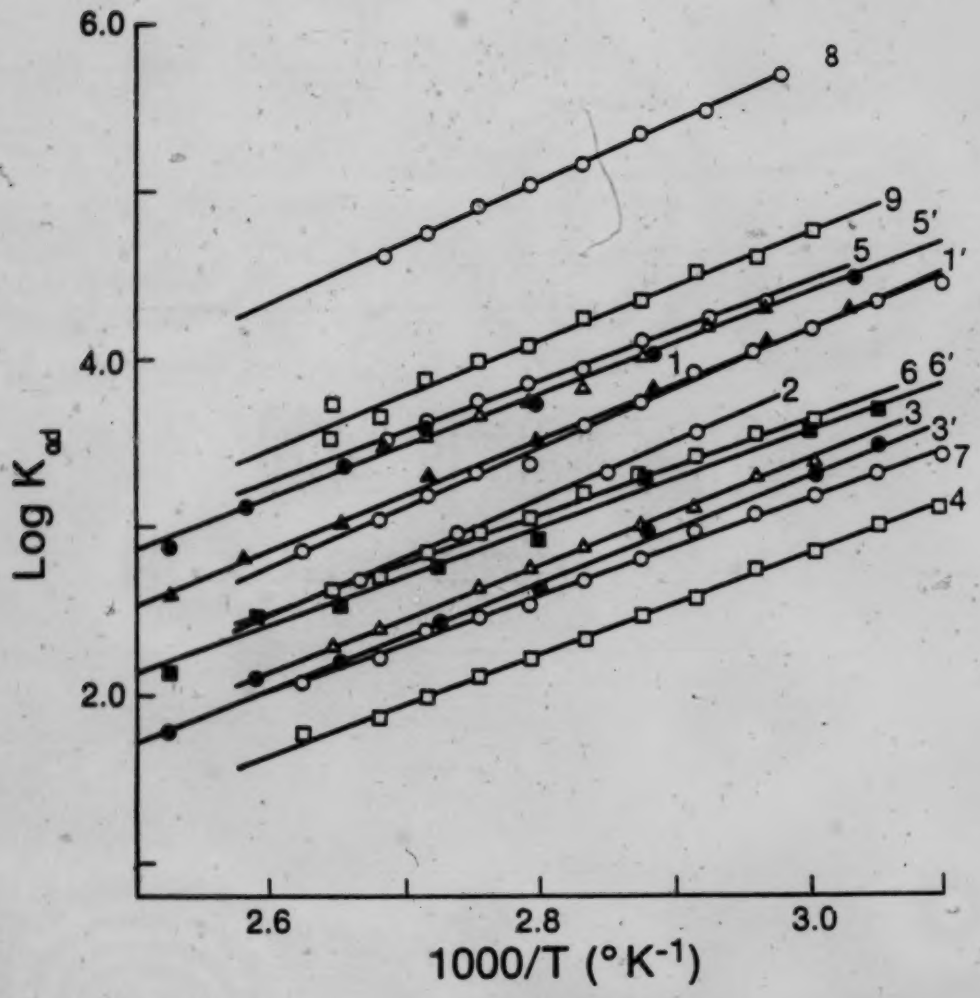

Figure 6.3. van't Hoff plots of equilibrium constants of equilibria $A^- + Sl = A^-.Sl$. The numbers beside the plots correspond to the numbered reactions given in Table 6.2.

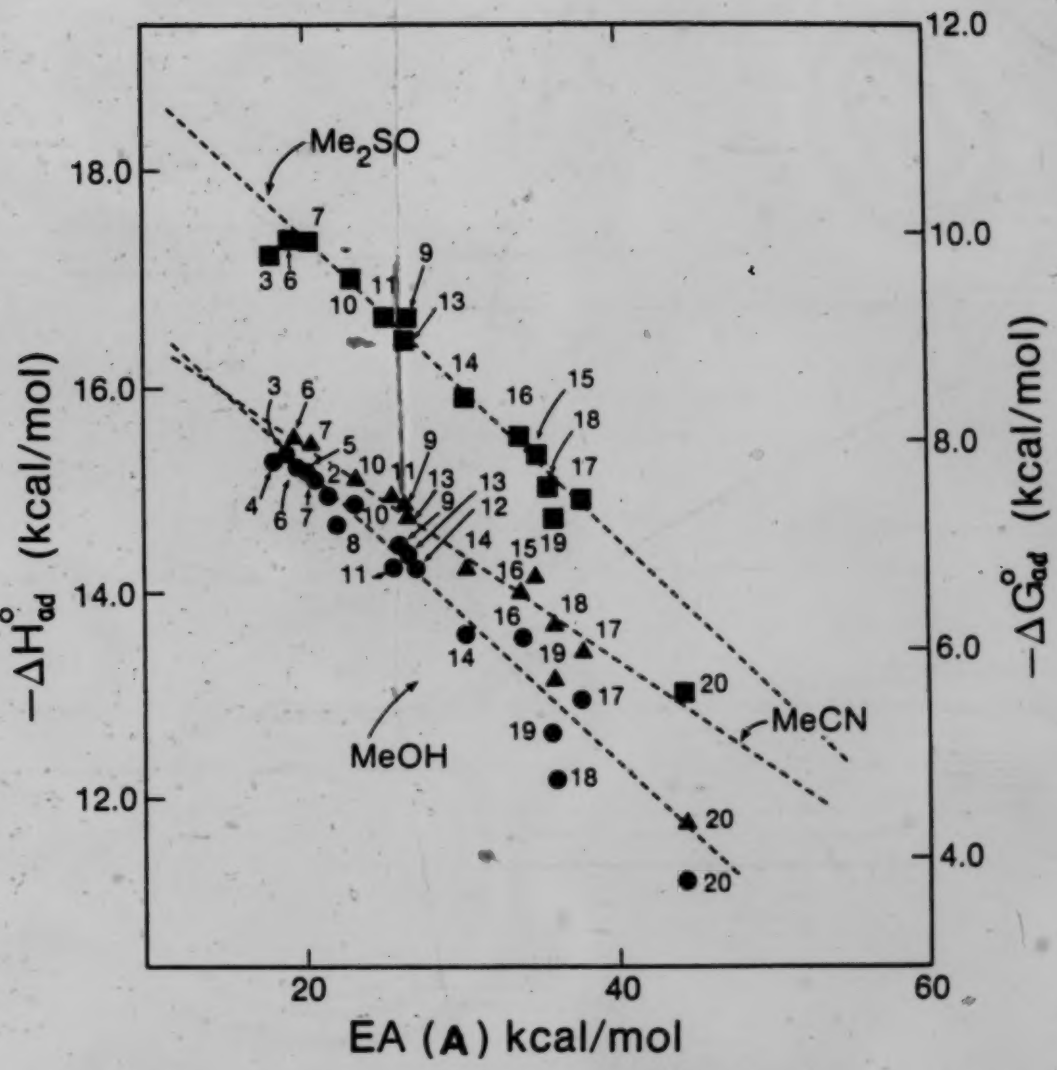

Figure 6.4. Plot of ΔG^0(70°C) and ΔH^0 for the reaction $A^- + Sl = A^-.Sl$ versus the electron affinity of A. The three plots are for Sl = DMSO, MeCN and MeOH. The actual A^- are identified by the number. All A^- used in the plot were anions of substituted nitrobenzenes XNB, substituent X is: 2,3-diMe (#1), 3-OMe(#2), 4-OMe(#3), 2-Me(#4), 3-Me(#5), 4-Me(#6), H(#7), 2-F(#8), 3-F(#9), 4-F(#10), 2-Cl(#11), 3-Cl(#12), 4-Cl(#13), 3-CF_3(#14), 2-CN(#15), 3-CN(#16), 4-CN(#17), 2-NO_2(#18), 3-NO_2(#19), 4-NO_2(#20). ΔH^0(ad) values are approximate and were obtained by assuming that ΔS^0_{ad} = -25.0 cals/deg, which is an average value for the entropy change given in Table 6.2, obtained from van't Hoff plots.

complexes become available.

6.2.2 Discussion of Bond Energies in $A^{\cdot}$.Sl and Their Significance to the Solvation of $A^{\cdot}$ in Polar and Dipolar Aprotic Solvent

Examining the ΔG^0_{ad} values in Table 6.1 for the dipolar aprotic solvent Sl = DMF and MeCN one finds that ΔG^0_{ad} for MeCN is generally little (~0.5 kcal/mol) more exothermic than that for DMF. On the other hand, the $-\Delta G^0_{ad}$ values for the protic MeOH do not maintain a constant difference with the aprotic DMF and MeCN, i.e., for methanol the exothermicity decreases faster with increasing electron affinity of A than is the case for DMF and MeCN. The relationships are illustrated in Figure 6.4, from which the data for DMF are omitted to reduce crowding in the figure. Examining Figure 6.4 one finds also the interesting result that the binding energies, $-\Delta G^0_{ad}$ for a given Sl decrease approximately linearly with increasing electron affinity of A.

Relative solvation energies of the ions $A^{\cdot}$ in a given liquid solvent can be obtained by a comparison of the gas phase electron affinities of A with polarographic half wave reduction potentials $E_{1/2}$. In the polarographic experiments, A is reduced to $A^{\cdot}$ in solution of the solvent Sl. The energy released in this reduction increases with the electron affinity of A. However, due to the presence of the solvent also the solvation energies of A and $A^{\cdot}$ influence the energy change[29], as shown earlier in chapter 4. For convenience the equations representing half wave reduction potentials and solvation energies are given below again, equations (6.4) to (6.6).

$$E_{1/2} + C_1 = EA - \delta\Delta G^0_s \qquad (6.4)$$

$$\delta\Delta G^0_s = \Delta G^0_s(A^{\cdot}) - \Delta G^0_s(A) \qquad (6.5)$$

$$E_{1/2} + C_2 \approx EA \qquad (6.6)$$

The constant C_1 contains the voltage of the standard cell coupled to the dropping mercury

electrode. Chen and Wentworth[29], assuming $\delta\Delta G_s^0$ does not change as A is changed, simplified the equations (6.4) to (6.6). Calibrating (6.6) to some known gas phase electron affinities, they determined the value of the constant C_2. Chen used equation (6.6) to evaluate "gas phase" EA's from experimental $E_{1/2}$ values. A plot of these solution-based "gas phase" electron affinities (solvent = MeCN) versus gas phase electron affinities obtained in the present investigation (Table 4.3) was shown in Figure 4.32 earlier in chapter 4. However, the Figure 4.32 also contains the electron affinities deduced from the spectroscopic measurements of charge transfer energies. Here our focus will remain confined to the data from half wave reduction potential measurements, which are open circles in Figure 4.32. The results from charge transfer energies are complicated by more assumptions being introduced to simplify the original equation representing charge transfer energies, to deduce "gas phase" electron affinities. The significance of these equations were discussed in Chapter 1. Had $\delta\Delta G_s^0$ been constant, the plot would have led to a slope equal to unity. The observed slope is 0.72. Since an approximately straight line is obtained, the $-\delta\Delta G_s^0$ must be decreasing approximately linearly with increasing electron affinity of A, as shown in equation (6.7)a.

$$-\delta\Delta G_s^0 \simeq C_3 - C_4\, EA(A) \qquad (6.7)a$$

$$-\Delta G_s^0(A^-) \simeq C_5 - C_4\, EA(A) \qquad (6.7)b$$

$$(C_4 = 0.28 \text{ for Sl} = MeCN)$$

It is known that $-\Delta G_s^0(A^-)$ is much larger than $-\Delta G_s^0(A)$, therefore the changes in $\Delta G_s^0(A)$ as A is changed will not have a large effect on $\delta\Delta G_s^0$. This assumption leads to equation (6.7)b which predicts a linear decrease in $-\Delta G_s^0(A^-)$ with the increase of EA(A). Recalling the result in Figure 6.4 we note that, both the binding free energy for A^-.Sl and solvation energy $-\Delta G_s^0(A^-)$ decrease approximately linearly with the increase of the EA(A).

The effect of the decrease of solvation energy with the increase of charge delocalization in the negative ion on the measured half wave reduction potential, and hence on the electron

affinities deduced from $E_{1/2}$ values can be observed directly from the results shown in Figure 6.5. Shown in Figure 6.5 are the half wave reduction potential values for some benzo- and naphthoquinones plotted against the electron affinities of the corresponding molecules. The EAs are present results from Table 4.3. The $E_{1/2}$ values are from Prince et al.[165] (Tables I and II, chapter II.1 of reference 165), who obtained reduction potentials by using cyclic voltametry in DMF. As is evident from the results depicted in Figure 6.5, the curve representing the experimental $E_{1/2}$ values is deviated from the unit slope line . The higher the electron affinity of the quinone, the larger is the deviation from the line of unit slope. That is the relative increase in $E_{1/2}$ values corresponding to electron affinity increase, decreases with the increase in electron affinity of the molecule. The above observation can be explained with the help of equation (6.4). The achievement of the increase of electron affinity in a conjugated system is due to the increased charge delocalization in the negative ion. As discussed in the preceeding paragraphs, this increased charge delocalization would reduce the solvation exothermicity of the ion, in other words, $\delta\Delta G_s^0$ would become more positive, for compounds of higher EA, compared to those of lower EA. Hence $E_{1/2}$ values of higher electron affinity molecules will be less relative to values one would expect for no change in $\delta\Delta G_s^0$ with the increase of electron affinity. The deviation of $E_{1/2}$ values from unit slope observed in Figure 6.5 is, therefore, in accord with the expected decrease in solvation energy of the negative ion, with increased charge delocalization.

The above results can be explained in more detail, at least qualitatively for A^--Sl binding energies, i.e., for the one molecule solvation of the ion. As mentioned earlier, an electron affinity increase in compounds A is generally obtained by adding electron withdrawing groups to the aromatic or conjugated system. The effect of these groups is to delocalize the negative charge. A particularly simple case is nitrobenzene, NB and 1,4-dinitrobenzene, 4-NO_2NB. The negative ions are shown in scheme 6.1. The introduction of the second nitro group increases the electron affinity, delocalizes the charge and thus increases the effective

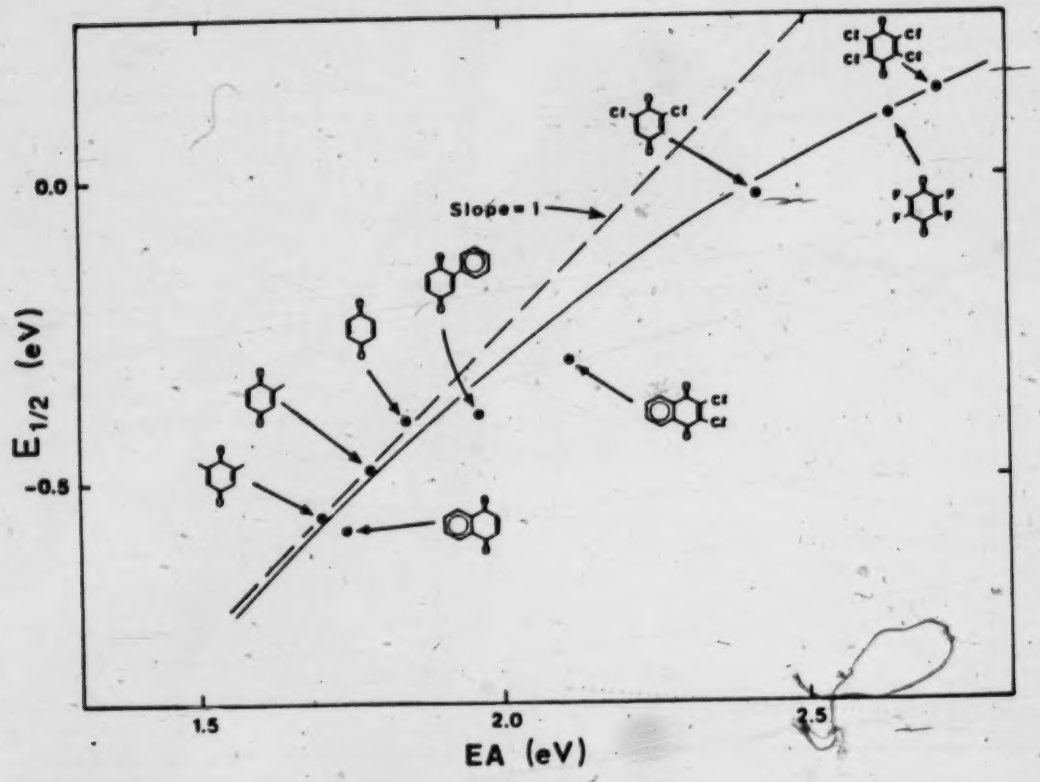

Figure 6.5. Plot of $E_{1/2}$, the half wave reduction potential values of some benzo- and naphthoquinones measured in DMF solution versus electron affinities of the corresponding quinones (Table 4.3). The deviation of the $E_{1/2}$ values from the unit slope increases with the increase of electron affinity. This deviation is attributed as due to the decrease in solvation exothermicity of the quinone negative ion as the electron affinity of the quinone is increased.

distance between the solvent molecule and the effective centre of the negative charge on the ion.

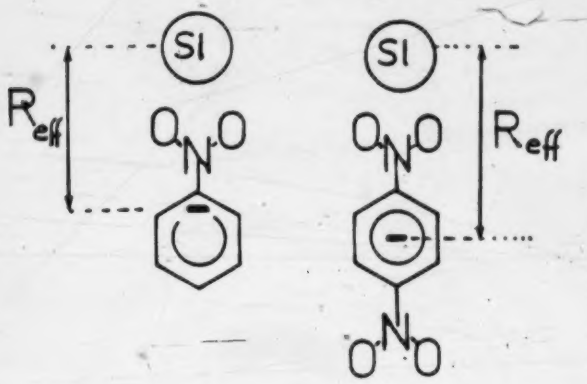

scheme 6.1

An increase in the radius necessarily leads to a decrease in the bond energy, since this is largely an electrostatic type interaction.

The greater decrease of the $A^{\cdot}$-Sl bond energy with the increase in EA(A), i.e., increase of effective radius R_{eff}, for the protic solvent MeOH relative to aprotic solvent MeCN, see Figure 6.4, is also easily rationalized in qualitative terms. While the molecular dipole in MeOH (1.7 Debye)[90] is largely located on the OH group and the smallness of the H-atom allows a close approach to the negative centre (hydrogen bond), molecular dipole in MeCN (4 Debye)[90] is due to a positive charge distribution which is diffuse, with most of the charge on the cyano-carbon and some on the methyl hydrogens[163-164]. In effect this locates most of the dipole on the cyano group, and this group cannot be approached closely by the negative ion as shown in scheme 6.2. It is obvious that an increase in the effective radius occurring for the change from $NB^{\cdot}$ to 4-$NO_2NB^{\cdot}$ will cause a relatively smaller decrease in the electrostatic bonding interaction with MeCN where R_{eff} is already large relative to MeOH whose R_{eff} is

smaller. This effect can be demonstrated by very simple model calculation.

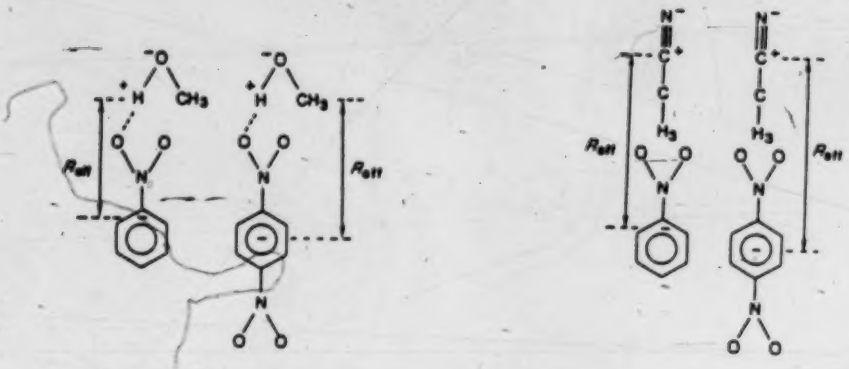

scheme 6.2

Selecting an EA(A) (see Figure 6.4) where $\Delta G^0_{ad}(A^-.MeOH) \simeq \Delta G^0_{ad}(A^-.MeCN)$ and assuming $R_{eff}(A^-.MeOH) = 3A$ and $R_{eff}(A^-.MeCN) = 4.5A$, the simple ion-dipole stabilization energy expression (6.8) leads to the same E for MeOH and MeCN when the correct dipole moments $\mu_D(MeOH) = 1.7$ Debye and $\mu_D(MeCN) = 4$ Debye are substituted in equation (6.8).

$$E = - e\mu_D/(R_{eff})^2 \qquad (6.8)$$

Increasing then both radii by the same amount, say 1A, to account for a charge delocalization in A corresponding to an EA increase of A, the -E obtained from (6.8) for methanol is found to decrease to 52% while that for MeCN decreases to only 67% of the original value. The smaller decrease for MeCN is in line with the observed changes in Figure 6.4.

The order of bond energies, $-\Delta G^0_{ad}(A^-.Sl)$ observed in Table 6.1 for the dipolar aprotic Sl is DMSO >> MeCN ≃ DMF >> THF. DMSO not only has a high dipole moment but its pyramidal shape keeps the two methyl groups partially out of the way and allows a relatively

closer approach to the negative ion[150]. The most weakly bonding Solvent tetrahydrofuran, THF (see structure below) not only has the weakest dipole moment but also has the largest steric hindrance for the approach of the negative ion to the positive end of the dipole.

THF

A clear demonstration that the location of the dipole within the molecule is very important can be obtained by determining binding energies with negative and positive ions. Positive ions can readily approach the negative end of the dipole in dipolar aprotic solvent like MeCN, DMF, DMSO, acetone etc. and therefore these molecules have binding energies to positive ions which are much stronger relative to those for negative ions of similar size[150].

The geometries of the $A^{\cdot}$.Sl complexes, shown in scheme 6.2 are somewhat arbitrary. They are based on the assumption that the highest negative charge density on the nitrobenzene negative ion is located on the oxygens of the nitro-group. Radom[122] has published results from STO-3G calculations for the nitrobenzene negative ion, as mentioned in the chapter 4. These include molecular electrostatic potential contour maps, which provide the first order interaction energy between a positive charge, the proton, and the unperturbed molecular anion[122]. They show the highest potential at the oxygens. The highest potentials are actually located about 1A above and below the oxygen atoms, i.e., above and below the plane of the molecular ion, as would be expected since the extra electron is in a π^{*} orbital.

The negative charge distribution in the variously substituted nitrobenzene radical anions may be quite complex, particularly so due to the shape of the π^{*} orbital which is occupied by the extra electron. A comparison of the electron affinities of substituted nitrobenzenes and those of substituted phenoxide radicals (chapter 4) shows that the effects of the substituents in both

negative ion systems is very much the same, even though only π orbitals are involved for the phenoxide ions while in the nitrobenzenes both π and π^* orbitals participate. This similarity indicates that resonance structures that can be used for the phenoxides, can be also used for the nitrobenzene radical anions. Use of this by analogy in behavior will be made in subsequent discussion.

An examination of the individual $-\Delta G^0_{ad}$ values for different A^- in Table 6.1 reveals some interesting trends. Most revealing are the data for isomeric nitrobenzenes. For NO_2 substituted nitrobenzenes one finds the order of bond energies to be for MeOH: 3-NO_2NB > 2-NO_2NB > 4-NO_2NB. The same order is observed also for the cyano substituted nitrobenzenes. On the other hand for the aprotic acetonitrile, MeCN and DMSO the order is 2-NO_2NB > 3-NO_2NB > 4-NO_2NB. We assume that the adduct molecule Sl bonds to the NO_2 group with geometries approximately as shown in scheme 6.2. As pointed out by Kebarle[14], in an earlier work the hydrogen bonding adduct (of MeOH) is much more affected by losses of electron density from the negative centre. The π withdrawing effect of the second NO_2 group (or the CN group) is strongest for 4-NO_2NB (or 4-CNNB) and weakest for 3-NO_2NB (or 3-CNNB). Therefore, one observes the strongest MeOH adduct to be to the 3-NO_2NB (or 3-CNNB) anion.

The dipolar aprotic molecules having their dipole located some distance away from the negative centre are less sensitive to the detailed charge distribution. They respond rather to more global changes, so that for them the allignment of the two negative charges carrying the NO_2 groups (or CN group) which occurs in the 2-XNB^-, is the most favorable one and leads to the strongest adduct. Presumably, in this adduct the aprotic solvent interacts with the negative charge of both substituents.

The adduct binding energies for the nitrobenzene anions substituted by the π donating and σ donating substituents CH_3O and F decreases in the order 4-XNB > 2-XNB > 3-XNB for both the protic MeOH and the aprotic MeCN, DMSO and DMF. This indicates that the increasing electron density on the NO_2 oxygen by the π donation from CH_3O and F which is strongest in 4-XNB^- has a favorable effect for both protic and aprotic adducts. Significantly

however, the difference between 4- and 3-substituted $NB^{\cdot}$ is larger for the protic MeOH than for the aprotic solvents (Table 6.1). This difference is in line with the expected greater sensitivity of the protic molecules to the negative centre to which it bonds.

The bond free energies ΔG^0_{ad} for $A^{\cdot}$ = 2-NO_2phenoxide and 4-NO_2phenoxide anion and Sl = MeOH, MeCN and DMSO are also given in Table 6.1. The correlation observed between the electron affinities of A and the bond energies in $A^{\cdot}$.Sl obviously does not include the phenoxide anions. Thus, while the phenoxides have the highest electron affinities and are thus expected to bond Sl least strongly, the bond energies $NO_2PhO^{\cdot}$.Sl are relatively high (Table 6.1). This effect is expected. The phenoxide anions are even electron systems where the extra electron occupies a bonding orbital which is less diffuse than the π^* orbital of the radical anions. Also bonding in the $PhO^{\cdot}$.Sl occurs to the phenoxy-oxygen and other things being equal one expects a larger negative charge density on this singly charged atom than for the two oxygens of the NO_2 group of the $NB^{\cdot}$. Measurements of the other bond energies for the substituted phenoxides $XPhO^{\cdot}$.Sl would have been of considerable interest. The NO_2-phenoxide anions were produced in the ion source by a reaction of NO_2^- or O_2^- with 2-ClNB and 4-ClNB. The reaction of NO_2^- with various substituted nitrobenzenes will be discussed later in this chapter. Unfortunately the preparation of other $XPhO^{\cdot}$ so far is possible in our apparatus only by deprotonation of the corresponding phenols[14], and the presence of the strongly acidic hydrogen in X-PhOH leads to the corresponding proton held dimers $XPhO^{\cdot}$.HOPhX as the completely dominant species, precluding thus the observation of the $XPhO^{\cdot}$.Sl.

While the phenoxide ions do not fall on the lines observed for the radical anions $A^{\cdot}$ in Figure 6.4, it is quite certain that the bond energies for $XPhO^{\cdot}$.Sl as a group themselves will fall on an approximately straight line when plotted versus EA(XPhO) or the gas phase acidity of XPhOH. An approximately linear relationship is known to exist[14,127] between the solvation energies and the phenoxides $XPhO^{\cdot}$ and the electron affinities of XPhO. The relationship is actually between the gas phase acidities and solution acidities of the substituted phenols. From this relationship since the bond energies D(XPhO-H) are expected to change very little one can deduce a linear inverse relationship between the electron affinities EA(XPhO) and solvation

energies of $XPhO^-$ ions. This relationship has the same origin as observed for A^-, i.e., the electron affinity of XPhO increases with increasing charge delocalization in $XPhO^-$ and increasing charge delocalization decreases the bonding in $XPhO^-$.Sl and the solvation energies of $XPhO^-$.

6.3 Binding Energies in A^-.B and A^-.A, where A and B are NO_2, Nitrobenzenes, Quinones and Perfluoromolecules

6.3.1 Measurements and Results

The determinaiton of binding energies of adducts, A^-.B or A^-.A follows the same procedure, discussed in more details earlier in this chapter in connection with A^-.Sl binding energies (section 6.2.1). The measurements were done by studying the ion-neutral equilibria (6.8).

$$A^- + A = A^-.A \qquad (6.8)$$
$$A^- + B = A^-.B$$

Three different types of A^-.B complexes were studied. These were (i) adducts of NO_2^- and $2\text{-}NO_2NB^-$ with various substituted nitrobenzenes and quinones etc., (ii) adducts of miscellaneous A^- ions (including Cl^-) and B molecules, where A and B are some aromatic hydrocarbons, SF_6 and other perfluoro aromatic and nonaromatic compounds, and (iii) A^-.A adducts.

Experiments in which NO_2 was one of the reactants lead to the observation of the three different types of reactions. (a) Electron transfer: $A^- + NO_2 = A + NO_2^-$, (b) adduct formation: $NO_2^- + A = NO_2^-.A$, and (c) some of the compounds A were converted to

phenoxy negative ion on reaction with NO_2^-. For example, 4-NO_2NB leads to the formation of 4-NO_2PhO$^-$ negative ion, via reaction (6.9).

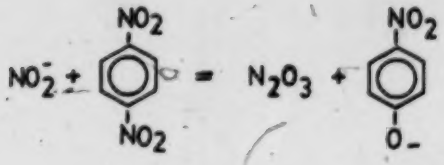

(6.9)

The oxy-negative ion forming reaction is isomer specific. The results shown in Figure 6.6 illustrate the ion concentration changes indicating the occurrence of three reactions (a) to (c), mentioned above involving NO_2 and NO_2^-. The observed faster decay of nitrobenzene negative ions compared to other ions in Figure 6.6, is due to the electron transfer from 4-NO_2NB$^-$ and 3-NO_2NB$^-$ to NO_2, since NO_2 has higher electron affinity than either dinitrobenzenes (Table 4.3). The significance of rate constants for these electron transfer reactions is discussed in chapter 3 and results are provided in Table 3.1.

The formation of the adducts NO_2^-.A by reaction (6.8) is also observed in Figure 6.6. In both trials (a) and (b), this adduct reaches equilibrium with NO_2^-. The constant ion ratio $[NO_2^-.A]/[NO_2^-]$ leads to the constant vertical distance between the ions in the logarithmic plot used. The results in Figure 6.6 indicate that 3-NO_2NB forms an adduct more stable than 4-NO_2NB, since the adduct NO_2^-.A intensity is greater for the 3-NO_2NB isomer, for nearly equal [A] in both trials (a) and (b).

Shown in Figure 6.7 are determinations of K_{ad} at different ion source pressures. The results demonstrate that K_{ad} (NO_2^-.A) is invariant of the concentration of the neutral reactants and carrier gas. The temperature dependence of K_{ad} was determined for a limited number of compounds A. The resulting van't Hoff plots are shown in Figure 6.8 and the derived ΔH^0_{ad}, ΔS^0_{ad} and ΔG^0_{ad} values are given in Table 6.3. The majority of the reactions (6.8) involving NO_2^-.A were determined at 150°C only and the total results are given in Table 6.4. The ΔH^0_{ad}

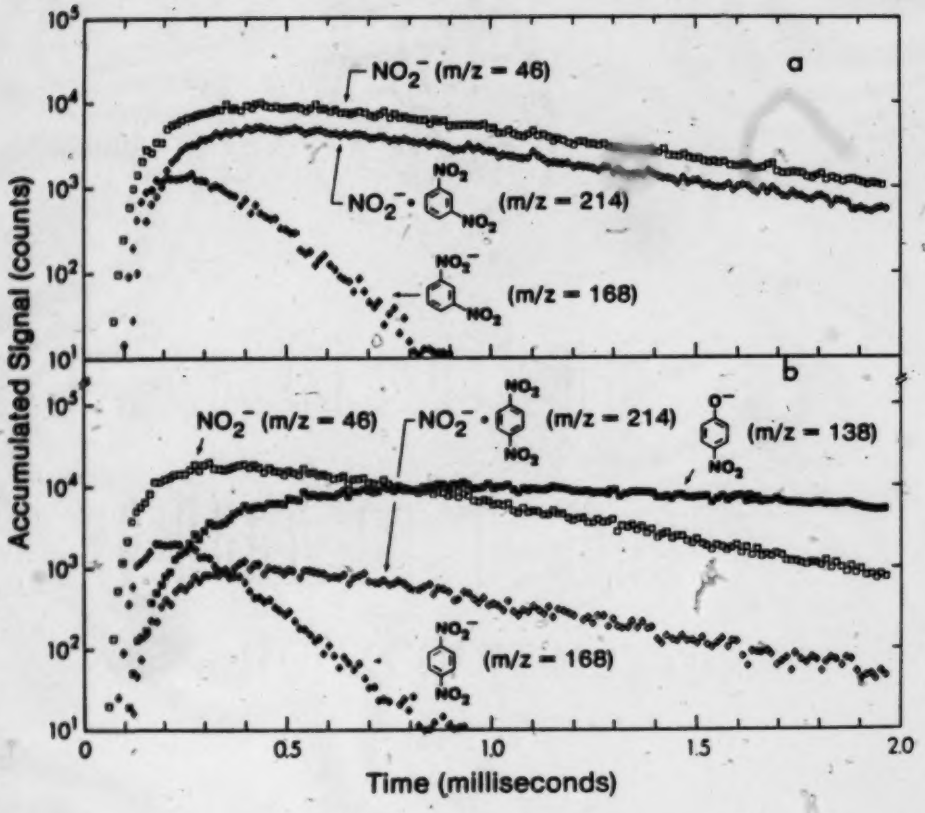

Figure 6.6. Observed ion intensity changes after ionising electron pulse determined at 150°C. (a) 2.8 mtorr methane, 0.8 mtorr NO_2 and 0.6 mtorr 1,3-dinitrobenzene. Electron transfer from 1,3-dinitrobenzene negative ion to NO_2 reduces the concentration of this ion. Adduct NO_2^-.3-NO_2NB reaches equilibrium with NO_2^-. (b) 4.0 torr methane, 1.0 mtorr NO_2, 0.8 mtorr 1,4-dinitirobenzene. The reactions are as in (a), however, the additional reaction (6.10) leading to 4-NO_2 phenoxide ion is also observed.

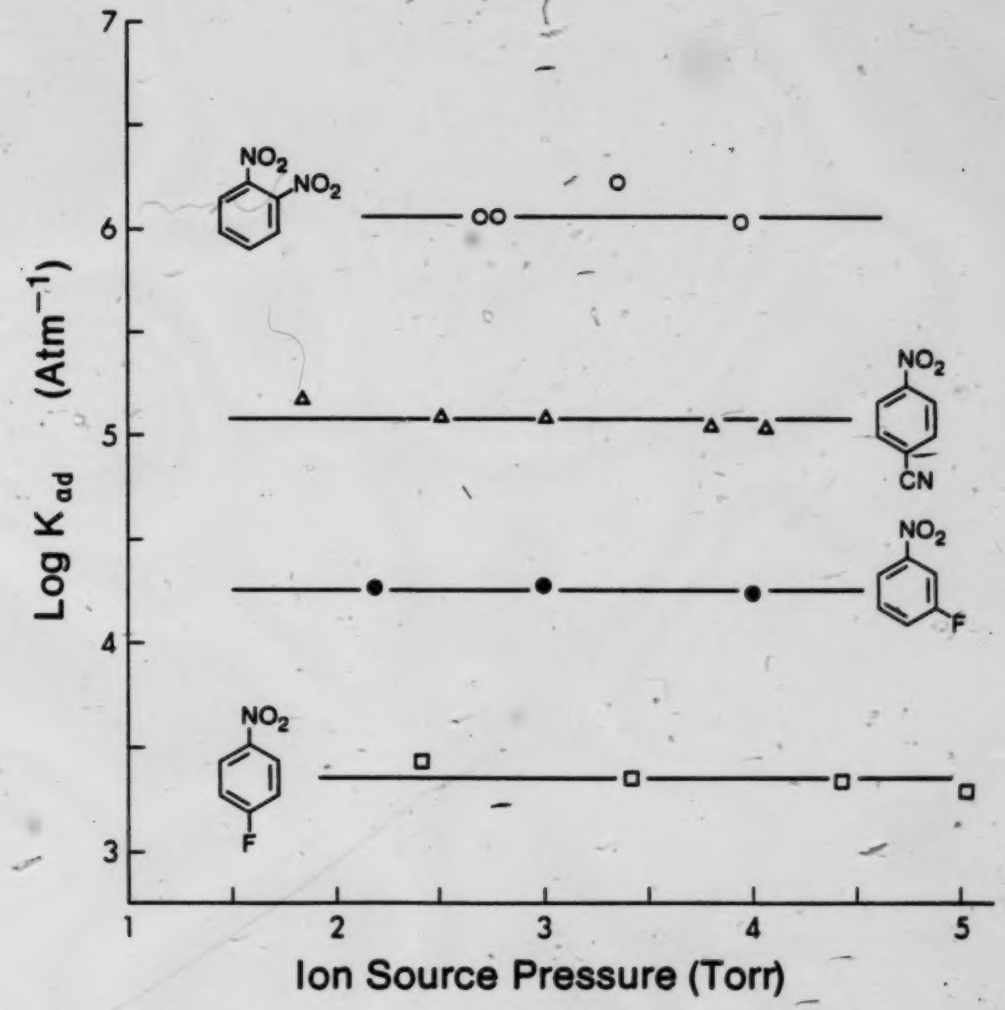

Figure 6.7. Equilibrium constants K_{ad} at 150°C for the reaction $NO_2^- + A = NO_2^-.A$ versus total ion source pressure. The results demonstrate the invariance of K_{ad} with the total pressure.

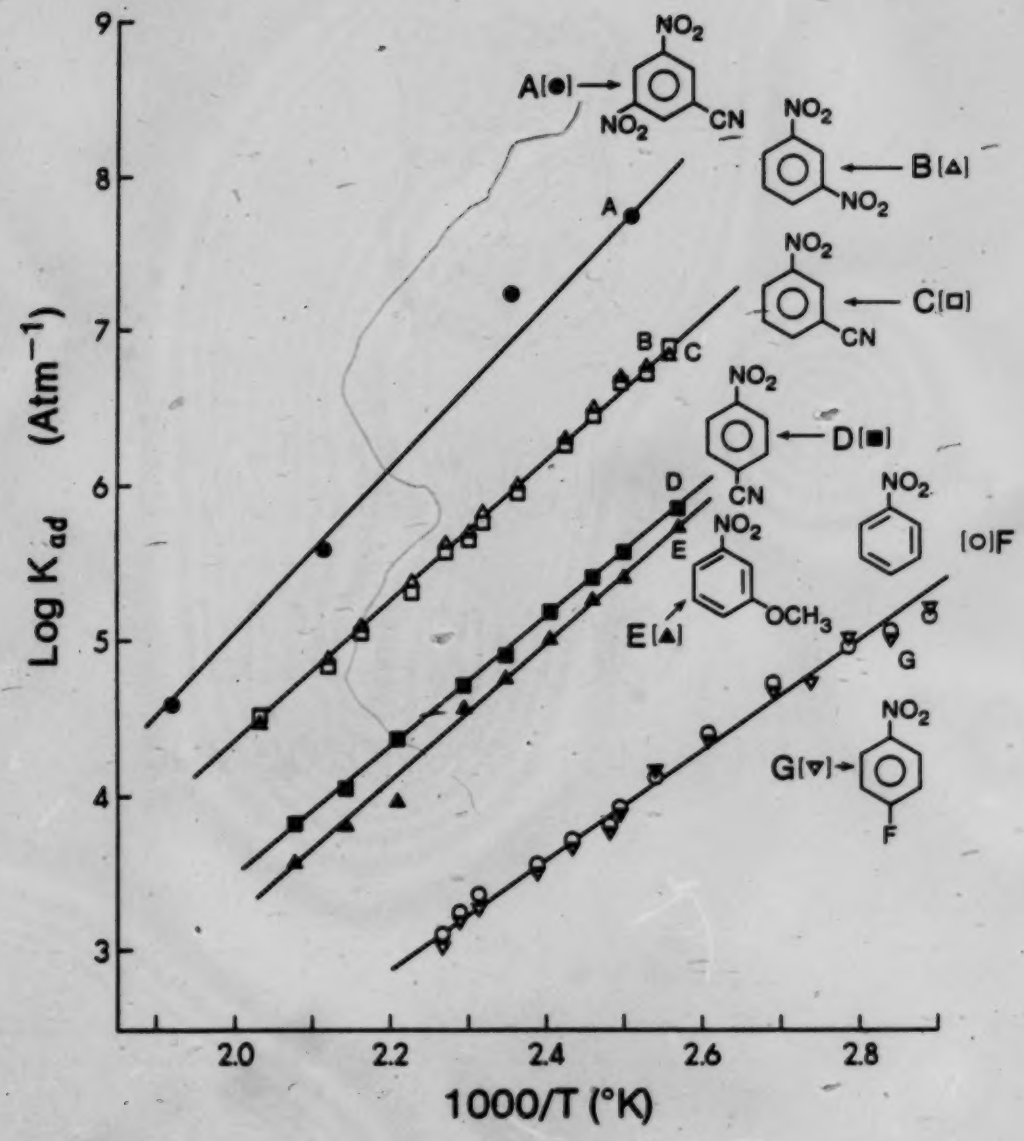

Figure 6.8. van't Hoff plots of the equilibrium constants K_{ad} for the reaction NO_2^- + A = NO_2^-.A.

Table 6.3: Thermochemical data[a] for the reactions: $NO_2^- + A = NO_2^-.A$ obtained from van't Hoff plots (Fig. 6.6).

A[b]	$-\Delta H^0_{ad}$ (kcal/mol)	ΔS^0_{ad} (cal/deg)	$-\Delta G^0_{ad}$(300K) (kcal/mol)
3,5-diNO_2BN	23.5	-23.7	16.4
3-NO_2NB	21.2	-22.6	14.4
3-CNNB	20.0	-20.0	14.0
4-CNNB	18.8	-21.5	12.4
4-FNB	15.0	-19.6	9.1
3-OCH_3NB	20.5	-26.3	12.6
NB	14.2	-17.5	8.9

[a]Standard state 1 atm. Estimated errors: ΔH^0 values ±2.0 kcal/mol, ΔS^0 values ±3.0 cal/deg.

[b]BN and NB stand for benzonitrile and nitrobenzene respectively.

Table 6.4: Thermochemical[a] data for the adduct forming reaction: NO_2^- + A = NO_2^-.A and rate constants for oxy-negative ion forming reaction: NO_2^- + X-NB = NB-O$^-$ + X-NO.

A[b]	EA(A) kcal/mol	$-\Delta G^0_{ad}$(150°C) kcal/mol	$-\Delta H^0_{ad}$ kcal/mol[c]	k[d] cc molecule^{-1} s^{-1}
3,5-diNO_2BN	49.9	13.6	22.1(23.5)	2×10^{-10}
4-NO_2NB	46.2	9.2	17.7	1×10^{-10}
2-NO_2NB	38.2	11.6	20.1	2×10^{-11}
3-NO_2NB	38.2	11.4	19.9(21.2)	
BQ	44.1	<1.9	<10.4	
4-CNNB	39.5	9.7	18.2(18.8)	
2-CNNB	37.1	11.6	20.1	5×10^{-12}
3-CNNB	36.1	11.5	20.0	
3-CF_3NB	32.6	9.7	18.2	
3-ClNB	29.5	8.3	16.8	
4-ClNB	29.0	6.4	14.9	
2-ClNB	26.3	8.3	16.8	3×10^{-13}
3-FNB	28.4	8.3	16.8	
4-FNB	25.8	6.4	14.9(15.0)	
2-FNB	24.8	8.7	17.2	1×10^{-12}
3-OCH_3NB	24.1	9.1	17.6(20.5)	
4-OCH_3NB	21.1	9.6	18.1	
NB	23.2	7.0	15.5(14.2)	
3-CH_3NB	22.8	6.7	15.2	
4-CH_3NB	22.0	6.4	14.9	
2-CH_3NB	21.3	5.8	14.3	5×10^{-14}

[a]The equilibrium constants for the formation of NO_2^-.A are measured at one temperature (150°C) only. The ΔH^0 values are obtained by assuming entropy change = -20.0 cals/deg uniformly, an average value of the results from van't Hoff plots given in Table 6.3.

[b]BN stands for benzonitrile, BQ for p-benzoquinone, and NB for nitrobenzene.

[c]The enthalpy changes in brackets are from direct measurements through van't Hoff plots.

[d]Rate constants for oxynegative ion forming reaction NO_2^- + X-NB = $^-$O-NB + X-NO. The rate constants involving other nitrobenzenes not given in the table are very small.

values in Table 6.4 are deduced by assuming uniformly ΔS^0_{ad} = -20.0 cals/deg. an average one could deduce from the results obtained from van't Hoff plots (Figure 6.8) provided in Table 6.3.

Given in Table 6.5 are the results for the formation of $2\text{-}NO_2NB^-.A$ measured only at 70°C (343K). ΔH^0_{ad} values for the adduct forming reaction (6.8) for $A^- = 2\text{-}NO_2NB^-$ are obtained by assuming ΔS^0_{ad} = -25.0 cals/deg.

The results from the studies of temperature dependence of the equilibria (6.8) for $Cl^-.A$ and other $A^-.B$, where A and B are perfluorinated compounds are shown in Figure 6.9. The resulting thermochemical quantities such as ΔH^0_{ad}, ΔS^0_{ad}, and ΔG^0_{ad} are given in Table 3.7 (earlier in chapter 3) and Table 6.6. The results from equilibria measurements involving $A^-.A$ are given in Table 6.7.

6.3.2 Discussion of Results

(i) Oxy-anion Forming Reactions

Before starting the discussion about binding energies, a brief discussion of reactions forming oxy-negative ions involving NO_2^- will be given. The general reactions involving NO_2^- and substituted nitrobenzenes, XNB is given by equation (6.10),

$$NO_2^- + X\text{-}NB = ONB^- + XNO \qquad (6.10)$$

where ONB^- is the nitro substituted pnenoxide ion. The specific example is shown by equation (6.11), where X = Cl in the ortho position, also shows a formal representation of the

Table 6.5: Thermochemical results[a] for the reaction, $2\text{-}NO_2NB^{\cdot} + A = 2\text{-}NO_2NB^{\cdot}.A$.

A[b]	$-\Delta G^0_{ad}(343K)$ kcal/mol	$-\Delta H^0_{ad}$ kcal/mol
$3\text{-}OCH_3NB$	7.8	16.4
$4\text{-}OCH_3NB$	8.2	16.8
$2\text{-}CH_3NB$	5.3	13.9
$3\text{-}CH_3NB$	5.8	14.4
$4\text{-}CH_3NB$	6.0	14.6
NB	5.5	14.1
2-FNB	7.2	15.8
3-FNB	6.6	15.2
4-FNB	5.3	13.9
$3\text{-}CF_3NB$	8.0	16.6
2-ClNB	7.2	15.8
3-ClNB	6.9	15.5
3-CNNB	7.6	16.2

[a]The free energy changes are measured only at one temperature (343K), given in column 2 and no temperature dependence of the free energy changes was studied. The enthalpy values given in column 3 are obtained by assuming entropy change = -25.0 cals/deg.

[b]NB stands for nitrobenzene.

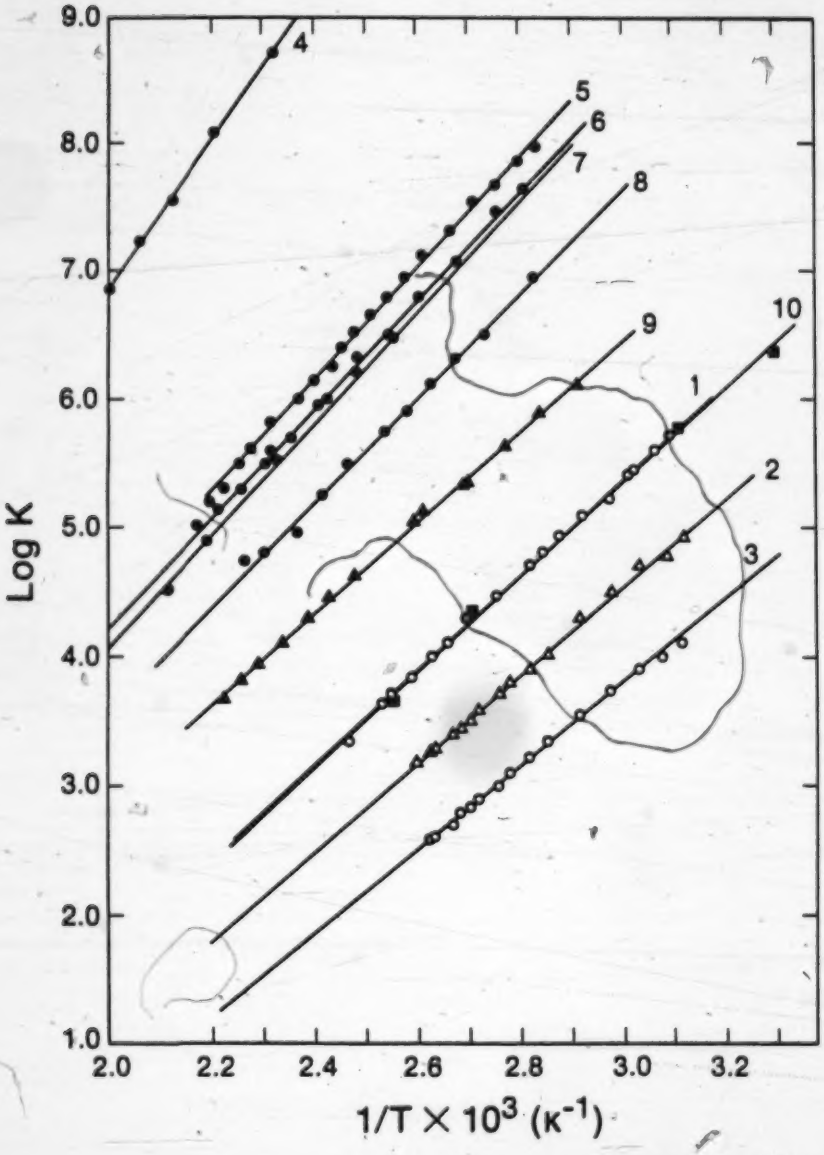

Figure 6.9. van't Hoff plots of equilibrium constants for adduct forming reaction: A^- + B = A^-.B. Standard state is 1.0 atm. Numbers correspond to the reactions forming adducts A^-.B as follows: #1 (SF_6^-.3-CF_3NB), #2 (SF_6^-.3-FNB), #3 (SF_6^-.NB), #4 (Cl^-.F_4BQ), #5 (Cl^-.4-CNNB), #6 (Cl^-.3-CF_3NB), #7 (Cl^-.C_6F_5CN), #9 (Cl^-.NB), #10 (Cl^-.C_6F_6).

Table 6.6: Binding energies[a] in Cl^--A from the study of equilibria: $Cl^- + A = Cl^-.A$.

	A	$-\Delta G^0$(300K) kcal/mol	$-\Delta H^0$ kcal/mol	$-\Delta S^0$ cal/deg
1	PhH	3.6	9.6[b]	
2	PhCl	6.6	12.6[b]	
3	PhCN	10.0	16.0	
4	$PhNO_2$ = NB	10.5	16.3(16.5)[b]	19.4
5	3-FNB	12.3	18.7	21.2
6	4-CNNB	14.0	20.0	20.0
7	3-CF_3NB	14.1	19.5	17.9
8	BQ (p-benzoquinone)	9.5		
9	SF_6	<<1.8		
10	C_7F_{11}	<<1.8		
11	C_6F_6	8.8	16.8	25.9
12	C_6F_5CN	13.5	21.3[c]	
13	1,4-diCNC_6F_4	14.6(378K)	24.4[c]	
14	F_4BQ	20.2		
15	PhF	5.9[d]	11.9[b,d]	
16	$PhOCH_3$	7.3[d]	13.3[b,d]	

[a]Standard state is 1 atm. NB and BQ stand for nitrobenzene and p-benzoquinone respectively.

[b]Enthalpy change values are obtained from corresponding free energy changes assuming ΔS^0 = -20.0 cal/deg.

[c]ΔS^0 = -25.9 cal/deg.

[d]data from ref. 168.

Table 6.7: Thermochemical data[a] for the clustering reaction: $A^- + A = A_2^-$.

A^b (μ_D)	$-\Delta G^0$(343K) kcal/mol	$-\Delta H^0$ kcal/mol[c]	$-\Delta S^0$ cal/deg
2,3-diCH_3NB	7.2	17.2	
3-OCH_3NB (4.54 D)	10.2	20.2	
4-OCH_3NB (5.26 D)	10.7(10.7)	20.7(19.5)	(29.5)
2-CH_3NB (3.7 D)	7.4	17.4	
3-CH_3NB (4.2 D)	8.0	18.0	
4-CH_3NB (4.4 D)	8.0	18.0	
NB (4.3 D)	7.6	17.6	
2-FNB	8.9	18.9	
3-FNB	8.2(8.3)	18.2(18.3)	(29.3)
4-FNB (2.87 D)	7.2	17.2	
2-ClNB (4.63 D)	9.0	19.0	
3-ClNB (3.72 D)	8.3	18.3	
4-ClNB (2.81 D)	7.1	17.1	
3-CF_3NB	8.9(8.9)	18.9(17.7)	(25.4)
MaAn	9.7	19.7	
2-CNNB (6.24 D)	11.1	21.1	
3-CNNB (3.81 D)	10.0	20.0	
4-CNNB (0.00 D)	7.8(7.9)	17.8(18.3)	(30.3)
2-NO_2NB (6.10 D)	10.4	20.4	
3-NO_2NB (3.87 D)	9.1	19.1	
4-NO_2NB (0.00 D)	5.7	15.7	
3,5-diNO_2BN	9.0	19.0	
BQ (0.00 D)	<1.6	<11.6	
NpQ	<1.6	<11.6	
F_4BQ	8.4	18.4	

[a]Results of thermochemical quantities in brackets are obtained from van't Hoff plots.

[b]NB stands for nitrobenzene, BN for benzonitrile, BQ for p-benzoquinone, NpQ for 1,4-naphthoquinone and MaAn for maleic anhydride. The values in brackets are experimental dipole moments in debye units from ref. 90.

[c]ΔH^0 values which are not in brackets are calculated by assuming ΔS^0 = -29.0 cal/deg.

presumed chemical transition state.

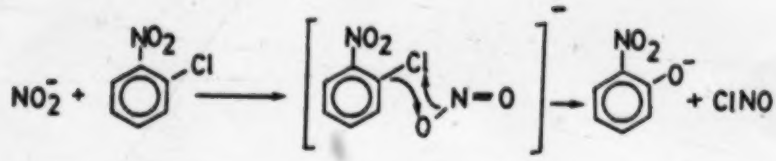

(6.11)

The formation of the neutral XNO product is required by the thermochemistry of the reaction. The general reaction given by (6.10) must be exothermic in order to be observed under the experimental conditions used. An exact calculation of ΔH^0 for the reaction (6.11) cannot be made since ΔH_f^0 $(X\text{-}NB)_g$ values are not available, however approximate calculations are possible with the use of a cycle which was written for X-NB = 2-ClNB.

$$NO_2^- + ClNB + H = ONB^- + ClNO + H$$

$$\Delta H^0 = EA(NO_2) + D(O\text{-}NO) - D(O\text{-}H) + D(NB\text{-}Cl) - D(NB\text{-}OH) + D(NBO\text{-}H) - EA(NBO) - D(Cl\text{-}NO) \qquad (6.12)$$

The values for various quantities in equation (6.12) in kcal/mol are: $EA(NO_2)$ = 53.0, $D(O\text{-}NO)$ = 73.2[166], $D(O\text{-}H)$[167] = 104.0, $D(NB\text{-}Cl) - D(NB\text{-}OH) \approx -15.0$, $D(NBO\text{-}H) - EA(NBO)$ = 19.5[14b], $D(Cl\text{-}NO)$ = 38.2[166]. The only approximate number is $D(NB\text{-}Cl) - D(NB\text{-}OH) \approx -15.0$. The numerical value actually corresponds to $D(Ph\text{-}Cl) - D(Ph\text{-}OH)$ = 15.0[167]. Examining the values in equation (6.12) one finds that the oxy-negative ion formation would be endothermic by 26.0 kcal/mol and thus be impossible in the absence of exothermic Cl-O bond formation, for which ΔH^0 [equation(6.12)] = -11.5 kcal/mol.

While the nitrite ion, NO_2^- is known to engage in S_N2 reactions in condensed phase, reactions corresponding to equation (6.10), to our knowledge, have not been observed. The

decrease of solvation from the small nitrite ion to the large transition state ion is probably a major factor in preventing the occurrence of this reaction in solution. The reaction is enhanced in the gas phase not only by the absence of unfavorable solvation energy changes but also by the presence of "chemical activation". At the low pressures used, the energy released on formation of the NO_2^-.XNB complex is not immediately removed by third body collisions and is thus available for use in overcoming the barrier attendant with the formation of the chemical transition state.

(ii) Binding Energies in NO_2^-A, 2-NO_2NB$^-$.A and A$^-$.A

Shown in Figure 6.10 is a plot of binding energies of NO_2^- to A (from Table 6.4) versus the electron affinities of A (from Table 4.3). One observes a good correlation i.e., an approximate proportionality in the increase of binding energies in NO_2^-.A with the increase of electron affinities of A. The stabilities of the X-NB.NO_2^- adducts (Table 6.4 and Figure 6.10) are in the following order, for X= NO_2> CN > CF_3 > F ≃ Cl > H > CH_3. This is the same order as is observed for the electron affinities of X-NB. The relative NO_2^- bonding abilities of the ortho, meta and para isomers of X-NB also show some interesting regularities. For the strongly stabilizing substitutents X = NO_2, CN the observed stability order is ortho ≥ meta >> para. The same stability order is found for weakly stabilizing substituents F and Cl. However, for electron donating substituents, such as X = CH_3, OCH_3 etc. an opposite order para ≥ meta > ortho is obtained.

An earlier theoretical and experimental investigation by Kebarle and coworkers[168] pertaining to adducts of Cl^-.A between a variety of molecules A and Cl^- showed that the negative ion interacts with the most protic hydrogen in the molecule A. This was true not only for oxygen acid adduct molecules, such as phenols and carboxylic acids, with which the interactions are clearly hydrogen bonding, but also for compounds such as, benzene and substituted benzenes. While the binding energies observed with the latter group of compounds were lower, it made sense also to consider these interactions as essentially hydrogen bonding. The only benzenes with electron withdrawing substituents for which calculations were made[168] were fluorobenzene and 1,3-difluorobenzene. The most stable adducts predicted by the

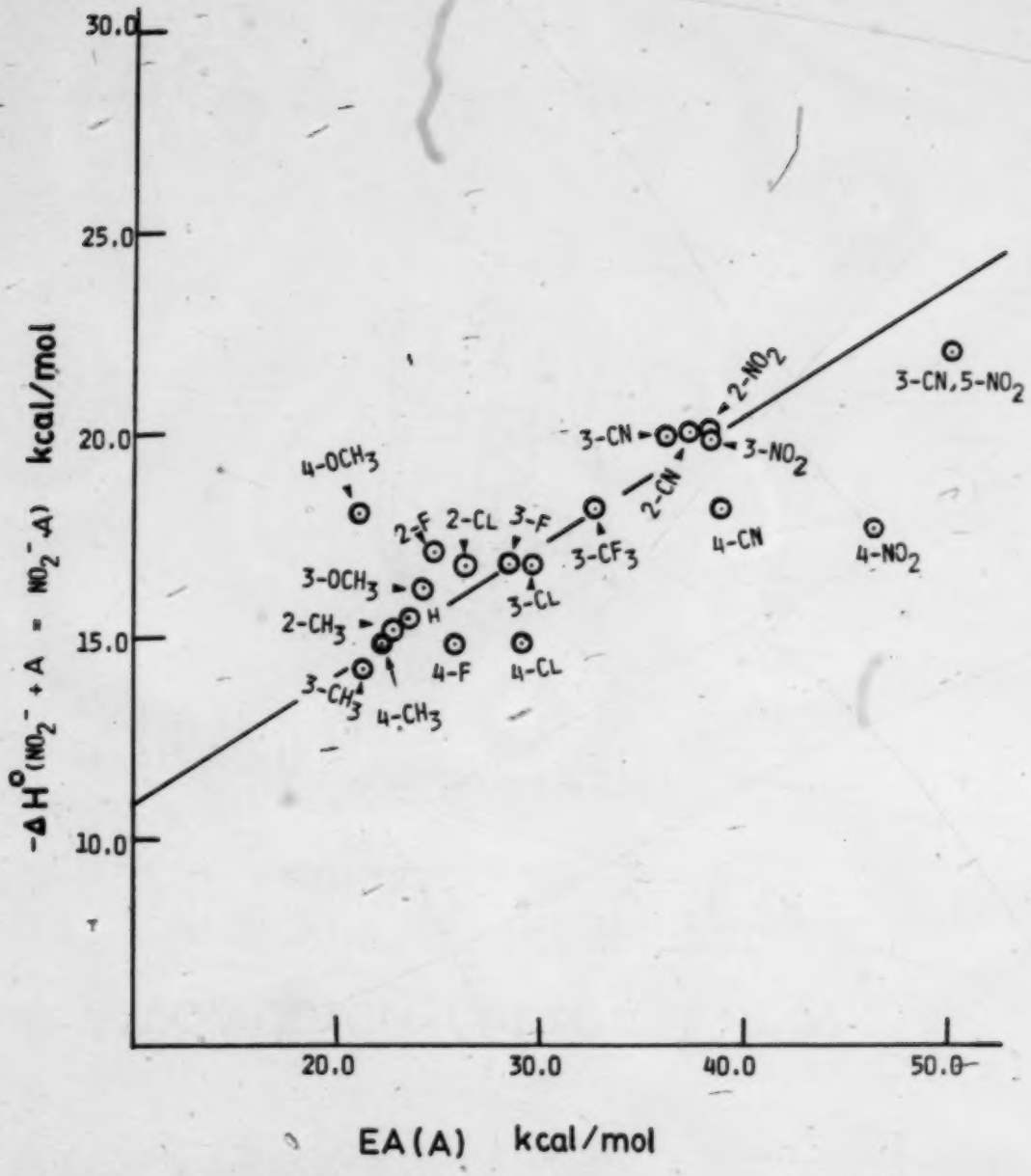

Figure 6.10. Plot of ΔH^0 for reactions $NO_2^- + A = NO_2^- \cdot A$ against electron affinities of A. A good correlation is obtained between the binding energies, $D(NO_2^- \cdot A)$ and electron affinities of A.

calculation[168] are shown in structures I to IV below, where the numbers in brackets are the calculated bond energies[168] in kcal/mol.

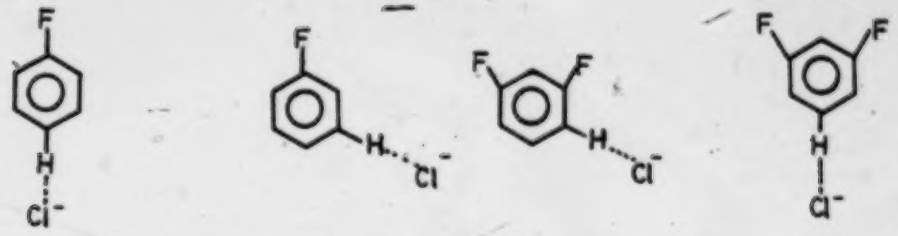

I(10.3) II(10.8) III(10.9) IV(12.9)

Fluorine has an electron withdrawing field/inductive effect. This effect is expected to increase the protic character of the aromatic hydrogens. But F is also a weak π donor and the π donation produces a small relative increase of electron density on the carbons ortho and para to the F and this in turn should reduce the protic character of the ortho and para hydrogens. The prediction from the theoretical calculations[168], that the structures II and IV are the most stable, is therefore, in line with the expected substituent (X = F) effect in aromatic systems.

The molecules for which measurements were made with Cl^- and NO_2^- are NB, 3-FNB, 4-CNNB and 3-CF_3NB; see Tables 6.4 and 6.6, for example. The corresponding adduct stabilities are: 16.3, 14.2; 18.7,16.8; 20.0, 18.8; and 19.5, 18.2; respectively for the clusters of Cl^-, NO_2^-; with four molecules given in the order above. Thus the bonding of the above two ions to neutral molecules is of quite similar magnitude, with NO_2^- giving a slightly weaker interaction. The increased delocalization of the the negative charge in the NO_2^- ion compared to that in Cl^- ion is probably responsible for the weaker interaction in NO_2^-.A.

Considering the information presented above, which indicate that the NO_2^-.A adducts are held together at least partly by hydrogen bonding forces, it becomes possible to interpret the observed relationship between NO_2^-.A and the electron affinity of A, shown in Figure 6.10. On formation of the negative ion A^- the electron enters the lowest unoccupied (π^*) orbital in A whose energy is decreased and the $\dot{E}A(A)$ is increased, by the presence of electron withdrawing substituents (and an opposite effect for the presence of electron donating substituents). The

same type of substituents (electron withdrawing) also increase the protic character of the hydrogens in the conjugated system of A and thus increase the (H)bonding ability of A toward negative ions like Cl^- and NO_2^-.

However, since the molecules A examined in Figure 6.10 often have large dipole moments, additional stabilization could occur from classical ion-dipole interaction between the negative ion and the neutral molecules A. If the ion-dipole stabilization is present in NO_2^-.A adducts, it will be reflected in the stability of NO_2^-.A involving isomers of A, where there is a large difference of dipole moments between isomers.

As an illustration, the experimental values of dipole moments of the three dinitrobenzene isomers are: 6.0 D, 3.8 D, 0.0 D respectively for ortho, meta, and para isomers. Thus one would expect the increase in stability of NO_2^-.A in the same order of increase in dipole moments of A. The expected stability order from ion-dipole interaction is in agreement with the observed binding energies of NO_2^- to A, the three dinitrobenzenes. Similarly one can explain the stability order of other NO_2^-.X-NB isomeric adducts given in Table 6.4 and shown in Figure 6.10.

Shown in Figure 6.11 is the plot of binding energies of NO_2^- to A molecules against the binding energies in 2-NO_2NB^-.A. The points in the figure roughly fall on a straight line. The results shown in Figure 6.11 therefore, predict that the binding energies in NO_2^-.A and 2-NO_2NB^-.A are similar i.e., an increase or decrease in binding energies in a similar fashion with the change of A, however the latter binding energies are weaker. The relatively lower binding energies of 2-NO_2NB^- to A compared to that of NO_2^- to A is not surprising. The negative charge of NO_2^- is rather localized in three atoms while that in 2-NO_2NB^- the charge is more delocalized with the ring and the NO_2 group and this will lead to the weaker interaction .

The results shown in Figure 6.10 and 6.11 are for complexes where the negative ion is kept the same while the neutral molecules, A were varied. An increase in binding energies in NO_2^-.A or NO_2NB^-.A was observed with the increase of electron affinities of A. Shown earlier in Figure 6.4 were results where the neutral molecules Sl are kept the same while the negative ions A^- (where A represents substituted nitrobenzenes) were varied and an opposite effect, the

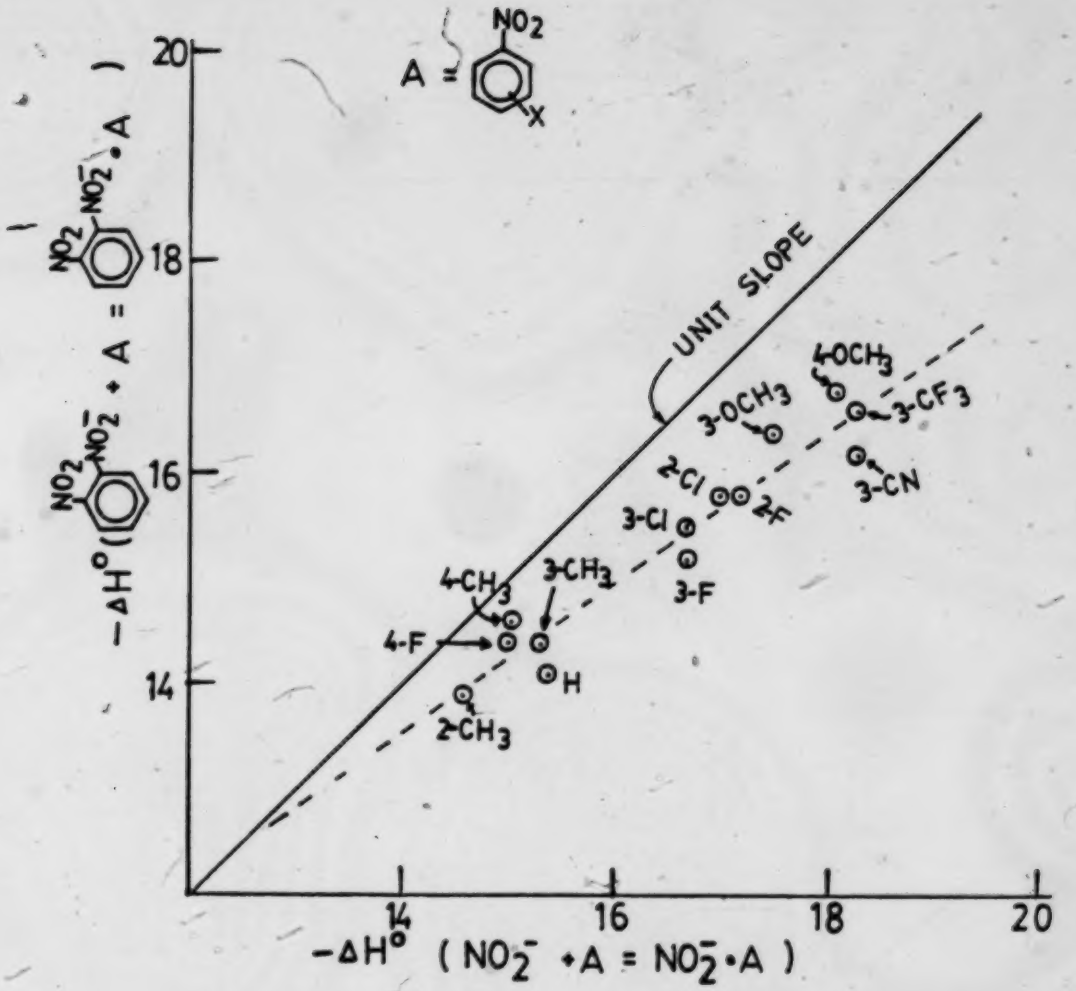

Figure 6.11. Plot of ΔH^0 (2-NO_2NB^- + A = 2-NO_2NB^-.A) against ΔH^0 (NO_2^- + A = NO_2^-.A). NB stands for nitrobenzene.

decrease in binding energies in $A^-.Sl$ is observed with the increase of electron affinities of A. The binding energies of A^- to A, however do not show any such correlation with the electron affinities of A as shown in Figure 6.12 (see also Table 6.7). The lack of correlation in the results shown in Figure 6.12 is probably due to the cancellation of the two opposing effects demonstrated earlier in Figures 6.4, 6.10, and 6.11. However, one can understand the change in binding energies in A_2^-, where the different A are isomers. For all electron withdrawing substituents NO_2, CN, Cl, F etc. the ortho isomer forms the strongest cluster and the order of bond strength is ortho ≥ meta >> para, while for electron donating substituents an opposite order para ≥ meta > ortho is observed in Figure 6.12 and Table 6.7. These orders in stability of $A^-.A$ are in line with the order of dipole moments[90] of isomers of A and this means that the strength of the molecular dipole of A in the $A^-.A$ adduct is the factor that dominates the bonding.

To examine the dependence of the binding energies in $A^-.A$ on the dipole moments of A, plotted in Figure 6.13 are binding energies in $A^-.A$ against experimental dipole moments[90] of A, also given in Table 6.7. Only few dipole moment values for A are available[90] from measurements in gas phase. The majority of them are measured in liquid benzene. It is observed[90] for some molecules for which the dipole moments are obtained in gas phase and also in liquid benzene, that the dipole moment values obtained in two different media differ only by 0.5 D or less. We used dipole moments of some molecules obtained in liquid benzene, which are not available from gas phase measurements. The results plotted in Figure 6.13 show a clear dependence of dipole moments of A on binding energies in $A^-.A$. Least square fitting (excluding the values for 4-NO_2NB and 4-CNNB) of results in Figure 6.13 gives a slope 1.1 and an intercept of 4.1 kcal/mol. The unusually high binding energies in $A^-.A$, for A = 4-NO_2NB, and 4-CNNB are not clear. The relatively higher binding energies observed for X = OCH_3 is probably due to interaction of methoxy hydrogen(s) to the negative ions rather than a aromatic hydrogen. An earlier investigation[169] regarding $Cl^-.A$ also showed binding energies in $Cl^-.H_3COPh$ is relatively higher compared to that observed in other $Cl^-.A$, where A were substituted aromatic hydrocarbons. The methoxy substituent is a strong π donor and weak σ

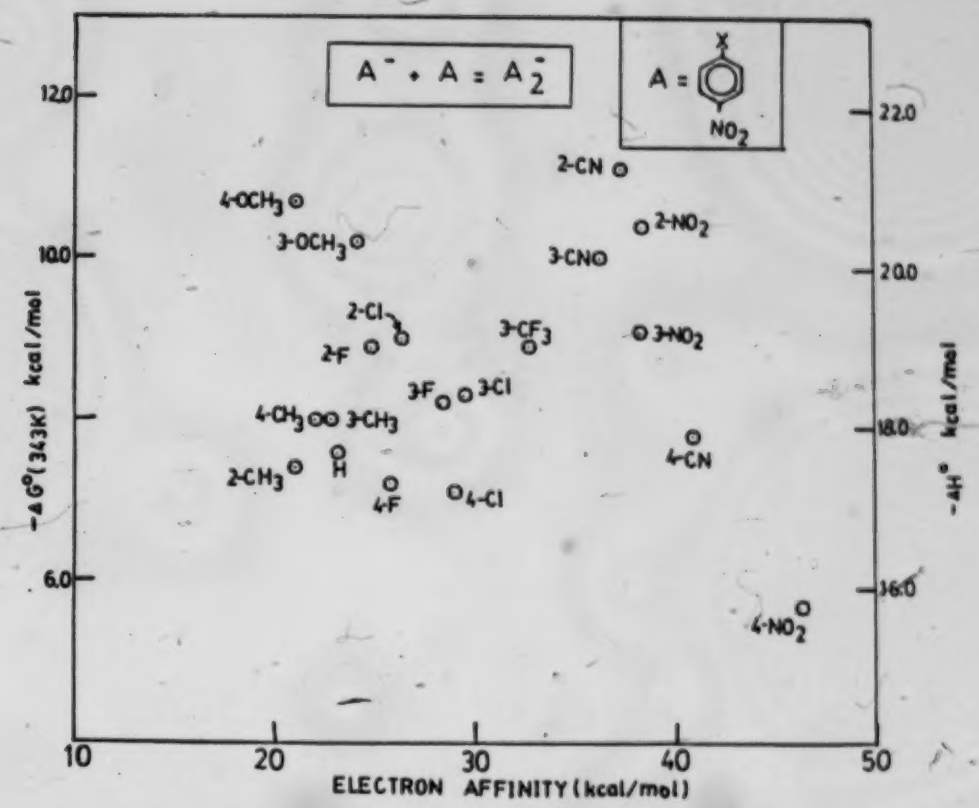

Figure 6.12. Plot of ΔG^0_{ad}(343K) for reactions $A^- + A = A^-.A$ against the electron affinities of A. Approximate enthalpy changes are given on the right hand side ordinate of the figure. These values are obtained by assuming entropy change = -29.0 cals/deg. No correlation is found to exist between $D(A^-\text{-}A)$ and the electron affinities of A in the figure.

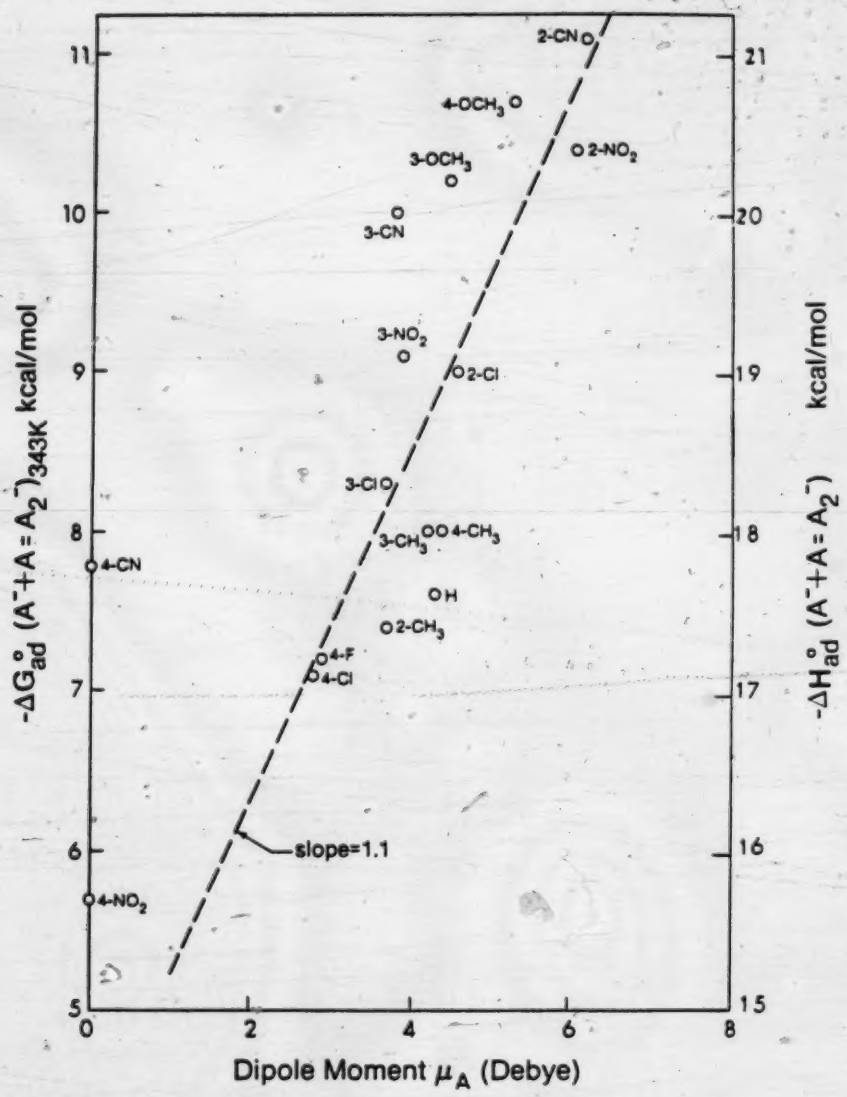

Figure 6.13. Plot of binding energies in $Cl^-.A$ adducts against dipole moments of A (ref. 90).

acceptor. The strong π donation develops partial positive charge on the oxygen atom of the methoxy group as shown below.

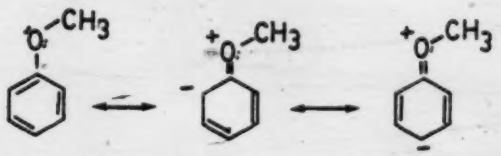

Which means that, negative ions probably interact with OCH_3 hydrogens of anisole or substituted anisoles, since they are in the region of excess positive charge. Further, since there is a possiblity of participation of more than one hydrogen in interacting with the negative ion in anisole or substituted anisoles, this will lead to stronger interaction.

In examining the factors influencing the binding energies in the adducts A^--B and A^--A, the possibile role of electron transfer from the negative ion to the neutral molecules is not considered. The observed increase of binding energies of A^-.B with increasing electron affinities of B and decreasing electron affinities of A may be also a consequence of charge transfer from A^- to B.

(iii) Binding Energies of Cl^- to A Molecules

The investigation involving the determination of binding energies of Cl^- to A molecules given in Table 6.6 obtained from van't Hoff plots shown in Figure 6.9 and some one-temperature measurements at 300K, is an extension of the previous work from this laboratory[168-169]. All the results provided in Table 6.6, except otherwise mentioned, are from the present investigation. Binding energies in three adducts, Cl^-.A, from the previous work[168-169] are redetermined. While binding energies (ΔG^0_{ad}, 300K) of Cl^- to PhH and PhCl are observed to be the same in the present study. However, that of Cl^- to NO_2Ph is observed to be much higher (10.5 kcal/mol in the present study versus 7.1 kcal/mol[168-169]). The present

result is supported by the observed binding energy of Cl^- to PhCN, which is 10.0 kcal/mol (see Table 6.6), a value much higher than 7.1 kcal/mol reported[168-169] for $Cl^-.NO_2Ph$.

Shown in Figure 6.14 is the plot of binding energies for the reactions: $Cl^- + A = Cl^-.A$, where A are some monosubstituted benzenes versus the substituent constants $\sigma_p^-(g)$, for gas phase phenol acidites, also used earlier in Figures 4.25 and 4.29 from Taft[127]. One observes a good correlation of $Cl^-.A$ adduct binding energies with the substituent constants σ_p^-, except for A = anisole, for which the observed binding energy in $Cl^-.A$ is much higher relative to the prediction from substituent constant for OCH_3. As discussed earlier the binding energies of other negative ions such as NO_2^-, XNB^- to anisoles are also observed to be higher. The greater stability of adducts observed involving aromatics containing OCH_3 group was discussed earlier in this section and was explained as due to the interaction of negative ions with the OCH_3 hydrogen(s) rather than the aromatic hydrogen of the ring.

Also given in Table 6.6 are binding energies of Cl^- with some perfluoro compounds, such as SF_6, $CF_3C_6F_{11}$, C_6F_6, C_6F_5CN etc. It is interesting to note that SF_6 and perfluorocarbons such as, $CF_3C_6F_{11}$ do not form measureable adducts with Cl^-, under experimental conditions used, while C_6F_6 and other substituted perfluorobenzenes form strong complexes with Cl^-. As shown earlier in Table 3.7, other negative ions such as, $3\text{-}NO_2NB^-$, $4\text{-}NO_2NB^-$ also do not form stable adducts with SF_6 or $CF_3C_6F_{11}$. On the other hand binding energies of SF_6^-, $CF_3C_6F_{11}^-$ to nitrobenzenes, X-NB are quite large (Table 3.7).

It is of considerable interest to enquire into the reasons for the large difference in the bond energies $D(SF_6^-\text{-}A)$ and $D(SF_6\text{-}A^-)$. A more general examination of the bonding involved will be of importance also for other $(A.B)^-$ systems.

The temperature dependence of adduct forming equilibria (6.8) involving perfluoro-molecules are shown in Figure 6.9 and tabulated in Tables 3.7 and 6.6. The results discussed earlier in this section for equilibria (6.8) indicated that the adducts of negative ions formed essentially of hydrogen bonded structures. Thus when B = benzenes, the electron withdrawing substitutents on the benzene induce partial positive charges on the aromatic hydrogens and the resulting most positive hydrogens engage in hydrogen bonding to the negative

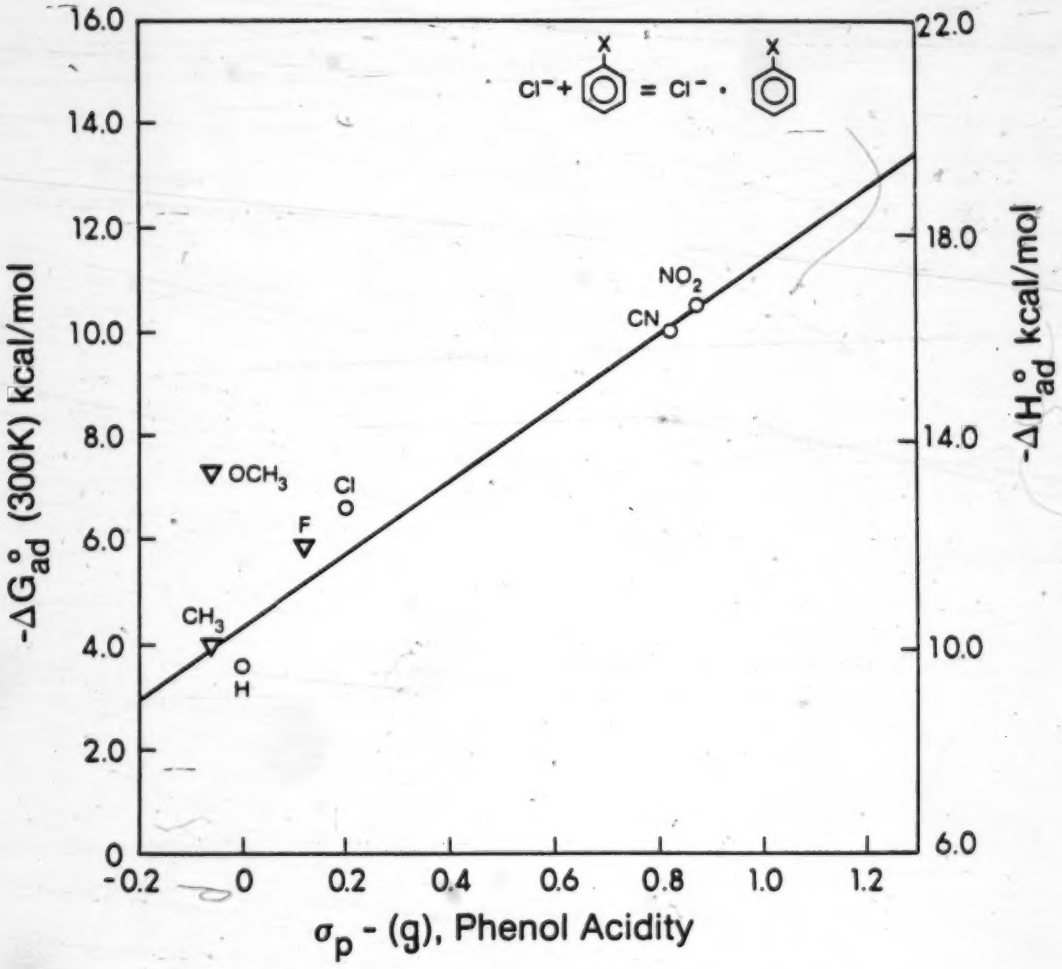

Figure 6.14. Plot of $-\Delta G^0_{ad}$(300K) for reactions Cl^- + A = Cl^-.A against Hammet type substituent constants, σ_p^-(g) for gas phase phenol acidities due to Taft (ref. 127).

ion. The occurrence of this type of bonding was supported by results from STO-3G calculations[168]. The type of bonding proposed for SF_6^-.A and SF_6.A^- is illustrated in Figure 6.15, where A = 3-CF_3NB. The similarity between the bonding observed in SF_6^-.A (Table 3.7), Cl^-.A (Table 6.6) and NO_2^-.A (Table 6.4) is evident when one examines the order of bond energies for the three anions. Thus D(SF_6^--A) decreases in the order of A = 3-CF_3NB, 3-FNB, NB; the same order is observed for D(Cl^--A) and D(NO_2^--A). The order is dictated by the decreasing electron withdrawing power of the substituents in benzene. The weakest Cl^-.A bond is found for A = PhH, benzene (Table 6.6) where electron withdrawing substituent is absent. The binding energies in SF_6^-.A are smaller than those of Cl^-.A, a result that could have been anticipated from the larger size of SF_6^- relative to Cl^-. However, the difference is not very large. The relatively strong bonding in SF_6^-.A may be due to the high electronegativity of the fluorine atoms. Thus the rather small F atom of SF_6^-, involved in the H-bonding shown in the Figure 6.15, probably has a relatively large net negative charge and this makes it a very suitable hydrogen bond acceptor.

On the other hand everything is unfavorable to bonding in A^-.SF_6 and Cl^-.SF_6. A^-.SF_6 or Cl^-.SF_6 were not detected in the present work (see Tables 3.7 and 6.6). SF_6 is not suitable for bonding because it has the wrong charge distribution. Thus the S^+-F^- bond dipoles in SF_6 result in dodecapole with negative charge on the outside of the molecule which shields the SF_6 from interaction with the negative centres in A^- (see Figure 6.15) or with Cl^-.

The geometries of $CF_3C_6F_{11}$ or $CF_3C_6F_{11}^-$ are not known. The observation of strong bonding in $CF_3C_6F_{11}^-$.A and the failure to see any A^-.$CF_3C_6F_{11}$ and Cl^-.$CF_3C_6F_{11}$, properties similar to what observed in case of adducts involving SF_6 and SF_6^-; suggest that the bonding patterns in $CF_3C_6F_{11}^-$.A and A^-.$CF_3C_6F_{11}$ are similar to those in SF_6^-.A and SF_6.A^- shown in Figure 6.15.

Considering the weak bonding observed for A^-.SF_6, A^-.$CF_3C_6F_{11}$, Cl^-.SF_6 and Cl^-.$CF_3C_6F_{11}$, one might have expected that A^-.C_6F_6 would be also weakly bonded. Results for the binding energies in Cl^-.C_6F_6, Cl^-.C_6F_5CN, Cl^-.$C_6F_4(CN)_2$ are given in Table 6.6. Surprisingly however, C_6F_6 bonds quite strongly in spite of the fact that it does not have a

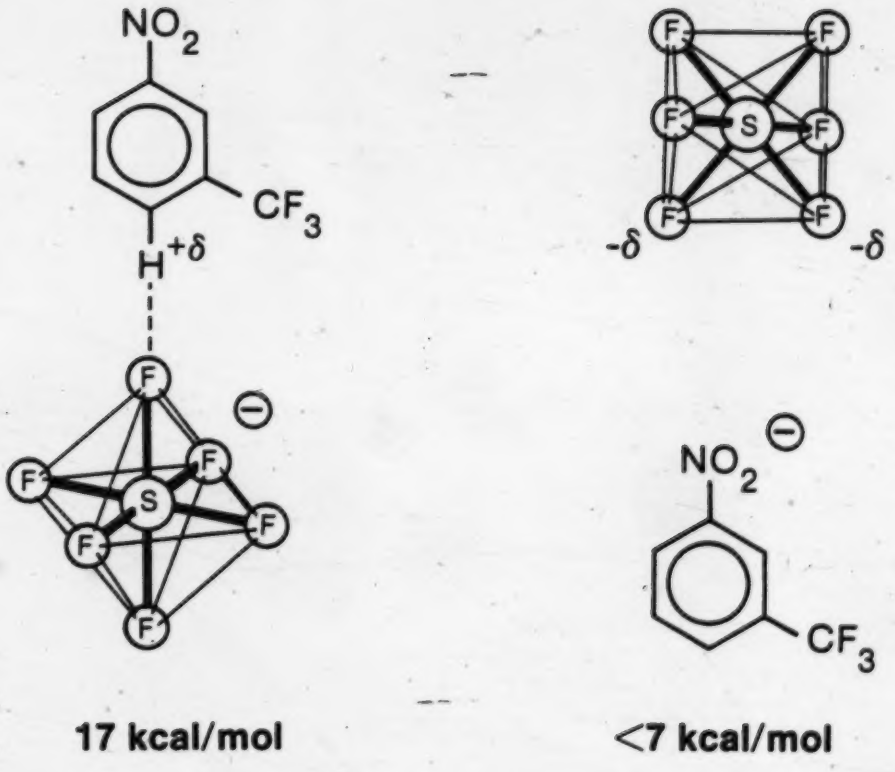

Figure 6.15. Possible bonding structures of $SF_6^-.B$ and $SF_6.B^-$, where B = 3-CF_3NB.

protic hydrogen. The binding energy with negative ion increases when F is substituted with a stronger electron withdrawing substitutents, such as CN. Thus $D(Cl^{-}\text{-}C_6F_6) = 16.8$, $D(Cl^{-}\text{-}C_6F_5CN) = 21.3$, and $D(Cl^{-}\text{-}C_6F_4(CN)_2) = 24.4$ in kcal/mol, see Table 6.6.

A recent experimental and detailed theoretical investigation involving cluster ions $F^{-}.PhH$ and $F^{-}.C_6F_6$ by Hiraoka et al.[170] also showed very strong interaction of F^{-} with C_6F_6. Thus, $D(F^{-}\text{-}PhH) = 15.3$ and $D(F^{-}\text{-}C_6F_6) = 27.5$ kcal/mol[170]. The unusual (high) binding energy in $F^{-}.C_6F_6$ is explained[170] as due to considerable charge transfer i.e., a covalent type bond formation between F^{-} and a C-atom of C_6F_6. The obtained geometries from theoretical calculation[170] for $F^{-}.PhH$ and $F^{-}.C_6F_6$ using 3-21G + p basis set are shown in Figure 6.16. F^{-} interacts with PhH through hydrogen bonding, resulting in a small distortion of the PhH geometry. The $F^{-}.C_6F_6$ geometry is distorted significantly relative to that of C_6F_6 (C-C = 1.37A and C-F = 1.35A), and $F^{-}.C_6F_6$ is found to have the geometry of the tetrahedral intermediate, shown in Figure 6.16. The halide ion is taken in as a substituent. The covalent bond(C-F = 1.403A) formation is clearly shown, and the perfluorobenzene ring is deformed accordingly from D_{6h} symmetry. The negative charge is almost equally distributed to seven F-atoms. The geometry is similar to that of the Meisenhiemer complex[188-190], equation (6.13).

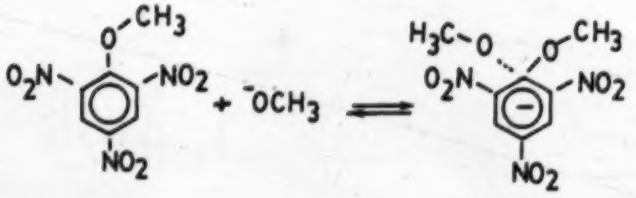

(6.13)

The presence of six electron withdrawing F atoms makes the C atoms of the ring partially positively charged to accept the F^{-} electron density. When F^{-} interacts with C_6F_6, F-F exchange repulsion is brought about, which operates to deform the C_6F_6 structure. The deformation lowers the energy level of the LUMO through $\pi^{*}\text{-}\sigma_{C\text{-}F}$ orbital mixing[170]. This

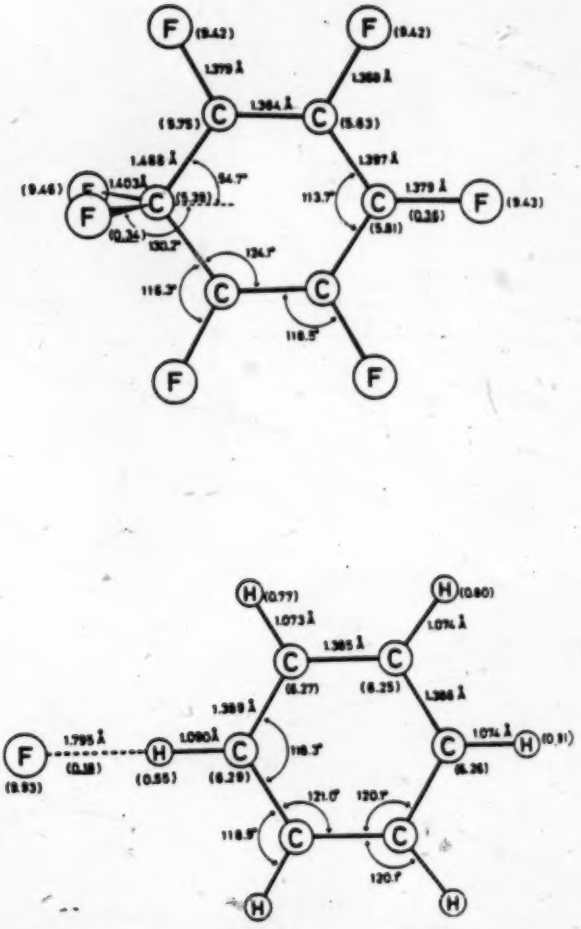

Figure 6.16. Structures of $F^{-}.C_6F_6$ and $F^{-}.C_6H_6$ from theoretical calculations due to Hiraoka et al. (ref. 170).

energy lowering of LUMO promotes the $F^- \rightarrow C_6F_6$ charge transfer.

The relatively weaker interaction of Cl^- with C_6F_6 (16.8 kcal/mol) obtained in the present investigation compared to that of F^- with C_6F_6 (27.5 kcal/mol)[170] is probably due to the larger size of the chloride ion which can not approach as close as F^- can and therefore the interaction is weaker. The presence of strong electron withdrawing substituents like CN in C_6F_6 will make the carbon atoms of the ring more positively charged than that in C_6F_6 and therefore, the interaction with negative ion will increase. This prediction agrees well with the experimental results shown in the Table 6.6 (reactions 11 to 13).

7. APPLICATION OF ELECTRON AFFINITIES AND THE STABILITIES OF A^- AND ADDUCTS OF A^- IN NEGATIVE ION ANALYTICAL MASS SPECTROMETRY

The knowledge of electron affinities of molecules and the binding energies of A^- to various neutral molecules is of fundamental significance to several areas of analytical mass spectrometry[11-12,171-180]. One such area is negative ion analytical mass spectrometry.

The formation of negative ions by interaction of electrons and analytes can occur by three different mechanisms:

$$AB + e^- \rightarrow AB^- \qquad \text{resonance capture} \qquad (7.1)$$

$$AB + e^- \rightarrow A^{\cdot} + B^- \qquad \text{dissociative resonance capture} \qquad (7.2)$$

$$AB + e^- \rightarrow A^+ + B^- + e^- \qquad \text{ion pair production} \qquad (7.3)$$

Each of these processes shows strong dependence on electron energy. If the electrons are thermal or near thermal ($E_e \approx 0.0$ eV), molecular negative ions are formed due to resonance capture. Dissociative electron capture is observed with electrons in the energy range 0 - 15 eV, while ion-pair production usually requires electron energies above 10 eV. Under conventional electron impact conditions (40 - 80 eV electrons and source pressure in the range 10^{-5} to 10^{-7} torr), formation of negative ions occur predominantly by the ion-pair mechanism. At the much higher pressures at which a CI source is operated, many low energy electrons are present which can lead to the formation of a stable molecular negative ion, if the analyte molecule has a positive electron affinity or to a negative CI mass spectrum in the presence of a suitable reagent gas.

In a negative chemical ionisation experiment a high yield of thermal electrons is obtained from the "reagent gas". This is followed by electron capture by an analyte with positive electron affinity, equation (7.1) or, dissociative electron capture, reaction (7.2). In pulsed positive and negative ion chemical ionisation mass spectrometry (PPNICI)[171] CH_4 and

isobutane yield Bronsted acids RH^+ like, CH_5^+, $C_2H_5^+$ etc. in the positive ion mode. The RH^+ reacts with the analyte molecule M and leads to the formation of MH^+. In the negative ion mode CH_4 and isobutane act as the source of thermal electrons. Many organic analytes capture low energy electrons and undergo dissociative electron capture to produce low mass fragments[182]. Few analytes capture thermal electrons to form stable molecular ions. Most organic samples have to be derivatized to increase the volatility and the electron capture cross section and/or electron affinity.

It has been observed in the present investigation that in general compounds A, with electron affinity values greater than ~ 0.5 eV form molecular negative ion A^- by resonance electron capture in a HPMS source, which is not different from a NICI source. Shown in Figure 7.1 are the electron affinities of four different classes of molecules, whose electron affinities are divided by a dotted line at 0.5 eV. Electron affinities of molecules above the dotted line in Figure 7.1 were determined by electron transfer equilibria measurements in the present investigation. However electron affinities of compounds below the dotted line were not determined in the present investigation, they were taken from the literature because molecular negative ions of those compounds were not observed in the HPMS source.

The results described above and shown in Figure 7.1 can be explained on the basis of thermal electron detachment from negative ions A^- of lower electron affinity molecules A. It was discussed earlier in chapter 4 in connection with C_6F_6 and $C_6F_6^-$ and in chapter 5 in connection with azulene negative ion, Az^-, that the intensities of both $C_6F_6^-$ {$EA(C_6F_6) = 0.52$ eV} and Az^- {$EA(Az) = 0.7$ eV} decrease much faster in the ion-source at temperatures above ~150°C. The faster decay of these two ions at higher temperatures is due to thermal electron detachment from Az^- and $C_6F_6^-$, see chapter 5. It is also shown in chapter 5 that the electron detachment rate becomes faster with the increase of temperature of the ion source. The negative ions A^- of molecules of low electron affinity ($EA < 0.5$ eV) will detach electrons at much lower temperature, at a faster rate. Therefore the molecular negative ions of low electron affinity molecules are not generally observed in a NICI ion source at the normal operating condition. Further molecules of low electron affinity have very low thermal electron capture

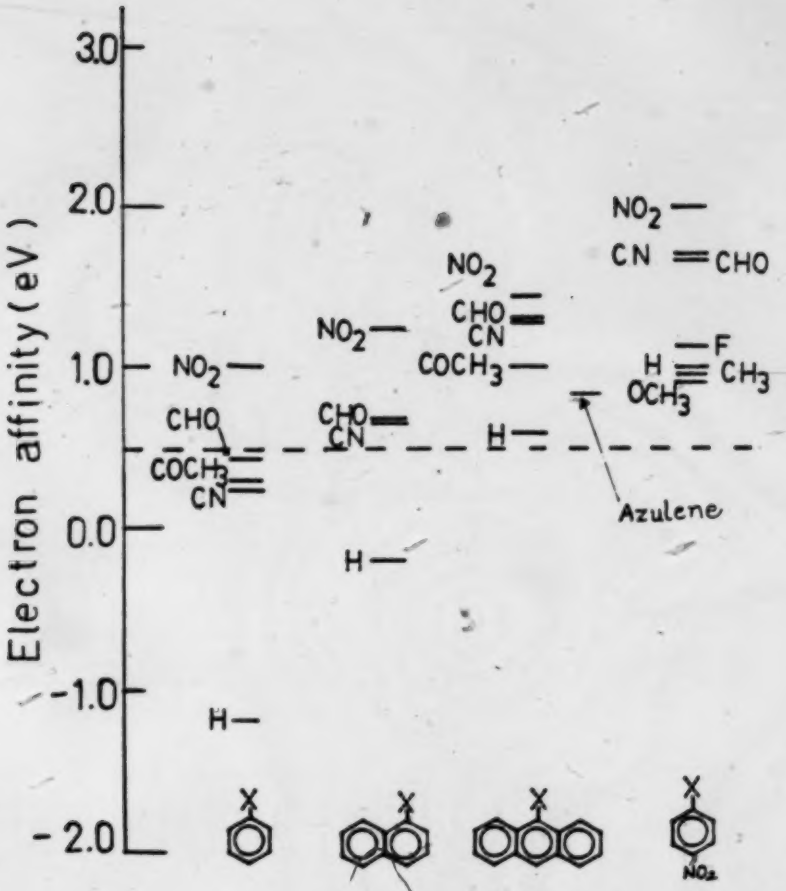

Figure 7.1. Electron affinities of four different classes of compounds are shown. The electron affinity values above the dotted line were obtained experimentally through electron transfer equilibria, while those under the line are from literature: benzene and naphthalene; Jordan (ref. 124); benzonitrile, benzaldehyde and acetophenone; Chen (ref. 33). The dotted line indicates that electron affinities less than ~0.5 eV could not be measured from electron transfer equilibria measurements, probably the ions are lost by rapid thermal electron detachment from the negative ion.

coefficient[25]. Therefore, the formation of initial molecular negative ion intensity by electron capture will be also low, which will be further destroyed by thermal electron detachment. The above observation offers an unique opportunity to distinguish between isomeric compounds whose electron affinities are separated by the line of 0.5 eV in Figure 7.1.

Buchanan et al.[12a,175] and Iida[172] demonstrated that some polycyclic aromatic hydrocarbons (PAHs) could be selectively detected on the basis of electron affinities by electron capture CIMS, provided the electron affinity of one of them is higher than 0.5 eV, while that of the other is lower. The one with higher EA forms A^- while the other does not, in NICI MS ion source. Thus fluorenthene (EA = 0.63 eV) and pyrene(EA = 0.45 eV) both with m/z = 202; azulene (EA = 0.7 eV) and naphthlene (EA = -0.15 eV) both with molecular weight 128 were readily distinguished[12a,172,175]. Similarly two isomers of benzopyrene: benzo[a]pyrene (EA = 0.64 eV) were easily differentiated from benzo[e]pyrene (EA = 0.35 eV) both have m/z = 252.

The dependence of the formation of molecular ions upon electron capture thus allows compounds to be differentiated without the use of authentic standards. Only the electron affinity values need to be known. Since the reliable experimental EA values were not available, Buchanan et al.[12a] used HMO coefficients to deduce electron affinity values. The present determination of electron affinities would be of much help in such investigations.

Polycyclic aromatic hydrocarbons which contain a saturated 5-membered ring as for example, compounds 1 and 2 have lower electron affinities than PAHs containing fully unsaturated 5- or 6-membered ring. The former compounds are not expected to form the molecular ion A^-. However, fluorene 1 and other flourene-derived compounds, except 9-methyl fluorene 2 exhibit[12a] ions corresponding to $(A + 14)^-$. No satisfactory reason is given,

however.

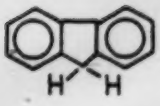

1

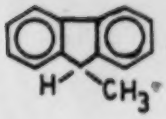

2

The formation of $(A + 14)^{+}$ for fluorene based compounds would allow isomeric fluorene and fluorenthene based compounds such as 3 and 4 to be distinguished from one another and also from the isomeric compound 5.

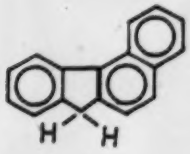

3

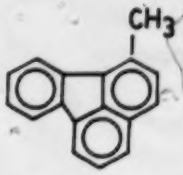

4

5.

All three compounds have molecular weight, m/z = 216. Compound 3 would be observed at m/z = 230, 4 at 216 and 5 would not form any molecular ion.

Wise and Buchanan[180] observed that the isomeric discrimination in some cases could be obtained by working at low CI gas pressure. This observation suggests that similar isomeric discrimination also could be achieved in a conventional electron capture detector for GC at low pressures. Using the same principle Hilpert et al.[179] were able to analyse two particulate materials, an urban air particulate and a diesel particulate, for PAH and alkalated-PAH by GCMS using EI and NICI techniques. The selectivity of NICI made it possible to differentiate methyl fluorenthene from methylpyrene in extracts of particulate materials. It was also possible to differentiate methylbenzo[e]pyrene from isomeric methylbenzo[a]pyrene and

methylbenzofluoranthene.

In addition to the presence of molecular ion A^-, cluster ions, $(A + X)^-$ could be utilized selectively to identify certain classes of compounds. Hunt et al.[171] using PPNICI mass spectrometry were able to analyse some sulfur containing compounds in the presence of hydrocarbon mixtures. In PPNICI technique mixtures of O_2 with 10% H_2 is used as reagent gas. Electron bombardment of oxygen at 1 torr yields O_2^+ and O^+ in the positive ion mode and O_2^- and O^- in the negative ion mode. Addition of 10% hydrogen to the reagent gas eliminates O^- from the reagent spectrum (reaction (7.4)) and simplifies the CI spectrum obtained from aromatic compounds.

$$O^- + H_2 \rightarrow H_2O + e \qquad (7.4)$$

In positive ion mode O_2^+ produces A^+ from the analyte A by charge exchange reaction (7.5).

$$A + O_2^+ \rightarrow O_2 + A^+ \qquad (7.5)$$

In negative ion mode, CI spectra of nonsulfur containing aromatics show an abundent A + 15 ion formed by two possible reactions: equations (7.6) and (7.7).

$$A^- + O_2 \rightarrow (M\text{-}H+O)^- + OH \qquad (7.6)$$

$$A + O_2^- \rightarrow (M\text{-}H+O)^- + OH \qquad (7.7)$$

In contrast to the above results, negative ion CI spectra of aromatic sulfides such as

dibenzothiophene, 6, exibit ions corresponding to A^- and $(A + O_2)^-$.

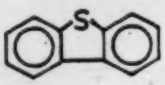

6

The above examples show that a mixture of a nonsulfur aromatic compound and an aromatic sulfide of the same unit mass can be easily analysed using PPNICI mass spectrometry[171]. Spectra of the two compounds show an unresolved doublet due to A^+ on the positive ion trace but only the nonsulfur aromaticcompound should produce an ion 15 mass unit higher on negative ion trace and the aromatic sulfide should show an ion of 32 mass unit higher on the negative trace.

The studies of the reactions involving NO_2 and NO_2^- discussed in chapter 6 (section 6.3) in the present investigation indicate that use of NO_2 and NO_2^- as NCI reagent gas and ion, can be of advantage in certain situations. The results in Table 4.3 demonstrate that NO_2^- will be specific reagent leading to A^- ions for compounds with relatively high electron affinity i.e., higher than $EA(NO_2)$ = 53 kcal/mol. Clustering of A by NO_2^- will be a less specific reaction. As discussed in section 6.3 of chapter 6, the binding energies in $NO_2^-.A$ do not change very much with the change of A, where A were substituted benzenes and quinones, such that binding energies could not be of any use for selective detection of molecules A by chemical ionisation experiments.

Superimposed on the electron transfer and clustering reactions are the oxyanion forming reactions discussed in section 6.3. These reactions are very selective. Typical analytes undergoing the reactions with NO_2^- are nitrobenzenes, XNB, having electron affinity values lower than ~40 kcal/mol and do not form oxyanions, while the ortho isomers invariably do, see Table 6.4. Therefore, in the NO_2-NCI spectrum of low EA substituted nitrobenzenes, an observations of two ions, one corresponding to $NO_2^-.A$, another to $(A\text{-}X+O)^-$ where X is either CN, Cl, F, or CH_3 signals the presence of an ortho isomer. At higher source temperatures the cluster ion

intensities would decrease, as described above, but the oxygenated anions of the ortho isomers would be increased as was the case for the corresponding ion of cyanodinitrobenzene in Figure 7.2. Shown in Figure 7.2 is the formation of phenoxy anion by reaction of NO_2^- with A = cyanodinitrobenzene at two differnt temperatures. At 125°C, free NO_2^- intensity is low since most of NO_2^- are bound as NO_2^-.A adduct. Phenoxide formation out of adduct is slow. At 250°C concentration of adduct NO_2^-.A being low, a high concentration of free NO_2^- is available and phenoxide formation is fast. For all compounds studied here which have EA values greater than 40 kcal/mol, rapid oxygenation reactions were observed in the NO_2-doped methane. For all of these compounds, ions of the type $(A-X+O)^-$, where X is either NO_2, Cl or F, were major species in the NO_2 NCI spectrum. For compounds with EA > 53 kcal/mol, electron transfer from NO_2^- will also produce a molecular ion A^-. Additional details about these reactions were given in section 6.3 and Table 6.4.

One final observation concerning the potential use of NO_2 for NCI is worthy of note. In Figure 7.3 the mass spectra observed with the reaction mixture consisting of methane, tetrafluorobenzoquinone and NO_2 in the ion source is shown (spectrum b). Also shown (spectrum a) is a mass spectrum recorded without NO_2 in the ion source. The effect of NO_2 is quite spectacular. The single molecular anion at m/z = 180 in spectrum a is converted by the presence of NO_2 to several ions of similar intensity in spectrum b. Of the ions observed in spectrum b, only the ions at m/z = 177 and m/z = 226 correspond to ion types which were observed for the other compounds in this study, $(A-F+O)^-$ and $A.NO_2^-$ respectively. While an explanation of the complete NO_2-NCI spectrum is not apparent at this time, a highly unusual synergistic effect between NO_2 and this perfluorinated, high electron affinity molecule is indicated. If this interaction with NO_2 is found to be typical of molecules in this class, it may better provide a basis for their specific detection and analysis.

Knowledge of electron transfer reactions and electron affinities of molecules aslo were shown to play an important role in negative ion FAB mass spectrometry[11,173]. Lloyd et al.[11] have shown that quinones, though have high electron affinities (Table 4.3) do not form Q^- by electron capture in a FAB source when introduced in a glycerol matrix. This is in accord with

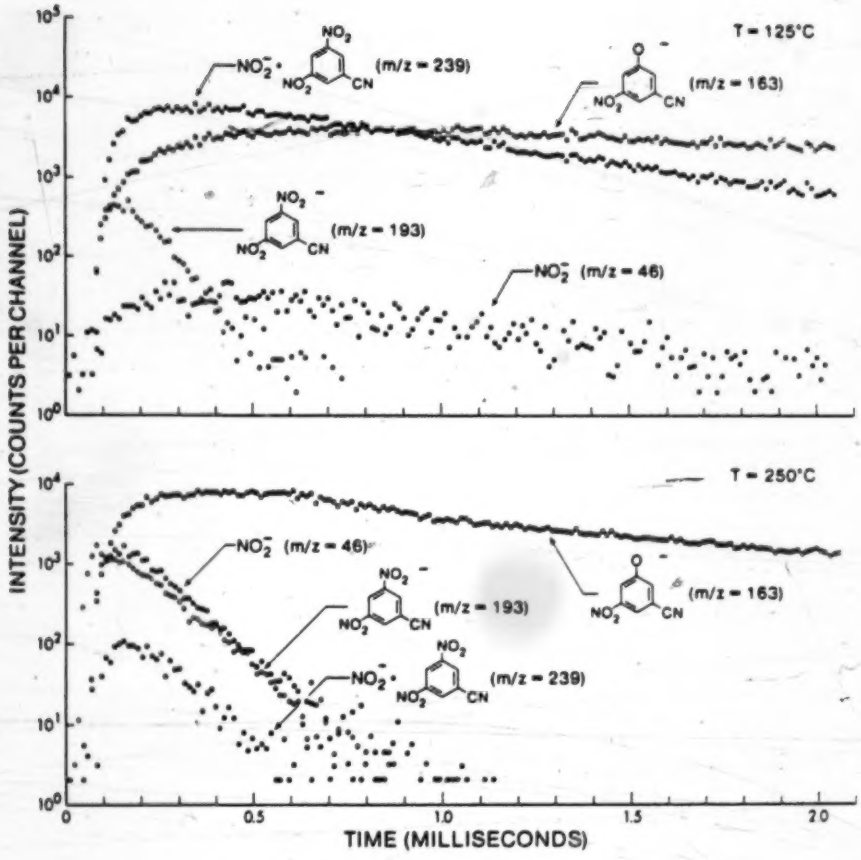

Figure 7.2. Formation of phenoxy anion by reaction of NO_2^- with A = 3,5-dinitrobenzonitrile at two different temperatures. At 125°C, free NO_2^- concentration is low, since most NO_2^- is bound as adduct NO_2^-.A. Phenoxide formation out of adduct is slow. At 250°C concentration of adduct is low, a high concentration of NO_2^- is available and phenoxide formation is fast. The pressure of various gases are: methane = 4.0 torr, NO_2=2.3 mtorr and A = 2.6 mtorr.

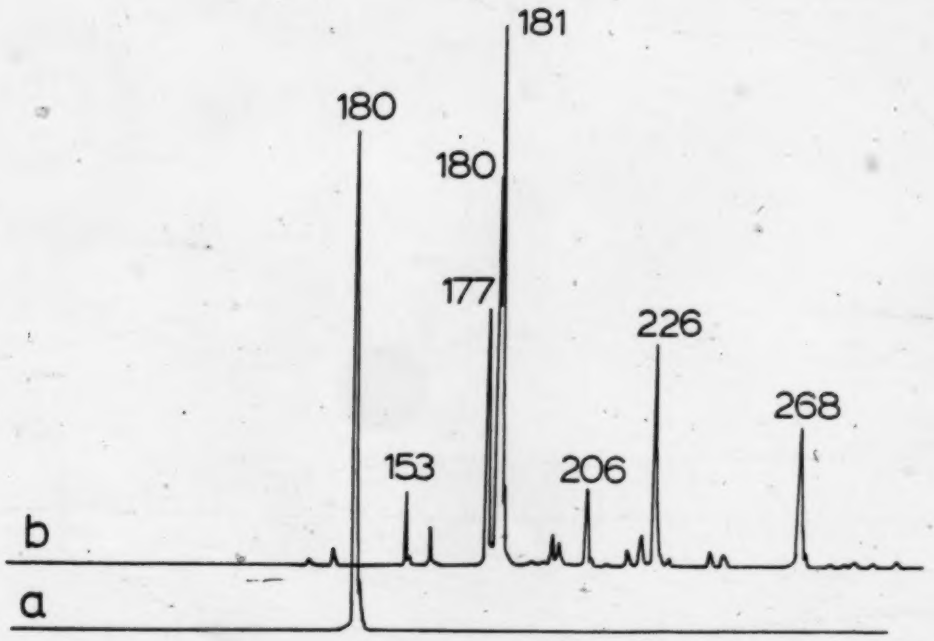

Figure 7.3. Pulsed electron negative ion mass spectrum of fluoranil. t = 150°C, methane = 3.0 torr, (a) 0.8 mtorr fluoranil, (b) 0.8 mtorr fluoranil and 4.0 mtorr NO_2. NCI spectra of fluoranil (without NO_2) produces a single ion, spectrum (a), presence of NO_2 leads to the formation of a number of ions due to reaction of fluoranil negative ion with NO_2.

the observation that quinones especially p-benzoquinone have low thermal electron capture coeffecients discussed in chapter 4, section 4.2. In fact benzoquinone is observed to capture no thermal electron in the present investigation. However, in sulfolane matrix the abundance of quinone negative ions, Q^-, increase significantly[11]. The enhancement of the sensitivity of Q^- in sulfolane matrix could be due to electron transfer from the fragment ions (from the matrix) such as SO_2^- (m/z = 64) to the quinone Q. Since the electron affinity of SO_2 is only 1.1 eV (see Table 4.3), while quinones have much higher electron affinities (>1.5 eV, see Table 4.3), electron transfer reaction (7.8) would occur efficiently.

$$SO_2^- + Q \rightarrow SO_2 + Q^- \qquad (7.8)$$

This is supported by the observation of the fact that the apparent decrease in the intensities of the matrix ions, m/z = 64 and m/z = 119 is approximately equal to the increase of intensity of quinone negative ion, Q^-, m/z = 450 (vitamin K_1)[11]. Thus sulfolane is a useful matrix for detection of compounds A with relatively high electron affinities and of low thermal electron capture cross section. The mechanism of formation of A^- appears to involve electron transfer from m/z = 64 and 119 ions.

8. SUGGESTIONS FOR FURTHER WORK

8.1 Determination of Electron Affinities

The measurements of electron affinities reported in the present investigation can be extended further with the following systems.

8.1.1 Polycyclic Aromatic Hydrocarbons, PAHs

Polycyclic aromatic hydrocarbons, PAHs belong to a group of tremendous biological significance, because most of the PAHs are carcinogenic[183]. These compounds are known to have positive electron affinities. Electron affinities of some polycyclic aromatic hydrocarbons are reported by Wentworth et al.[34] and Becker and Chen[120], measured with the help of a pulsed electron capture detector in gas phase. There are many more polycyclic aromatic hydrocarbons whose electron affinities are yet to be determined. Unfortunately, these compounds have low vapour pressures and therefore, the electron transfer equilibria involving PAHs can not be determined in a similar fashion as was done for other systems in the present study.

A special type of sample inlet system is necessary to study these molecules. In order to measure equilibria involving this group of compounds a temperature controlled heating probe must be used for direct sample inlet into the ion source. The concentration of the PAHs in the ion source can be obtained by measuring the observed pseudo first order rate constant , ν at a given temperature T for electron transfer to PAH, equation (8.1).

$$A^{\cdot} + PAH \rightarrow A + PAH^{\cdot} \qquad (8.1)$$

The concentration of PAH is related to ν by equation (8.2), where k is the bimolecular electron transfer rate constant which is probably equal to the Langevin-ADO predicted rate constant $\approx 10^{-9}$ cc/(molecule.s), unless there is a substantial barrier in the reaction coordinate for the

electron transfer reaction (8.1).

$$\nu = k\,[PAH] \qquad (8.2)$$

Once the concentrations of the neutral species A and PAH are known in the ion source at a temperature, T, the determination of equilibrium constant K for the reaction (8.1) and the evaluation of EA and all other thermochemical quantities follow the established procedure discussed in greater detail in chapter 4.

Apparently the electron affinity of PAHs are not very high (<2.0 eV). Since a large number of molecules are available at present in that range (see Table 4.3) with very small electron affinity differences, "kinetic bracketing technique" could also be applied towards the determination of electorn affinities of PAHs. The advantage of "kinetic bracketing technique" is that the concentration of neutral molecules is not necessary to be known. Only the direction of the electron transfer reaction (8.1) is crucial.

8.1.2 Extension of the Electron Affinity Scale to Higher Electron Affinity Values

Upon examination of the Figures 4.8 and 4.9 and Table 4.3, one observes that the molecule of highest electron affinity reported in this investigation is 3.1 eV for tetracyano ethylene and there is no other molecule whose electron affinity is between 2.8 and 3.1 eV. Molecules of higher electron affinites are important to spectroscopists, in connection with the formation of charge transfer complexes in solution[19] discussed in chapter 1. A few of them are for example, tetracyanoquinodimethane (TCQM), dichlorodicyanobenzoquinone (DDQ) and tetracyanobenzoquinone (TCQ).

To our knowledge no gas phase electron affinities are reported for DDQ and TCQ. However, Compton and Cooper[143] reported the determination of electron affinity for TCQM to be 2.8 eV, obtained from alkali beam collisional ionisation technique. This value seems to be much low compared to the electron affinity of tetracyanoethylene, EA(TCNE) = 3.1 eV

reported in the present investigation. The electron affinity of DDQ and TCQ are also expected to be very high. Unfortunately, these compounds have low volatility. Electron affinity of these compounds can be obtained with the same procedure suggested for the determinations involving PAHs.

Metallic fluorides are also known to have very high electron affinities. No direct determination of electron affinities of metallic fluorides are reported. However, some indirect determinations involving bond dissociation energies are available[184-185]. These indirect determinations were based on the formal cycle (8.3). The electron affinity $EA(MF_n)$ then could be deduced via equation (8.4).

$$\begin{array}{ccc} MF_n^- & \xrightarrow{D(MF_{n-1}\text{-}F^-)} & MF_{n-1} + F^- \\ \uparrow & & \downarrow \\ MF_n & \xrightarrow[D(MF_{n-1}\text{-}F)]{} & MF_{n-1} + F \end{array} \qquad \begin{array}{l} \\ -EA(MF_n) \\ \\ \end{array} \qquad \begin{array}{l} \\ EA(F) \\ \\ \end{array} \qquad (8.3)$$

$$EA(MF_n) = - D(MF_{n-1}\text{-}F) + D(MF_{n-1}\text{-}F^-) + EA(F) \qquad (8.4)$$

The determination of electron affinities via (8.4) involves the use of three experimental quantities, two of them are bond dissociation energies. In general, bond dissociation energies are not known accurately. Sidorov et al.[184-185] obtained binding energies in $MF_{n-1}\text{-}F$ and $(MF_{n-1}\text{-}F)^-$ from ion molecule equilibria studies at high temperatures (>1000°C). Such an approach gives good results for substances with well known vapour pressure. However, vapor pressure of many metal fluorides is not known, and is very sensitive to interaction with the material of the effusion cell of the high temperature mass spectrometer or with impurities. In contrast, electron affinity determination via electron transfer equilibria measurements, equation (1.1) provides more accurate values. However, molecules of known electron affinity values in the appropriate range are necessary in order to study electron transfer equilibria. Unfortunately,

accurate electron affinity values in the appropriate range necessary for the measurement of electron transfer equilibria involving MF_n are not available at the present time. The electron affinity scale has to be extended with molecules of further high electron affinity values. In suitable cases "kinetic bracketing techinique" can also be applied.

Another area where the knowledge of electron affinity is important involves organometallic chemistry. Very little information of the electron affinities of organometallic compounds are available in the literature. The determination of electron affinities, electron transfer kinetics and other negative ion properties of this group of compounds in gas phase will represent a significant step towards the characterization of this important group of molecules.

8.2 Determination of Binding Energies of Charge Delocalized Anions with Multiple Solvent Molecules

In the present investigation only binding energies of charge delocalized anions, A^- with one solvent molecule, Sl were determined. As discussed in chapter 6 it was observed that the binding energy $D(A^-\text{-Sl})$ decreases with the increase of electron affinity of A. It was shown in Figure 4.32 that the electron affinities deduced from the results obtained from solution based measurements, such as half wave reduction potential values etc. are generally lower for molecules of higher electron affinities and is higher for molecules of lower electron affinities compared to the corresponding gas phase electron affinity values reported in the present investigation and tabulated in Table 4.3. Qualitatively, this can be shown as a consequence of the decrease of the sovation exothermicity of charge delocalized anions, A^-, with the increase of electron affinity of A (chapter 4, section 4.2.3). This observation is in line with the observed binding energies for one molecule solvation to A^-. However, a more rigorous inside information regarding the solvation energies in condensed phase can be obtained by studying the binding energies of A^- to many solvent molecules step wise, equation (8.5). Kebarle and coworkers[5,186-187] have demonstrated that the difference in reactivity of organic ions in different solvents is rather due to the interactions of the ion with the closest solvent molecules rather than the bulk properties of the solvent.

$$A^-(Sl)_{n-1} + Sl = A^-(Sl)_n \qquad (8.5)$$

However, information regarding multiple solvent molecule association with small ions such as, Na^+, K^+, F^-, Cl^-, Br^-, I^- etc. is only known. It would be of considerable interest to investigate reactions like (8.5), where A^- are ions of large organic molecules discussed in chapter 6.

The binding energies of charge delocalized anions to solvent molecules are rather weaker compared to those of small ions such as F^-, Cl^- etc. Therefore, in order to measure equilibria (8.5) for higher n values, involving charge delocalized anions, a differently designed ion source, which could be cooled down to much lower temperature (~ -100°C) has to be used. Fortunately this type of ion source with cooling facilities have been in use for long time in this laboratory. The only problem one might encounter is the condensation of low volatile materials in the source. However, since the concentration of the neutral molecule A is not necessary to be known, and they have high electron capture coefficients[25], by using trace amount of A, the condensation problem can be avoided. The determination of binding energies of charge delocalized negative ions with multiple solvent molecules stepwise is an important project to be undertaken. The results from the study of equilibria, such as (8.5) involving charge delocalized anions will also provide information related to solvent reorganization energies, an important quantity necessary to explain the kinetics of electron transfer reactions in solution by Mercus theory[78].

8.3 Meisenheimer Type Complexes

In the course of determination of binding energies of various negative ions with molecules having positive electron affinity (chapter 6), some interesting results were obtained. The negative ion Cl^-, for example, forms no observable cluster with SF_6 or, $CF_3C_6F_{11}$ and was explained as due to unfavorable charge distribution in SF_6. Thus, in SF_6 the negative charge is located on the outside of the molecule i.e., on the F atoms, which prevents negative ions to approach. Interestingly however, C_6F_6 bonds quite strongly with Cl^-. Since π-cloud represents

regions of negative charge, apparently C_6F_6 should also not be suitable for electrostatic bonding with Cl^-. Hiraoka et al.[170] very recently observed that like Cl^-, F^- also forms very strong complex with C_6F_6.

Theoretical calculation showed that[170] $F^-(C_6F_6)$ has a geometry of tetrahedral intermediate. The geometry is similar to those of the Meisenheimer complex[188-190]. A 'Chemical' type bond with $F^- \rightarrow C_6F_6$ charge transfer is suggested[170] to be formed, where the F^- enters the ring as a substituent, the negative charge being delocalized equally over all seven F atoms. This explains the reason for the strong interaction of F^- with perfluorobenzene in $F^-.C_6F_6$.

It is also observed in the present investigation as discussed in chapter 6 that if F of perfluororobenzene is replaced with stronger electron withdrawing substituents, such as, CN the binding energy of the negative ion with the CN-substituted perfluorobenzene is higher than that with unsubstituted perfluorobenzene. The increased electron withdrawing makes the carbon atoms of the ring more positive and hence promotes charge transfer from Cl^-. Binding energy increases further when another CN-group is substituted for F, see Table 6.6. Since the interaction of Cl^- (or, F^-) with C_6F_6 or any other perfluorobenzene with strong electron withdrawing substituent is some kind of covalent bond fomation, with halide ion being taken in as a substituent on the ring, the further clustering of the negative ion with another neutral molecule would be very weak. While the existence of Meisenheimer complex is established in organic synthesis, there have been no studies on the determination of binding energies of halide or other ions in such complexes.

It would be interesting to investigate further the binding energies of Meisenheimer type complexes in gas phase. Additional investigations with many different negative ions and different perfluoro aromatics, aromatic compounds with many strong electron withdrawing substituents etc. might provide insights into the nature of bonding involved.

BIBLIOGRAPHY:

1. Compton, R. N. in "Photophysics and Photochemistry in the Vaccum Ultraviolet", S. P. McGlynn et al (eds), D. Reidel publishing Co. 1985, pp.261.

2. Widlt, R. Astrophys. J. 1939, 89, 295.

3. Mead, R. W.; Stevens, A. E. and Lineberger, W. C. in "Gas Phase Ion Chemistry", M. T. Bowers (eds), Academic press, NY. 1984, 3, 214.

4. Drzaic, P. S.; Marks, J. and Brauman, J. I. in "Gas Phase Ion Chemistry", M. T. Bowers (eds), Academic press, NY. 1984, 3, 168.

5. Kebarle, P. Ann. Rev. Phys. Chem., 1977, 28, 445.

6. Ferguson, E. E.; Fehsenfeld, F. C. and Albritton, D. L. in "Gas Phase Ion Chemistry", M. T. Bowers (eds), Academic press, NY. 1979, 1, 45.

7. Lovelock, J. E. Nature 1961, 187, 49.

8. Lovelock, J. E. Anal. Chem. 1963, 35, 474.

9. Wentworth, W. E. and Chen, E. C. M. J. Chromatography, 1979, 186, 99.

10. Freeman, G. R. Rad. Res. Rev. 1968, 1, 1.

11. Lloyd, J. R. and Cotter, M. L. Proc. 33rd Ann. Conf. Am. Soc. Mass Spec. San Diego, CA, 1985, pp. 817.

12. (a) Buchanan, M. V. and Olrich, G. Org. Mass Spectrom. 1984, 19, 486. (b) Harrison, A. G. "Chemical Ionisation Mass Spectrometry", CRC press, Boca raton, Fl. 1983.

13. Hiraoka, K.; Yamdagni, R. and Kebarle, P. J. Am. Chem. Soc. 1973, 95, 6833.

14. (a) McMahon, T. B. and Kebarle, P. J. Am. Chem. Soc. 1976, 98, 3399. (b) *ibid.* 1977, 99, 2222.

15. Cumming, J. B.; Magnera, T. F. and Kebarle, P. Can. J. Chem. 1977, 55, 3474.

16. Bartmess, J. E. and McIver, R. T. in "Gas Phase Ion Chemistry", M. T. Bowers (eds), Academic press, NY. 1979, 2, 88.

17. Szwarc, M. Prog. Phys. Org. Chem. 1968, 6, 323.

18. Briegleb, G. Angew. Chem. Int. Ed. Engl. 1964, 3, 617.

19. Foster, R. Organic Charge Transfer Complexes, Academic press, London. 1969.

20. Mulliken, R. S. J. Am. Chem. Soc. 1950, 72, 600.

21. Newton, M. D. and Sutin, N. Ann. Rev. Phys. Chem. 1984, 34, 437.

22. Klinger, R. J.; Mochida, K. and Kochi, J. K. J. Am. Chem. Soc. 1979, 101, 6626.

23. Amatore, C.; Pinson, J.; Saveant, J. M. and Thiebalt, A. J. J. Am. Chem. Soc. 1981, 103, 6930.

24. Rich, P. R. Farad. Diss. Chem. Soc. 1982, 74, 3183.

25. Christophorou, L. G. Adv. Elec. Elec. Phys. 1978, 46, 55.

26. Trumpower, B. L. (eds), "Functions of Quinones", Academic press, N.Y. 1982.

27. Christodoulides, A. A.; McCorkie, D. L. and Christophrou, L. G. Elec. Mol. Inter. Appls. 1985, 2, 423.

28. Wentworth, W. E. and Chen. E. C. M. J. Chromatography, 1979, 186, 99.

29. Chen, E. C. M. and Wentworth, W. E. J. Chem. Phys. 1975, 63, 3183.

30. Chen. E. C. M. and Wentworth, W. E. J. Phys. Chem. 1983, 87, 45.

31. Wentworth, W. E. and Becker, R. S. J. Am. Chem. Soc. 1962, 82, 4263.

32. Wentworth, W. E.; Becker, R. S. and Tang, R. J. Phys. Chem. 1967, 71, 1652.

33. Wentworth, W. E.; Kao, L. W. and Becker, R. S. J. Phys. Chem. 1975, 79, 1161.

34. (a) Wentworth, W. E.; Chen, E. and Lovelock, J. E. J. Phys. Chem. 1966, 70, 445. (b) Lovelock, J. E. and Ferber,G. J. Atom. Environ. 1982, 16, 1467.

35. Helbing, R. K. B. and Rothe, E. W. J. Chem. Phys. 1969, 51, 1607.

36. Leffered, C. B.; Jackson, W. M. and Rothe, E. W. J. Chem. Phys. 1973, 58, 5801.

37. Mathur, B. P.; Rothe, E. W.; Tang, S. Y.; Mohajon, K. and Reck, G. P. J. Chem. Phys 1976, 64, 1247.

38. Mathur, B. P.; Rothe, E. W.; Tang, S. Y. and Reck, G. P. J. Chem. Phys. 1976, 65, 565.

39. Mathur, B. P.; Rothe, E. W. and Reck, G. P. J. Chem. Phys. 1977, 67, 337.

40. Dispert, H. and Lacman, K. Chem. Phys. Letts. 1977, 47, 533.

41. *ibid*, Int. J. Mass Spectrom. Ion Phys. 1978, 28, 49.

42. Nalley, S. J.; Compton, R. W.; Schweinler, H. C. and Anderson, V. E. J. Chem. Phys. 1973, 59, 4125.

43. Compton, R. N.; Reinherdt, P. W. and Cooper, C. D. J. Chem. Phys. 1975, 63, 3821.

44. *ibid*, 1978, 68, 2023; 4360.

45. Cooper, C. D.; Naff, W. T. and Compton, R. N. *ibid*, 1975, 63, 2752.

46. Cooper, C. D.; Frey, W. F. and Compton, R. N. *ibid*, 1978, 69, 2367.

47. Lifshitz, C.; Hughes, B. M. and Tiernan, T. O. Chem. Phys. Letts. 1970, 7, 469.

48. Tiernan, T. O.; Hughes, B. M. and Lifshitz, C. J. Chem. Phys. 1971, 55, 5692.

49. Hughes, B. M.; Lifshitz, C. and Tiernan, T. O. *ibid*, 1973, 59, 3162; 3182.

50. Lifshitz, C.; Tiernan, T.O. and Hughes, B. M. J. Chem. Phys. 1973, 59, 3182; *ibid*, 1980, 72, 789.

51. Refaey, K. M. A. and Franklin, J. L. *ibid*, 1976, 65,1994.

52. *ibid*, 1976, 64, 4810.

53. *ibid*, Int. J. Mass Spec. Ion. Phys. 1977, 23, 13.

54. Refaey, K. M. A. J. Chem. Phys. 1976, 65, 2002.

55. Refaey, K. M. A. Int. J. Mass Spec. Ion Phys. 1976, 21, 21.

56. Fehsenfeld, F. C.; Ferguson, E. E. and Schmeltekoff, A. L. J. Chem. Phys. 1966, 45, 1844.

57. Dunkin, D. B.; Fehsenfeld, F. C. and Ferguson, E. E. Chem. Phys. Letts. 1972, 15, 257.

58. Bacock, L. M. and Streit, G. E. J. Chem. Phys. 1981, 75, 3864.

59. Streit, G. E. *ibid*, 1982, 77, 826.

60. Fukuda, E. K. and McIver, R. T. J. Chem. Phys. 1982, 77, 4942.

61. Cellota, R. J.; Bennett, R. A. and Hall, J. J. J. Chem. Phys. 1974, 60, 1740.

62. Feldmann, D. Z. Naturforsch. Teil, 1970, A25, 621.

63. Caldwell, G. and Kebarle, P. J. Chem. Phys. 1984, 80, 577.

64. Grabowski, J. J.; Van Doren, J. M.; DePuy, C. H. and Bierbaum, V. M. *ibid*, 1984, 80, 575.

65. Rothe, E. W.; Tang, S. Y. and Reck, G. P.J. Chem. Phys. 1975, 62, 3829.

66. Farragher, A. L. and Page, F. M. Trans. Farad. Soc. 1965, 61, 3072; 1967, 63, 2369.

67. Page, F. M. and Goode, G. C. "Negative Ions and Magnetron", Wiley Intersc., NY. 1969.

68. Klots, C. E.; Compton, R. N. and Raaen, V. F. J. Chem. Phys. 1974, 60, 1177.

69. Latimer, W. M.; Pitzer, K. S. and Slansky, C. M. J. Chem. Phys. 1939, 7, 108.

70. Bradsley, J. N. and Mandl, F. Rep. Prog. Phys. 1968, 31, 471.

71. Eberson, L. Adv. Free Radical Biol. Med. 1985, 1, 19.

72. Birch, A.J; Subba Rao, G. Adv. Org. Chem. 1972, 8, 1.

73. Bordwell, F. G. and Bausch, M. J. J. Am. Chem. Soc. 1986, 108, 1985.

74. Kerber, R. C.; Urry, G. W. and Kornblum, N. J. Am. Chem. Soc. 1965, 87, 4520.

75. Marcus, R. A. J. Chem. Phys.1956, 24, 966; 979.

76. Henglein, A.; Muccinie, G. A. J. Chem. Phys. 1959, 31, 1426.

77. Rains, L. J.; Moore, H. W. and McIver, R. T. J. Chem. Phys. 1978, 68, 3309.

78. McIver, R. T. and Fukuda, E. K. "Lecture Notes In Chemistry", Hartman, H.; Wanzek, K. P. (eds), Springer, Berlin. 1983, pp. 164.

79. Fukuda, E. K. and McIver, R. T. J. Phys. Chem. 1983, 87, 2993.

80. Fukuda, E. K. and McIver, R. T. J. Am. Chem. Soc. 1985, 107, 2291.

81. McIver, R. T. Rev. Sci. Instrum. 1978, 49, 111.

82. Beauchamp, J. L. Ann. Rev. Phys. Chem. 1971, 22, 527.

83. Ferguson, E. E.; Fehsenfeld, F. C. and Schmeltekopf, A. L. Adv. At. Mol. Phys. 1969, 5, 1.

84. Hiraoka, K. and Kebarle, P. J. Am. Chem. Soc. 1975, 97, 4179.

85. Durden, D. A. Ph. D. Thesis, University of Alberta, 1968.

86. Arshadi, M. R. Ph. D. Thesis, University of Alberta, 1969.

87. Cunningham, A. J.; Payzant, J. and Kebarle, P. J. Am. Chem. Soc. 1972, 94, 7627.

88. Su, T. and Bowers, M. T. Int. J. Mass Spectrom. Ion Phys. 1975, 17, 211.

89. Herbst, E.; Patterson, T. A. and Lineberger, W. C. J. Chem. Phys. 1974, 61, 1300.

90. McClellan, A. L. "Tables of Experimental Dipole Moments", W. H. Freeman and Co., San Fransisco. 1963.

91. (a)Drzaic, P. S. and Brauman, J. I. J. Am. Chem. Soc. 1982, 104, 13. (b) *ibid*, Chem. Phys. Letts. 1981, 83, 508.

92. (a) Fehsenfeld, F. C. J. Chem. Phys. 1970, 53, 2000.(b) *ibid*, 1971, 54, 438.

93. Heneghan, S. P. and Benson, S. W. Int. J. Chem. Kinet. 1983, 15, 109.

94. Lifshitz, C. J. Phys. Chem. 1983, 87, 3474.

95. Chen. C. L. and Chentry, P. J. J. Chem. Phys. 1979, 71, 3847.

96. Foster, M. S. and Beauchamp, J. L. Chem. Phys. Letts. 1975, 31, 482.

97. (a) Fessenden, R. W.; Schuler, R. H. J. Chem. Phys. 1966, 45, 1845.(b) Morton, J. R.; Preston, K. F.; Tait, J. C. J. Chem. Phys. 1975, 62, 2029.

98. Hay, P. J. J. Chem. Phys. 1982, 76, 502.

99. Brion, C. E. Int. J. Mass Spectrom. Ion Phys. 1969, 3, 197.

100. Sen Sharma, D. K. and Kebarle, P. J. Am. Chem. Soc. 1982, 104, 19.

101. Olmsted, W. N. and Brauman, J. I. J. Am. Chem. Soc. 1977, 99, 4219; Ferneth, E. and

Brauman, J. I. J. Am. Chem. Soc. 1976, 98, 7891.

102. Magnera, T. F. and Kebarle, P. in "Ionic Processes the Gas Phase", A. Ferreira (eds), Reidel, Dordrecht, Netherlands. 1984.

103. Caldwell, G.; Magnera, T. F. and Kebarle, P. J. Am. Chem. Soc. 1984, 106, 959.

104. Richardson, D. E. J. Phys. Chem. 1986, 90, 3697.

105. Marcus, R. A. and Sutin, N. Inorg. Chem. 1975, 14, 213.

106. Sutin, N. Prog. Inorg. Chem. 1983, 30, 441.

107. Herzberg, G. "Infrared and Raman Spectra", van Nostrand, NY. 1945.

108. Hirao, K. J. Chem. Phys. 1985, 83, 1433; Hirao, K. (Private communication with Dr. Kebarle).

109. Milligan, D. E. and Jacox, M. E. J. Chem. Phys. 1971, 55, 1003.

110. Rosenstock, H. M.; Draxl, K.; Steiner, B. W.; Herron, J.T. J. Phys. Chem. Ref. Data Sup. 1, 1977, 6.

111. Lias, S.; Liebman, J. F. and Levin, R. D. J. Phys. Chem. Ref. Data 1985, 13, 695.

112. Traeger, J. C. and McLaughlin, R. G. J. Am. Chem. Soc. 1981, 103, 3647.

113. Stull, D. R.; Prophet, H. JANAF Thermochmical Tables, NBS, Washington D.C., 1971.

114. Paul, M. A. "Principles of Chemical Thermodynamics", First edn. McGraw-Hill Inc., 1951, pp. 708.

115. Woo, S. B.; Helmy, E. M.; Mauk, P. H. and Paszek, A. P. Phys. Rev A. 1981, 24, 1380.

116. Dispert, H. and Lacman, K. Hans-Meitner-Inst. Kern. Forsch. Berlin. 1975, HMI-B 198, 34.

117. Lyons L. E. and Palmer, L. D. Aust. J. Chem. 1976, 29, 1919.

118. Leffert, C. B.; Tang, S. Y.; Rothe, E. W. and Cheng, T. C. J. Chem. Phys. 1974, 61, 4929.

119. Compton, R. N. and Cooper, C. D. J. Chem. Phys. 1973, 59, 4140.

120. Becker, R. S. and Chen, E. J. J. Chem. Phys. 1966, 45, 240.

121. Hindle, A. L.; Poppinger, D. and Radom, L. J. Am. Chem. Soc. 1978, 100, 4681.

122. Birch, A. J.; Hindle, A. L. and Radom, L. J. Am. Chem. Soc. 1980, 102, 3370.

123. Burrow, P. D.; Micheda, J. A. and Jordan, K. D. J. Am. Chem. Soc. 1976, 98, 1295; 6392; 7178.

124. Jordan, K. D. and Burrow, P. D. Accts. Chem. Res. 1978, 11, 341.

125. (a) Heilbronner, E. and Bock, H. "Das HMO-Modell Und Seine Anwendung", Verlat

Chemie, Bergstr. 1968, pp. 333. (b) Streitwieser, Jr. A."MO Theory for Organic Chemists", John Wiley and Sons, NY. 1966.

126. Heinis, T.; Chowdhury, S. and Kebarle, P. (to be submitted for publication).

127. Fujio, M.; Mclver, R. T.and Taft, R. W. J. Am. Chem. Soc. 1981, 103, 4017.

128. Hamano, H. and Kondo, H. Bull. Chem. Soc. Jpn. 1979, 41, 157.

129. Taft, R. W.and Lewis, I. C. J. Am. Chem. Soc. 1958, 80, 2436; 1960, 81, 5343.

130. Hoefnagel, A. J. and Wepester, B. M. J. Am. Chem. Soc. 1973, 95, 5357.

131. Rozeboom, M. D.; Tegmo-Larsson, I.; Houk, K. N. J. Org. Chem.1981, 46, 2338.

132. Collins, P. M.; Christophorou, L. G.; Charney, E. L. and Carter, J. G. Chem. Phys. Letts. 1970, 4, 646; J. Chem. Phys. 1970 , 52, 4413.

133. Heinis, T.; Chowdhury, S.; Scott, S. and Kebarle, P. (to be submitted for publication).

134. Frazier, J. R.; Christophorou, L. G.; Carter, J. S. and Schwindler, H. C. J. Chem. Phys. 1978, 69, 3807.

135. Jordan, K. D. and Burrow, P. D. J. Chem. Phys. 1979, 71, 5384.

136. Symons, M. C. R.; Selby, R. C.; Smith, I. G. and Bratt, S. W. Chem. Phys. Letts. 1977, 48, 100.

137. Millefiori, S.; Millefiori, A. and Granozzi, G.; J. Mol. Structure, 1982, 89, 247.

138. Schegoleva, L. N.; Bilkis, I. I. and Schastrev, P. V. Chem. Phys. 1983, 82, 343.

139. Yim, M. B. and Wood, D. E. J. Am. Chem. Soc. 1976, 98, 2053.

140. (a)Heilbronner, E. "Molecular Spectroscopy", Institute of Petroleum, London.1976.(b) Brundle, C. R.; Robins, M. B.; Kuebler, N. A. J. Am. Chem. Soc. 1972, 94, 1466.

141. Cooper, C. D. and Compton, R. N. J. Chem. Phys. 1974, 60, 2953.

142. *ibid*, 1974, 60, 2424.

143. Compton, R. N.; Reinhardt, P. W. and Cooper, C. D. J. Chem. Phys. 1974, 60, 2953.

144. Modelli, A.; Distefano, G. and Jones, D. Chem. Phys. 1982, 73, 395.

145. Lyons, L. E. and Palmer, L. D. Chem. Phys. Letts. 1973, 21, 442.

146. Bately, M. and Lyons, L. C. Nature, 1962, 196, 573.

147. Kebarle, P. In "Ions and Ion Pairs In Organic Reactions", M. Szwarc (eds), Wiley Interscience, 1972.

148. Herron, J. T.; Rosenstock, H. M.; Shields, W. R. Nature (London), 1965, 206, 611.

149. Peover, M. E. J. Chem. Soc., 1962, 2540.

150. Magnera, T. F.; Caldwell, G.; Sunner, J.; Ikuta, K. S. and Kebarle, P. J. Am. Chem. Soc. 1984, 106, 6140; Kebarle, P.; Caldwell, G.; Magnera, T. F. and Sunner, J. Pure & Appl. Chem. 1985, 57, 339.

151. Robinson, P. J. and Holbrook, K. A. "Unimolecular Reactions", Wiley Interscience, NY. 1972.

152. Stull, D. R.; Westrum, Jr., E. F.; Sinke, G. C. The Chemical Thermodynamics of Organic Compounds, Wiley Interscience, NY. 1969, pp. 458.

153. Pitzer, K. S. "Quantum Chemistry", Prentice Hall Englewood Cliffs, NJ. 1954, Table A18-4.

154. Becker, E. D.; Charney, E.; Anno, T. J. Chem. Phys. 1965, 42, 942.

155. Pack, L. and Phelps, A. V. J. Chem. Phys. 1966, 44, 1870.

156. Lindinger, W. and Albiriton, D. L. J. Chem. Phys. 1975, 62, 3520.

157. Rodiguin, N. M. and Rodiguina, E. N. "Consecutive Chemical Reactions", van Nostrand, Princeton, 1964.

158. McDaniel, E. W. "Collision Phenomena in Ionised Gases", Wiley Interscience, NY. 1964.

159. Hurst, G. S.; Stockdale, J. A. and O'kelly, L. B. J. Chem. Phys. 1963, 38, 2572.

160. Wojnarovits, L. and Foldiak, G. J. Chromatography, 1981, 206, 511.

161. Hogg, A. M.; Kebarle, P. J. Chem. Phys. 1965, 43, 449; Hogg, A. M.; Haynes, R. N.; Kebarle, P. J. Am. Chem. Soc. 1966, 88, 28; Lau, Y. K.; and Kebarle, P. Can. J. Chem., 1981, 59, 151.

162. Bathgate, R. H.; Moelwyn-Hughes, E. A. J. Chem. Soc. 1959, 2642; Parker, A. J. Chem. Rev. 1964, 69, 1.

163. Davidson, W. R.; Kebarle, P. J. Am. Chem. Soc. 1976, 98, 6125; Yamdagni, R.; Kebarle, P. J. Am. Chem. Soc. 1972, 94, 2940.

164. Yamabe, S.; Hirao, K. Chem. Phys. Letts. 1981, 84, 598; Hirao, K.; Yamabe, S. and Sano, M. J. Phys. Chem. 1982, 86, 2626.

165. Prince, R. C. et al in "Functions of Quinones", B. L. Trumpower (eds), Academic press, 1982, pp. 29.

166. Wagman, D. D.; Evans, W. H.; Parker, V. B.; Hallow, I.; Bailey, S. M. and Schumn, R. H. NBS US Tech. Note 270-3. 1968.

167. Weast, R. C. (eds) "Handbook of Chemistry and Physics", CRC press, Boca Raton, Fl. 79th edn. 1979, pp. 1078.

168. French, M. A.; Ikuta, S. and Kebarle, P. Can. J. Chem. 1982, 60, 1907.

169. French, M. A. Ph. D. Thesis, University of Alberta, 1977.

170. Hiraoka, K.; Mizure, S. and Yamabe, S. J. Chem. Phys.(in press).

171. Hunt, D. F.; Stafford, G. C.; Crow, F. W. and Russel, J. W. **Anal. Chem.** 1976, 48, 2098; Robinson, C. J. and Cook, G. C. **Anal. Chem.** 1971, 43, 1425.

172. Iida, Y. and Daishema, S. **Chem. Letts.** 1983, 273.

173. Clayton, E. and Wakefield, A. J. C. J. **Chem. Soc. Chem. Commun.** 1984, 969.

174. Chowdhury, S. and Kebarle, P. "Electron Affinities of Compounds M and Presence of M^+ and Clusters of M^- in NICI". Presented at the 34th Annu. ASMS Conf., Cincinnati, 1986.

175. Buchanan, M. V.; Wise, M. B. and Rubin, I. B. "Investigations of the Mechanisms Responsible for Isomeric Discrimination of Polycyclic Aromatic Hydrocarbons". 34th Annu. ASMS Conf., Cincinnati, 1986.

176. Kassel, D.; Kayganich, K. and Watson, J. T. "Detection of Chlorine Adducts Under Conditions for ECNCI MS". 34th Annu. ASMS Conf., Cincinnati, 1986.

177. Das, P. R. and Pramanik, B. N. "NCI MS of some Nitro Compounds". 34th Annu. ASMS Conf., Cincinnati, 1986.

178. Campbell, J. A.; Kallos, G.; Herman, E. and Patric, D. "NICI MS for Isomer Differentiation of Nitrogen Heterocyclic, Sulfur Heterocyclic and Mixed Heterocyclic Compounds". 34th Annu. ASMS Conf., Cincinnati, 1986.

179. Hilpert, L. R. "Determination of PAH and Alkalated-PAH in Particulate Extracts Using NICI MS". 34th Annu. ASMS Conf., Cincinnati, 1986.

180. Wise, M. B. and Buchanan, M. V. "Electron Capture Processes at Reduced Pressures for Selective Detection". 34th Annu. ASMS Conf., Cincinnati, 1986.

181. Dougherty, R. C.; Dalton, J. and Brios, F. J. **Org. Mass Spectrom.** 1972, 6, 1171.

182. Christophorou, L. G. **Atomic and Molecular Radiation Physics**, Wiley Interscience, NY. 1971, Chapter 6.

183. Hecht, S. S.; Melikian, A. A. and Amin, S. **Acc. Chem. Res.** 1986, 19, 174.

184. Chilingarov, N. S.; Korobov, M. V.; Sidorov, L. N.; Mitkin, V. N.; Shipachev, V. A. and Zemskov, S. V. **J. Chem. Thermo.** 1984, 16, 965.

185. Badtiev, E. B.; Chilingarov, N. S.; Korobov, M. V.; Sidorov, L. N. and Sorokin, I. D. **High Temp. Sci.** 1982, 15, 93.

186. Dzidic, I. and Kebarle, P. J. **Phys. Chem.** 1970, 74, 1466.

187. Kebarle, P.; Davidson, W. R.; French, M.; Cumming, J. B. and McMahon, T. B. **Farad. Discuss. Chem. Soc.** 1977, 64, 220.

188. Meisenheimer, J. **Liebigs. Ann. Chem.** 1902, 323, 205.

189. Artmkina, G. A.; Egorov, M. P. and Beletskaya, I. P. **Chem. Revs.** 1982, 82, 427.

190. Terrier, F. **Chem. Revs.** 1982, 82, 77.